
PEDESTRIAN WHOLE BODY GROUND CONTACT MECHANISMS AND HEAD INJURY ASSESSMENT FOLLOWING VEHICLE IMPACT

SHI SHANG, BENG., MSC.



A thesis submitted to the University of Dublin, Trinity College in partial fulfilment of the requirements for the degree of

Doctor of Philosophy

April 2020

Supervisor

Dr. Ciaran K. Simms

Internal Examiner

Dr. David Taylor

External Examiner

Dr. Michael Gilchrist

Declaration

I declare that this thesis has not been submitted as an exercise for a degree at this or any other university and it is entirely my own work.

I agree to deposit this thesis in the University's open access institutional repository or allow the library to do so on my behalf, subject to Irish Copyright Legislation and Trinity College Library conditions of use and acknowledgement.

Shi Shang, April 2020

Abstract

According to the WHO, there are an estimated 1.35 million road-traffic related deaths each year, with pedestrians constituting approximately 22% of this figure, which justifies the necessity of research into vehicle-pedestrian collisions. Previous researchers have primarily focused on the injuries that pedestrians experience as a result of contact with the vehicle, however, ground related injuries and the mechanisms have been largely neglected. Accordingly, the purpose of this study is to significantly strengthen the understanding of pedestrian ground contact, to investigate what factors influence pedestrian ground contact injury severity, and to determine injury prevention strategies.

An analysis of GIDAS vehicle-pedestrian crash data showed that head, thorax, and upper/lower extremities injuries are the most frequent pedestrian ground related injuries. The severity of ground related injuries is greatly affected by vehicle speed and pedestrian age. Older pedestrians are more at risk of suffering thorax injuries. Logistical analysis indicates that normalized bonnet leading edge height (NBLEH) is a predictor of the risk of AIS2 + ground related injuries. Prevention of all ground related pedestrian injuries for vehicle impact speeds below 40 km/h would bring very substantial injury cost reductions.

An analysis of real-world vehicle-pedestrian collision videos from Youtube has been done in Chapter 5 to provide a basic understanding of pedestrian ground contact mechanism. The study consisted of 29 videos and examined the influencing factors that affect the mechanisms of pedestrian ground contact. It was observed that pedestrian projection increases with the vehicle speed, while smaller NBLEH resulted in larger pedestrian rotations, which indicates the potential effects that vehicle front shape has on the resulting pedestrian ground contact injuries.

Six cadaver tests were conducted in LBA, IFSTTAR, Aix-Marseille University, France, which provided data relating to the pedestrian's kinematics during ground contact. It was observed that there is approximately 500ms of continued interaction between the pedestrian and the vehicle until separation occurs, which is followed by a flight period of around 200ms, finally terminating during ground contact. The linear accelerations in ground contact for vehicle impact speeds of 20 and 30 km/h are generally higher than the acceleration in the

vehicle contact The predicted risk of rotationally induced brain injury caused by ground contact is high for the 20 km/h test, highlighting the risk of pedestrian injuries from ground contact even at very low speeds.

Validation of both the MB and FE pedestrian models is yet to be completed in ground contact, therefore, a robust comparison of the pedestrian's motion in MADYMO environment with the pedestrian's motion in the cadaver test footage was conducted, thus revealing the competency of the MB model to predict the pedestrian's trajectory during a collision. It shows that contact characteristics of vehicle front-end greatly influence pedestrian post-impact kinematics and the induced injury predictions. In two of these reconstructed simulations, the MB pedestrian model bounded off the vehicle in a dissimilar motion to the motion observed in the staged tests. Although the pedestrian model failed to represent all the cadaver tests with exact kinematics, the model is partially suitable for use in a virtual test system (VTS) under low speed impact configurations.

An inverse method based on a Virtual Test System (VTS) was used to correlate the distribution of impact parameters (vehicle speed, pedestrian height and pedestrian gait) with the predicted injuries, thus allowing the weighting of each parameter (Weighted Injury Costs) with its predicted injury to be determined. VTS showed that there was no significant difference in the WIC scores for the two shapes 'Good shape' and 'poor Shape') in each category of vehicle. Although for the van and SUV categories, the differences become significantly large under test samples of 120. The good shape vehicles are at least not worse in pedestrian-friendly than the poor shape vehicles.

Together these studies provide significant new insights into pedestrian ground contact kinematics and injuries.

Acknowledgement

This study was sponsored by the Scholarship from the China Scholarship Council (CSC) and the Faculty of Engineering, Mathematics & Science of Trinity College Dublin.

I would like to thank all those who have helped and supported me throughout this research. But first, I would like to thank Prof. Ciaran Simms, my supervisor, who always shares the professional guidance and the explanation very patiently and encourage me not afraid of expressing my opinions to the research. His high efficiency makes sure that he always gave me feedback as soon as he can. I benefited greatly by his profession, serious study and deep investigation on research. It is my pleasure to have the opportunity to do my PhD research with Ciaran and I look forward to continuing work with him in the future.

I would like to thank Prof. Dietmar Otte from the Medical University of Hannover, Germany for the in-depth pedestrian accident data, Prof. Pierre-Jean Arnoux, Dr. Catherine Masson, and Max Py from Laboratory of Applied Biomechanics Faculty of Medicine North, France for the cadaver tests conduction, Mr. David Teeling from Denis Wood Associates, Ireland, for part of the contribution of MBIM analysis, Dr. Guibing Li from Hunan University of Science and Technology, China for assistance with the virtual test system interpretation, and Francoise Dotraux from Euro NCAP, Belgium for the pedestrian safety test results of specified vehicle models.

I also would like to thank all of the staff in the department, and everyone who shared the office with me throughout my study: Ger, Guibing, Greg, Kevin, Kian, Micheal, Melika, Niamh, Parth, Richard, and Tiefang. I have a highly wonderful time in Ireland for the last half three years and I will cherish the memories forever.

I would like to thank Prof. Jun Xu from the Department of Automotive Engineering, Beihang University, who supervised me during my master's. He taught me a lot and lead me to the academic field. I would not be at this level without his patient and professional guidance. I am always amazed at his hard-working style and continuous fresh ideas. I look forward to continuing to work with Jun in the future.

Finally, I would like to thank my family and friends, they have always been on my side and supportive. I would like to express my sincere gratitude to my parents, for their continued concern, support and everything they have done for me.

Content

Abstract.....	I
Acknowledgement.....	III
Content.....	V
List of Figures.....	XI
List of Tables.....	XVII
Publications	XIX
Glossary	XXI
1. Introduction.....	1
1.1. Background	1
1.2. Proposed research approaches.....	4
2. Literature Review	7
2.1. Overview of pedestrian ground contact during a vehicle collision.....	7
2.2. Head-brain Injury and the criteria	7
2.2.1. Head-brain injury	7
2.2.2. Head brain injury criteria	8
2.3. Materials and methods used in the studies of pedestrian ground contact injury.....	12
2.3.1. In-depth accident databases analysis	12
2.3.2. Crash reconstruction using MB/FE pedestrian models.....	14
2.3.3. Real-world crash video analysis	23
2.3.4. Cadaver/dummy/impactor test.....	25
2.4. Relative methods will be applied	29
2.4.1. Virtual Test System (VTS).....	29
2.4.2. Model Based Image Matching (MBIM)	31
2.5. What is known about pedestrian ground related injuries	32
2.5.1. The severity of pedestrian ground contact injuries	32

2.5.2. Vehicle speed effect on ground related injuries	34
2.5.3. Vehicle type effect on the pedestrian ground related injuries	36
2.5.4. Pedestrian size effect on ground related injuries	38
2.5.5. Other effects on ground related injuries.....	39
2.6. Absence of information on ground contact injuries	40
2.7. Summary	40
3. Proposed research to understand pedestrian ground related injury	43
3.1. Introduction	43
3.2. Methods.....	43
3.2.1. Detailed accident analysis to understand the nature of the ground contact	43
3.2.2. Video analysis of real-world collisions	43
3.2.3. Staged tests with cadavers to provide better information on ground contact and model assessment information.....	44
3.2.4. Multibody model assessment based on the cadaver tests	44
3.2.5. Virtual test system (VTS) approach to reduce or prevent ground contact injuries	45
4. Study 1: Analysis of pedestrian ground contact injuries from detailed German accident database	47
4.1. Introduction	47
4.2. Methods.....	49
4.2.1. GIDAS data.....	49
4.2.2. Statistical analysis.....	52
4.3. Results	54
4.3.1. Overview of ground related injuries	54
4.3.2. Effect of vehicle impact speed on pedestrian ground related injury	56
4.3.3. Effect of pedestrian age on pedestrian ground related injury	58
4.3.4. Effect of vehicle production year on pedestrian ground related injury.....	59
4.3.5. Effect of vehicle front shape on pedestrian ground related injury	60

4.3.6. Potential reduction in ground contact injury costs.....	62
4.4. Discussion	63
4.5. Conclusion.....	66
5. Study 2: Video analysis of real-world collisions	69
5.1. Introduction	69
5.2. Methods.....	69
5.2.1. Videos of real-world vehicle-pedestrian collisions.....	69
5.2.2. Estimation of vehicle speed, projection distance.....	71
5.3. Results	71
5.3.1. The relationship between vehicle speed and pedestrian projection distance	72
5.3.2. The relationship between Normalized BLEH and whole-body rotations.....	72
5.4. Discussion	73
5.5. Conclusion.....	74
6. Study 3: Kinematics and dynamics of pedestrian head ground contact by cadaver testing program	77
6.1. Introduction	77
6.2. Methods.....	79
6.2.1. Cadaver Test Setup	79
6.2.2. Video Data Analysis.....	88
6.2.3. Head injury assessments	89
6.3. Results	90
6.3.1. Pedestrian kinematics during the whole process of vehicle impact.....	90
6.3.2. Head injury risk assessments	98
6.4. Discussion	102
6.4.1. Whole-body kinematics during the complete pedestrian impact process.....	102
6.4.2. Head kinematics throughout the impact process	103
6.4.3. Head ground contacts.....	103

6.4.4. Head accelerometer filtering.....	105
6.4.5. Head Linear versus rotational loading ground contact	105
6.4.6. Comparison with real-world crash video	106
6.4.7. Unexpected Results.....	107
6.5. Conclusion.....	109
7. Study 4: Assessment of multibody pedestrian model compared with real pedestrian during the crash	111
7.1. Introduction	111
7.2. Materials and methods.....	113
7.2.1. Multibody vehicle models.....	113
7.2.2. Pedestrian models	114
7.2.3. Movement input of the MB vehicle models.....	116
7.2.4. Contact characteristic applied on the MB vehicle model	119
7.2.5. Ground contact stiffness.....	120
7.3. First round of simulation and results	125
7.3.1. Pedestrian kinematics.....	126
7.3.2. Pedestrian head trajectories.....	134
7.3.3. Pedestrian head injury criteria assessments	136
7.4. Sensitivity study	137
7.4.1. Sensitivity study of pedestrian initial joint angle.....	138
7.4.2. Sensitivity study of bending of pedestrian model.....	140
7.5. Second round of reconstruction.....	141
7.6. Discussion	143
7.7. Conclusion.....	145
8. Study 5: Assessment of vehicle front-end shape on pedestrian ground related injury considering a weighted impact configuration.....	147
8.1. Introduction	147

8.2. Materials and methods	148
8.2.1. Pedestrian accident distribution	148
8.2.2. Pedestrian model.....	150
8.2.3. Vehicle model.....	151
8.2.4. Numerical simulation.....	152
8.2.5. Weighted Injury cost	152
8.2.6. Simulation test sample	153
8.3. Results	153
8.4. Discussion	155
8.5. Conclusion.....	155
9. Discussion	157
9.1. Pedestrian ground contact injuries from real-world accident database.....	157
9.2. Pedestrian kinematics observed from real-world collision videos.....	159
9.3. Kinematics and dynamics of pedestrian head ground contact from cadaver tests ..	159
9.4. Multi-body pedestrian model assessment for ground contact.....	161
9.5. Vehicle shape effect on ground related injury costs based on a virtual test system	162
9.6. Potential practical work to reduce the risk and severity of ground related head injuries	162
9.7. Summary	163
10. General Conclusion and Future Work.....	167
10.1. General Conclusion	167
10.2. Future work	168
References.....	171
Appendices.....	185
Appendix A. Subsystem impactor tests stiffness calculation, adapted from [Martinez <i>et al.</i> 2007]	185
Stiffness calculation from headform tests.....	185

Stiffness calculation from legform test	186
Stiffness calculation from Upper legform test	186
Appendix B. Real-world crash video sequences used in Chapter 5	187
Appendix C. Sequence of vehicle-pedestrian impact for cadaver test 01 with video data	198
Appendix D. Simulation test sample (STS) used in Chapter 8	199

List of Figures

Figure 1.1 Sequences of pedestrian-vehicle impact and pedestrian-ground impact captured from one of a series of cadaver tests	3
Figure 1.2 Study plan.....	6
Figure 2.1 Sagittal view of the simplified brain and skull anatomy diagram, adapted from [Shang <i>et al.</i> 2018d].....	8
Figure 2.2 WSTC head injury tolerance curve, adapted from [Lissner <i>et al.</i> 1960].....	9
Figure 2.3 Relation of <i>HIC</i> score and the probability of skull fracture [Hertz 1993], adapted from [Tillmann 2006]	10
Figure 2.4 The relationship between <i>BrIC</i> (based on CSDM and MPS and formulation given by Equation 2.2 and the probability of brain injury risk at a different level of severity, adapted from [Takhounts <i>et al.</i> 2013]	11
Figure 2.5 Relationship between brain shear strain and head angular speed & acceleration. Critical strains: 0.2 (heavy dashed line), 0.15 (heavy solid line), 0.1 (dashed line) and 0.05 (solid line), adapted from [Margulies and Thibault 1992].....	12
Figure 2.6 Ellipsoid pedestrian models, from left to right; 3-year-old child, 6-year-old child, small female, mid-size male and large male, adapted from [TNO 2017].....	14
Figure 2.7 Geometry and the mass distribution of the MB 50th percentile adult pedestrian model developed by [Yang and Lovsund 1997], adapted from [Yang and Lovsund 1997]	15
Figure 2.8 THUMS models and applications, adapted from [TOYOTA]	15
Figure 2.9 GHBMC human models, adapted from [Elemance]	16
Figure 2.10 Numerical vehicle-pedestrian impact scenario combined FE vehicle shape and MB pedestrian model, adapted from [Shi <i>et al.</i> 2018]. The numbers of degree indicating the post-vehicle impact rotation angles of pedestrian before landing on the ground.	17
Figure 2.11 Occurrences of the six impact mechanisms for each vehicle type for the adult pedestrian impacts at all vehicle impact speeds (20, 30 and 40 km/h), adapted from [Crocetta <i>et al.</i> 2015]	18
Figure 2.12 Effect of speed on most severe injury source, adapted from [Kendall <i>et al.</i> 2006]	19
Figure 2.13 Average launch speed of 50th percentile male (a); Average launch angle of 50th percentile male (b), adapted from [Hamacher <i>et al.</i> 2012].....	19
Figure 2.14 Dimensional parameters of vehicle front-end structure. Bonnet leading edge	

height (H) bonnet length (L), bonnet angle (α), and windshield angle (θ) are indicated, adapted from [Yin <i>et al.</i> 2017].....	20
Figure 2.15 Coupling effect of H and α on HIC_{15} at all impact speeds (20, 30, and 40 km/h), adapted from [Yin <i>et al.</i> 2017].....	20
Figure 2.16 Pedestrian orientation at $t=450$ ms after impact, for car impact velocity of 40 km/h and 0.8G braking, adapted from [Gupta <i>et al.</i> 2017].....	21
Figure 2.17 A sequence of lateral views of vehicle-to-pedestrian interactions at initial impact. Left: SUV vs. pedestrian. Right: sedan vs. pedestrian, adapted from [Tamura <i>et al.</i> 2014].....	22
Figure 2.18 Comparison of selected TBI assessment parameters. (a) HIC_{15} due to primary and secondary head strikes; (b) max rotation acceleration due to primary and secondary head strikes; (c) HIP_{max} due to primary and secondary head strikes, adapted from [Tamura <i>et al.</i> 2014].....	23
Figure 2.19 Comparison of head-ground vertical impact speed from real-world videos analysed and from previously published predictions [Crocetta <i>et al.</i> 2015], adapted from [Barry and Simms 2016].....	24
Figure 2.20 Definition of vehicle-pedestrian crash scenarios, adapted from [Han <i>et al.</i> 2017].....	24
Figure 2.21 Distribution of pedestrian body landing region, adapted from [Han <i>et al.</i> 2017].....	25
Figure 2.22 Sequential photo of the dummy behaviour test, vehicle impact vel. 41.0km/h, adapted from [Taneda <i>et al.</i> 1973].....	26
Figure 2.23 Sequential sketch of four different patterns, adapted from [Taneda <i>et al.</i> 1973].....	27
Figure 2.24 Experimental test setup (a) and post ground impact conditions (b), adapted from [Hamacher <i>et al.</i> 2012].....	28
Figure 2.25 Illustration of Euro NCAP pedestrian test.....	28
Figure 2.26 Illustration of VTS for vehicle shape optimization based on the weighted injury cost, adapted from [Li <i>et al.</i> 2017b].....	30
Figure 2.27 The original video image (a) and the images of matched Poser skeleton model to the laboratory model in three views (b-d), adapted from [Krosshaug and Bahr 2005] ...	31
Figure 2.28 Injury Frequency of $n=293$ Pedestrians in Total (100% all persons), distinguished for primary and secondary impacted persons (100% each injured body regions).....	32

Figure 2.29 Classification tree for vehicle or road as a source of head impact and injury split by road user type, adapted from [Badea-Romero and Lenard 2013].....	34
Figure 2.30 Relative influence of pedestrian injuries caused by vehicle contact versus ground contact as a function of impact speed, adapted from [Ashton 1975].....	35
Figure 2.31 Proportion of pedestrian ground contact mechanisms by vehicle type, adapted from [Simms <i>et al.</i> 2011].....	37
Figure 2.32 Normalized bonnet leading edge height (NBLE/Pedestrian height) effect on pedestrian head ground impact speed and the time of impact for mechanism 1 from [Crocetta <i>et al.</i> 2015], adapted from [Crocetta <i>et al.</i> 2015].....	38
Figure 2.33 Qualitative comparison of children and adult pedestrian models regarding secondary impact, adapted from [Hamacher <i>et al.</i> 2012].....	39
Figure 2.34 Weighted injury cost for full braking versus controlled braking for different simulation test sample combinations, adapted from [Zou <i>et al.</i> 2019].....	39
Figure 4.1 Number of cases and percentage distribution of body regions injured by pedestrian ground contact for different AIS levels: (a) AIS 2, (b) AIS 3, (c) AIS 4, and (d) AIS 5.....	55
Figure 4.2 GIDAS cases with and without ground related injuries. At each MAIS level, the black columns show the total number of cases and red columns show the number of cases where the highest AIS injury is associated with ground contact.	55
Figure 4.3 Distribution of vehicle speeds for AIS 2, AIS 3 and AIS 4-5 ground related injuries (GRI).....	56
Figure 4.4 Distribution of vehicle speed for AIS2+ ground related injuries (GRI) across body regions.....	57
Figure 4.5 Distribution of pedestrian age for AIS2, AIS 3 and AIS 4-5 ground related injuries (GRI).....	58
Figure 4.6 Pedestrian age distribution for different body regions with AIS2+ ground related injuries.	59
Figure 4.7 Distribution of NBLEH for cases with AIS2, AIS3 and AIS4-5 ground related head injuries.....	60
Figure 4.8 Average AIS2+ ground related head injury risk as a function of NBLEH for different speed (km/h) and age (years) levels.	61
Figure 4.9 Distribution of gender for cases with AIS1+, AIS2, AIS3 and AIS4+ ground related injuries.....	65

Figure 5.1 Three sample sequences of vehicle-pedestrian collision captured by video	70
Figure 5.2 The relation of pedestrian projection and vehicle impact speed	72
Figure 5.3 The relation of Normalized BLEH and whole-body rotations	73
Figure 6.1 The general locations of the high-speed cameras	85
Figure 6.2 (a) Pre-impact scenario; (b) accelerometer positions and nominal orientations; (c) head accelerometer, CG and forehead marker positions.....	86
Figure 6.3 Knee joint angles of pedestrian pre-impact positions.....	87
Figure 6.4 Sample head MBIM matching using multi-view camera images	88
Figure 6.5 Sequences of vehicle-pedestrian impact for the six cadaver tests	92
Figure 6.6 PMHS head displacement in X and Z directions for each test	94
Figure 6.7 Pedestrian head impact location on vehicle.....	94
Figure 6.8 Head velocity time-histories from central difference (blue and cyan) with straight line approximations between major impact phases (black).	96
Figure 6.9 Filtered and unfiltered resultant head accelerometer time-histories during vehicle contact and ground contact	97
Figure 6.10 Comparison of head speed changes from MBIM and accelerometer.....	98
Figure 6.11 Summary of head injury indices for vehicle and ground contact	99
Figure 6.12 Comparison of <i>BrIC</i> scores between researchers performing MBIM.....	99
Figure 6.13 Comparison of linear velocity changes between researchers performing MBIM	101
Figure 6.14: Comparison of the relationship between <i>aHIC/3ms</i> linear head injury risk with the rotationally assessed AIS 3+ risk for Test 01-05 (the accelerometer malfunctioned in the ground contact in Test 06).....	105
Figure 7.1 Flow chart of assessing the multi-body models	113
Figure 7.2 The vehicle models with the simplified MADYMO models	114
Figure 7.3 The initial postures of PMHS pedestrians and the corresponding multi-body models.....	115
Figure 7.4 The steps of choosing the tracking point.....	116
Figure 7.5 The fitting curves of the motion of the tracking point.....	118
Figure 7.6 The comparison of input and output motions of checking points	119
Figure 7.7 Force-deformation contact characteristics of vehicle front components from different sources.....	120
Figure 7.8 Ground stiffness for each test calculated by two methods	122

Figure 7.9 Comparison of the accelerations obtained from simplified head model test by using K_1 and K_2 (the comparison of Test 06 was not given because the head acceleration was corrupted signal during ground contact)	123
Figure 7.10 Two Stiffnesses of ground (k_p for Test 01, Test 02, Test 05 and Test 06; k_a for Test 03 and Test 04) applied in MADYMO simulation.....	123
Figure 7.11 Comparison of acceleration peaks from cadaver tests and simplified MADYMO simulation in ground contact (the comparison of Test 06 was not given because the head acceleration was corrupted signal during ground contact)	124
Figure 7.12 Testing of hysteresis slope and unloading curve effect on the contact.....	125
Figure 7.13-1 Test 01: Sequences of vehicle-pedestrian impact experiment compared with MB simulations. Contact characteristic of vehicle front applied from (Green model: EU NCAP; Blue model: Martinez; Red model: Mizuno).....	128
Figure 7.14 Comparison of pedestrian forehead trajectories between PNHS experiments and mathematic simulations	135
Figure 7.15 Comparison of head injury indices from vehicle and ground contact.....	137
Figure 7.16 Initial joint angle effect on HIC and $BrIC$ from ground contact.....	139
Figure 7.17 Pedestrian ground contact mechanisms from different initial hip angle from Table 7.3.....	139
Figure 7.18 Sequence of baseline MB pedestrian model (orange) and the model with added bending kinematics in vehicle crash	140
Figure 7.19 Comparison of pedestrian landing mechanisms between PMHS tests and MB reconstructions (Pink model: First round; Blue model: Second round)	142
Figure 7.20 Comparison of head injury indices from PMHS tests, 1 st round and 2 nd round simulations	143
Figure 8.1 Distribution of pedestrian height in vehicle crashes from PCDS and GIDAS database.....	149
Figure 8.2 Pedestrian stances for different gait parameters (%) of the gait cycle, adapted from [Untaroiu <i>et al.</i> 2009].....	149
Figure 8.3 Distribution of vehicle impact speed in vehicle crashes from PCDS and GIDAS database.....	150
Figure 8.4 MADYMO pedestrian models, 3 years old, 6 years old, 5% percentile, 160cm (scaled), 170cm (scaled), 50% percentile, 180cm (scaled), 95% percentile and 190cm (scaled), from left to right.....	150

Figure 8.5 Description of vehicle front shape parameters and MB vehicle-pedestrian impact scenario151

Figure 8.6 WIC comparison between poor shape vehicles and good shape vehicles154

Figure 9.1 The idea of the inflatable safety vest163

List of Tables

Table 2.1 Common head brain injuries and related mechanisms, adapted from [Yang 2005]	8
Table 2.2 Threshold for <i>HIC</i> score in different AIS levels, adapted from [Payne and Patel 2001].....	10
Table 2.3 Distribution of sources of head injury and resultant injury severity for adults by the class of vehicle, adapted from [Roudsari <i>et al.</i> 2005].....	33
Table 4.1 Medical and auxiliary cost of injury severity, adapted from ISO 13232-5:2005 [ISO 2005]	52
Table 4.2 Permanent partial incapacity (PPI) determination, adapted from ISO 13232-5:2005 [ISO 2005]	52
Table 4.3 Magnitudes of effect sized <i>d</i> and <i>r</i> for ANOVA [Cohen 1988, Sawilowsky 2009]	53
Table 4.4 Detailed information for the MAIS4/5 ground related injury cases	56
Table 4.5 ANOVA comparisons of vehicle speeds for different AIS categories.....	57
Table 4.6 Chi-squared Test of differences in ground related/non-ground related AIS 2+ whole-body injury cases for newer versus older vehicles (adults only).....	59
Table 4.7 Fisher’s Exact Test of differences in ground related/non-ground related AIS 2+ head injury cases for newer versus older vehicles (adults only).....	60
Table 4.8 Logistic regression results for speed, age and NBLEH vs ground related AIS 2+ head injuries (age 18+)	61
Table 4.9 -1 Total and ground related injury cost (US\$): (A) Cases with vehicle impact speed < 20km/h.....	62
Table 4.10 Average proportion of ground related injury cost for different speed categories	63
Table 6.1 Summary of PMHS tests performed.....	81
Table 6.2-1 External anthropometry	82
Table 6.3 Three different vehicles used in the impact experiments.....	84
Table 6.4 Expected ground contact mechanisms [Crocetta <i>et al.</i> 2015].....	85
Table 6.5 Key vehicle and ground contact events (s)	91
Table 6.6-1 Intraclass correlation coefficients for two independent MBIM researchers for vehicle contact	100

Table 6.7 Summary of head/vehicle contact injury assessments	101
Table 6.8 Summary of head/ground contact injury assessments	101
Table 6.9 Expected and observed pedestrian ground contact mechanisms [Crocetta <i>et al.</i> 2015]	101
Table 6.10 Expected and observed ground contact speeds [Crocetta <i>et al.</i> 2015].....	102
Table 6.11 Contact location for suitable cadaver tests	104
Table 6.12 Reasons for unsuitable cadaver tests.....	104
Table 6.13 Head ground contact stiffness	104
Table 6.14 Cases around 20 kph from Chapter 5 and Chapter 6	107
Table 6.15 Cases around 30 kph from Chapter 5 and Chapter 6	107
Table 7.1 The input parameter of the MB ball (simplified head model)	121
Table 7.2-1 Comparison of key events (s) of Test 01	126
Table 7.3 Initial angles of joint sensitivity study	138
Table 7.4 Comparison of <i>HIC</i> and <i>BrIC</i> in ground contact from baseline pedestrian model and the damping model.....	141
Table 8.1 A simulation test sample (STS) considering 6 vehicle impact speeds, 5 pedestrian heights and 4 pedestrian gait stances	153

Publications

Journal publications

Shang, S., Otte, D., Li, G., Simms, C. (2018). Detailed assessment of pedestrian ground contact injuries observed from in-depth accident data. *Accident Analysis & Prevention*, 110, 9-17.

<https://doi.org/10.1016/j.aap.2017.10.011>

Shang, S., Masson, C., Teeling, D., Py, M., Ferrand, Q., Arnoux, P.J., Simms, C (2020). Kinematics and dynamics of pedestrian head ground contact: a cadaver study. *Safety Science*, 127, 104684.

<https://doi.org/10.1016/j.ssci.2020.104684>

Shang, S., Masson, C., Llari, M., Arnoux, P.J., Py, M., Simms, C. Assessment of a Multi-body pedestrian model compared with real pedestrian during the crash experiment. *In preparation*.

Shang, S., Simms. Assessment of vehicle front-end shape on pedestrian ground related injury considering a weighted impact configuration. *In preparation*.

Conference abstracts

Shang, S., Otte, D., Simms, C. (20-21 January 2017). Investigation of pedestrian injuries caused by ground contact during traffic accidents. Bioengineering in Ireland Conference Proceedings, 2017, Templepatrick, Northern Ireland.

Shang, S., Otte, D., Simms, C. (13-15 September 2017). Pedestrian-ground contact injuries observed from German in-depth accident data. IRCOBI Conference Proceedings, 2017, Antwerp, Belgium.

Shang, S., Arnoux, P.J., Masson, C., Py, M., Simms, C. (26-27 January 2018). A preliminary vehicle dummy impact test for validation of multi body pedestrian ground contact simulation. Bioengineering in Ireland Conference Proceedings, 2018, Meath, Ireland.

Shang, S., Otte, D., Li, G., Simms, C. (25-27 April 2018). An inverse method to reduce pedestrian-ground contact injuries. IRCOBI Asia Conference Proceedings, Lonavala, India.

Shang, S., Arnoux, P.J., Masson, C., Py, M., Simms, C. (8-12 July 2018). Comparison of pedestrian head trajectories between a dummy test and a multi-body model simulation. World Congress of Biomechanics, 2018, Dublin, Ireland.

Shang, S., Masson, C., Arnoux, P.J., Py, M., Simms, C. (12-14 September 2018). Preliminary assessment of the Madymo pedestrian model for predicting pedestrian ground contact kinematics. IRCOBI Conference Proceedings, 2018, Athens, Greece.

Shang, S., Arnoux, P.J., Masson, C., Py, M., Simms, C. (18-19 January 2019). Pedestrian head kinematics during ground contact. Bioengineering in Ireland Conference Proceedings, 2019, Limerick, Ireland.

Shang, S., Teeling, D., Masson, C., Arnoux, P.J., Py, M., Ferrand, Q., Simms, C. (11-13 September 2019). Pedestrian head injuries in ground contact: a cadaver study. IRCOBI Conference Proceedings, 2019, Florence, Italy.

Glossary

AM50	Adult Male 50 th Percentile
AIS	Abbreviated Injury Scale
ANOVA	Analysis Of Variance
APROSYS	Advance Protection System
BCH	Bumper Center Height
BL	Bumper Lead
BLEH	Bonnet Leading Edge Height
BrIC	Brain Injury Criterion
CIDAS	German In-Depth Accident Study
CNCAP	China New Car Assessment Programme
CSDM	Cumulative Strain Damage Measure
DAI	Diffuse Axonal Injury
EEVC	European Experimental Vehicle Committee
Euro NCAP	European New Car Assessment Programme
FE	Finite Element
FFC	Femur Force Criterion
GHBMC	Global Human Body Models Consortium
GIDAS	German In-Depth Accident Study
HIC	Head Injury Criterion
HIP	Head Impact Power
IC	Injury Cost
ICC	Intraclass Correlation Coefficients
IFSTTAR	The French Institute of Science and Technology for Transport, Development and Networks
ISO	International Organization for Standardization
JNCAP	Japan New Car Assessment Programme
LBA	Laboratory of Biomechanics and Application
LTV	Light Truck Vehicle
MB	Multi-body
MBIM	Model Based Image Matching

MPS	Maximum Principal Strain
NBLEH	Normalized Bonnet Leading Edge Height
NCAC	National Crash Analysis Center
NHTSA	National Highway Traffic Safety Administration
OTS	On the Spot
PCDS	Pedestrian Crash Analysis Center
PMHS	Post-mortem Human Subject
STS	Simulation Test Sample
SUV	Sport Utility Vehicle
TBI	Traumatic Brain Injury
THUMS	Total Human Model for Safety
TI	Tibia Index
TTI	Throacic Trauma Index
UBrIC	Universal Brain Injury Criterion
VC	Viscous Criterion
VTS	Virtual Test System
VRUs	Vulnerable Road Users
WHO	World Health Organization
WIC	Weighted Injury Cost
WSTC	Wayne State Tolerance Curve

1. Introduction

1.1. Background

Vehicle crashes are one of the major causes of accidental injury and death in road traffic. Pedestrians are often categorized as Vulnerable Road Users (VRU) since they do not benefit from crash protection features common on most passenger vehicles [Simms and Wood 2009]. The World Health Organization (WHO) estimates about 270,000 pedestrian fatalities occur annually following road traffic collisions [WHO 2013]. Researchers [Simms 2005, Simms and Wood 2009, Rosén *et al.* 2011, Niebuhr *et al.* 2016, Li *et al.* 2017a, Yin *et al.* 2017] have provided a good understanding of the relationship between vehicle speed, front-end design, and pedestrian injury outcome and the European Union has announced that relevant tests must be passed by new cars for pedestrian safety. Some vehicle companies have proposed ideas such as improved front-end designs, external airbags and applied pop-up bonnets to reduce the injury risk to pedestrians.

Most pedestrians have an initial (primary) contact with the vehicle (windshield, bonnet, bumper, etc) and then also a secondary impact with the ground after being hit by the vehicle in a whole process of the crash (as shown in Figure 1.1). However, in collision research, there has been much less focus on pedestrian ground contact injuries, and prevention strategies. Distinguishing whether injuries to pedestrians were sustained by contact with the vehicle or with the ground generally presents a challenge for collision investigators [Otte and Pohlemann 2001, Neal-Sturgess *et al.* 2007] and the distribution and risk factors for pedestrian ground contact injuries remains poorly understood. The effects of head–vehicle contact and the following head–ground contact often make it difficult to identify the head injury mechanism. Nonetheless, despite uncertainty in attributing injuries to vehicle or ground contact, accident data analysis [Otte and Pohlemann 2001] shows that pedestrian ground contact injuries are also significant. Otte and Pohlemann [Otte and Pohlemann 2001] analysed the 1985-1999 German in-depth Accident Study (GIDAS) data and found that 65 percent of pedestrians had injuries from ground contact. However, the severity and distribution of injuries were not clearly reported, and the front-end shape of the vehicle fleet has since changed significantly.

It is widely accepted in the field of vehicle safety that pedestrian ground contact mechanisms are highly variable [Simms and Wood 2006, Kerrigan *et al.* 2007, Li *et al.* 2018], but in recent years studies have been conducted to investigate the mechanism of injury generation from pedestrian contact with the ground [Simms and Wood 2006, Simms *et al.* 2011, Crocetta *et al.* 2015, Han *et al.* 2017, Yin *et al.* 2017]. These have focused on head injuries (associated with head ground impact speed or head injury criterion), since head injuries are one of the most frequent and the most severe injuries due to ground contact. Overall, the literature provides some detail on pedestrian head injuries from ground contact, but the whole-body distribution of ground contact injuries is not reported and risk factors for ground injuries remain poorly understood from collision data. A biomechanical analysis of the relationship between pedestrian head ground injuries and vehicle type remains incomplete.

Computational studies have addressed pedestrian ground contact [Kendall *et al.* 2006, Tamura and Duma 2011a, Tamura *et al.* 2014, Crocetta *et al.* 2015, Yin *et al.* 2017] and these studies observed a strong influence of the initial impact boundary on pedestrian ground contact mechanism. The bonnet leading-edge height (BLEH) influences ground contact kinematics [Simms *et al.* 2011, Hamacher *et al.* 2012, Crocetta *et al.* 2015, Yin *et al.* 2017] implying that vehicle front-end shapes positively influence the pedestrian ground contact. However, no pedestrian models have been validated for ground contact, although preliminary comparisons with video recordings of pedestrian collisions show some verification [Barry and Simms 2016, Han *et al.* 2017, Han *et al.* 2018b]. Previous validation has only focused on the first few hundred milliseconds of a vehicle-pedestrian impact.

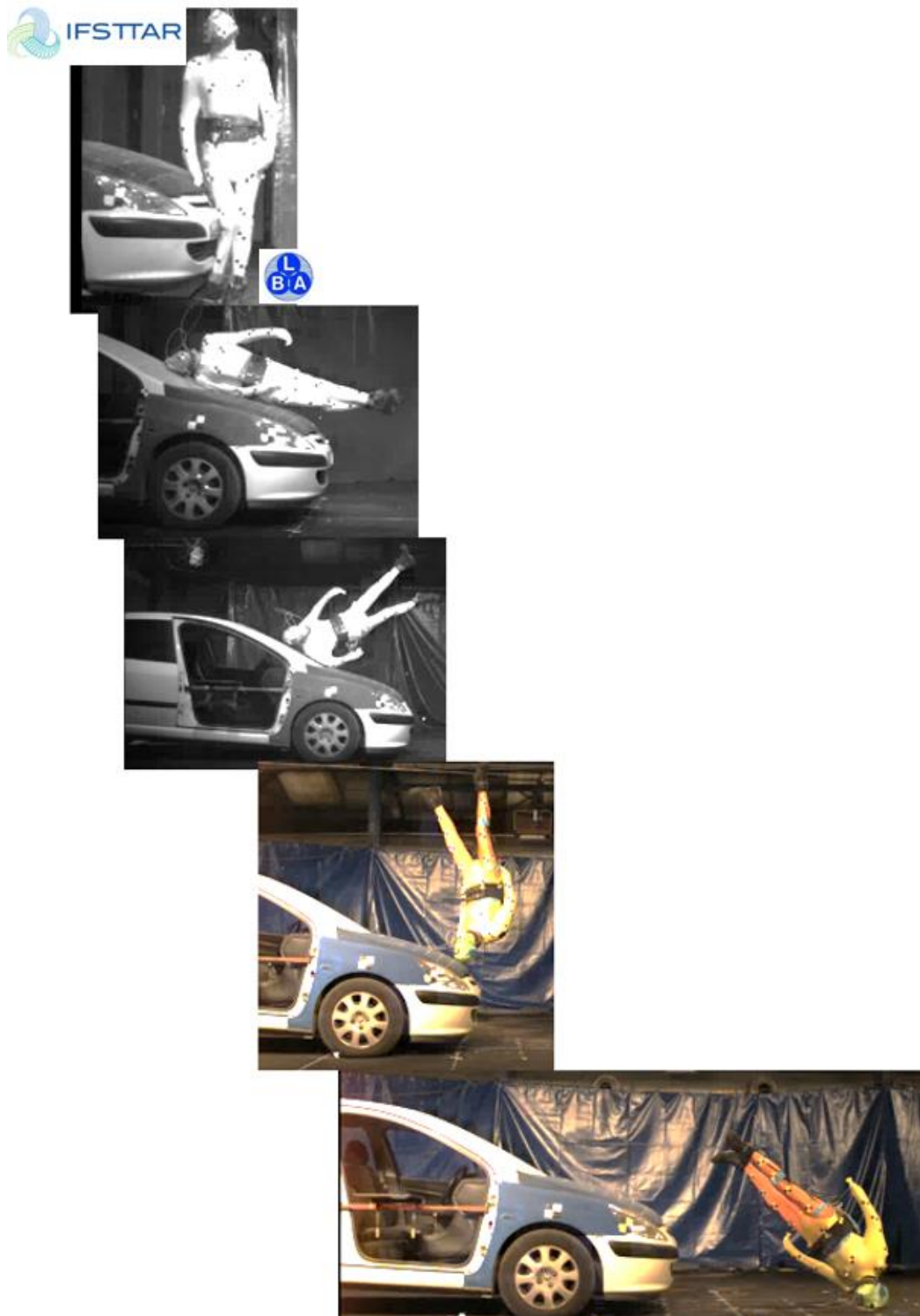


Figure 1.1 Sequences of pedestrian-vehicle impact and pedestrian-ground impact captured from one of a series of cadaver tests¹

¹ The cadaver tests were conducted as part of this research aiming at studying the pedestrian post vehicle contact kinematics and head ground impact mechanisms in detail. The tests were performed at the Laboratory of Applied Biomechanics (LBA) Faculty of Medicine North, IFSTTAR, Aix-Marseille University under the collaborate help of Prof. Pierre-Jean Arnoux, Dr. Catherine Masson, Max Py, and Quentin Ferrand.

1.2. Proposed research approaches

The principal biomechanical tools available for injury analysis are the reconstruction of real-world accidents using post-accident evidence, assessment of large-scale accident databases, staged physical tests using cadavers and crash test dummies, computational modelling using multibody and finite element models and video analysis of cases where public video cameras have recorded the accident event in sufficient detail. The objective of this research is to significantly strengthen our understanding of pedestrian ground contact mechanisms and injuries by using currently available information to identify the factors that influence pedestrian ground contact. The following points illustrate the research that was undertaken to achieve the aims of the project.

- 1) Analyzing the large-scale accident databases to have a better understanding of the global nature of pedestrian ground contact injuries and understand how do the influencing factors affect pedestrian ground contact mechanisms and injuries. A set of GIDAS database involving vehicle-pedestrian contact from 2000 to 2015 was used to find the influencing factors that have a significant effect on pedestrian ground contact. The SPSS software is applied in this step for relevant statistical analysis.
- 2) Analyzing available videos of vehicle-pedestrian contact to have a basic understanding of the kinematics of pedestrian ground contact. Moreover, real-world videos could provide a reference for designing and running pedestrian cadaver impact tests. A number of real-world videos of a vehicle-pedestrian crash are accessible for analysis.
- 3) Analyzing the available real dummy/cadaver test video footage for detailed ground impact reconstructions for pedestrian-vehicle impact cases. In this step, additional dummy/cadaver tests were commissioned and conducted with LBA, IFSTTAR to obtain the detailed kinematics of pedestrian ground contact. The kinematics of pedestrians during the whole process of the crash will be analyzed.
- 4) Reanalyzing the vehicle cadaver pedestrian impact tests to provide data for human body model assessment. Assessing the ability of existing multibody (MADYMO) human body models to reproduce pedestrian ground contact kinematics afterwards.

Assess the MB model to reconstruct the cadaver tests and to perform the parametric study. MB human and vehicle models could be used to reconstruct the dummy/cadaver test.

- 5) Assess vehicle front shape effect on reducing ground contact injuries by using Virtual Test System (VTS) which covers a broad range of real-world accident scenarios.

The study plan is demonstrated in Figure 1.2. It is necessary to have a general understanding of pedestrian ground contact by first reviewing the previous literature. Secondly, analyzing a real-world vehicle-pedestrian in-depth accident database and collision videos can provide valuable information such as the effect of the influencing factors on the risk and the severity of ground related injuries. However, the videos are not clear enough to observe pedestrian ground contact in detail. It was decided therefore to conduct a series of cadaver tests to capture the whole process of pedestrian ground contact. In the meantime, the cadaver tests can be used to validate the usage of multibody pedestrian models in a virtual test system (VTS). VTS and cadaver tests will be conducted to prove the results from accident analysis and video analysis.

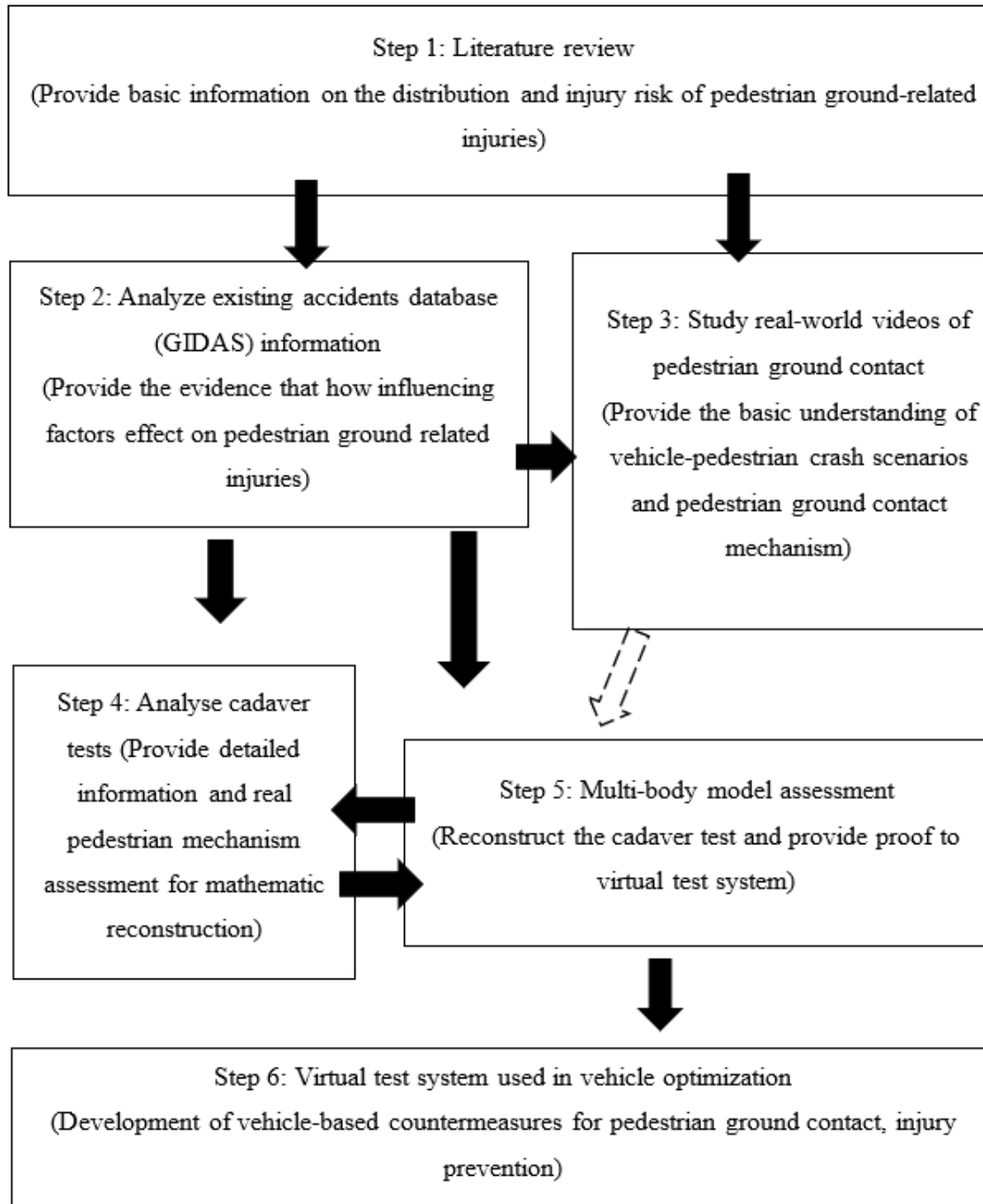


Figure 1.2 Study plan

2. Literature Review

A comprehensive literature review of the risk and mechanism of pedestrian ground related head injuries is necessary because it describes how the proposed study is related to previous work. The most widely used methods and techniques in the field of pedestrian safety are real-world accident database (from hospitals or in-depth studies) analysis, experimental impact tests (by using cadaver, pedestrian dummy, and impactor), crash reconstruction with numerical models (multi-body models or finite element models). Therefore, a review of the relevant research related to an overview of pedestrian ground contact, in-depth accident databases, real-world video analysis, cadaver tests, the MB/FE pedestrian models that previous researchers have used, the methods they applied, what is known about pedestrian ground contact, as well as the absence information are all presented in this chapter. In addition, the previous and current work performed by researchers show the gap between what is known and what is unknown, which indicates the potential guideline of our research.

2.1. Overview of pedestrian ground contact during a vehicle collision

Pedestrian safety is a very serious problem which needs to be given more attention. [WHO 2015] reports that approximately 264,000 pedestrians die from road traffic accidents each year worldwide. For the whole process of a vehicle-pedestrian collision, the pedestrian may sustain injuries both from primary contact with the vehicle and from secondary contact with the ground. Researchers have exerted a great deal of effort on analysing active and passive techniques for pedestrian-friendly vehicles. However, few focused on the injuries from ground contact, even though the ground related head injuries account for a relatively large proportion of pedestrians head injuries [Otte and Pohlemann 2001, Badea-Romero and Lenard 2013]. Head, upper and lower extremities are the most frequently injured body parts for AIS2+ ground related injuries [Guillaume *et al.* 2015].

2.2. Head-brain Injury and the criteria

2.2.1. Head-brain injury

After being impacted by the vehicle, the head (Figure 2.1 illustrates a sagittal view of head anatomy, which is from an FE head model) is one of the most frequent body regions to suffer injuries subjected to ground contact [Otte and Pohlemann 2001, Yang 2005, Shang *et al.*

2018d]. Injuries like scalp contusion, skull fracture, concussion and diffuse axonal injury are the most common head-brain injuries in vehicle-pedestrian crashes, see Table 2.1.

Table 2.1 Common head brain injuries and related mechanisms, adapted from [Yang 2005]

Injury	Mechanism
Skull fracture	Contact force
Coup contusion	Contact force
Contrecoup contusion	Deceleration and contact force
Extradural hematoma	Contact force
Subdural hematoma	Linear and rotational acceleration
Concussion	Rotational motion and relative motion between brain and skull
Diffuse axonal injury	Rotational motion

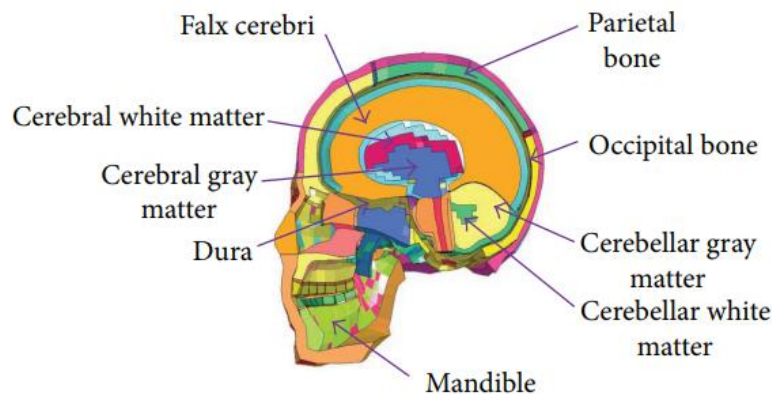


Figure 2.1 Sagittal view of the simplified brain and skull anatomy diagram, adapted from [Shang *et al.* 2018d]

2.2.2. Head brain injury criteria

HIC (Head Injury Criterion), is the most frequently used head injury criteria for assessing the severity of head injuries caused by a translational acceleration in multi-body simulations and impactor tests [Chawla *et al.* 2000, Carter *et al.* 2005, Marjoux *et al.* 2008, Tamura *et al.* 2014]. The *HIC* was originally developed by [Versace 1971] based on the WSTC (Wayne State Tolerance Curve) [Lissner *et al.* 1960]. The WSTC (Figure 2.2) shows a relationship between head linear acceleration threshold for a skull fracture and the duration of the corresponding loading on the head.

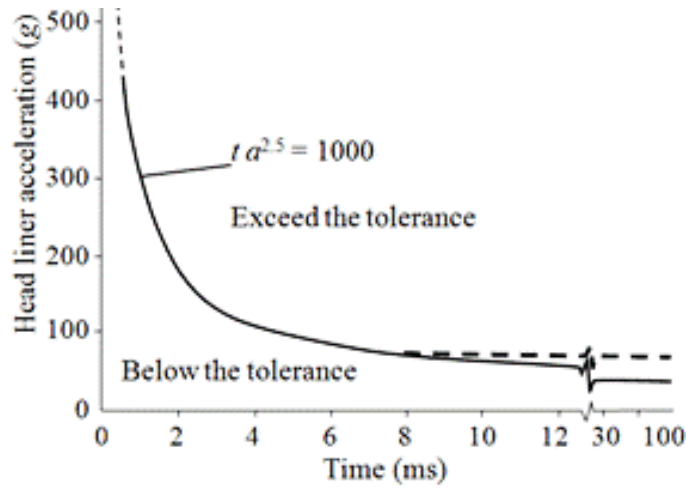


Figure 2.2 WSTC head injury tolerance curve, adapted from [Lissner *et al.* 1960]

The US NHTSA (National Highway Traffic Safety Administration) then proposed a final version of function to obtain the *HIC* score, as Equation 2.1 shows,

$$HIC = \left\{ \left[\frac{1}{t_2 - t_1} \int_{t_1}^{t_2} a_m(t) dt \right]^{2.5} (t_2 - t_1) \right\}_{max} \quad \text{Equation 2.1}$$

where t_1 is the initial time and t_2 is the final time to get the maximum *HIC* value, a_m is the resultant acceleration (units of g) of head CG with time duration $(t_2 - t_1)$ constrained to be less than 36 ms or 15 ms. The time duration which maximises the expression in Equation 2.1 is the *HIC* interval. The expression in brackets is the average acceleration during *HIC* interval. The relationship between *HIC* value and skull fracture in Figure 2.3 shows there is an approximately 50% risk of suffering skull fracture when *HIC* is 1000. Payne and Patel [Payne and Patel 2001] proposed the *HIC* score associated with different AIS (Abbreviated Injury Scale) levels, as shown in Table 2.2, which has been used for assessing head injury costs in numerical studies [Li *et al.* 2016].

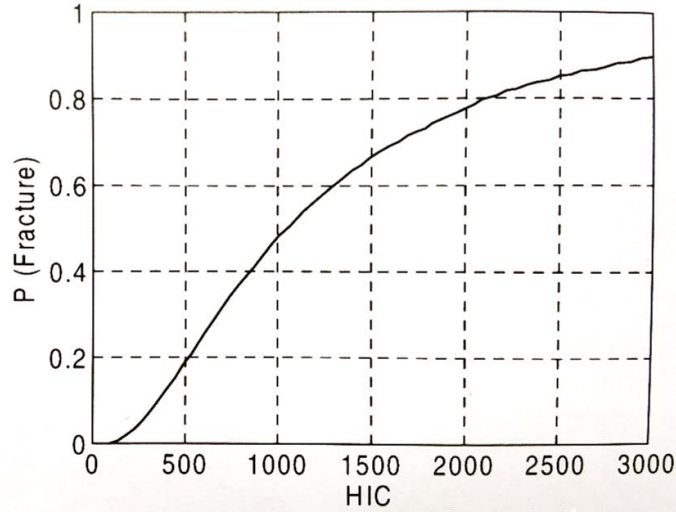


Figure 2.3 Relation of *HIC* score and the probability of skull fracture [Hertz 1993], adapted from [Tillmann 2006]

Table 2.2 Threshold for *HIC* score in different AIS levels, adapted from [Payne and Patel 2001]

Head Injury criteria	Injury criteria level	AIS level	Description of injury level
<i>HIC</i>	<520	1	No fracture
	520-900	2	Linear fracture
	900-1,255	3	Depressed fracture
	1,255-1,575	4	Open fracture
	1,575-1,860	5	Large haematoma
	>1,860	6	Non survivable

Sudden rotation of the head could result in severe brain injuries during impact [Kimpara and Iwamoto 2012]. The Brain Injury Criterion (*BrIC*), is used to assess the risk of rotationally induced brain injuries [Takhounts *et al.* 2013] in vehicle crash and sport accidents [Tierney *et al.* 2018]. The *BrIC* score is found from the peak components of the body local head angular velocities:

$$BrIC = \sqrt{\left(\frac{\omega_x}{\omega_{xC}}\right)^2 + \left(\frac{\omega_y}{\omega_{yC}}\right)^2 + \left(\frac{\omega_z}{\omega_{zC}}\right)^2}, \quad \text{Equation 2.2}$$

where ω_x , ω_y and ω_z are the peak values of head angular velocity components while ω_{xC} , ω_{yC} and ω_{zC} are the critical values based on the correlation with maximum principal strain (MPS) and cumulative strain damage measure (CSDM). *BrIC* is associated with the risk of injury severity at different levels, as shown in Figure 2.4.

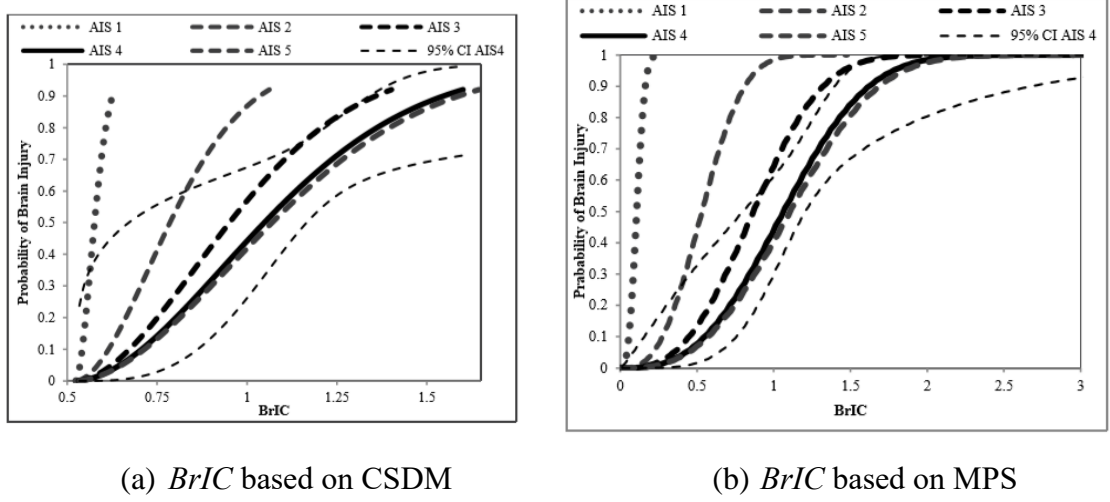


Figure 2.4 The relationship between *BrIC* (based on CSDM and MPS and formulation given by Equation 2.2) and the probability of brain injury risk at a different level of severity, adapted from [Takhounts *et al.* 2013]

Based on the *BrIC*, Gabler *et al.* [Gabler *et al.* 2018, Gabler *et al.* 2019] developed a second-order system, *UBrIC* (universal brain injury criterion), for assessing the maximum brain strain based on the angular velocities and accelerations.

$$UBrIC = \left\{ \sum_i \left[\omega_i^* + (\alpha_i^* - \omega_i^*) e^{-\frac{\alpha_i^*}{\omega_i^*} r} \right]^r \right\}^{\frac{1}{r}} \quad \text{Equation 2.3}$$

where ω_i^* and α_i^* are the maximum magnitudes of head angular velocity and angular acceleration in different directions ($i = x, y, z$) and ω_i^* and α_i^* are normalized by the critical values: $\omega_i^* = \omega_i / \omega_{icr}$ and $\alpha_i^* = \alpha_i / \alpha_{icr}$. Figure 2.5 illustrates the modelling linking rotationally induced brain injury, shear strain, to head angular speed/acceleration [Margulies and Thibault 1992].

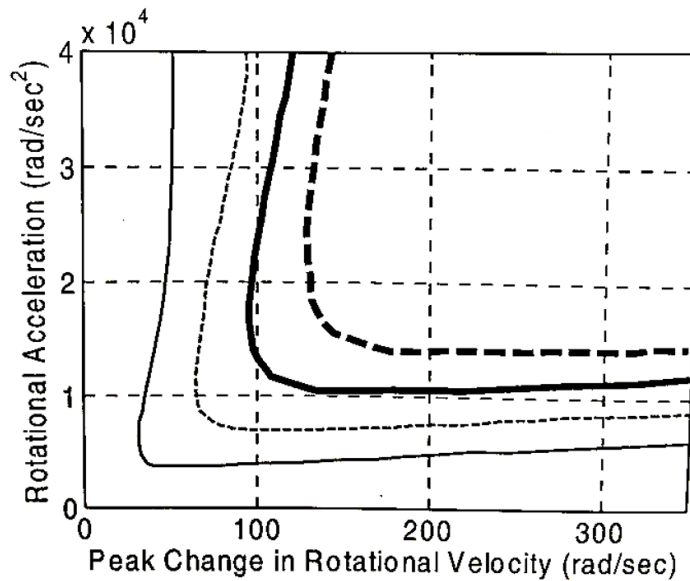


Figure 2.5 Relationship between brain shear strain and head angular speed & acceleration. Critical strains: 0.2 (heavy dashed line), 0.15 (heavy solid line), 0.1 (dashed line) and 0.05 (solid line), adapted from [Margulies and Thibault 1992]

2.3. Materials and methods used in the studies of pedestrian ground contact injury

The most widely used methods and techniques in the field of pedestrian safety are real-world accident database, e.g. from hospital [Arregui-Dalmases *et al.* 2010] or in-depth study analysis, experimental impact tests (by using cadaver, pedestrian dummy, and subsystem impactor), crash reconstruction with numerical models (multi-body models or finite element models).

2.3.1. In-depth accident databases analysis

Analyzing the accident data helps the researchers understand the cause or causes of an accident as well as the outcomes. Several in-depth accident analysis institutions such as (GIDAS), UK On-the-Spot (OTS), China In-Depth Accident Study (CIDAS), Pedestrian Crash Data Study (PCDS), etc., are established and developed for decades (while PCDS and UK OTS are not running till this moment).

The German In-Depth Accident Study (GIDAS) is a joint Federal Highway Research Institute (BASt) and the German Association for Research in Automobile Technology (FAT) project started in 1999 [GIDAS 2017]. GIDAS analyzed each real-world collision with about

3600 parameters and documented around 150 photos. The important information of vehicle, environment and road traffic participant are also collected, and the crashes are then constructed and simulated. GIDAS aims to monitor the road traffic situation by analyzing the database to detect positive and negative trends. In addition, the vehicle industry could improve their technology and safety based on the study. It has been widely used in studies of vehicle-pedestrian collisions [Otte and Pohlemann 2001, Yao *et al.* 2008, Otte 2010, Otte *et al.* 2012, Li *et al.* 2017a].

China In-Depth Accident Study (CIDAS) is a joint project by the China Automotive Technology & Research Center (CATRC) and several car companies that started in 2011 [CIDAS 2017]. For each case, more than 2000 items of information are documented. Currently, the project has collected more than 3000 road traffic crash cases in China, and the database has been widely accepted, which is reflected by its application in legislation, vehicle safety technology and C-NCAP tests. The CIDAS database is also used in accident analysis and vehicle optimization [Chen *et al.* 2014a, Chen *et al.* 2014b, Li *et al.* 2015, Ding *et al.* 2016, Zeng *et al.* 2016].

The UK On the Spot (OTS) accident research is a project that investigates road traffic accidents in-depth to build an accident database to find the causes of crashes and the causes of injuries [Badea-Romero and Lenard 2013, Barrow *et al.* 2014]. From 2000 to 2010, about 500 crashes per year were documented and analyzed. Factors relating to the vehicle, human and environment are analysed in detail during pre-impact, impact, and post-impact for each case [Hill *et al.* 2001]. OTS was funded by the Department for Transport and the Highways Agency and its aims are providing essential resources which could assist safety professionals in their efforts to make all road users safe in the UK.

Pedestrian Crash Data Study (PCDS) was a project implemented by the National Highway Traffic Safety Administration (NHTSA) from 1994-1998. More than 500 pedestrian crash cases were documented with detailed information on the pedestrian, driver and vehicle. Each case has 144 different variables. PCDS aimed to provide detailed pedestrian crash reconstruction data and it is frequently used in analysing the circumstances of the crashes [Isenberg and Chidester 1998, Jarrett and Saul 1998, Stammen *et al.* 2002, Mizuno and Ishikawa 2005, Zhang *et al.* 2008]. [Zhang *et al.* 2008]'s investigation on PCDS vehicle to

pedestrian impact database found that 17.3% of the coded injuries were from the ground.

2.3.2. Crash reconstruction using MB/FE pedestrian models

Numerical simulations with multi-body (MB) pedestrian models and finite element (FE) pedestrian models are widely used to reconstruct the crash and parametric studies in the field of pedestrian safety. MADYMO ellipsoid 50th percentile (mid-size) male pedestrian model is one of the most used MB models [Simms and Wood 2006, Serre *et al.* 2007, Hamacher *et al.* 2012, Crocetta *et al.* 2015, Yin *et al.* 2017, Shang *et al.* 2018c]. The model is 174cm height and 75.7kg weight. It consists of 52 rigid bodies and the outer surface is described by 64 ellipsoids and 2 planes. It has been validated with blunt impact tests [Viano 1989, Kajzer *et al.* 1990, Kajzer *et al.* 1993, Bouquet *et al.* 1994] and PMHS subjects [Ishikawa *et al.* 1993a, Yang *et al.* 2000]. Injury criteria values for each body region (head, chest, abdomen, spine, extremities *et. al*) can be obtained to assess the injury severity [TNO 2017]. Computational efficacy is a typical advantage of simulating MB model. Besides the 50th percentile pedestrian model, there is also a 3-year-old child, 6-year-old child, 5th percentile female model, etc., see Figure 2.6.

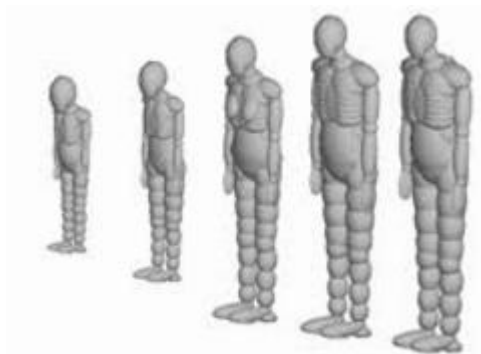


Figure 2.6 Ellipsoid pedestrian models, from left to right; 3-year-old child, 6-year-old child, small female, mid-size male and large male, adapted from [TNO 2017]

[Yang and Lovsund 1997] developed another 3D MB pedestrian model with an emphasis on the head and lower extremities. This model consists of fifteen body segments and connected by fourteen joints, as shown in Figure 2.7. The leg segments are breakable which can simulate the response of the knee and leg fracture from vehicle contact. The model has been used for decades for parametric studies and crashes reconstructions [Liu and Yang 2003, Yao *et al.* 2008, Shi *et al.* 2018].

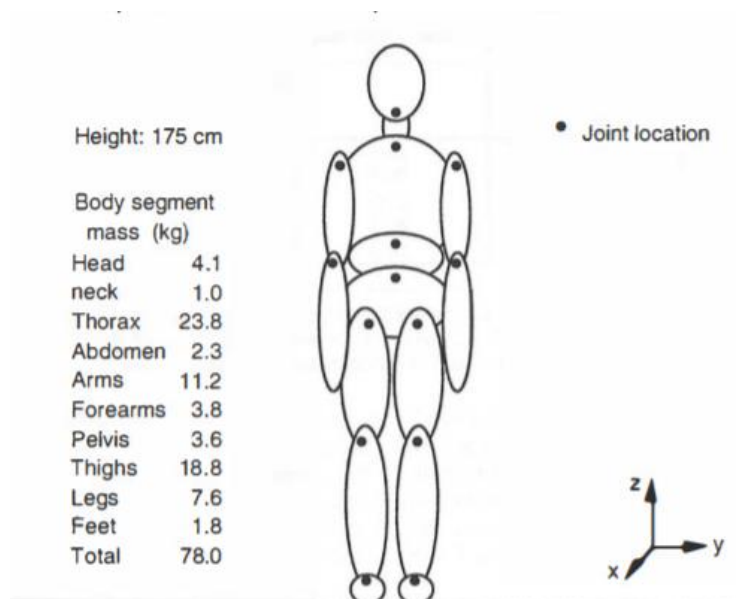


Figure 2.7 Geometry and the mass distribution of the MB 50th percentile adult pedestrian model developed by [Yang and Lovsund 1997], adapted from [Yang and Lovsund 1997]

The finite element model of the total human model for safety (THUMS) has been used to reconstruct vehicle-pedestrian collisions [Yasuki 2006, Yasuki and Yamamae 2010, Tamura *et al.* 2014]. THUMS is developed and validated [Kimpara *et al.* 2006, Shigeta *et al.* 2009] by Toyota Motor Corporation and Toyota Central R&D Labs. Sitting models and standing models (see Figure 2.8) can be simplified to represent the occupants and pedestrians in detail not only the outer surface but also muscles, bones, ligaments, tendons, and internal organs [Iwamoto *et al.* 2002]. It can be used to simulate vehicle crashes and then to assess the injuries, identify safety problems and find the solutions [Watanabe *et al.* 2011].

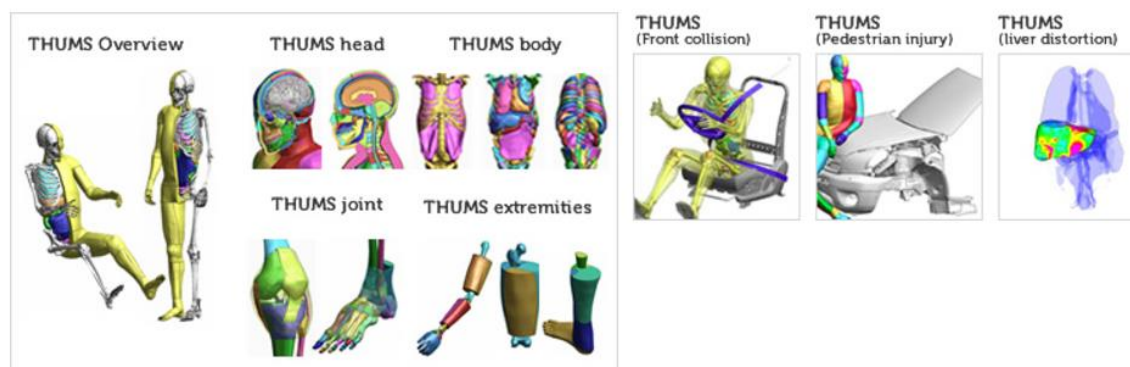
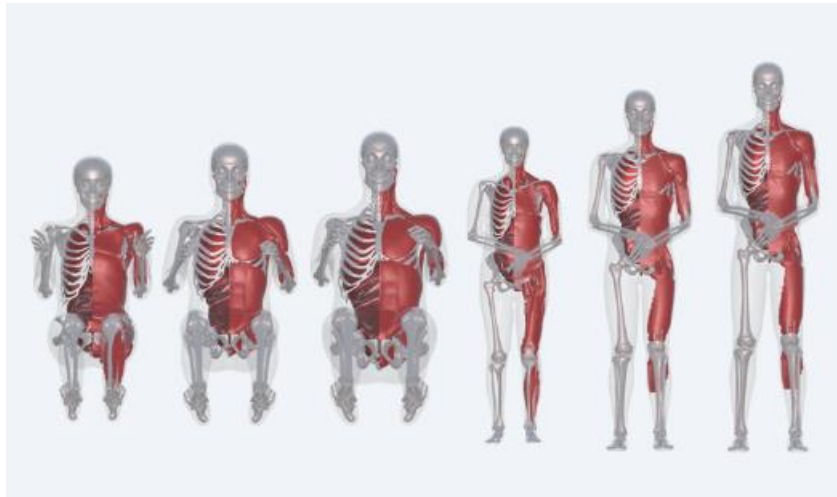


Figure 2.8 THUMS models and applications, adapted from [TOYOTA]

Global Human Body Models Consortium (GHBMC) is another FE pedestrian model developed by [Elemance] for crash-induced injury metrics and criteria. As shown in Figure 2.9 (a) and (b), different sizes of detailed human models and simplified human models are

developed [Gayzik *et al.* 2011, Meng *et al.* 2017, Untaroiu *et al.* 2018], respectively. The simplified model has fewer elements which makes the run time up to 50 times faster versus the detailed models. GHBMC pedestrian models have been increasingly used for simulating vehicle-pedestrian crashes [Decker *et al.* 2019]. However, all current MB and FE pedestrian models have only been validated for vehicle contact, and the validation for pedestrian's movement in the air and the ground contact are still missing [Decker *et al.* 2019].



(a) Detailed GHBMC Models



(b) Simplified GHBMC models

Figure 2.9 GHBMC human models, adapted from [Elemance]

Xu *et al.* [Xu *et al.* 2016a, Shang *et al.* 2018d] combined the MB model and FE model to simulate the vehicle electric self-balancing scooter (ESS) crashes. They used an FE car model and an MB pedestrian model plus an MB ESS model to simulate the crash at MADYMO platform and then used the FE head model to repeat the head-ground contact at LS-DYNA platform. In this way, it combined the accuracy of the FE head model as well as the efficiency of the MB model. Other researchers [Gupta and Yang 2013, Shi *et al.* 2018]

combined the FE vehicle model and MB pedestrian model for the collision reconstructions, as shown in Figure 2.10, which considered the accuracy of the vehicle front shape.

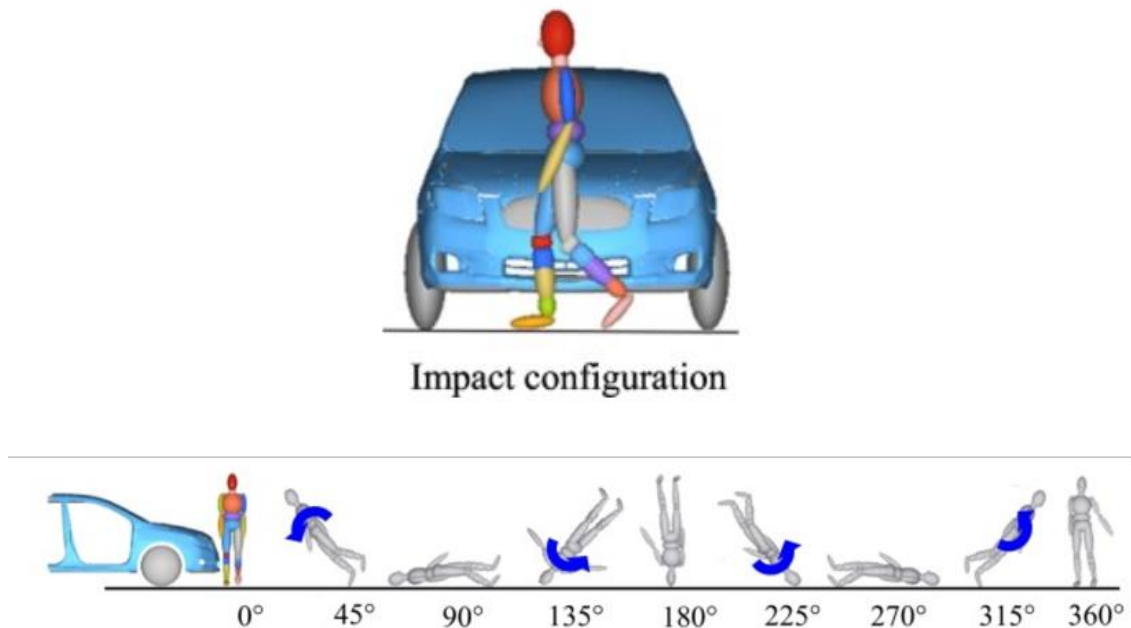


Figure 2.10 Numerical vehicle-pedestrian impact scenario combined FE vehicle shape and MB pedestrian model, adapted from [Shi *et al.* 2018]. The numbers of degree indicating the post-vehicle impact rotation angles of pedestrian before landing on the ground.

Reconstructing vehicle-pedestrian crashes by simulating with multi-body (MB) model models is widely used in the field of safety to observe pedestrian kinematics and to predict head injuries during the process of the crash due to its computational efficiency.

Simms and Wood [Simms and Wood 2006] analyzed vehicle-pedestrian contact and vehicle ground contact and compared head/pelvis/chest injury severities by simulating multi-body human/vehicle models using MADYMO. Several crash scenarios with different pre-impact pedestrian postures were selected and simulated. Results show that compared to the head-vehicle contact, pedestrian ground contact force was more variable and unpredictable due to different pedestrian initial stance. Researchers [Simms *et al.* 2011, Crocetta *et al.* 2015, Yin *et al.* 2017] also checked vehicle front shape's effect on mechanisms of pedestrian ground contact injuries by using MADYMO human/vehicle models. Different vehicle shapes and pedestrian sizes were selected to simulate the vehicle-pedestrian crash. Simms *et al.* [Simms *et al.* 2011] found that there was a correlation between bonnet leading-edge height and *HIC* score caused by ground contact and the body angle at the instant of ground contact was also correlated with the *HIC* score. Crocetta *et al.* [Crocetta *et al.* 2015] summarized six typical

pedestrian ground impact mechanisms (see Figure 2.11) based on the pedestrian ground contact angle by simulating a series of impact conditions by using different vehicle types, different pedestrian sizes as well as different vehicle speeds. Vehicle type, pedestrian height and vehicle speed were found as factors influencing ground contact mechanism and head ground contact speed. Head-ground contact speeds for different mechanisms were varied significantly. In addition, the distribution of impact mechanisms was strongly associated with vehicle type (see Figure 2.11). Compared to low fronted vehicles like the sedan and compact car, big SUV and van were more aggressive to the pedestrians.

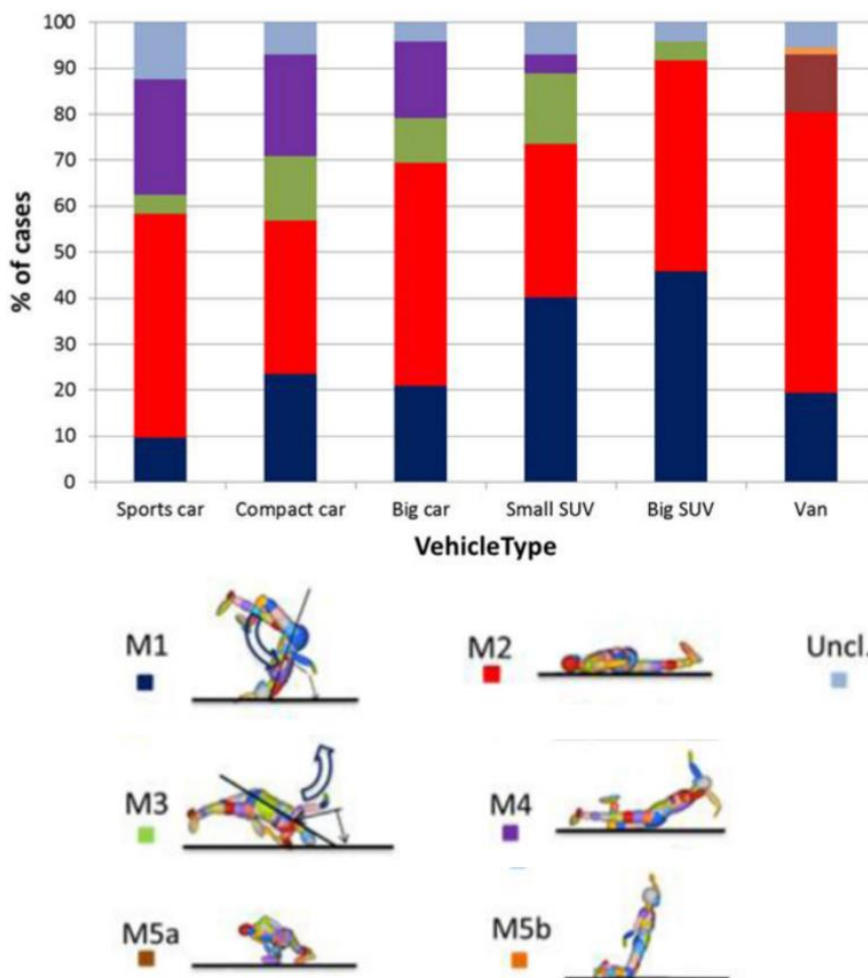


Figure 2.11 Occurrences of the six impact mechanisms for each vehicle type for the adult pedestrian impacts at all vehicle impact speeds (20, 30 and 40 km/h), adapted from [Crocetta *et al.* 2015]

Kendall *et al.* [Kendall *et al.* 2006] simulated 40 vehicle-pedestrian collisions to determine if the risk of pedestrian head injury was greater from impact with the vehicle or impact with the ground. The results show that with the vehicle speed increase, risk of head injury from both vehicle contact and ground contact tends to rise, but injury risk due to ground contact

is less predictable. They conclude that at lower speeds cases, the vehicle tends to pose a greater risk of injury than does the ground, while at higher vehicle speeds cases, the probability of injury from both the vehicle and ground is typically very large (see Figure 2.12). However, the results are doubtful due to the very limited number of simulations.

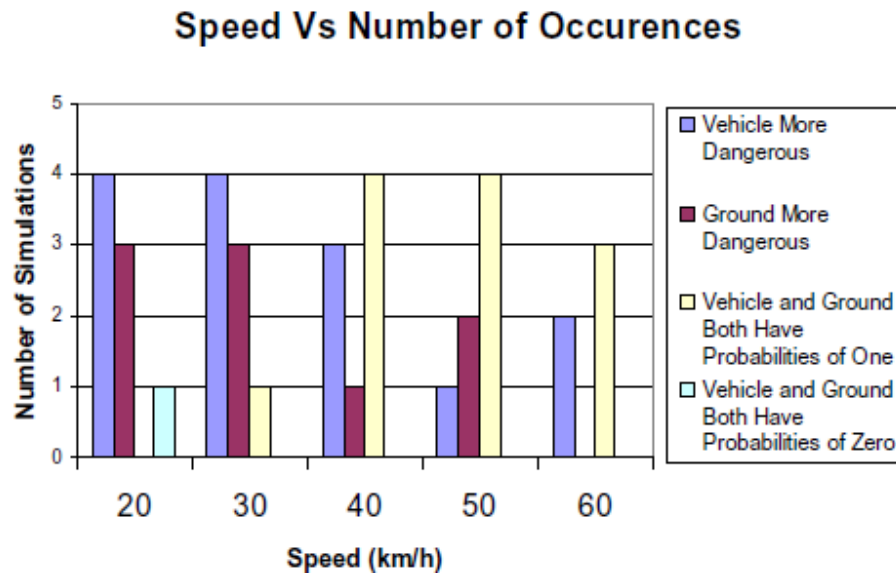


Figure 2.12 Effect of speed on most severe injury source, adapted from [Kendall *et al.* 2006]

In 2012, Hamacher *et al.* [Hamacher *et al.* 2012] used different vehicle classes (Compact Car, Sedan, Van, SUV, OneBox, Sports Car) models and pedestrian models on MADYMO platform to investigate the influence of vehicle type on pedestrians' kinematics. The results indicated that high bonnet leading edge (BLE, reflected on vehicle type) concerning the pedestrian posture as well as large bonnet and windshield angles increase the risk of a head impact on the ground (as shown in Figure 2.13). But this needs to be validated against real-world collisions.

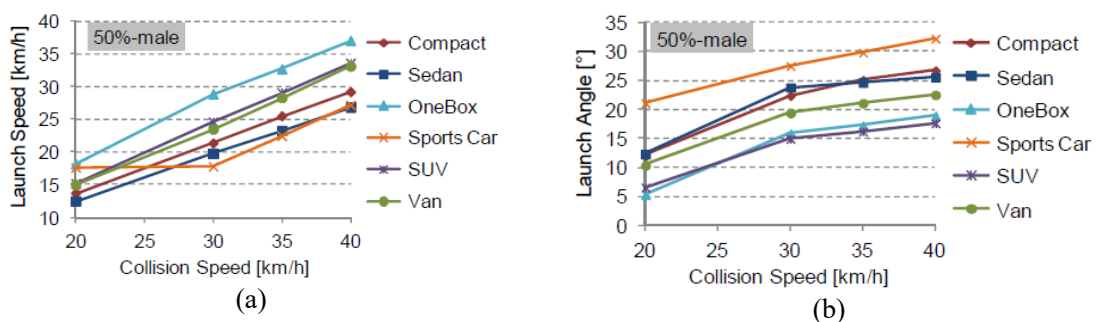


Figure 2.13 Average launch speed of 50th percentile male (a); Average launch angle of 50th percentile male (b), adapted from [Hamacher *et al.* 2012]

Yin *et al.* [Yin *et al.* 2017] conducted a set of parametric simulations in MADYMO platform to understand how vehicle front-end dimensional parameters affect the severity of head injuries resulted from secondary impact with the ground. Bonnet leading edge height, bonnet angle, bonnet length and windshield angle, which can briefly evaluate the profile of a vehicle (as shown in Figure 2.14), are selected as the main parameters as the variables. By comparing the posture and head injury criterion (HIC) at the instant of head ground contact for the impact scenario with different vehicle front end parameters, bonnet leading edge (BLE) height is found to be the top governing factor among the four, then followed bonnet angle, bonnet length and windshield angle (see Figure 2.15). The main conclusions are consistent with the results of Hamacher *et al.* [Hamacher *et al.* 2012]'s study.

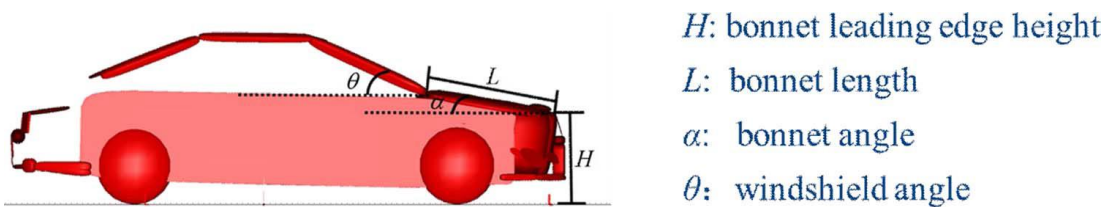


Figure 2.14 Dimensional parameters of vehicle front-end structure. Bonnet leading edge height (H) bonnet length (L), bonnet angle (α), and windshield angle (θ) are indicated, adapted from [Yin *et al.* 2017]

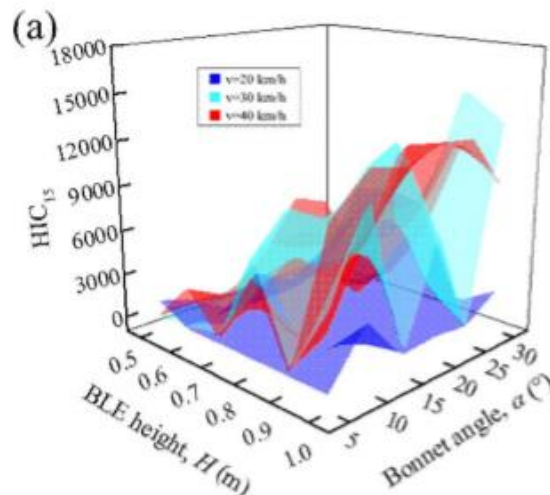


Figure 2.15 Coupling effect of H and α on HIC_{15} at all impact speeds (20, 30, and 40 km/h), adapted from [Yin *et al.* 2017]

A recent study proposed a method to reduce the risk of pedestrian injury from secondary ground contact by adding external adhesive coated pedestrian airbags on the vehicle bonnet [Gupta *et al.* 2017]. The impact scenario of a 50th percentile male with a sedan front surface

as well as an adhesively-coated airbag was modelled. The human body was comprised of rigid bodies with freely rotating joints. Adhesive properties were calibrated based on ball drop tests. Experiments and simulation results indicated that the adhesively-coated airbag may prevent flight, or reduce pedestrian rebound speed, resulting in reducing the injuries caused by ground contact (as shown in Figure 2.16), but it has not been turned into a real product yet. Besides, the influence of adhesive materials on pedestrians' skin is not taken into consideration.

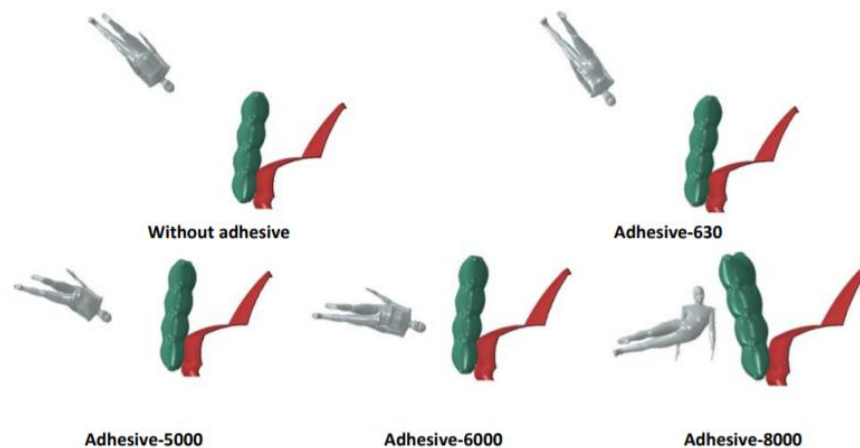


Figure 2.16 Pedestrian orientation at $t=450\text{ms}$ after impact, for car impact velocity of 40 km/h and 0.8G braking, adapted from [Gupta *et al.* 2017]

Finite element (FE) human and vehicle models are another way used to reconstruct the vehicle-pedestrian impact crash due to the realistic configurations. Tamura *et al.* [Tamura *et al.* 2014] performed a series of parametric studies on vehicle-pedestrian crashes by using full scale FE vehicle models and pedestrian FE model (see Figure 2.17). with detailed head model. The influences of different vehicle front shapes on post-impact kinematics and the severity of Traumatic Brain Injury (TBI) are investigated and the TBI assessment parameters caused by primary contact and secondary contact are compared (see Figure 2.18). As the results are shown in Figure 2.18, the predicted injury indices from ground contact are generally higher than in primary impact except the *HIC* obtained in the category of SUV with the impact speed of 40km/h , see Figure 2.18 (a), the *HIC* score from vehicle contact dramatically increased from 25km/h to 40km/h , making the injury severity higher than from ground contact. It is revealed that pedestrian kinematics and subsequent kinetics are unpredictable and are significantly affected by the vehicle front structure and vehicle impact speed. Besides, even when pedestrians were impacted by a vehicle with a low speed (25km/h), pedestrian ground contact could result in severe head injuries. The study indicated the importance of vehicle industry to focus on pedestrian ground injury.

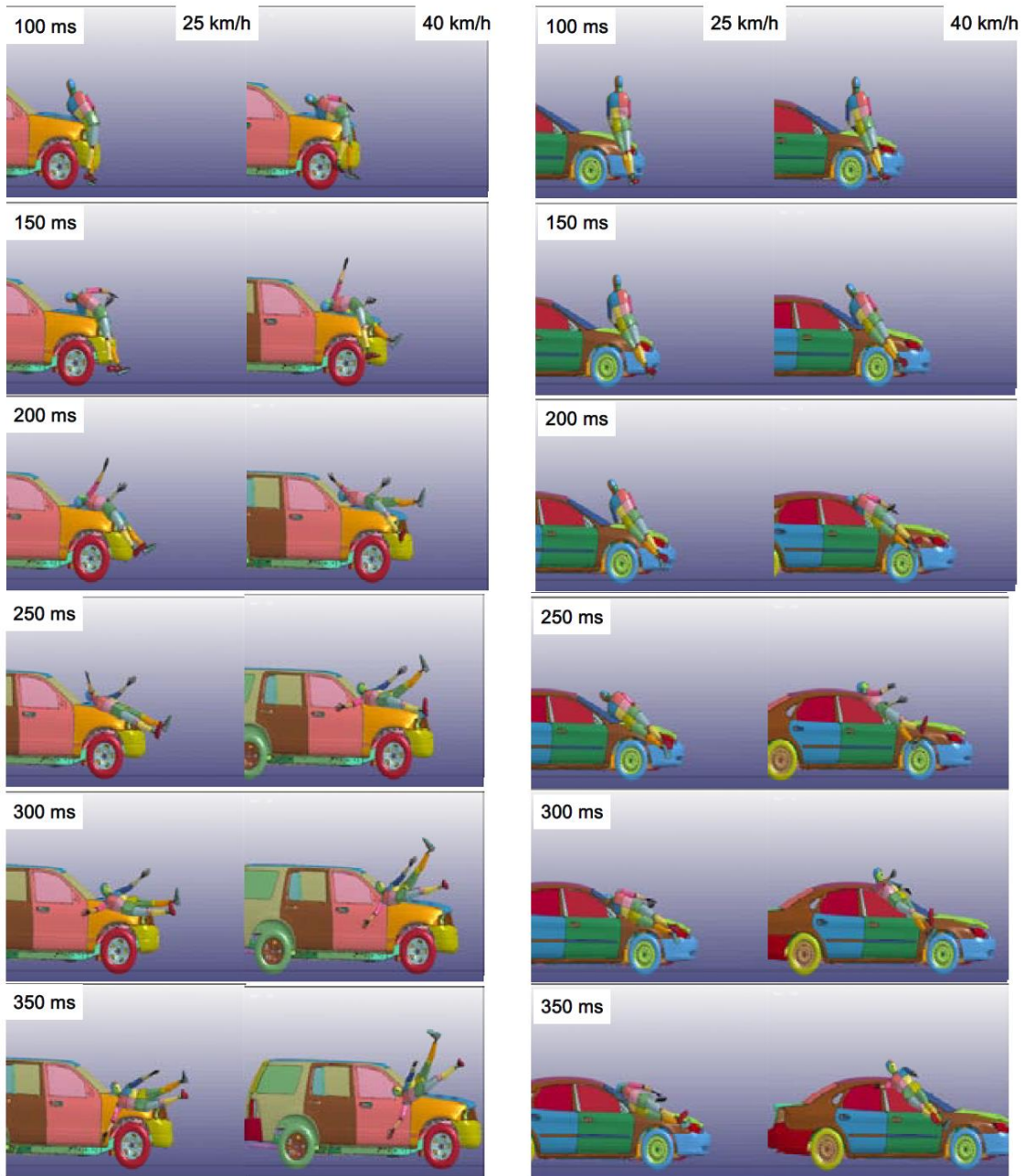


Figure 2.17 A sequence of lateral views of vehicle-to-pedestrian interactions at initial impact. Left: SUV vs. pedestrian. Right: sedan vs. pedestrian, adapted from [Tamura *et al.* 2014]

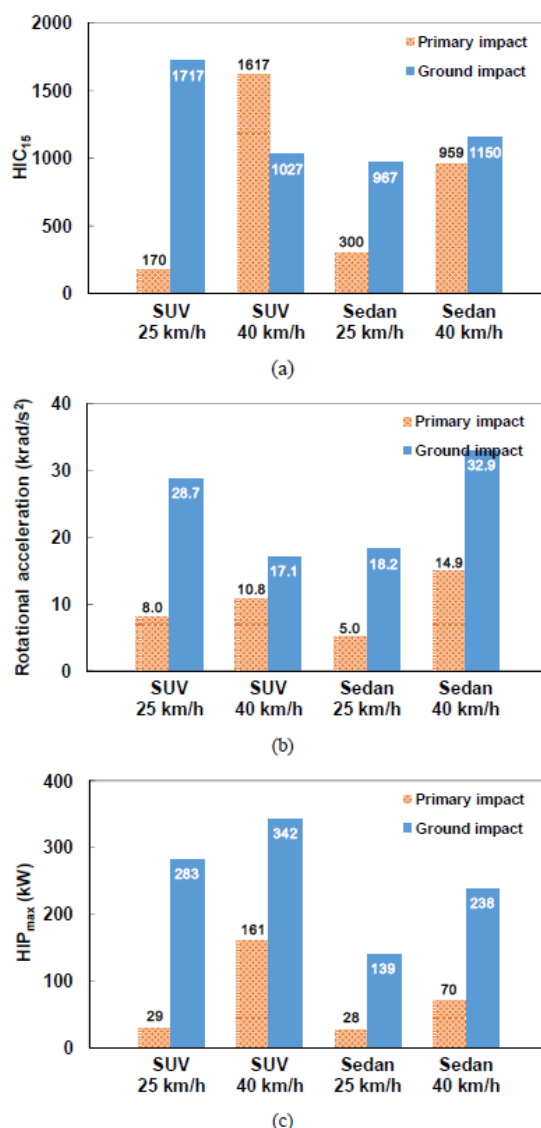


Figure 2.18 Comparison of selected TBI assessment parameters. (a) HIC_{15} due to primary and secondary head strikes; (b) max rotation acceleration due to primary and secondary head strikes; (c) HIP_{max} due to primary and secondary head strikes, adapted from [Tamura *et al.* 2014]

2.3.3. Real-world crash video analysis

Nowadays, the process of pedestrians' kinematics during real-world vehicle crash are easy to be captured because of the development of technology such like car driving recorder, surveillance video etc. Barry and Simms [Barry and Simms 2016] used real-world collision videos (from Youtube) to assess pedestrian ground impact categories. Distance tracker Matlab code, stopping distance formula were applied to estimate vehicle speed. Then, head-ground impact speed was calculated. It was found for each impact categories, the average head-ground impact speed is 1m/s lower compared to the speeds from MB model simulations [Crocetta *et al.* 2015]. But the global trends are similar, as shown in Figure 2.19.

Mechanism	1	2	3	4	5a/b	Other
N	11	5	2	4	0	7

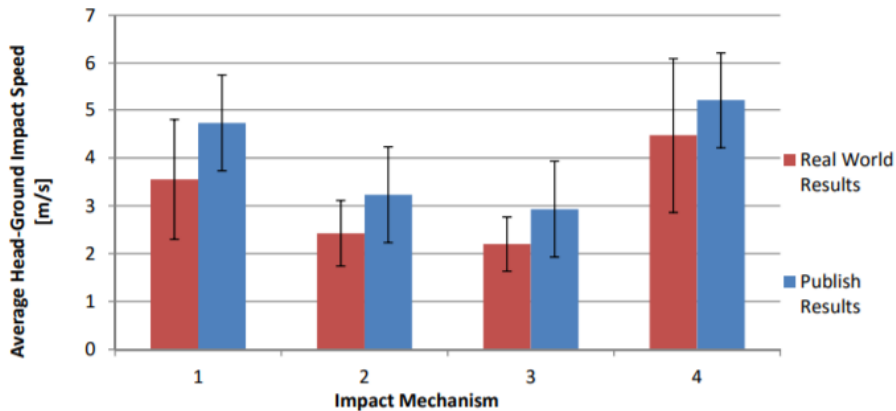


Figure 2.19 Comparison of head-ground vertical impact speed from real-world videos analysed and from previously published predictions [Crocetta *et al.* 2015], adapted from [Barry and Simms 2016]

Han *et al.* [Han *et al.* 2017] analyzed 200 pedestrian cases which downloaded and selected from the Internet (Youtube and Youku) with video information (accident scenarios, pedestrian avoidance motion, pedestrian kinematics and trajectory during ground contact) to make a clear understanding of pedestrian behavior. Besides vehicle-pedestrian contacts, vehicle-ground contacts are also examined. Vehicle impact speeds were estimated based on the relation of time and calculated vehicle traveled distance. By analyzing the videos, the vehicle-pedestrian impact scenarios were presented as Figure 2.20. Avoidance motions were observed in 66% of all 200 vehicle-pedestrian crashes while 14% could not be categorized due to the incompleteness of the videos. The landing postures were classified basing on the first impact body region to the ground. Lower extremity and head are found to be the most frequent first landing regions (distributions are shown in Figure 2.21).

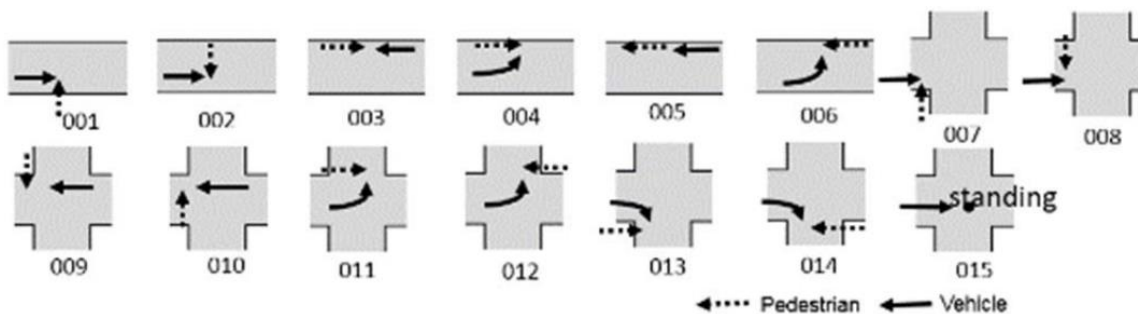


Figure 2.20 Definition of vehicle-pedestrian crash scenarios, adapted from [Han *et al.* 2017]

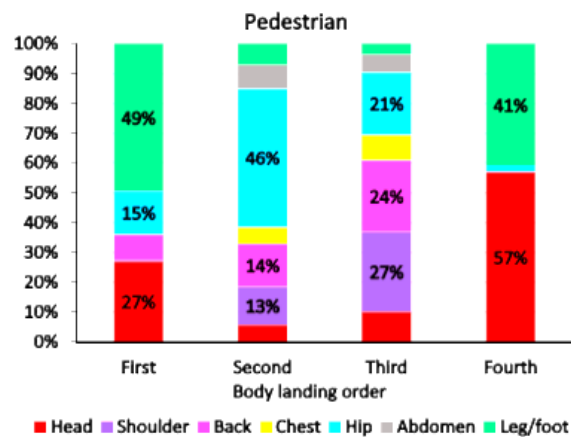


Figure 2.21 Distribution of pedestrian body landing region, adapted from [Han *et al.* 2017]

2.3.4. Cadaver/dummy/impactor test

Only limited information on pedestrian ground impact could be obtained from previous cadaver tests [Taneda *et al.* 1973, Hamacher *et al.* 2012]. A set of dummy tests (as shown in Figure 2.22) which conducted in 1970s [Taneda *et al.* 1973] has indicated that the trajectory of secondary collision differs according to vehicle speeds, vehicle front shape and other factors. Four different patterns (see Figure 2.23) were classified based on the pedestrian-ground contact posture. In terms of the body parts hitting the ground, the head is always the first region to have collision with the ground at 20km/h. While at 20-30km/h, the lower extremities strike the ground first. To improve pedestrian safety in traffic accidents, [Cavallero *et al.* 1983] analysed 50 cadaver tests to study the vehicle front shape influence on pedestrian kinematics and injuries in 1980's. The results showed that the head-ground contact locations were random. Besides this, calculating the average head-ground contact speed showed there is no certain vehicle shape seems helpful to reduce ground contact injuries. By doing full scale cadaver tests, [Subit *et al.* 2008] described the pedestrian kinematics and injuries when they hit by vehicles. They also found vehicle shape is a primary factor which determines the whole-body kinematics of pedestrians [Kerrigan *et al.* 2007].

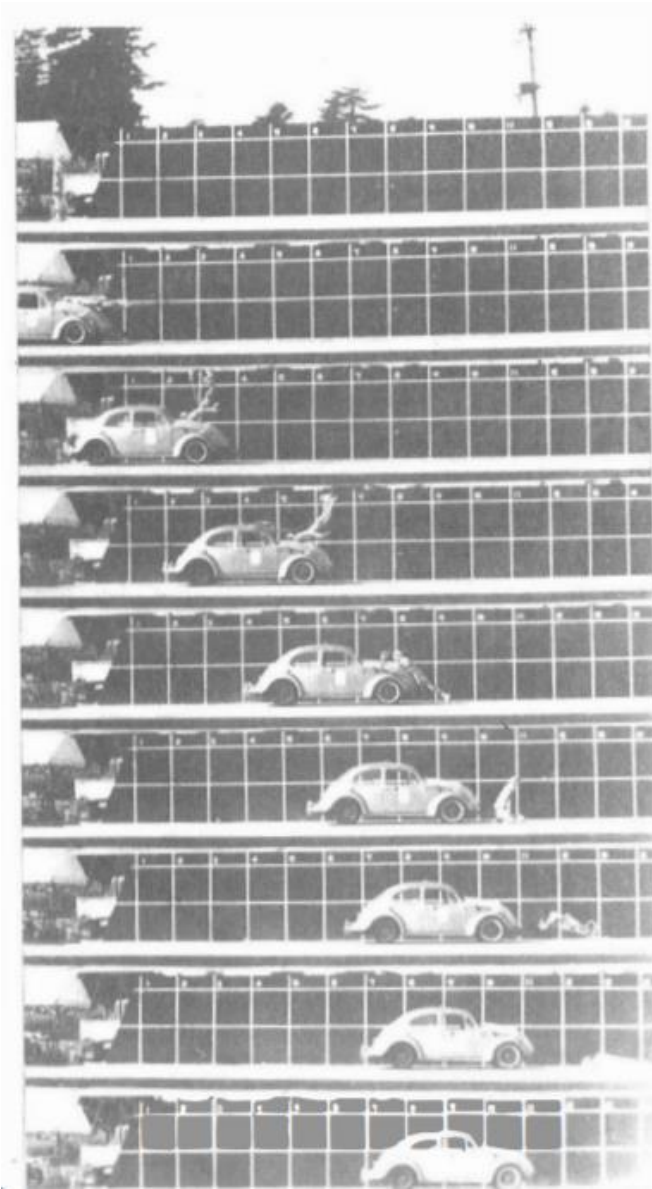


Figure 2.22 Sequential photo of the dummy behaviour test, vehicle impact vel. 41.0km/h, adapted from [Taneda et al. 1973]

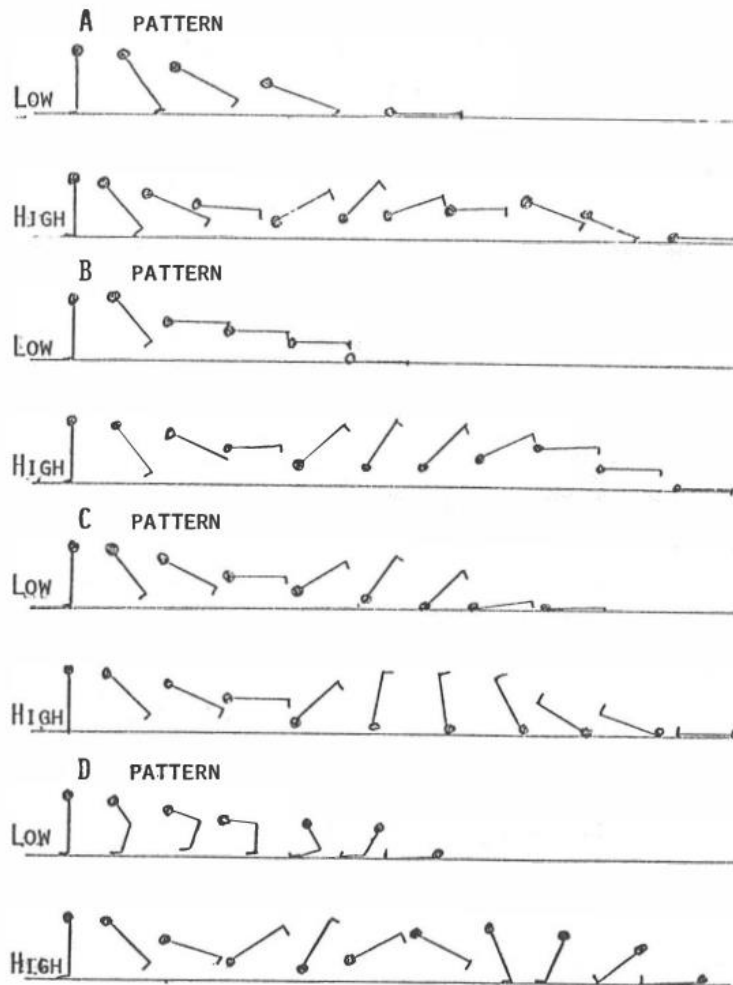
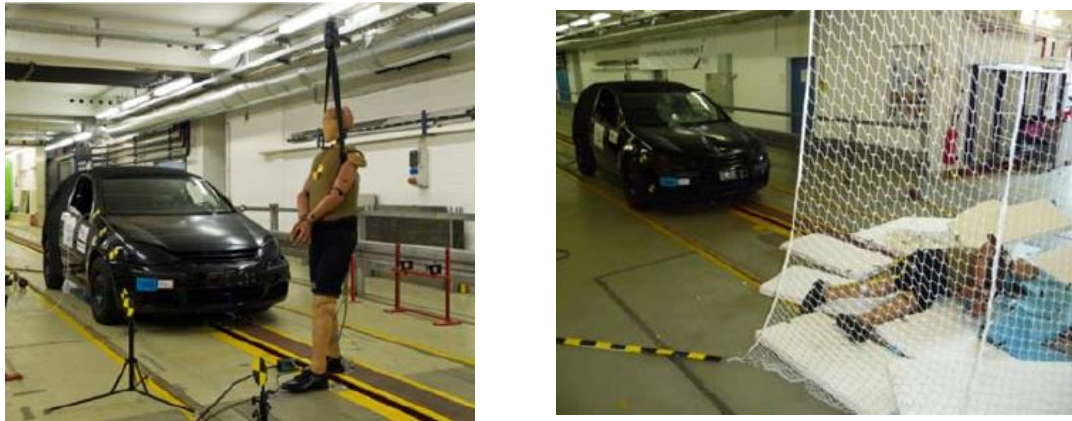


Figure 2.23 Sequential sketch of four different patterns, adapted from [Taneda *et al.* 1973]

A series of dummy tests [Hamacher *et al.* 2011] were conducted to assess of the active and passive technical measures for pedestrian protection, even though the tests mainly focused on pedestrian vehicle contact, post-impact pedestrian kinematics can also be drawn [Hamacher *et al.* 2012]. Polar-II pedestrian dummy are used in these tests (see Figure 2.24). Tests show that vehicle speed affect pedestrian post-impact kinematics, i.e. higher vehicle speed results more rotation angles (The angles pedestrian rotates in the air before hitting the ground). At 40km/h, the dummy rotated almost 270 degrees before impacting with the ground.



(a) Pre-impact

(b) Post-impact

Figure 2.24 Experimental test setup (a) and post ground impact conditions (b), adapted from [Hamacher *et al.* 2012]

Subsystem such like headform impactor and legform impactors are always used for pedestrian safety tests by impacting with vehicles with specified speeds and angles [Lawrence and Hardy 1998, Maki *et al.* 2003, Ponte *et al.* 2004, Martinez *et al.* 2007, Abvabi *et al.* 2010, Euro-NCAP 2010, Strandroth *et al.* 2011]. Take Euro NCAP pedestrian test for example, lower legform, upper legform, child headform and adult headform are applied to test the torque, contact force of the leg bumper/bonnet leading edge impacts and *HIC* scores for head windshield/ bonnet impact, as illustrated in Figure 2.25. Detailed procedures to obtain the force-deflection curves are attached in Appendix A.

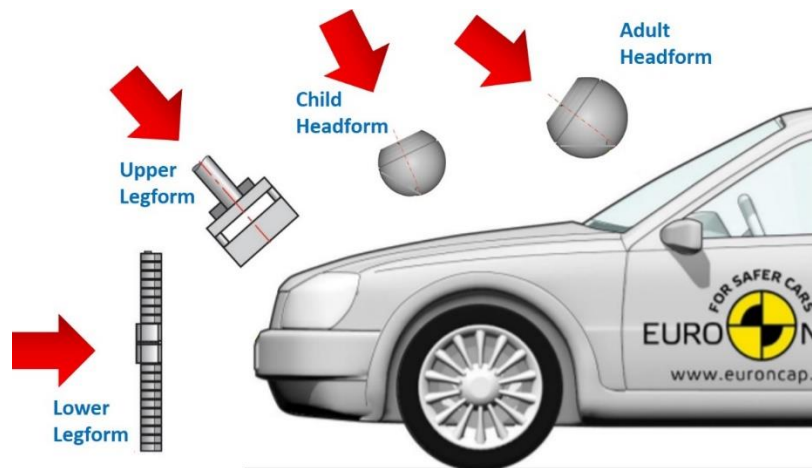


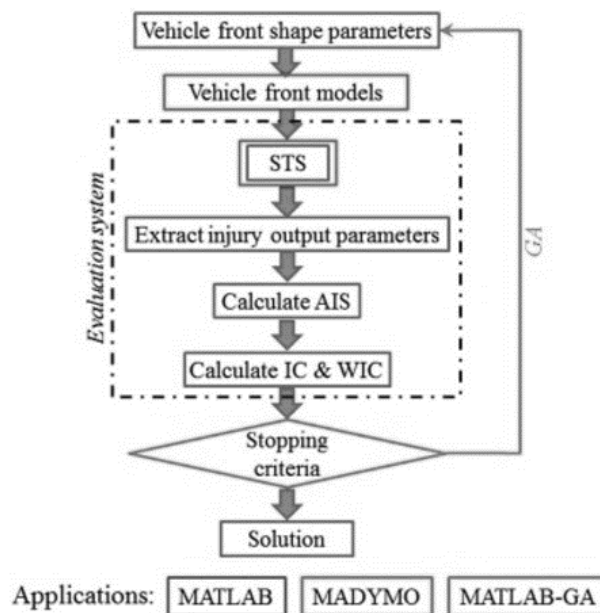
Figure 2.25 Illustration of Euro NCAP pedestrian test

2.4. Relative methods will be applied

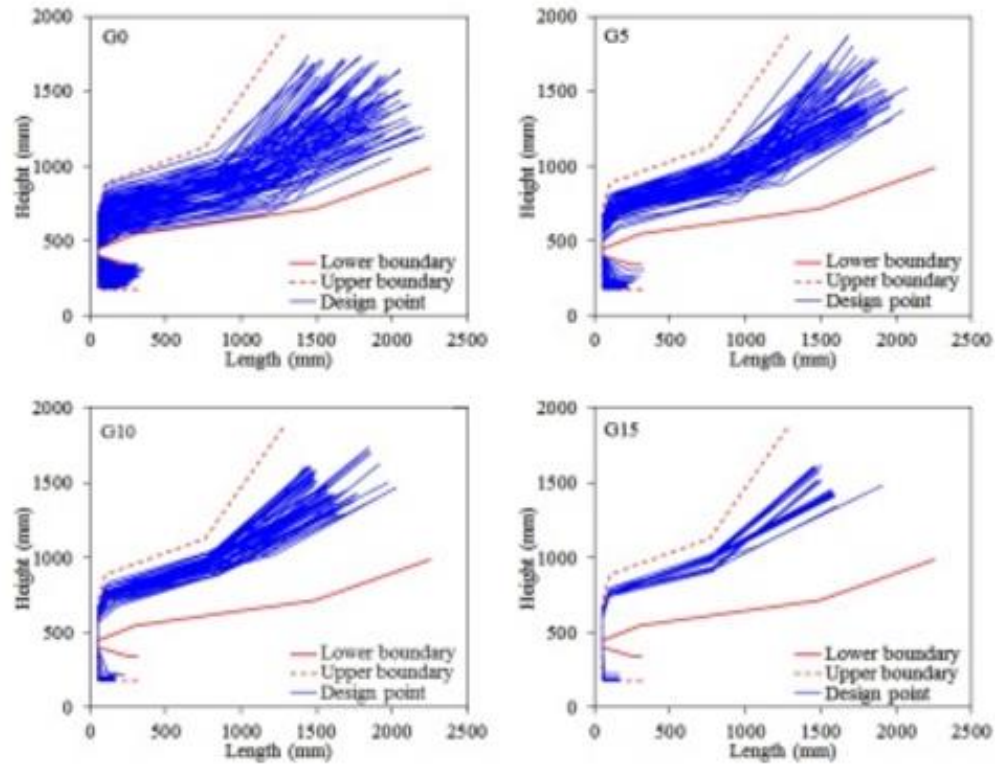
Other relative methods such like Virtual Test System (VTS) and Model Based Image Matching (MBIM), which has not been particularly used in pedestrian ground contact but will be applied in this study, are also reviewed.

2.4.1. Virtual Test System (VTS)

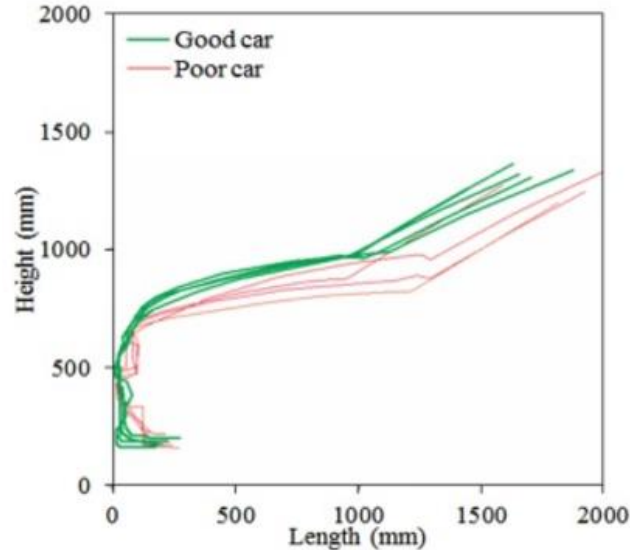
Li *et al.* [Li 2016, Li *et al.* 2016, 2017b] defined a Virtual Test System (VTS) to assess the vehicle front end design effect on pedestrian injuries with a weighted distribution of crash configuration on Madymo platform. Then an optimization method on vehicle front shape was proposed to minimize the weighted injury cost based on a genetic algorithm (GA), as the flow chart shown in Figure 2.26 (a). After the optimization of generations [Figure 2.26 (b)], good shape and poor shape cars [Figure 2.26 (c)] were obtained, which means that vehicle shape resulted in least weighted injury cost and largest weighted injury cost.



(a) The optimization framework of VTS, adapted from [Li *et al.* 2017b]



(b) Optimization design points of generation 0 (G0), 5 (G5), 10 (G10), and 15 (G15) based on genetic algorithm, adapted from [Li *et al.* 2017b]



(c) Profiles of the vehicles meeting the trends of predicted 'good' (low injury cost) and 'poor' (high injury cost) shapes, adapted from [Li *et al.* 2017b]

Figure 2.26 Illustration of VTS for vehicle shape optimization based on the weighted injury cost, adapted from [Li *et al.* 2017b]

2.4.2. Model Based Image Matching (MBIM)

Model Based Image Matching (MBIM) was introduced by [Krosshaug and Bahr 2005] for reconstructing human motion from video sequences basing on the traditional motion analysis. The basic process of MBIM is to build a virtual environment on Poser platform to match the customized environment in the background videos. Then fit the Poser skeleton human model to the laboratory model frame by frame by manually adjusting the model's segments and joints (as illustrated in Figure 2.27). The whole motion of the laboratory would be reconstructed and the time histories of translation and joint angle could be extracted with a customized Matlab script. Tierney *et al.* [Tierney *et al.* 2015, Tierney *et al.* 2016, Tierney *et al.* 2018] used MBIM to provide a technique for the assessment of 3-D linear and angular motion in the event of head impact.

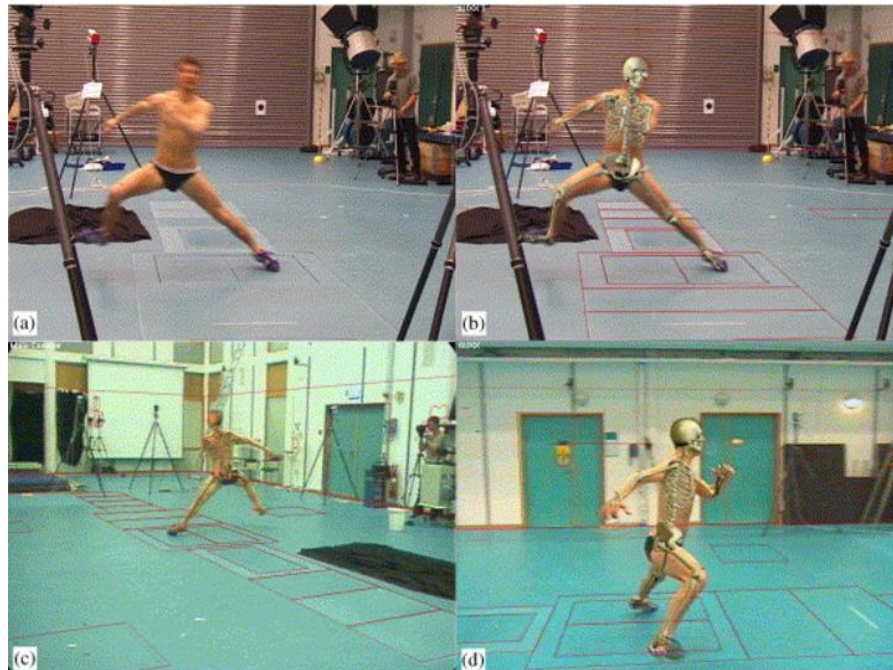


Figure 2.27 The original video image (a) and the images of matched Poser skeleton model to the laboratory model in three views (b-d), adapted from [Krosshaug and Bahr 2005]

2.5. What is known about pedestrian ground related injuries

2.5.1. The severity of pedestrian ground contact injuries

Tamura *et al.* [Tamura *et al.* 2014] pointed that pedestrian may suffer Traumatic Brain Injury (TBI) caused by ground contact even at low impact speeds. A set of GIDAS accident data collected from 1985 to 1999 was analyzed for a study [Otte and Pohlemann 2001] specifically aimed at pedestrian ground contact injuries. The distribution of primary injuries (due to contact with vehicle) and secondary injuries (due to contact with the ground) are analyzed (see Figure 2.28). 65% of the documented pedestrians suffered injuries by ground contact. About 61.6% of them suffered same or higher injury severity due to ground impact while 38.4 % of them suffered higher injury severity due to primary impact with vehicle. And for those who suffered head injuries, more than 60% of them had their head injuries due to contact with the ground. Through data analysis, the study also presented that vehicle speed, bonnet height and throwing distance of the flying pedestrian are some major influence factors for ground related injuries. However, the valuable information of relationship between vehicle speed/front end shape/pedestrian age and ground related injury risk are still missing. The injuries involved in this study were not classified based on the severities.

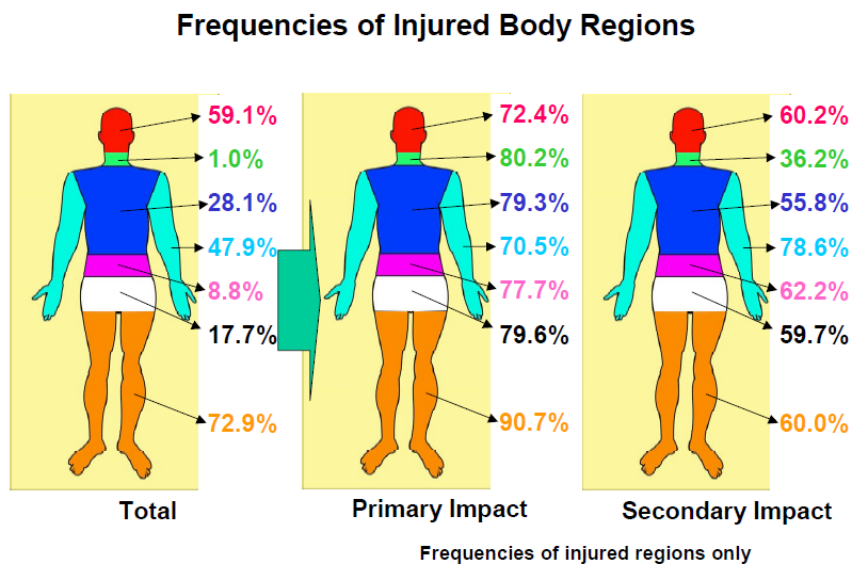


Figure 2.28 Injury Frequency of n=293 Pedestrians in Total (100% all persons), distinguished for primary and secondary impacted persons (100% each injured body regions)

Roudsari *et al.* [Roudsari *et al.* 2005] analyzed a set of PCDS data which involving passenger vehicles (PV) and light truck vehicles (LTV) to evaluate the effect of vehicle type on pedestrian's trajectory and the injury severity and sources. It is found that for PV-pedestrian

crash, the ground take responsibility of 7% of head injuries while the percentage is 39% for LTV crash (as shown in Table 2.3). Besides, the ground is the lead source of upper extremity injury [Roudsari *et al.* 2005], which indicated the LTV's aggressiveness to pedestrians as well as the importance of ground related injuries.

Table 2.3 Distribution of sources of head injury and resultant injury severity for adults by the class of vehicle, adapted from [Roudsari *et al.* 2005]

Source of injury	PVs		LTVs	
	Number (%) of injuries	Mean (±SD) AIS	Number (%) of injuries	Mean (±SD) AIS
Windshield	211 (63%)	2.7 ± 1.4	13 (7%)	2.6 ± 1.7
Hood surface	38 (11%)	2.7 ± 1.5	56 (33%)	2.6 ± 1.4
A pillar	29 (9%)	3 ± 1.3	15 (8%)	3.3 ± 1.6
Cowl	16 (5%)	3 ± 1.5	12 (6%)	3.3 ± 1.6
Front header	13 (4%)	2.7 ± 1.7	3 (2%)	4.3 ± 0.6
Other parts of vehicle ^A	5 (1%)	—	5 (3%)	—
Ground	23 (7%)	1.7 ± 1.1	68 (39%)	2.6 ± 1.6
Total	335 (100%)	2.6 ± 1.5	172 (100%)	2.7 ± 1.5

In terms of the various sources of head injury during the crash, researchers [Badea-Romero and Lenard 2013, Guillaume *et al.* 2015] carried out in-depth studies to have a better understanding of vehicle and ground related pedestrians' injuries, what would help to orient the safety actions. A set of 205 accidents cases from the UK On-the-Spot (OTS) study involving pedestrians and cyclists with head injuries was reviewed in detail [Badea-Romero and Lenard 2013]. According to the results of classification tree analysis (Figure 2.29), on the pedestrian side with head injuries, 48% of them had head injuries are subjected to ground contact. For those pedestrians, 26.4% of them sustain moderate or more serious injuries. The ratio is 35.9% for the cases with head injuries caused by vehicle-head contact. Another study [Guillaume *et al.* 2015] of pedestrians injury sources was based on an analysis of a sample (100 in-depth investigations and reconstructions of vehicle-pedestrian crashes from 2009 to 2011 continuously collected in an area of Paris) of CACIAUP database. Results have showed a high number or proportion of the injuries caused by ground contact. When the vehicle speed is less than 50km/h, ground related injuries account 27.5% for AIS2+ injuries. While when the vehicle speed is limited to 30km/h, the proportion of AIS2+ ground related injuries in AIS+ injuries had risen to 57%. Head, upper and lower extremities are the main injured body parts for AIS2+ injuries caused by contact with the ground.

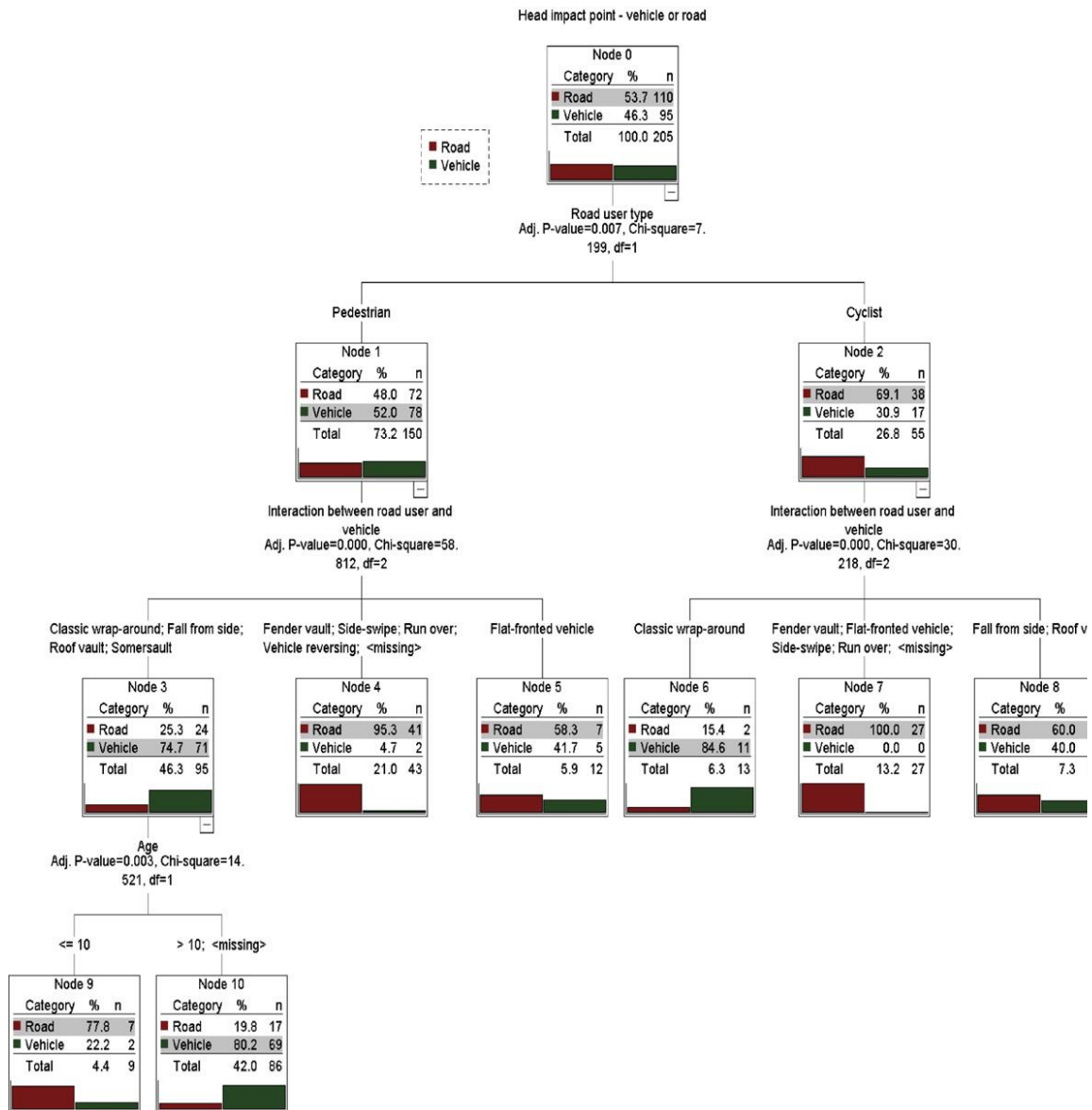


Figure 2.29 Classification tree for vehicle or road as a source of head impact and injury split by road user type, adapted from [Badea-Romero and Lenard 2013]

2.5.2. Vehicle speed effect on ground related injuries

Vehicle speed is widely considered as one of the leading factors causing pedestrian fatalities [Anderson *et al.* 1997, Hussain *et al.* 2019] and it highly affect pedestrian projection distance and injuries from ground contact in vehicle crash [Otte and Pohlemann 2001, Wood *et al.* 2005, Kendall *et al.* 2006, Simms and Wood 2006, Shang *et al.* 2017] even though it is variable and less predictable.

A 1970's accident study [Ashton 1975] used at-the-scene investigation, made by the Accident Research Unit of the Dept. of Transportation and Environmental Planning at the

University of Birmingham, to study the causes of pedestrian head injuries. Results showed that the severity of ground related injuries is higher than from vehicle contact when the impact speed is below 7m/s (as shown in Figure 2.30). However, when vehicle speed is higher than 40 km/h, pedestrians suffer an obvious high risk to have severe head injuries from contact with the vehicle.

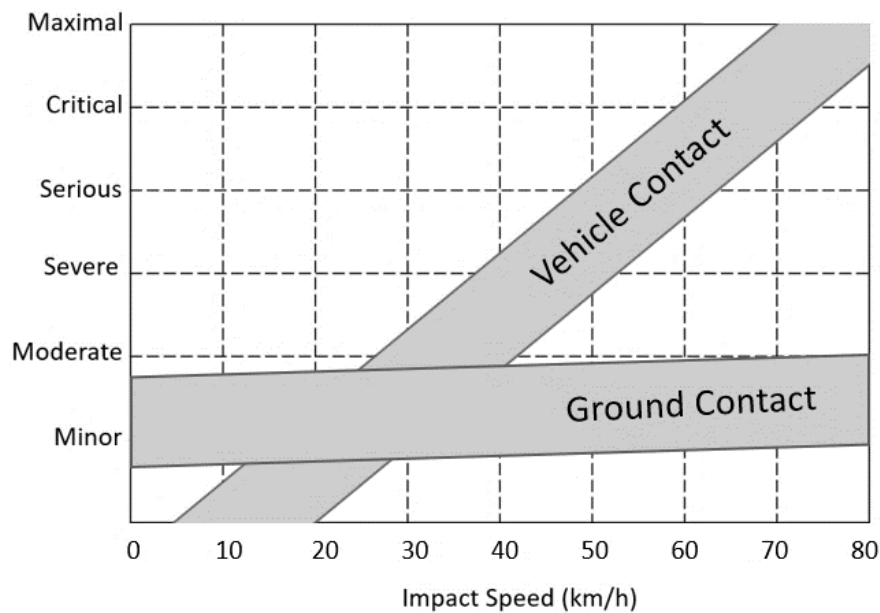


Figure 2.30 Relative influence of pedestrian injuries caused by vehicle contact versus ground contact as a function of impact speed, adapted from [Ashton 1975].

Kendall *et al.* [Kendall *et al.* 2006] simulated a series of vehicle-pedestrian collisions and found that risk of head injury from both vehicle contact and ground contact tends to rise with the vehicle speed increase, but injury risk caused by secondary ground contact is less predictable. They also found that at lower speeds cases, the vehicle tends to pose a greater risk of injury than does the ground, while at higher vehicle speeds cases, the injury risk from both the vehicle and ground is typically large. Similarly, [Simms and Wood 2006] simulated vehicle crash with different pre-impact position and found that the severity of injuries from different body parts (pelvis, chest and head) caused by secondary ground contact showed different trends with the impact speed increases. At all speed cases, head injury indices (HIC_{36} and 3ms) in ground contact are less than those from vehicle contact. At low vehicle impact speeds, chest and pelvic injuries from the ground impact are more serious than for the vehicle impact.

Hamacher *et al.* [Hamacher *et al.* 2012] investigated the vehicle-pedestrian collision speed effect on pedestrian-ground contact mechanism. The results indicated that the higher impact speed resulted in larger average launch speed and launch angle (as shown in Figure 2.13) when pedestrian ground contact happened. Based on an analysis of MB simulations, Shi *et al.* [Shi *et al.* 2018] found that the relationship between vehicle speed and pedestrian landing rotation angle is significant. By analyzing a set of real-world vehicle-pedestrian crash videos, [Han *et al.* 2018a, Li *et al.* 2018] also indicated that vehicle impact speed is one of the influencing factors which determines pedestrians' landing kinematics.

2.5.3. Vehicle type effect on the pedestrian ground related injuries

Previous investigations [Ishikawa *et al.* 1993b, Simms and Wood 2006] indicated that front shape of the vehicle, especially the BLEH (Bonnet leading edge height), greatly influences the kinematics of pedestrians after the impact. An analysis of real-world collision database found that head injuries were more frequently suffered for vehicles with BLEH ≥ 70 cm. While pedestrians were observed more frequent thorax injuries when BLEH < 70 cm. The study of Roudsari *et al.* [Roudsari *et al.* 2005] showed that LTVs (Light Trucks and Vans), which have significantly higher BLEH than passenger sedans, resulted in a higher risk of head injuries subjected to ground contact (39% vs 7%).

In order to investigate the influence of vehicle shape on pedestrian ground contact injuries, [Simms *et al.* 2011] modelled and simulated a number of vehicle-pedestrian impact scenarios with different vehicle shapes and vehicle impact speeds. Results showed that pedestrian ground impact mechanisms are highly dependent on vehicle shape, see Figure 2.31. They found a relationship between vehicle front bonnet edge height and the head HIC score obtained from contact with the ground and suggested that higher bonnet leading edge produced more serious injuries.

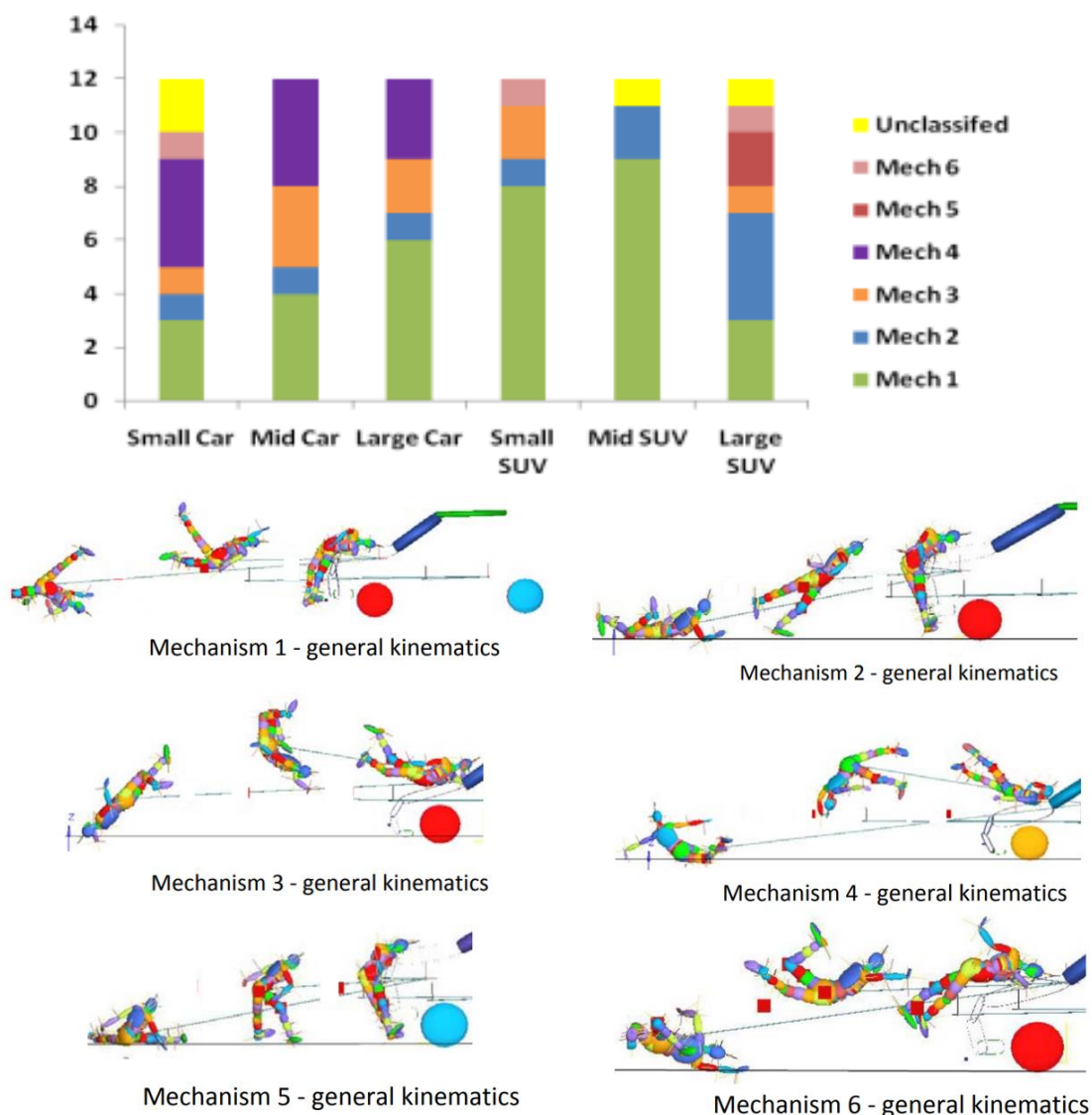
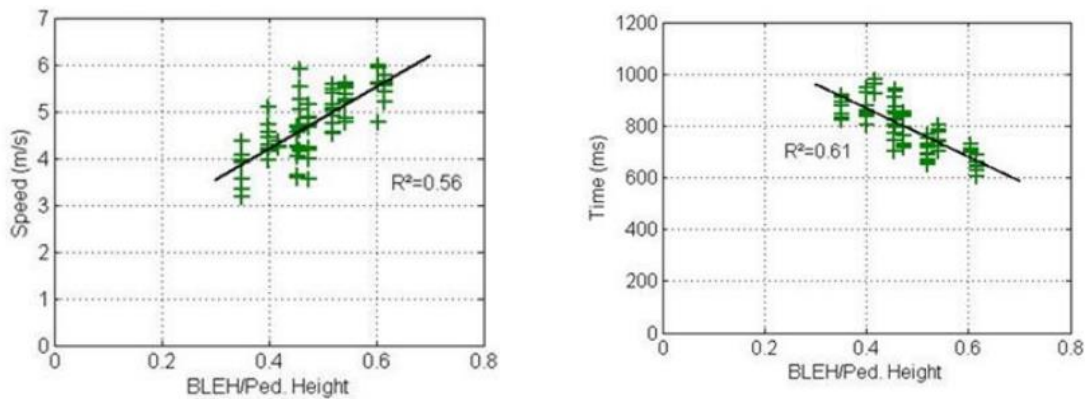


Figure 2.31 Proportion of pedestrian ground contact mechanisms by vehicle type, adapted from [Simms *et al.* 2011]

Yin *et al.* [Yin *et al.* 2017] built and simulated a series of MB vehicle-pedestrian crash scenarios to study how bonnet leading-edge height, bonnet angle, bonnet length and windshield angle effect on head injury severities subjected to secondary ground impact. By comparing the posture and head *HIC*, they found that the bonnet leading edge height (BLEH) was the top dominating factor (see Figure 2.15). Hamacher *et al.* [Hamacher *et al.* 2012] investigated the vehicle shape effect on pedestrian ground contact mechanism by simulating the vehicle-pedestrian crash scenarios with different vehicle types by using MB models. Similar to the result of [Yin *et al.* 2017], the high BLEH with relevant pedestrian posture, large bonnet angle and windshield angle increase the risk of a head ground contact.

Crocetta *et al.* [Crocetta *et al.* 2015] investigated the vehicle front end height associated with pedestrian height effect on ground contact mechanism by simulating vehicle-pedestrian crashes with different vehicle shapes. Results showed that higher NBLEH resulted in larger head ground impact speed [Figure 2.32 (a)] and also made the head ground impact occurred earlier [Figure 2.32 (b)]. Tamura *et al.* [Tamura *et al.* 2014] also indicated that pedestrian kinematics and ground impact mechanisms are significantly affected by the shape of the vehicle front structure.



(a) Relation of BLEH/ pedestrian height and Head ground impact speed (b) Relation of BLEH/ pedestrian height and Head ground impact time

Figure 2.32 Normalized bonnet leading edge height (NBLE/Pedestrian height) effect on pedestrian head ground impact speed and the time of impact for mechanism 1 from [Crocetta *et al.* 2015], adapted from [Crocetta *et al.* 2015]

2.5.4. Pedestrian size effect on ground related injuries

Crocetta *et al.* [Crocetta *et al.* 2015] indicated the NBLEH effect on pedestrian ground contact mechanisms and head ground impact speed. Thus, pedestrian size (height) is a significant factor which can affect pedestrian post-impact kinematics. By simulating the crash scenarios at MADYMO platform, Hamacher *et al.* [Hamacher *et al.* 2012] assessed the pedestrian ground contact based on criteria which formed by the launch speed, throw distance, flight height, etc. Results showed the children model and adult models received different scores for sedan and van involved crashes (see Figure 2.33).

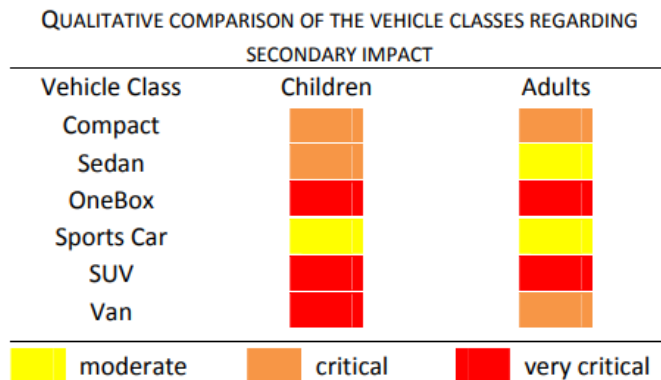


Figure 2.33 Qualitative comparison of children and adult pedestrian models regarding secondary impact, adapted from [Hamacher *et al.* 2012]

2.5.5. Other effects on ground related injuries

Zou *et al.* [Zou *et al.* 2019] first analyzed the potential braking effect on the pedestrian ground related injuries by controlling the braking in multi-body simulations. Results obtained from different combination of a simulation test sample (vehicle speeds, pedestrian sizes and pedestrian gaits) showed that the weighted injury cost (associated with injury severity) from ground contact can frequently be reduced by using controlled braking rather than full braking, as shown in Figure 2.34.

Pedestrian pre-impact posture (orientation, gait, joint angle etc.) can also influence the impact direction of angle [Chen *et al.* 2015], the kinematics of the body, and thus change the mechanisms of ground impact as well as the level of injury severity [Simms and Wood 2006, Shi *et al.* 2018].

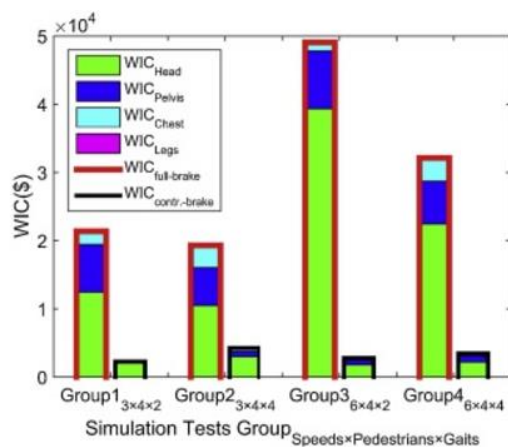


Figure 2.34 Weighted injury cost for full braking versus controlled braking for different simulation test sample combinations, adapted from [Zou *et al.* 2019].

2.6. Absence of information on ground contact injuries

Compared with the study of pedestrians being impacted by vehicles, the specific studies of pedestrian ground contact appear few. The analysis of ground related injuries based on the GIDAS database is 19 years ago [Otte and Pohlemann 2001]. The data cannot represent the current situation of the characteristics of vehicle-pedestrian collisions because the vehicles are improving. Also, the injury distribution and comparison between ground related injuries and vehicle-related injuries are too ambiguous. Moreover, the relation of pedestrian ground related injuries and influencing factors were not stated clearly. Similarly, the video analysis of ground contact indicated the relation of vehicle shape and pedestrian ground contact mechanism is unclear [Han *et al.* 2017]. Besides, the injuries of the crashes recorded in the videos are unknown. For the multibody reconstruction models, the pedestrian models are not validated for the ground contact [Crocetta *et al.* 2015, Yin *et al.* 2017]. Therefore, it needs to do experimental or cadaver tests to have a reference to assess the capability of the models. Some information could be obtained from cadaver or dummy tests [Hamacher *et al.* 2011, Hamacher *et al.* 2012], but few were aimed to pedestrian ground contact up to now. Some studies have indicated that vehicle shape affects pedestrian ground contact injuries, but the relevant method for reducing or eliminating injuries caused by ground contact is not proposed.

2.7. Summary

In this chapter, relevant studies of pedestrian ground contact have been reviewed. Section 2.1 presents an overview of pedestrian injuries due to ground contacts. Pedestrian ground contact should be given more attention due to the massive and severe injuries it may cause, especially the head injuries [Otte and Pohlemann 2001, Badea-Romero and Lenard 2013]. In Section 2.2, methods such as cadaver/dummy tests [Taneda *et al.* 1973, Hamacher *et al.* 2012], numerical simulation analysis with MB/FE reconstruction [Kendall *et al.* 2006, Simms and Wood 2006, Simms *et al.* 2011, Crocetta *et al.* 2015, Yin *et al.* 2017], in-depth crash data analysis [Ashton 1975, Otte and Pohlemann 2001, Neal-Sturgess *et al.* 2007, Badea-Romero and Lenard 2013, Guillaume *et al.* 2015], and real-world video analysis [Barry and Simms 2016, Han *et al.* 2017], applied in previous studies on ground contact are introduced. Even though the vehicle is the first and main source of pedestrian injuries, ground related injuries account for a considerable proportion [Otte and Pohlemann 2001, Badea-Romero and Lenard 2013]. Researchers have paid attention to reduce the injuries

subjected to vehicle contact by improving the vehicle designs [Nagatomi *et al.* 2005, Oh *et al.* 2008, Hutchinson *et al.* 2011, Masoumi *et al.* 2011]. The importance of ground contact should now also draw more attention.

The absence of information on ground contact for previous studies can be concluded as:

- 1) No recent systematical study on pedestrian ground contact or important relationship between influencing factors and ground related injuries are not observed from the real-world crash database.
- 2) Insufficient detailed information of real-world pedestrian post-impact kinematics and mechanisms.
- 3) Most current PMHS tests focused on pedestrian-vehicle impact, no detailed study on pedestrian response after vehicle contact, especially the process of pedestrian ground contact.
- 4) Both the MB pedestrian models and the FE pedestrian models were only validated for vehicle contact, the feasibility of representing pedestrian ground contact is uncertain.
- 5) Effect of vehicle shape on ground injuries is still uncertain even though it is widely accepted that vehicle shape does influence pedestrian post-impact kinematics.

Based on the information of current gap between the valuable results already observed and the missing information of ground contact, the proposed work aiming at pedestrian ground contact head injuries are introduced in Chapter 3, which proposed to have a more detailed and comprehensive understanding. The proposed work is presented in Chapter 3 points out the potential work which may cross the gap.

3. Proposed research to understand pedestrian ground related injury

3.1. Introduction

The literature review in Chapter 2 indicates what researchers have done on pedestrian ground contact as well as the research that has yet to be completed. Few researchers have focused on ground contact due to its unpredictability, which provides an opportunity to better understand pedestrian ground contact injuries as a precursor to developing potential injury countermeasures. Several methods proposed in section 3.2 could help to have a more detailed understanding of the mechanism and risk of ground related injuries.

3.2. Methods

3.2.1. Detailed accident analysis to understand the nature of the ground contact

An analysis of the GIDAS database from 2000 to 2015 is applied to analyze ground related injuries comprehensively in this study. It is better to have a more detailed overview of the distribution of pedestrian ground related injuries as well as a comparison with vehicle-related injuries. The previous study [Otte and Pohlemann 2001] generally pointed out some factors affecting pedestrian ground contact. But it is better to determine in detail how factors such as vehicle speed, pedestrian age, vehicle front shape, sex etc., influence the risk and severity of ground related injuries and find the relationships between them. Injuries from contact with the ground are categorized based on the severity level and body region. The influence of older/newer vehicles on injury risk is also studied. Potential reduction in ground contact injury costs is stated to show the ecological benefits of reducing and eliminating the ground contact. Relevant statistical analysis by using Shapiro-Wilk test, Kruskal-Wallis test, Chi-Squared and Fisher's Exact Tests are presented in Chapter 4.

3.2.2. Video analysis of real-world collisions

Analyzing real-world crash videos is an intuitive way to observe pedestrian post-vehicle

impact kinetics and then present the relationship between influencing factors and outcomes. But there are limited conclusive conclusions in previous studies [Barry and Simms 2016, Han *et al.* 2017]. Therefore, an analysis of real-world collision videos is presented in Chapter 5.

3.2.3. Staged tests with cadavers to provide better information on ground contact and model assessment information

A series of cadaver impact tests were proposed and designed to study pedestrian kinematics and dynamics for post vehicle contact in detail. The impact speeds and the pedestrian's initial position were set based on real-world video analysis. Compared to the numerical simulations, reconstructing vehicle-pedestrian collisions with cadaver tests is a way to reflect the mechanism in more near to true circumstances. Multi-view videos of the whole impact process are captured by high-speed cameras and the accelerometer data provided the detailed kinematics and kinetics, which enables forensic experts to assess injuries from contact with the ground. In addition, cadaver tests could be used to validate the numerical models such as MADYMO pedestrian model. Relevant studies of experimental/cadaver tests are presented in Chapter 6.

3.2.4. Multibody model assessment based on the cadaver tests

The staged PMHS impact tests can provide references to assess the capability of MB models to reconstruct the scenarios. Vehicle models were built based on the real vehicles tested and the pedestrian models were also scaled to the same size as the cadaver for each test. The cadaver tests were reconstructed in a MADYMO environment and the subsequent collisions were simulated. The pedestrian's overall kinematics, ground contact mechanisms and head injuries were then extracted and assessed by comparing the results to those from the cadaver tests. The models are assessed in Chapter 7.

3.2.5. Virtual test system (VTS) approach to reduce or prevent ground contact injuries

Previous studies [Simms *et al.* 2011, Tamura *et al.* 2014, Crocetta *et al.* 2015, Han *et al.* 2017, Yin *et al.* 2017] have indicated that vehicle front shape like bonnet leading-edge height, bonnet angle and windshield angle have a discernable effect on pedestrian injuries from ground contact. However, few methods are proposed [Khaykin and Larner 2016, Gupta *et al.* 2017] aiming at reducing or eliminating the secondary ground contact injuries. Therefore, a method of VTS in the current study is inspired from Li *et al.* [Li *et al.* 2016], in which the weighting was used to represent different collision scenarios within a wide range, is proposed to reduce injuries from ground contact by changing the dimensions of vehicle front shape (see Chapter 8). During the processes of vehicle optimization [Li *et al.* 2016], a poor shaped vehicle profile, in which a pedestrian suffered the highest weighted injury (a combination of vehicle and ground contact injuries) and a good shaped (pedestrian suffered lowest weighted injury) vehicle profile are produced for each vehicle category (sedan, SUV and van). The parameters of these six vehicle shapes are employed in the current study to test the weighted injury costs from contact with the ground. The aim of the VTS is to determine the extent that a vehicle's shape can affect ground-related injuries with real-world collision distributions.

4. Study 1: Analysis of pedestrian ground contact injuries from detailed German accident database¹

4.1. Introduction

This chapter is based on a published paper [Shang *et al.* 2018d]. The World Health Organization estimates about 270,000 pedestrian fatalities occur annually following road traffic collisions [WHO 2013]. There is now a good understanding of the relationship between vehicle speed, front-end design and pedestrian injury outcome [Simms 2005, Simms and Wood 2009, Rosén *et al.* 2011, Niebuhr *et al.* 2016, Li *et al.* 2017a]. And this is reflected in legislative tests and consumer test protocols for pedestrian protection in the European Union. Many modern vehicles have improved front-end designs and some have external airbags and pop-up bonnets for pedestrian protection. However, although most pedestrians struck by vehicles subsequently impact the ground, there has been much less focus on pedestrian ground contact injuries and the opportunities for their prevention. Pedestrian ground contact is mostly less severe than vehicle contact [Ashton and Mackay 1983], but the potential benefit of eliminating pedestrian ground contact injuries remains very high, though technically challenging to achieve. Distinguishing between pedestrian injuries from the vehicle versus the ground generally presents a challenge for collision investigators [Otte and Pohlemann 2001, Neal-Sturgess *et al.* 2007] and the distribution and risk factors for pedestrian ground contact injuries remains poorly understood. Otte and Pohlemann [Otte and Pohlemann 2001] analysed the 1985–1999 German in-depth Accident Study (GIDAS) data and found that 65 percent of pedestrians had injuries from ground contact. However, the severity and distribution of injuries were not clearly reported and the front-end shape of the vehicle fleet has since changed significantly. An analysis of the US Pedestrian Crash Data Study (PCDS) found 17% of pedestrian injuries were ground related [Zhang *et al.* 2008]. The PCDS data also showed that head injuries from ground contact were significantly increased following collisions with Light Trucks and Vans (LTVs) compared to

¹ Shang, S., Otte, D., Li, G., & Simms, C. (2018). Detailed assessment of pedestrian ground contact injuries observed from in-depth accident data. *Accident Analysis & Prevention*, 110, 9-17.

Shang, S contributed the conception and design of the study, analysis of data and drafting the article and revising the article

Otte, D contributed the acquisition and interpretation of GIDAS data

Li, G contributed part interpretation of statistical analysis

Simms, C contributed the conception and design of the study, the guide of the study and revising the article

passenger cars, and this was attributed to their higher bonnet leading edge heights [Roudsari *et al.* 2005]. A recent analysis of 150 pedestrian collision cases in the UK found almost half the head injuries were ground related, but vehicle contact injuries were more severe [Badea-Romero and Lenard 2013]. Analysis of 100 French pedestrian collisions [Guillaume *et al.* 2015] indicated that more than half of AIS 2+ injuries were ground related for vehicle speeds below 30 km/h. Overall, the literature provides some detail on pedestrian head injuries from ground contact, but the whole-body distribution of ground contact injuries is not reported and risk factors for ground injuries remain poorly understood from collision data.

Computational studies have addressed pedestrian ground contact [Kendall *et al.* 2006, Tamura and Duma 2011a, Tamura *et al.* 2014, Crocetta *et al.* 2015, Yin *et al.* 2017] and these studies observed a strong influence of the initial crash configuration on the pedestrian ground contact interaction. However, several also identified patterns governing the kinematics of ground contact [Kendall *et al.* 2006, Tamura and Duma 2011a, Tamura *et al.* 2014, Crocetta *et al.* 2015, Yin *et al.* 2017], determined by the inertial and geometric interaction of the pedestrian and vehicle front and also the collision speed. The bonnet leading-edge height influences ground contact kinematics [Simms *et al.* 2011, Hamacher *et al.* 2012, Crocetta *et al.* 2015, Yin *et al.* 2017], implying that in future an active restraint system could dynamically change the vehicle front-end shape to positively influence the pedestrian ground contact. However, no models have been validated for ground contact, although preliminary comparisons with video recordings of pedestrian collisions show some verification [Barry and Simms 2016].

Since the 1970s, several vehicle restraint concepts have been proposed to reduce pedestrian ground contact injuries: mechanical catching devices [Jehu and Peavson 1976] and recently an adhesive approach was patented by Google [Khaykin and Larner 2016]. Their concept is to apply an adhesive layer covered by a coating to the vehicle front-end which is activated during a collision such that the pedestrian adheres to the vehicle during the wrap phase. The aim is always to maintain the pedestrian on the bonnet top following impact, thereby preventing ground contact. However, none of these approaches has been implemented, reflecting the technical difficulties involved. Accordingly, a different approach to ground injury reduction may be needed. If relationships between vehicle shape and ground contact kinematics could be established from collision data similar to what has been predicted using

multibody models [Kendall *et al.* 2006, Tamura and Duma 2011a, Tamura *et al.* 2014, Crocetta *et al.* 2015], ground contact injury mitigation might be achieved through shape-changing technology (e.g. airbags) on the vehicle front, to simultaneously reduce vehicle contact injuries and also moderate the post-impact kinematics of the pedestrian. Notwithstanding the significant protective potential of crash avoidance technology, the effectiveness of current secondary pedestrian protection strategies is limited by their failure to protect against ground injuries. Therefore, the impetus for developing such countermeasures will grow as the risk posed to pedestrians by primary contact with the vehicle front reduces with improved front-end design [Untaroiu *et al.* 2007, Hu and Klinich 2012]. Pedestrian ground contact injuries at speeds below 40 km/h are of particular interest since pedestrian injuries from vehicle contact at these speeds are mostly survivable [Rosén *et al.* 2011].

However, prior to countermeasure development, a better understanding of the distribution and risk factors for pedestrian ground contact injuries in recent collisions is needed. The German in-depth Accident Study (GIDAS) is therefore used to assess the severity and distribution of pedestrian ground related injuries for collisions between 2000 and 2015 involving passenger cars, light trucks and vans. The database is also used to assess:

- (1) how do vehicle impact speed and pedestrian age influence pedestrian ground contact injuries?
- (2) Is the proportion of ground related injuries for newer model vehicles higher compared to older vehicles?
- (3) Does vehicle bonnet leading-edge height influence pedestrian ground related injuries?
- (4) What are the benefits of eliminating pedestrian ground contact for collisions below 20, 30 and 40 km/h?

4.2. Methods

4.2.1. GIDAS data

Pedestrian cases involving AIS 1+ ground related injuries from the German in-depth Accident Study (GIDAS) between 2000 and 2015 were used to analyse pedestrian ground contact injuries. For each case, the database includes the age, height and injured body parts and severity levels. An estimate for the vehicle speed and direction of motion of the

pedestrian and the source of each injury (vehicle or ground) was coded following detailed reconstruction of each case by an experienced team using 3-D laser scans of the scene, assessment of vehicle damage, the pedestrian projection distance and other evidence to produce a PC-crash reconstruction of the event. Based on all available evidence, the team assigned each injury to either vehicle or ground contact [Otte *et al.* 2003, Otte 2005]. There is as yet no gold standard method for coding the source of injuries for pedestrians, and the process entails uncertainty which is difficult to quantify. However, the following detailed approach was used, similar to the best practice guidelines proposed by the European Network of Forensic Science Institutes [ENFSI 2015]. Injuries were assessed using an internal GIDAS coding system as well as the 2005 Abbreviated Injury Scale (AIS) [Gennarelli and Wodzin 2006]. The AIS system defines the severity of individual injuries on a scale of one to six: AIS 1 = minor, AIS 2 = moderate, AIS 3 = serious, AIS 4 = severe, AIS 5 = critical and AIS 6 = fatal). In the internal GIDAS coding system, each injury is given a descriptor such as soft tissue lesion or haematoma and injuries are linked where possible to a common source, for example, a soft tissue lesion and an underlying bone fracture. Injuries are documented at four stages: (1) the on-the-spot team attending at the collision site, (2) using the hospital-based injury information, (3) the final medical report which includes X-rays and CT scans in the case of brain injuries and (4) the kinematic sequence estimated from the accident reconstruction. This information is combined to code the source of each injury. Scratch marks on soft tissues indicate a ground contact while depressed skull fractures typically indicate vehicle contacts (for example, the A-pillar). Injuries, where the source is doubtful or cannot be assigned, are coded as “unknown”. The following additional criteria were applied: (1) only cases involving a single vehicle striking a standing/walking/running pedestrian were included; (2) injuries (not cases) with uncertain/unknown sources were excluded; (3) only pedestrians struck by the vehicle front were included. The proportion of cases with ground related injuries at different AIS levels was assessed, as well as the distribution across different body regions and age and speed effects. To evaluate the relationship between ground related injuries and vehicle model year, two categories of vehicles were defined: “older vehicles” (models released prior to 2005, the year of the first implementation of the EU Directive on pedestrian safety [Union 2005] and “newer vehicles” (models since and including 2005). To evaluate the relationship between ground related injury and bonnet leading edge height (BLEH), the vehicle contours were established [The-Blueprints] and the BLEH was defined using the European Enhanced Vehicle-Safety

Committee Working Group 17 (EEVC WG17) [EEVC 2002] protocol, similar to [Li *et al.* 2017a]. Hip heights for pedestrians were estimated from the known pedestrian height in GIDAS using anthropometric regression relationships [Pheasant and Haslegrave 2016] and hence the normalized bonnet leading-edge height (NBLEH = BLEH/hip height) was estimated. Given the geometric interaction between pedestrian height and bonnet leading edge height for the principal point of contact on the vehicle, for the bonnet leading-edge height analysis, the pedestrians were categorized as either child (less than 12 years old), adolescents (12-17 years old) or adults (aged 18+). To assess the potential injury cost savings which could be achieved by preventing ground related injuries, the injury cost approach for medical and auxiliary costs from ISO: 13232-5, 2005 was utilized [Li *et al.* 2016] to compute injury costs below speed thresholds of 20, 30 and 40 km/h. These costs are based on a simplified model of samples of bioeconomic data. Medical costs include rehabilitation, chronic care, and vocational rehabilitation while ancillary costs are associated with lost wages and legal actions as well as the cost of replacing household/workplace contributions. Costs of permanent partial incapacity due to lower extremity injuries are also accounted for. Injury costs may vary across country to country while they should satisfy the trend that severity level injuries cost more. Implementation of this approach works as follows: for each collision case, the total cost is calculated from the sum of all the individual medical and ancillary costs of each coded injury (the costs vary with AIS level and body region injury). The cost associated with lower extremity injuries is based on the permanent partial incapacity score, see Table 4.1 and Table 4.2. The cost of a fatality is coded separately in Table 4.2, regardless of the injuries coded.

Table 4.1 Medical and auxiliary cost of injury severity, adapted from ISO 13232-5:2005 [ISO 2005]

Body region	AIS injury severity level	Medical cost (\$)	PPI	Ancillary cost (\$)
Head	1	784	-	2 664
	2	3 807	-	10 818
	3	14 169	-	47 819
	4	72 349	-	91 497
	5	263 306	-	320 571
Neck	3	20 509	-	76 267
	4	440 037	-	391 007
	5	530 695	-	463 314
Thorax	1	696	-	1372
	2	3 410	-	10 886
	3	10 147	-	31 051
	4	19 577	-	46 853
	5	32 790	-	64 256
Abdomen	1	696	-	1 372
	2	3 410	-	10 886
	3	10 147	-	31 051
	4	19 577	-	46 853
Leg			07	27 370
	2	7 881	15	58 650
	3	22 732	22	86 020
			27	105 570
			38	148 580

Fatality cost is \$596 580

Table 4.2 Permanent partial incapacity (PPI) determination, adapted from ISO 13232-5:2005 [ISO 2005]

If		PPI
$N_{F,3} + N_{K,2} + N_{T,3} + N_{T,2}$	≥ 3	38
$N_{F,3} + N_{K,3} + N_{K,2} + N_{T,3} + N_{T,2}$	$= 2$	27
$N_{F,3}$ or $N_{K,2}$ or $N_{T,3}$	$= 1$	15
$N_{T,2}$	$= 1$	07

$N_{I,J}$ is the number of injured frangible leg components I of AIS level J,
F, T, K are femur, tibia and knee component, respectively.

4.2.2. Statistical analysis

Data analysis was performed using IBM SPSS Statistics software [IBM 2015]. The Shapiro-Wilk test was used to check whether a given parameter was normally distributed. Analysis of variance (ANOVA) was applied to normally distributed datasets to assess the difference between the means as well as the effect size [Cohen 1988, Sawilowsky 2009], see Table 4.3. Otherwise, the Kruskal-Wallis Test was used to test for differences in the median. The Chi-Squared and Fisher’s Exact Tests were employed to assess a possible bias in cases involving

newer versus older vehicles in suffering AIS 2+ ground related injuries. The threshold for statistical significance was set at the 5% level. Logistic regression and odds ratios have been successfully applied to the relationship between vehicle shape and pedestrian injuries from vehicle contact [Yao *et al.* 2008, Li *et al.* 2017a], and this approach was therefore applied to assess the influence of NBLEH on AIS 2+ ground related head injury outcome. Logistic regression (LR) is applied to obtain odds ratio in the presence of multi-variables. By analysing the association of all variables (such as vehicle speed, vehicle shape, pedestrian age, height, etc) together, LR could avoid the confounding effects. The sigmoid curve generated by logistic regression could show the probability from 0 to 1. The logistic model and injury probabilities are:

$$\text{logit}(p) = \log\left(\frac{p}{1-p}\right) = \beta_0 + \beta_1 * x_1 \dots + \beta_i * x_i \quad \text{Equation 4.1}$$

$$p = \frac{\exp(\beta_0 + \beta_1 * x_1 \dots + \beta_i * x_i)}{1 + \exp(\beta_0 + \beta_1 * x_1 \dots + \beta_i * x_i)} \quad \text{Equation 4.2}$$

where p is the probability of an AIS 2+ ground related injury, β_i are the coefficients estimated using the method of maximum likelihood and x_i are the predictors (vehicle speed, pedestrian age and NBLEH). Predictor multicollinearity was assessed to check the tolerance (Tol) and the variance inflation factor (VIF). A VIF maximum cut-off of 2.5 was applied [Midi *et al.* 2010]. Odds ratios (OR) were used to estimate the change in injury odds per unit increase in the corresponding predictor variable while keeping remaining variables fixed. Confidence Intervals (CI) at the 95% level were constructed.

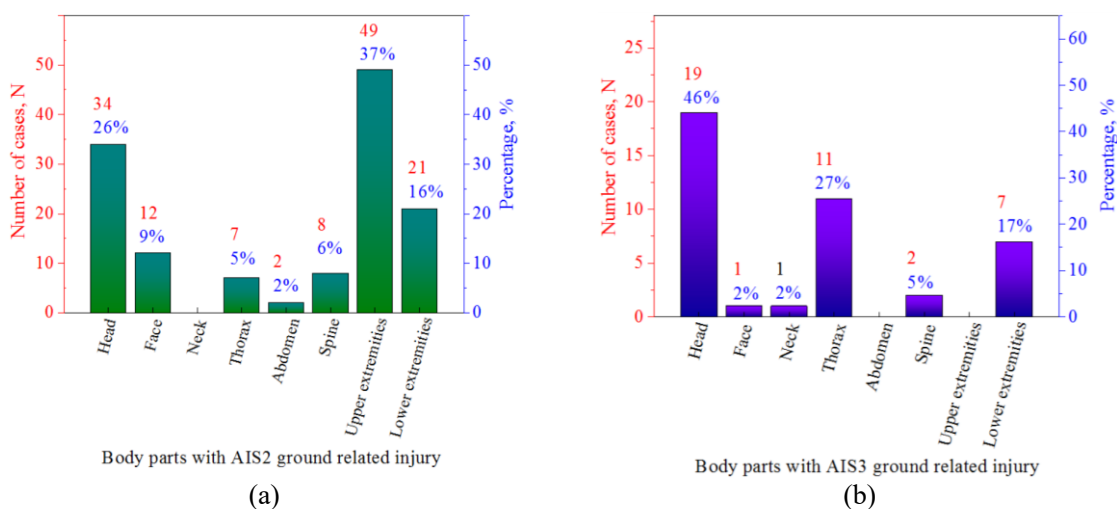
Table 4.3 Magnitudes of effect sized d and r for ANOVA [Cohen 1988, Sawilowsky 2009]

<i>Effect size</i>	<i>d</i>	<i>r</i>
Very small	0.10	0.050
Small	0.20	0.100
Medium	0.50	0.243
Large	0.80	0.371
Very large	1.20	0.514
Huge	2.00	0.707

4.3. Results

4.3.1. Overview of ground related injuries

Figure 4.1 shows the body region injury distributions at different AIS levels. Figure 4.1(a) shows that for cases with AIS 2 ground related injuries, the head (26%) and upper (37%) and lower extremities (16%) were the most frequently injured body regions. Avulsion of the scalp, brain injuries and skull fracture were typical AIS 2 ground related head injuries. For the upper and lower extremities, there were several de-gloving injuries but fracture accounted for 87% of cases. Figure 4.1(b) shows that for cases with AIS 3 ground related injuries, the head (46%), thorax (27%) and legs (17%) were the most frequently injured body regions. Among AIS 3 head injuries, 63% were brain injuries including brain edema and intracerebral hematoma, while the remaining injuries were skull fractures. The thorax injuries involved pulmonary injury, haemothorax, haemopneumothorax and fracture of multiple ribs. The upper/lower extremities injuries were all fractures. Figure 4.1(c) shows five cases with AIS 4 head injuries (cerebral hematoma, skull fracture), three cases with AIS 4 thorax injuries (fracture of multiple ribs with flail chest) and one case with an AIS4 abdominal injury (hepatic rupture). Figure 4.1(d) shows three AIS 5 ground related head injuries (cerebral hematoma, skull fracture), three AIS 5 ground related spinal injuries (laceration of the spinal cord) and a single AIS 5 thorax injury (fracture of the ribs with flail chest). Few lower extremities injuries are coded as AIS 5 and AIS 5 face injuries or upper extremities injuries do not exist. Thus spinal injuries account for a substantial proportion of AIS 5 ground related injuries.



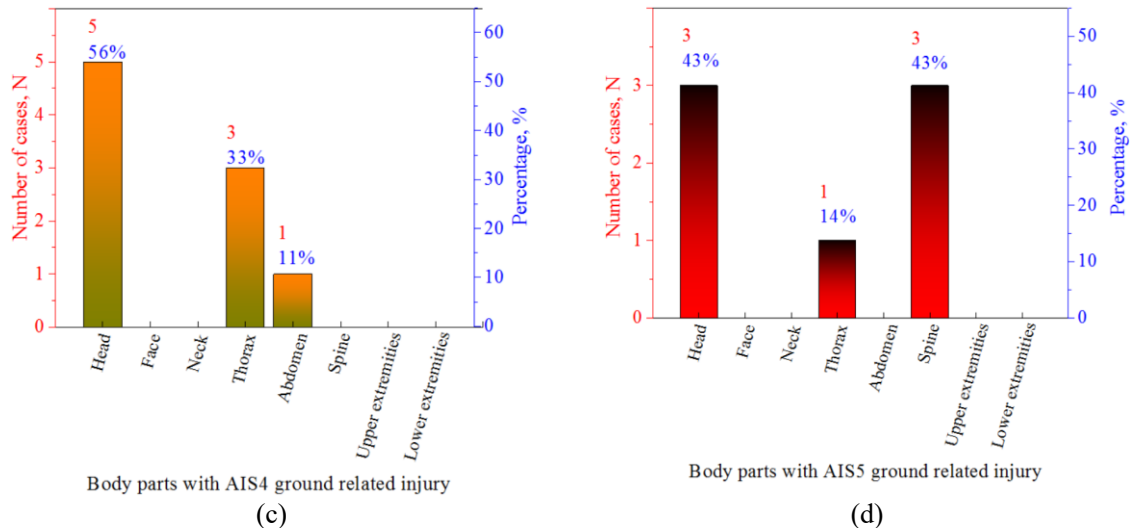


Figure 4.1 Number of cases and percentage distribution of body regions injured by pedestrian ground contact for different AIS levels: (a) AIS 2, (b) AIS 3, (c) AIS 4, and (d) AIS 5.

Figure 4.2 presents the proportion of injuries associated with ground contact at each AIS level, showing that 43% (n=527) of cases had injuries resulting from ground contact. When the maximum AIS was 1, the ground was coded as the source of an AIS 1 injury in 57% (n=424) of cases. Similarly, when the maximum AIS was 2, the ground was coded as the source of an AIS 2 injury in 24% (n=73) of cases. This proportion reduces steadily with increasing AIS level. Table 4.4 shows detailed information for the eight cases involving ground related MAIS 4 and 5 injuries. The vehicle speeds varied from 15 to 55 km/h and the vehicles involved were mostly sedans. Three of these cases were fatal and in one case the pedestrian was over 80 years old.

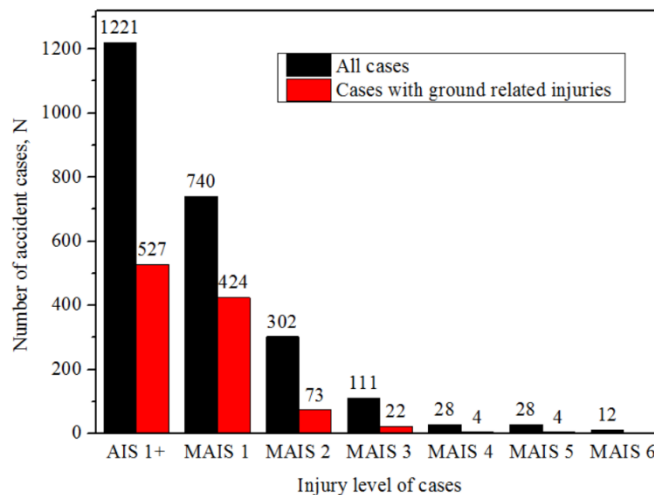


Figure 4.2 GIDAS cases with and without ground related injuries. At each MAIS level, the black columns show the total number of cases and red columns show the number of cases where the highest AIS injury is associated with ground contact.

Table 4.4 Detailed information for the MAIS4/5 ground related injury cases

No.	Vehicle type	Vehicle speed (km/h)	Sex (M/F)	Age (years)	Height (cm)	NBLEH	MAIS	Fatal (Y/N)
1	BMW 3 series (1998 - 2007)	37	M	79	NA	NA	5	N
2	Volvo 300 (1976 - 1990)	38	F	72	NA	NA	5	N
3	Ford Mondeo (2000 - 2007)	39	M	73	159	0.91	5	N
4	Smart Fortwo (1998 - 2006)	46	M	43	162	0.78	5	Y
5	VW T5 (2003 -)	15	F	55	160	1.33	4	N
6	Mits. Galant (1997 - 2003)	50	F	63	160	0.88	4	Y
7	VW Passat V (1996 - 2005)	55	F	89	153	0.92	4	Y
8	Honda Civic V (1991 - 1995)	NA	M	8	130	1.03	4	N

4.3.2. Effect of vehicle impact speed on pedestrian ground related injury

Figure 4.3 shows the distribution of vehicle speed for AIS 2, 3 and 4-5 ground related injuries (AIS 4 and 5 are combined as there are few cases). ANOVA analysis showed that mean speed differences between AIS 2 and AIS 3 were not significant, see Table 4.5 and Figure 4.3. However, the mean speeds for AIS 2 and AIS 3 were both significantly lower than for AIS 4-5.

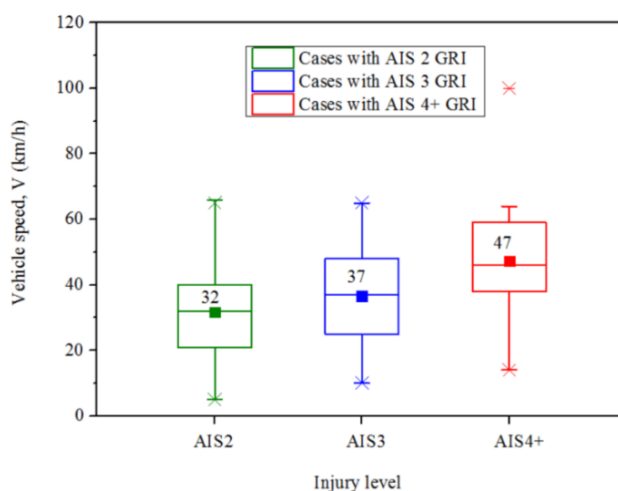


Figure 4.3 Distribution of vehicle speeds for AIS 2, AIS 3 and AIS 4-5 ground related injuries (GRI).

Table 4.5 ANOVA comparisons of vehicle speeds for different AIS categories

Group	N	Mean	Std. Deviation	Effect size r	Standard	Sig.	
AIS 2	107	31.7	13.4	vs. AIS 3	-0.18	Small	0.081
				vs. AIS 4+	-0.40	Large	< 0.001
AIS 3	35	36.7	14.2	vs. AIS 2	-0.18	Small	0.081
				vs. AIS 4+	-0.28	Medium	0.021
AIS 4+	14	47.3	15.1	vs. AIS 2	-0.40	Large	< 0.001
				vs. AIS 3	-0.28	Medium	0.021

Figure 4.4 shows the speed distributions for AIS 2+ ground related injuries to the head, thorax, spine, upper extremities and lower extremities. The Kruskal-Wallis test showed significant median speed differences between upper extremities and head injuries ($P=0.044$), upper extremities and thorax injuries ($P=0.024$), upper extremities and spine injuries ($P=0.011$), lower extremities and thorax injuries ($P=0.039$) and lower extremities and spine injuries ($P=0.018$).

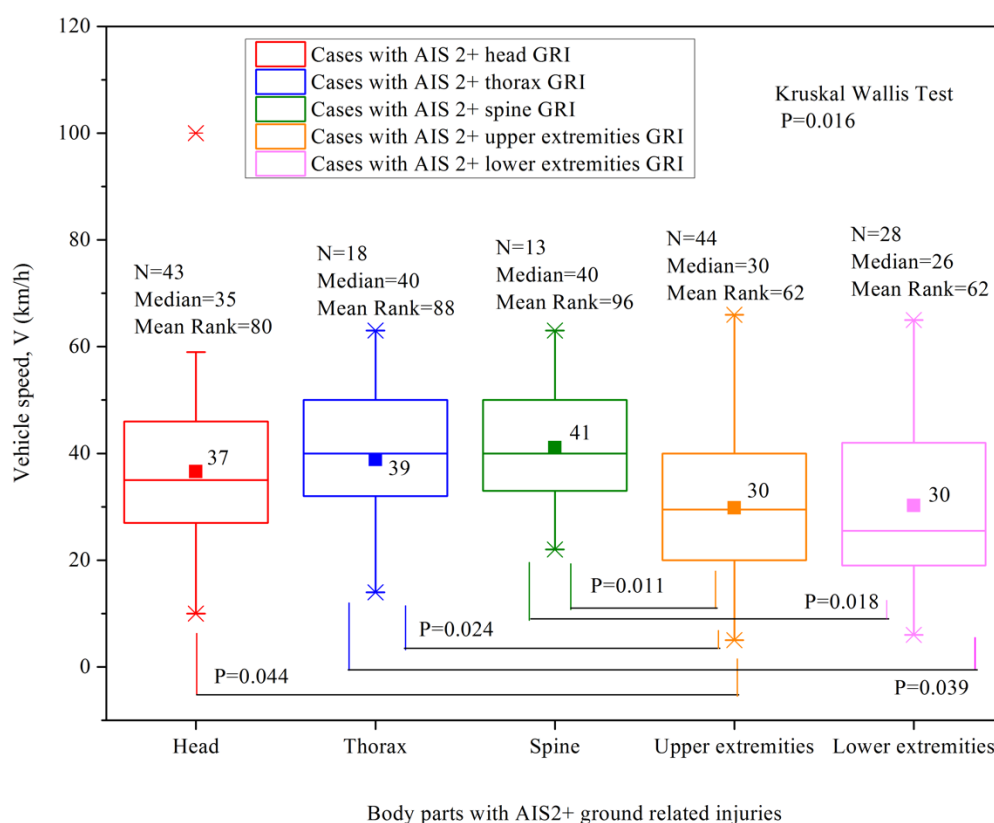


Figure 4.4 Distribution of vehicle speed for AIS2+ ground related injuries (GRI) across body regions.

4.3.3. Effect of pedestrian age on pedestrian ground related injury

Figure 4.5 shows the pedestrian age distributions for AIS 2, AIS 3 and AIS 4-5 ground related injuries. The Kruskal-Wallis test showed significant median age differences between AIS 2 and AIS 3 ($P=0.025$) and between AIS 2 and AIS 4+ categories ($P=0.009$). The age distributions for AIS 2+ ground related injuries to the head, thorax, spine, upper extremities and lower extremities are shown in Figure 4.6. The Kruskal-Wallis Test shows the increased age-associated with thorax injuries is significant ($P = 0.028$). Pairwise comparisons of pedestrian age for injuries to the different body regions show the median pedestrian age for ground related thorax injuries is higher than for head injuries ($P=0.001$), spinal injuries ($P=0.029$), upper extremities injuries ($P=0.007$) and lower extremities injuries ($P=0.041$).

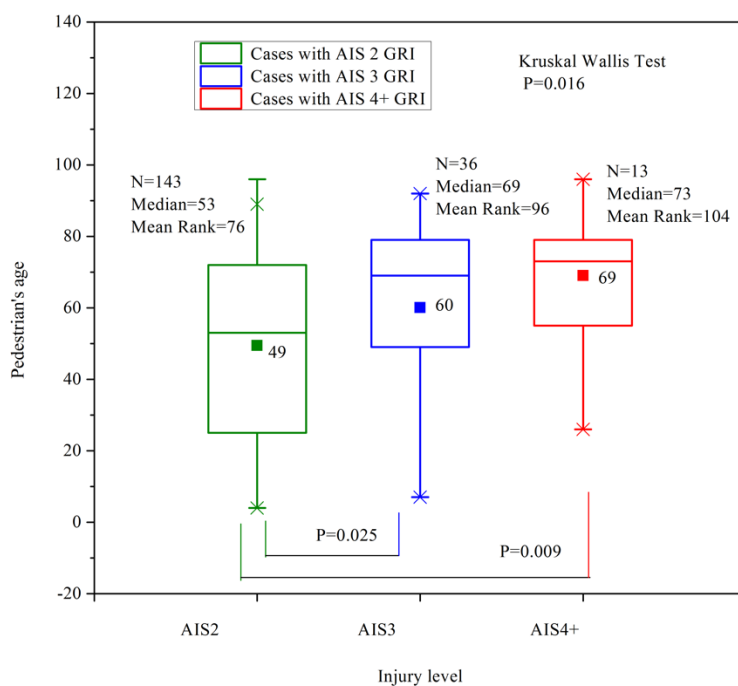


Figure 4.5 Distribution of pedestrian age for AIS2, AIS 3 and AIS 4-5 ground related injuries (GRI).

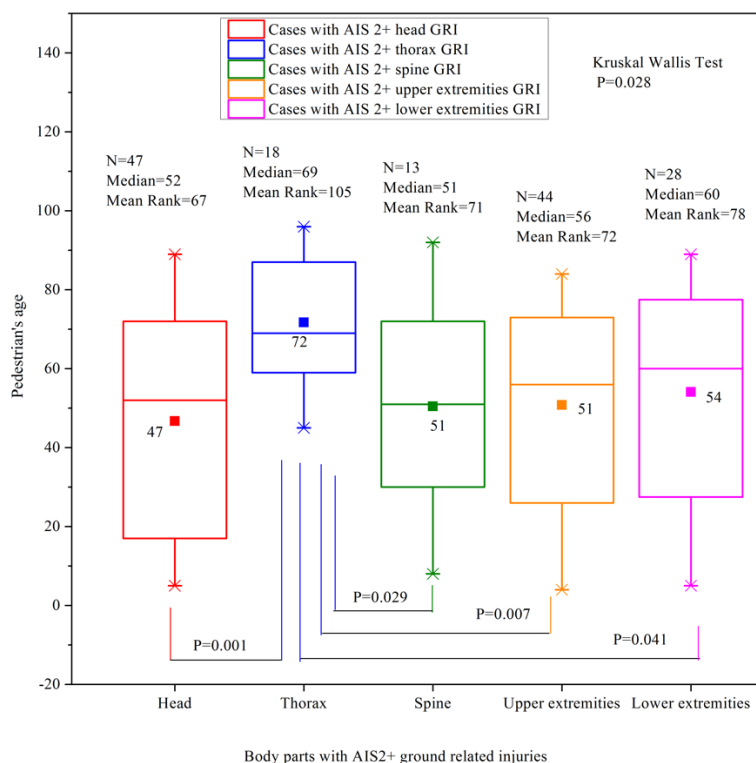


Figure 4.6 Pedestrian age distribution for different body regions with AIS2+ ground related injuries.

4.3.4. Effect of vehicle production year on pedestrian ground related injury

Chi-squared tests and Fisher’s Exact Test show the proportion of adult pedestrian cases with AIS 2+ ground related injuries for all body regions (Table 4.6) and the head only (Table 4.7) for older (pre-2005) versus newer vehicles (since 2005). No significant differences were observed.

Table 4.6 Chi-squared Test of differences in ground related/non-ground related AIS 2+ whole-body injury cases for newer versus older vehicles (adults only)

	Cases with AIS 2+ ground related injuries	Cases without AIS 2+ ground related injuries	Pearson Chi-Square	P-value
Older vehicles	109	645	0.039	0.528
Newer vehicles	6	47		

Table 4.7 Fisher’s Exact Test of differences in ground related/non-ground related AIS 2+ head injury cases for newer versus older vehicles (adults only)

	Cases with AIS 2+ ground related head injuries	Cases without AIS 2+ ground related head injuries	P-value
Older vehicles	32	722	0.611
Newer vehicles	2	51	

4.3.5. Effect of vehicle front shape on pedestrian ground related injury

Figure 4.7 shows the relation between NBLEH and AIS 2, AIS 3 and AIS 4-5 ground related head injuries. The median NBLEH increases from 0.86 for AIS 2 to 0.91 for AIS 3 and 0.95 for AIS 4-5. However, the Kruskal-Wallis Test shows these differences are not significant (P=0.366). There are only four AIS 4-5 ground related head injuries.

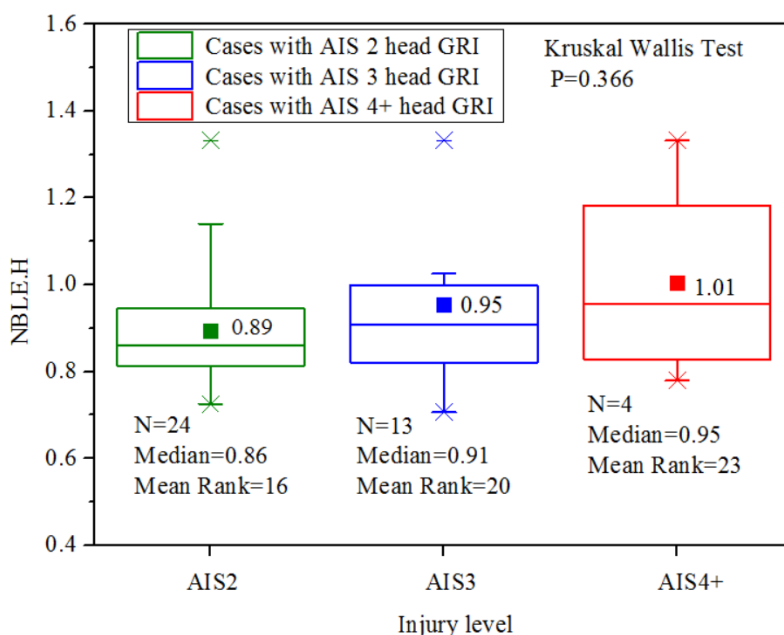


Figure 4.7 Distribution of NBLEH for cases with AIS2, AIS3 and AIS4-5 ground related head injuries.

The multicollinearity detection showed it is feasible to perform logistic regression of AIS 2+ ground related head injuries as a function of speed, age and NBLEH for adults (VIF parameters all less than 2.5). Table 4.8 shows that for adult pedestrian cases the speed, age and NBLEH were all significant predictors of AIS 2+ ground related head injury. There were insufficient cases for meaningful logistical regression for the children and adolescent categories.

Table 4.8 Logistic regression results for speed, age and NBLEH vs ground related AIS 2+ head injuries (age 18+)

Parameter	Boundary values	β	P-value	OR (95% CI)
Constant	/	-9.665	/	/
Speed	3-116 km/h	0.029	0.019	1.029 (1.005-1.055)
Age	18-96 year	0.025	0.030	1.026 (1.002-1.050)
NBLEH	67-133%	4.693	0.011	109.234 (2.910-4100.470)

Based on Equation 4.1, Equation 4.2 and Equation 4.3, the average AIS2+ ground related head injury risk as a function of vehicle speed, pedestrian age and NBLEH can be described as:

$$p = \frac{\exp(-9.665 + 0.029 * \text{speed} + 0.025 * \text{age} + 4.693 * \text{NBLEH})}{1 + \exp(-9.665 + 0.029 * \text{speed} + 0.025 * \text{age} + 4.693 * \text{NBLEH})} \quad \text{Equation 4.3}$$

The average AIS2+ ground related head injury risks as a function of NBLEH for different speeds and ages are shown in Figure 4.8.

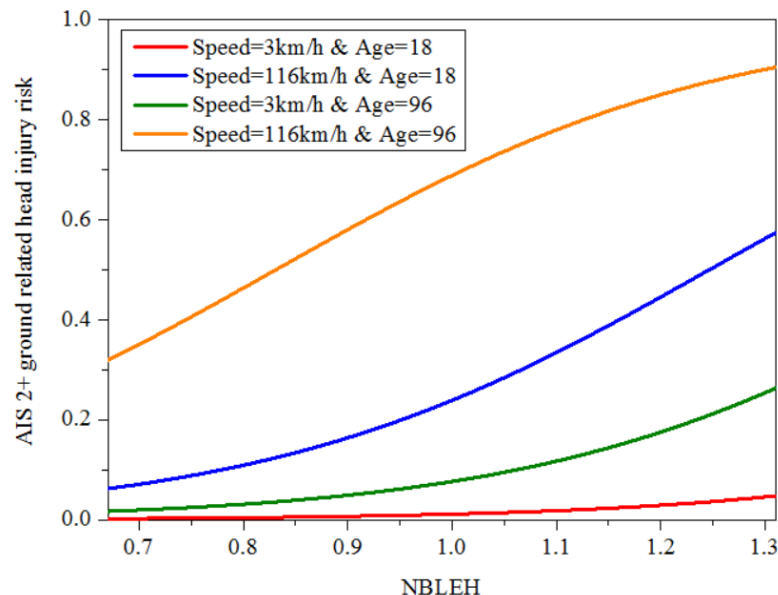


Figure 4.8 Average AIS2+ ground related head injury risk as a function of NBLEH for different speed (km/h) and age (years) levels.

4.3.6. Potential reduction in ground contact injury costs

Table 4.9 shows the proportion of calculated pedestrian injury costs for cases with vehicle collision speeds below 40 km/h, separated into categories of 0-20km/h, 0-30km/h and 0-40km/h. Based on this data, Table 4.10 shows the average proportion of ground related injury cost for vehicle collision speeds below 20, 30 and 40 km/h, respectively.

Table 4.9 -1 Total and ground related injury cost (US\$): (A) Cases with vehicle impact speed < 20km/h

Case No.	Total Injury Cost	Ground Related Injury cost (\$)	Ground Related Injury Percentage (%)	Case No.	Total Injury Cost (\$)	Ground Related Injury cost (\$)	Ground Related Injury Percentage (%)
1	70502	35251	50	12	38699	35251	91
2	141004	141004	100	13	70502	35251	50
3	70502	70502	100	14	120081	120081	100
4	141004	141004	100	15	238693	236625	99
5	45595	45595	100	16	141004	105753	75
6	10147	6896	68	17	109201	109201	100
7	81382	81382	100	18	147900	42147	29
8	596580	21521	4	19	105753	35251	33
9	164784	129533	79	20	29250	14625	50
10	596580	196823	33	21	123529	123529	100
11	524348	442966	84				

Table 4.9-2 Total and ground related injury cost (US\$): (B) Cases with vehicle impact speed \geq 20km/h & < 30km/h

Case No.	Total Injury Cost	Ground Related Injury cost (\$)	Ground Related Injury Percentage (%)	Case No.	Total Injury Cost (\$)	Ground Related Injury cost (\$)	Ground Related Injury Percentage (%)
22	38699	38699	100	37	96007	14625	15
23	109201	109201	100	38	73950	70502	95
24	132981	38699	29	39	49876	49876	100
25	70502	70502	100	40	49043	49043	100
26	21521	21521	100	41	123976	61988	50
27	141004	70502	50	42	118062	59031	50
28	105753	70502	67	43	73950	73950	100
29	115148	115148	100	44	90405	86957	96
30	53324	53324	100	45	38699	38699	100
31	112649	77398	69	46	130722	60220	46
32	156052	64978	42	47	202103	35251	17
33	116097	80846	70	48	874668	105753	12
34	109201	73950	68	49	251731	133669	53
35	70502	35251	50	50	392404	286651	73
36	51944	51944	100				

Table 4.9-3 Total and ground related injury cost (US\$): (C) Cases with vehicle impact speed ≥ 30 km/h & < 40 km/h.

Case No.	Total Injury Cost	Ground Related Injury cost (\$)	Ground Related Injury Percentage (%)	Case No.	Total Injury Cost (\$)	Ground Related Injury cost (\$)	Ground Related Injury Percentage (%)
51	596580	23780	4	70	55392	18073	33
52	194328	120378	62	71	109201	38699	35
53	73950	73950	100	72	280204	59031	21
54	88575	53324	60	73	94522	18073	19
55	205208	205208	100	74	194328	159077	82
56	112759	112759	100	75	152450	18073	12
57	72570	37319	51	76	176255	35251	20
58	100687	100687	100	77	69375	69375	100
59	176255	105753	60	78	53324	18073	34
60	187718	35251	19	79	170300	38699	23
61	183151	105753	58	80	596580	65436	11
62	92023	92023	100	81	596580	400677	67
63	144452	109201	76	82	782534	747283	95
64	314355	76449	24	83	831679	725926	87
65	101178	101178	100	84	331587	70502	21
66	179218	105268	59	85	41853	18073	43
67	56772	56772	100	86	53144	53144	100
68	412217	108578	26	87	596580	23780	4
69	154699	115312	75	88	194328	120378	62

Table 4.10 Average proportion of ground related injury cost for different speed categories

Speed range	Number of cases	Proportion of costs reduction
0-20 km/h	N=21	74%
0-30 km/h	N=50	72%
0-40 km/h	N=88	66%

4.4. Discussion

This study presents the first detailed review of the distribution of pedestrian ground contact injuries since 2001 [Otte and Pohlemann 2001]. Over half of AIS 1 injuries to pedestrians were coded as ground contact injuries, see Figure 4.2 Head injuries are distributed over all AIS levels except AIS 6 (there was no ground related AIS 6 injuries observed, though there were fatalities). However, the proportion of ground contact injuries reduces quickly as AIS level increases, with only 4/28 cases being from ground contact for both MAIS 4 and MAIS 5, similar to the general trend observed by Ashton and Mackay in the 1980s [Ashton and

Mackay 1983]. Higher vehicle speeds produce ground related injuries in the spine, thorax and head and these should be the focus of prevention efforts. However, severe and critical injuries from the ground were not only caused at high vehicle speed but also resulted from collisions by sedans at medium and low speed (see Table 4.4).

Increased vehicle speeds resulted in significantly higher injuries from ground contact, see Figure 4.3 and Table 4.5. However, two cases with AIS 4+ ground related injuries occurred at low vehicle speeds (< 20km/h). One was a 55-year-old female (case no.5 in Table 4.4) struck by a large van (NBLEH = 1.33) at 15 km/h, suffering a cerebral hematoma (AIS 4). The other case involved a 96-year-old male (not included in Table 4.4) as he was MAIS 6 from contact with the vehicle) who broke more than 5 ribs with flail chest caused by ground contact after being struck by a small sedan at 14 km/h, NBLEH = 0.91. There were also four high-speed cases (> 100 km/h) without AIS 2+ ground related injuries, and three of these were fatal with the windscreen contact coded as the highest AIS level. These detailed cases highlight the variability of ground related injuries and the importance of ground related injuries for some low-speed collision cases.

Age is an important factor for pedestrian ground related injuries, with significant age increases for higher AIS levels, see Figure 4.5. Although others [Niebuhr *et al.* 2016, Li *et al.* 2017a] observed similar trends for pedestrian injuries from vehicle contact, this has not previously been reported for ground related injuries. Furthermore, the data show for the first time that the average age of pedestrians with AIS 2+ thorax injuries from ground contact is substantially higher than for head, spine and upper/lower extremities injuries, see Figure 4.6. Thus, serious thorax injuries from ground contact are mostly associated with older people (> 60). Another real-world crash data analysis [Koppel *et al.* 2011] showed older drivers (> 65) suffered sustained a significantly higher proportion of thorax injury (30.9%) compared to of (18.5%) middle-aged drivers (41-55 y.o).

Table 4.6 and Table 4.7 show no statistically significant change in the proportion of ground related pedestrian injuries from newer vehicles (model year since 2005) compared to older vehicles (model year before 2005). However, there are only eight cases with AIS 2+ ground related head injuries for model years since 2005 and this analysis should be repeated when more cases become available.

Male pedestrians account for 48.2%, 43.2% and 57.1% of the cases involving AIS2, AIS3 and AIS4+ ground contact injuries, respectively (see Figure 4.9). Chi-squared Test shows no statistically significant difference in ground related injury levels between female and male pedestrian.

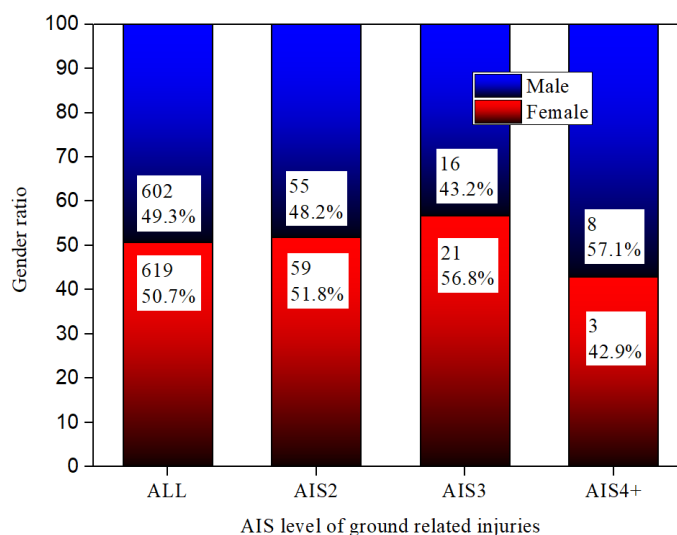


Figure 4.9 Distribution of gender for cases with AIS1+, AIS2, AIS3 and AIS4+ ground related injuries.

The logistic regression analysis shows for the first time a statistically significant influence of normalized bonnet leading-edge height on adult pedestrian head injury outcome from ground contact, see Table 4.8. This provides some support for recent computational modelling predictions which have identified relationships between vehicle shape and pedestrian ground contact injuries [Kendall *et al.* 2006, Tamura and Duma 2011a, Tamura *et al.* 2014, Crocetta *et al.* 2015]. Caution is however required since the present GIDAS data also show that increases in the median normalized bonnet leading edge height (NBLEH) with increasing AIS level are not statistically significant (Figure 4.7). This may be a reflection of the small number of cases at AIS 4-5 level and further evaluation is required as more cases become available.

The assessment of the potential injury cost savings if ground contact injuries from low-speed collisions were prevented showed very significant benefits, with more than half of the injury costs eliminated for all collisions below 40 km/h and almost three quarters of the injury costs

eliminated for collisions below 20 km/h. Given the relatively low injury risk from vehicle contact for pedestrians struck below 30 km/h [Rosén *et al.* 2011] and the move towards 30 km/h speed limits in many urban areas, implementation of technology such as the recent Google patent [Khaykin and Lerner 2016]. These injury data show that countermeasures to address ground contact injuries during lower speed collisions are needed if there are to be substantial further reductions in pedestrian injury costs. However, interventions will need substantial engineering development.

There are several limitations to this analysis. Most importantly, there is inevitable uncertainty in the coding of the source of each individual injury (ground versus vehicle), though the GIDAS methods have been well documented (Otte, 2001, 2004), and each case is the subject of detailed collision reconstruction. Ascertaining the source of brain and extremity injuries is likely to pose the most difficulties, while the source of soft tissue and bone fractures are usually easier to determine. There were only four SUV cases and 24 van cases with complete information, making an assessment of the effects of vehicle type impractical. Furthermore, individual pedestrian hip height was not available and was estimated based on overall pedestrian height. No information on pedestrian kinematics was available, hampering direct comparisons with previous multibody model predictions. The effects of pedestrian initial gait position were not considered (not recorded), even though the gait stance affects the kinematics and hence ground contact injuries [Simms and Wood 2006, Masson *et al.* 2007, Untaroiu *et al.* 2009, Crocetta *et al.* 2015]. Pedestrian orientation also affects injury outcome [Simms and Wood 2006], but this was also not considered since about 80% of pedestrians in the GIDAS data were laterally impacted. Vehicle speed for each case was calculated based mainly on available braking traces on the road and the pedestrian projection distance, wrap around distance and numerical reconstruction of the collision cases (Otte, 2001, 2004), and some uncertainty is inevitable.

4.5. Conclusion

The recent GIDAS pedestrian data show for the first time that head, thorax and upper/lower extremities injuries are the most important pedestrian ground related injuries following a vehicle impact, while upper/lower extremities injuries generally occur at lower AIS levels. Avulsion of the scalp, brain injuries, skull fracture and fractures of upper and lower extremities are frequent AIS 2 injuries from ground contact. For AIS 4 and 5 injuries,

cerebral hematoma, skull fracture, fracture of the ribs with flail chest and laceration of the spinal cord are common. Increasing vehicle speed and pedestrian age both adversely affect the severity of ground related injuries. The average vehicle impact speed for AIS 2+ ground related upper extremity injuries is significantly lower than for head, thorax and spine injuries. Older pedestrians are more at risk of thorax injuries. The proportion of ground related head injuries in AIS 2+ cases is higher for more recent vehicle models, but the difference is not statistically significant. Similarly, the median normalized bonnet leading-edge height is higher for AIS 4+ compared to AIS 2 head injuries from the ground, but again this difference was not statically significant and future assessment with larger sample sizes is needed. Prevention of all ground related pedestrian injuries for vehicle impact speeds below 40 km/h would bring very substantial injury cost reductions. These data provide significant motivation for the development and implementation of countermeasures to address pedestrian ground related injuries.

5. Study 2: Video analysis of real-world collisions

5.1. Introduction

Only a few studies of pedestrian secondary ground contact have analyzed real-world videos [Barry and Simms 2016, Han *et al.* 2017]. Analysing real-world videos is the most intuitive and the most authentic way to gain a basic understanding of pedestrian ground contact as it occurs in real-world collisions. In 2017, Han *et al.* summarized the distribution of a body landing region during ground contact from 160 real-world crash videos. Head and extremities were found to be the most frequent body region which impacts the ground first after being hit by the vehicles. Li *et al.* [Li *et al.* 2018] categorized the pedestrian landing mechanisms by observing 134 real-world accident videos. They found that vehicle impact speeds and kinematic trajectories were the dominating factors influencing landing mechanisms. Pedestrians who were thrown forward after vehicle contact and impact the ground without a clear rotational tendency was the highest (49.3%) observed mechanism in all 134 cases.

Even though the pedestrian ground impact mechanisms were observed and the effect of impact speed, vehicle type on pedestrian rotation angle, pedestrian trajectories were analyzed [Han *et al.* 2017], the effect of NBLEH on pedestrian ground contact in real-world collision has not been assessed. Therefore, videos of real-world vehicle-pedestrian collisions were collected and analyzed to:

- (1) gain a basic understanding of pedestrian ground contact mechanics.
- (2) assess how the influencing factors (including NBLEH) affect the kinematics mechanisms of pedestrian ground contact.

5.2. Methods

5.2.1. Videos of real-world vehicle-pedestrian collisions

Videos were obtained from online sources, i.e. Youtube, see the examples of video sequences demonstrated in Figure 5.1. Cases were selected with the following criteria applied:

1. Only one vehicle involved in vehicle-pedestrian collisions and the vehicle shape could be easily identified.
2. Pedestrians were first impacted by the front components of the vehicle.

3. The pedestrians had a secondary ground contact with the ground and the impact process was captured.

In total 29 cases were analysed in this study, the kinematic sequence of pedestrian are illustrated in Appendix B. Vehicle speeds, pedestrian projections were estimated with the same methods applied in [Barry and Simms 2016, Han *et al.* 2017]. For each case, parameters like vehicle speed, pedestrian rotation angle before landing on the ground, head-ground impact speed, vehicle bonnet leading-edge height, pedestrian height etc were recorded.

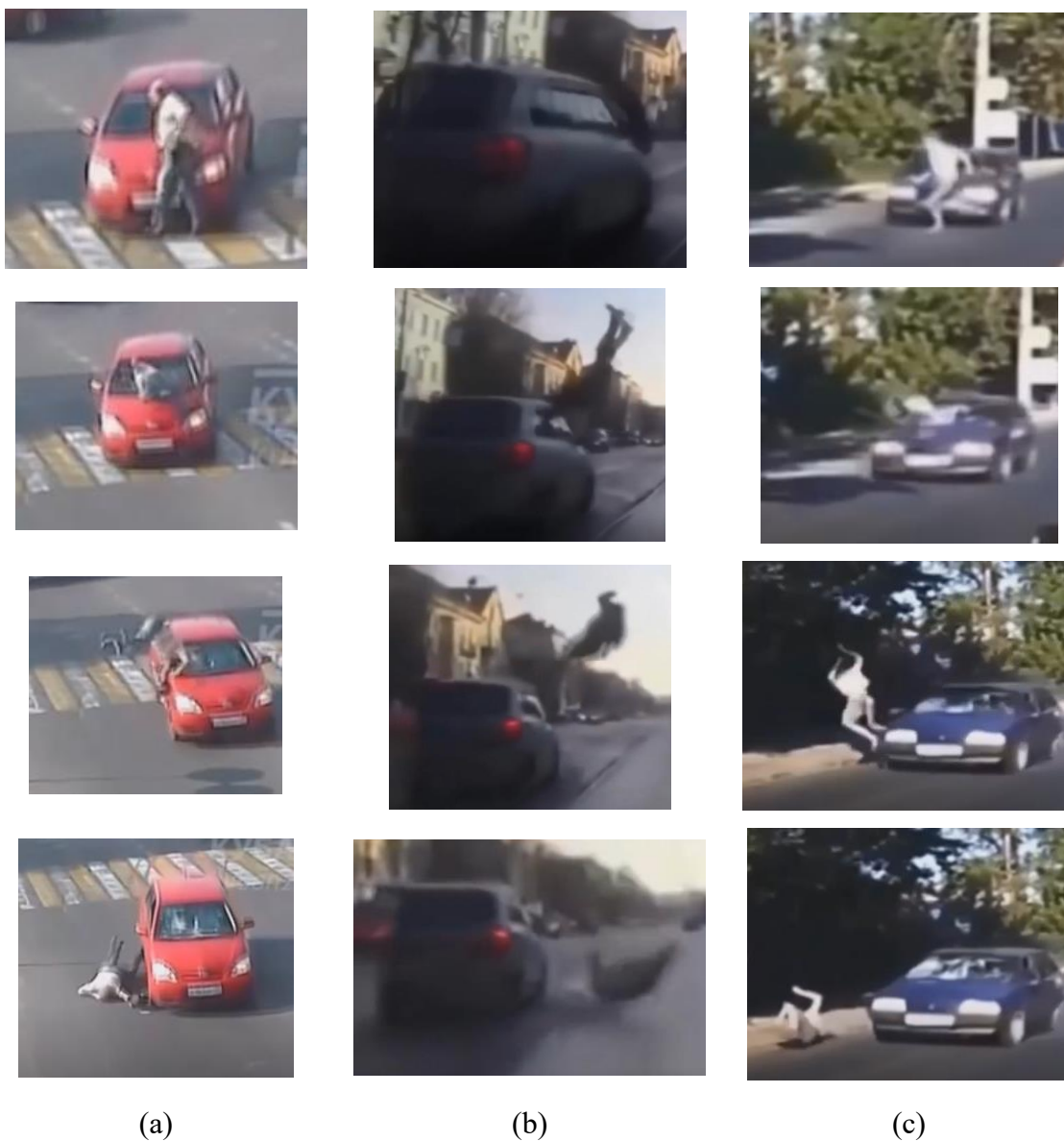


Figure 5.1 Three sample sequences of vehicle-pedestrian collision captured by video

5.2.2. Estimation of vehicle speed, projection distance

Since there is no detailed pedestrian and vehicle information of the crashes, visual estimation was used for estimating pedestrian heights, vehicle front end heights and vehicle lengths. Vehicle front end heights and projection distances were estimated based on the ratio of pedestrian heights. The time intervals were extracted by frame rates. The vehicle speed was calculated based on a particular distance and relevant interval.

$$S = L_V \times N \quad \text{Equation 5.1}$$

$$V = 3.6 \times S \times \frac{f}{m}, \quad \text{Equation 5.2}$$

where S is the distance vehicle travelled, L_V is the length of the vehicle, N is the distance travelled by the vehicle in multiples of the vehicle's length, f is the frame rate of the real-world videos, m is the number of the frames during the distance.

5.3. Results

The impact processes of vehicle-pedestrian contact, as well as the following pedestrian ground contact, were observed from the real-world videos. The collisions generally occurred when (1) the vehicle was turning left/right at the crossroads and hit the pedestrian; (2) the pedestrian suddenly emerged from the next lane and was impacted by the vehicle. In 15 of 29 cases, the evidence of voluntary motion (standstill, step back, stoop backwards, push the bonnet) of the pedestrian was observed even in a very short period. The head impacting the ground first was observed in 13 of 29 cases with different kinds of contact mechanisms. In most cases, the pedestrian was hit by the car on the thigh or hip first and then the body rotated forward to the windshield and had contact with the head. Following this, the pedestrian would either fall onto the ground directly or be thrown into the air, subsequently falling to the ground. The relation of vehicle speed and pedestrian projection and the relation of normalized bonnet leading edge height (NBLEH) and pedestrian whole-body rotation were studied.

5.3.1. The relationship between vehicle speed and pedestrian projection distance

Figure 5.2 shows the relationship between pedestrian projection and vehicle impact speed. The fitting curve indicated a general trend that higher vehicle speeds produce a larger pedestrian projection, which is as expected and is consistent with previous studies [Simms and Wood 2009]. It is also noted that in most of these selected cases, the impact speeds were between 15 km/h to 45 km/h excluding one case with a vehicle speed of 72 km/h (as shown in Figure 5.2). For this case, the incident vehicle was running the red light at a tremendous speed and then hit a pedestrian who was walking on the pavement. The pedestrian noticed the car was running toward him and moved back a step and made a self-protective reaction at the meantime.

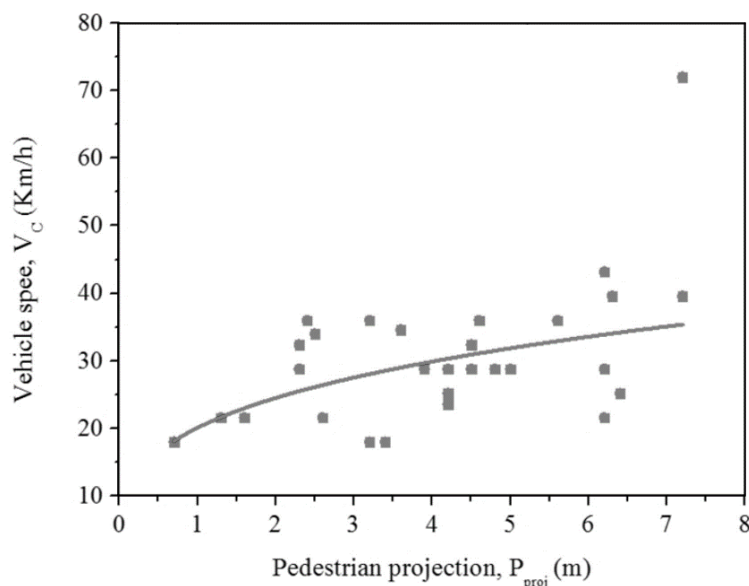
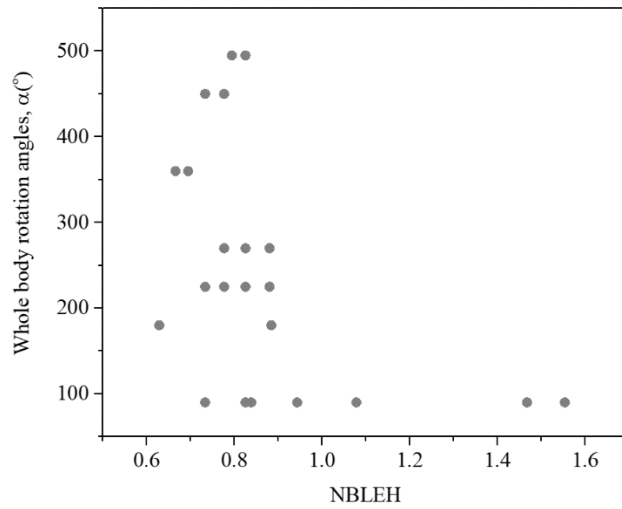


Figure 5.2 The relation of pedestrian projection and vehicle impact speed

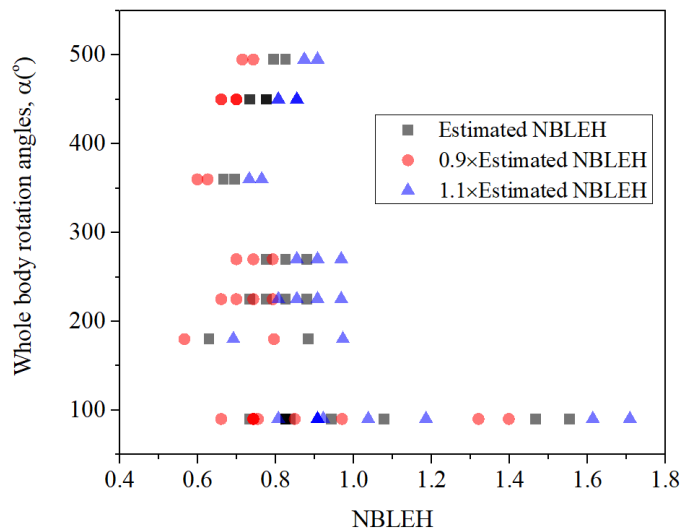
5.3.2. The relationship between Normalized BLEH and whole-body rotations

It is widely predicted from modelling studies [Bouquet *et al.* 1994, Simms *et al.* 2011, Crocetta *et al.* 2015, Yin *et al.* 2017] that vehicle bonnet leading edge height (BLEH) has a significant influence on pedestrian ground contact mechanism and hence injury outcome. The relation of estimated NBLEH and whole-body rotations Figure 5.3 (a) shows the relation of Normalized BLEH (NBLEH = BLEH/pedestrian hip height) and whole-body rotations in real-world collisions for the first time. An error analysis of possible effects of +10% or -10% in estimate change was conducted to check the reliability of the estimation, as shown in

Figure 5.3 (b). Results show that smaller NBLEH produces larger whole-body rotation angles. In addition, a sharp drop is observed after NBLEH>0.9 and large scatter below that.



(a) The relation of estimated NBLEH and whole-body rotations



(b) Error analysis of possible effects of +10% or -10% in estimate change

Figure 5.3 The relation of Normalized BLEH and whole-body rotations

5.4. Discussion

Twenty-nine online videos of real-world vehicle-pedestrian collisions were selected and analyzed. The vehicle speed and pedestrian heights/vehicle BLEH were estimated by extracting the footages of the videos. These real-world videos showed the complete process of a pedestrian being impacted by vehicles (hip/thigh was hit first and then the pedestrian

rotated towards to the bonnet/windshield to have a head vehicle impact) and how the secondary ground contact happened. The pedestrian usually had a head-vehicle contact after being hit by the vehicle, then fell onto to the ground. If the impact speed was obviously fast, the pedestrian would be hit and fly in the air with rotations. The footage visually provided the display of vehicle-pedestrian impact.

Unfortunately, it is difficult to ensure that the important parameters like vehicle speed and moving distance are correct or similar to the actual values because a great number of the videos were captured by a driving recorder fixed on a moving car and the estimating method might produce large errors. Moreover, the images are not clear enough to observe pedestrian-ground contact in detail and the videos are lack any pedestrian injury information. Even though the work was done earlier than [Han *et al.* 2018b], the resulting data still provides relevant insights into vehicle-pedestrian collisions.

Results showed that after being impacted by a vehicle, the pedestrian sustained a larger projection distance for larger vehicle impact speeds, as expected. It's justifiable to assert that the vehicle shape is an important parameter in the resulting pedestrian's motion because The relation of estimated NBLEH and whole-body rotations demonstrated the varying relationship between NBLEH and the resulting whole body rotation angles, which is the first time this has been clearly demonstrated using real-world accident data.

A sharp drop-off in rotation is observed as the normalised bonnet leading-edge height reaches pelvic height. The estimated vehicle impact speeds were almost all between 20 and 40 kph and given that injuries are likely from the vehicle contact for 40 kph collisions, that allows us to focus on 20 and 30 kph speeds for studying the ground contact. Finally, since these real-world videos are not clear enough it sets up the need for staged cadaver tests with high-quality videos.

5.5. Conclusion

29 real-world vehicle-pedestrian collision videos were collected and studied to investigate the effect that the shape of a vehicle's front has on the resulting pedestrian ground contact. The common collision scenarios involved cases in which a vehicle was turning left/right at

the crossroads and hit the pedestrian or the pedestrian suddenly emerged into the motor lane and was impacted by the vehicle. Pedestrians showed voluntary motion (standstill, step back, stoop backwards, push the bonnet) in more than half of the selected cases. The head impacted the ground first in nearly half of the cases, but the head ground contact mechanisms were quite different. As predicted, a correlation between larger vehicle speeds and greater pedestrian projection distances was found.

Smaller NBLEH resulted in larger pedestrian whole-body rotations, which is the first occasion of this phenomenon being observed, therefore indicating the potential influence of vehicle front-end shape on the resulting pedestrian injuries from contact with the ground.

6. Study 3: Kinematics and dynamics of pedestrian head ground contact by cadaver testing program¹

6.1. Introduction

The World Health Organization reports nearly 300,000 pedestrian fatalities from road traffic collisions annually [WHO 2013], with many more injured. Injuries occur during the primary vehicle contact and, following a period of flight after separation from the vehicle, significant injuries often also occur during the subsequent ground contact. In early collision reconstruction work, Ashton and Mackay [Ashton and Mackay 1983] showed that for vehicle impact speeds below about 25km/h, ground contact injuries exceed those of vehicle contact, but at higher speeds, injuries from vehicle contacts predominate.

Pedestrian kinematics and injuries in contacts with vehicles are generally well understood, with vehicle speed/shape/stiffness and pedestrian age/height/stance all influencing subsequent motion and injuries, e.g. [Simms 2005, Simms and Wood 2009, Rosén *et al.* 2011, Kalra *et al.* 2016, Niebuhr *et al.* 2016, Li *et al.* 2017a, Li *et al.* 2017b, Shang *et al.* 2018d]. However, pedestrian ground contact involves a wide range of contact orientations and a complex combination of slide, roll and bounce to rest. The resultant injuries and their mechanisms are not well understood as significant challenges persist in predicting the kinematics of this long timeframe event and in retrospectively attributing injuries observed to either vehicle or ground contact [Simms and Wood 2009]. However, a recent analysis of the German collision database [Shang *et al.* 2018d] GIDAS showed that the head, thorax and spine dominate AIS 4-5 ground contact injuries, and ground contact injury severity increases with both pedestrian age and vehicle speed, which stated in Chapter 4. That study also found that, for collisions below 40 km/h, about two-thirds of pedestrian injury costs were attributed to ground contact, again emphasising the importance of ground contact

¹ Shang, S., Masson, C., Teeling, D., Py, M., Ferrand, Q., Arnoux, P-J., & Simms, C. (2020). Kinematics and dynamics of pedestrian head ground contact: a cadaver study. *Safety Science*, 127, 104684.

Shang, S contributed the conception and design of the study, preparation and perform of the tests, analysis of data and drafting the article and revising the article

Masson, C contributed the acquisition of PMHS, preparation and perform of the tests

Teeling, D contributed part analysis of MBIM analysis

Py, M contributed the acquisition of PMHS, preparation and perform of the tests

Ferrand, Q contributed the acquisition of PMHS, preparation and perform of the tests

Arnoux, P-J contributed the acquisition of PMHS

Simms, C contributed the conception and design of the study, the guide of the study and revising the article

injuries for low impact speeds [Shang *et al.* 2018d]. Badeo-Romero and Lenard assessed UK collisions and also found a significant role for ground contact [Badeo-Romero and Lenard 2013].

Of particular interest is the manner in which pedestrian ground contact injuries are influenced by vehicle speed and design in the speed range 20-40 km/h since this could lead to vehicle-based methods to reduce the severity of ground contact injuries in cases where pedestrian injuries from vehicle contact are mostly survivable. Recent computational modelling studies have posited various relationships between vehicle shape and pedestrian ground contact injuries [Kendall *et al.* 2006, Tamura and Duma 2011b, Gupta and Yang 2013, Tamura *et al.* 2014, Crocetta *et al.* 2015, Gupta *et al.* 2015, Xu *et al.* 2016b]. In particular, Crocetta *et al.* [Crocetta *et al.* 2015] reported on six identifiable ground contact “mechanisms” distinguished by the amount of whole-body rotation of the pedestrian prior to ground contact, with average head impact speed varying between the different mechanisms. Some support for identifying the influence of vehicle design on pedestrian ground contact was found by Shang *et al.* [Shang *et al.* 2018d] who used GIDAS collision data to show that the normalised bonnet leading-edge height (bonnet height/hip height) is a risk factor for adult pedestrian AIS2+ ground related head injuries. Further, Han *et al.* [Han *et al.* 2018b] analyzed 200 videos of vehicle-pedestrian crashes and found that vehicle front shape and impact speed both influence pedestrian ground contact kinematics. However, no pedestrian models (multi-body or finite element) are validated for ground contact and establishing initial conditions and injury outcomes in real-world video cases is challenging.

Cadaver tests can overcome many of these difficulties and provide model validation data and thus have the potential to greatly strengthen our understanding of pedestrian ground contact. However, previous cadaver tests have mainly focused on vehicle contact, with limited reference to ground contact [Kerrigan *et al.* 2007, Masson *et al.* 2007, Subit *et al.* 2008, Paas *et al.* 2015] and dummy tests [Taneda *et al.* 1973, Hamacher *et al.* 2011]. In early work, [Cavallero *et al.* 1983] performed 150 cadaver and dummy tests and concluded that head-ground contact locations are random and that head-ground contact speed could not be predicted by knowing the vehicle shape. However, all tests were performed at 32 km/h, vehicle shapes have changed substantially since the 1980s and no ground contact kinematics (accelerations or velocity changes) or injuries were reported. More recently, several

pedestrian cadaver studies have been performed at the University of Virginia and the University of Marseille using a range of vehicle shapes and pedestrian sizes [Kerrigan *et al.* 2007, Subit *et al.* 2008, Paas *et al.* 2015], but these studies all focused on vehicle contact (mostly at 40km/h), and ground contact kinematics/injuries were not evaluated. In fact, the sequence of pedestrian motion following head contact on the bonnet top or windscreen has received little attention.

In summary, pedestrian ground contact kinematics and injuries remain poorly understood. Various computational model predictions of ground contact mechanisms have been presented, but model validation is so far lacking. Reconstruction of real-world collisions shows an important role for ground contact at lower vehicle speeds, but the role of vehicle design in mediating pedestrian ground contact injury outcome remains uncertain and existing cadaver test data which includes ground contact is very limited. Accordingly, the aims of the current study are to:

- 1) develop a series of staged vehicle impact tests using cadavers to study the complete kinematic chain of events in a pedestrian collision, starting with first vehicle contact and ending after the pedestrian comes to rest on the ground.
- 2) use these staged tests to assess pedestrian post-impact kinematics as well as head ground contact in detail, including linear and rotational components of head injury risk.
- 3) assess potential interactive effects of vehicle speed and normalised bonnet leading edge height (BLEH) on pedestrian head injury risk during ground contact.

These data will serve to clarify pedestrian ground contact mechanisms and provide validation data for future model assessment.

6.2. Methods

6.2.1. Cadaver Test Setup

As part of the Faculty of Medicine of Marseille, the Laboratory of Applied Biomechanics is enabled to perform full-body human testing from body donations. Six cadaver tests were conducted to study pedestrian ground contact at LBA, IFSTTAR, Aix-Marseille Université: Faculté de Médecine-secteur Nord Marseille, France, the pairs of the tests are shown Table 6.1. Winckler's preparation [Winckler 1974] or zinc chloride [Goodarzi *et al.* 2017] was used for tissue preservation. For each subject, up to 54 anthropometric measures were performed,

and the external anthropometries are listed in Table 6.2. The study was approved by the Ethical Committee of Aix-Marseille University. Three vehicle types (Table 6.3) were tested to achieve different normalized bonnet leading edge heights (NBLEH), and each vehicle type was tested twice with nominally the same conditions (different cadavers but approximately the same initial stance). In each repeated test, damaged vehicle components were replaced (bumper, bonnet or windshield) as necessary. The expected mechanism (Table 6.4) for each case based on the simulation study by Crocetta *et al.* [Crocetta *et al.* 2015] is also shown. Five high-speed cameras (1000 fps) were placed to capture the whole pedestrian trajectory (Figure 6.1). A dry run of dummy test [Shang *et al.* 2018a] was performed to estimate the projection and therefore determine the appropriate positions to place the cameras. Nominal impact speeds of 20 or 30km/h were applied.

Table 6.1 Summary of PMHS tests performed

Test number	Vehicle speed (km/h)	Pedestrian/ vehicle size	NBLEH	Expected mechanism (M1-M6) [Crocetta <i>et al.</i> 2015] – see Table 6.4
Test 01	30.5	Peugeot 307 (sedan) + (Male, 88 y/o, 1.74m, 66kg)	0.7	M1 (most frequent) or M3 (less frequent) mechanism for adults struck by compact car at 30 kph – Figure 8 in [Crocetta <i>et al.</i> 2015]
Test 02	30.4	Peugeot 307 (sedan) + (Male, 83 y/o, 1.72m, 69kg)	0.7	
Test 03	20.4	Citroen C4 (compact)+ (Male, 94 y/o, 1.67m, 64kg)	0.9	M2 (most frequent mechanism for adults struck by any vehicle at 20 kph) - Figure 7 in [Crocetta <i>et al.</i> 2015]
Test 04	21.0	Citroen C4 (compact)+ (Male, 83 y/o, 1.67m, 55kg)	0.9	
Test 05	30.1	Renault Kangoo II (van)+ (Female, 94 y/o, 1.58m, 38kg)	1.2	M2 (most frequent) or M1 (less frequent) mechanism for adults struck by a Van at 30 kph) - Figure 8 in [Crocetta <i>et al.</i> 2015]
Test 06	30.4	Renault Kangoo II (van)+ (Male, 86 y/o, 1.62m, 69kg)	1.1	

Table 6.2-1 External anthropometry

Anthropometry	Test 01	Test 02	Test 03	Test 04	Test 05	Test 06
1 total height	174	172	167	167	157	163
2 eyes / ground height	166	161	162	155	147	153
3 acromion / ground height	149	144	145	137	121	141.5
4 elbow / ground height	116	110	109	106	97	110
5 iliac spine / ground height	95	94	91	91	84	95
6 trochanter / ground height	88	89	82	86	78	89.5
7 hauteur interligne genoux/sol	46	46	45	44.5	42	49
43 ankle height	6	8	7	10	5	8.5
44 a arm high circumference	27.5	31.5	31	25.3	18	28.5
44 b arm low circumference	26	28	28	24	17.5	27
48 a forearm high circumference	27	24	28.5	25	16.3	25.7
48 b forearm low circumference	19	19	20	19	12.5	18
49 hand length	20	18	19	18	13	20
36 thigh high circumference	42	46	46.5	40.5	33.5	47.5
37 thigh low circumference	35.5	38	39	36	27	39.5
38 knee circumference	37.5	38	36.5	37.5	33	37
39 calf circumference	30.5	31	29.5	30.5	20	29
40 ankle circumference	26	25	26.5	26.5	22.5	25
41 foot width	10	10	10.5	10.5	7	85
42 foot length	27.5	27	26.5	22.5	20	23
10 shoulder width	43	48	39.5	40.5	28.5	36
20 axillary thoracic width	36	35	31	39	27	34
23 thorax width under sternum	35	34	31	31.5	24	31

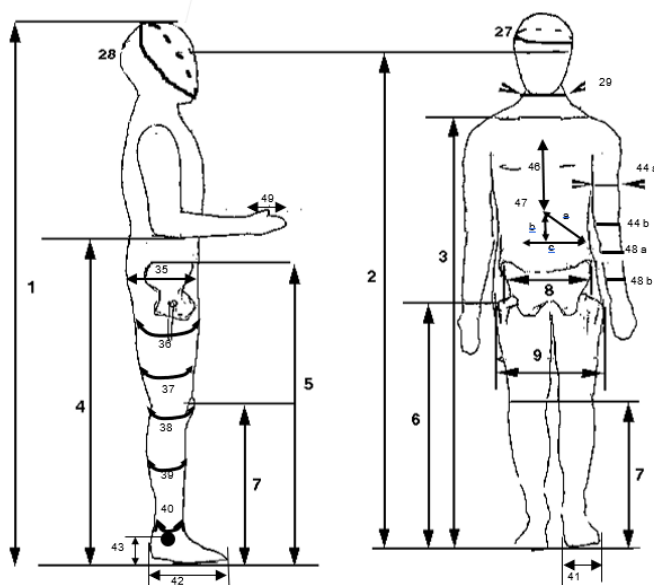


Table 6.2-2 External anthropometry (continued)

Anthropometry	Test 01	Test 02	Test 03	Test 04	Test 05	Test 06
30 abdomen width	37	36	29	37	26	33
8 pelvis width	35	35	26.5	26	26.5	28
9 bi-trochanter width	39	36	39	33	27	36
21 thoracic axillary thickness	27	22	23	12	9	12
24 thoracic thickness under sternum	-	22	18	18	15	21
33 abdomen thickness	18	17	17	14	25.5	21
35 buttocks thickness	16	17	19	14	12	15
26a head / forehead depth	26	21	19	18	16	18
26b head height	28	23.5	20	21.5	20	23
26c head width	17.5	18	16	14	12	15
27 head circumference	55.5	58	56	56	52	56.5
28 chin-occipital circumference	72	69	63	59	62	61
29 neck circumference	41.5	48	40.5	39	33.5	48
18 forearm + hand length	46	44	37	41.5	34	44.5
19 arm length	33.5	32	32	32	26	30
10 seat height	98	88	85	92	72	85
11 eyes / seat height	90	77	80	83	62	75
14 cervical / seat height	79	70	70	68	55	67
12 acromion / seat height	73	60	63	65	48	63.5
13 elbow / seat height	40	16	27	33	26	37
22 axillary thoracic circumference	93	104	93	89	79	98
25 thoracic circumference under sternum	85	93	87.5	75	77	101
31 abdominal circumference (navel)	83	88	78	75	78	91
32 pelvis circumference	88	94	90	87	72	96
16 knee / ground height	46	51	51	43	41	48
17 buttocks / knee length	40.5	52	38	30	35	29
34 pelvis / heel (stretched leg) length	88	93	93	82	78	97.5
45 T1 – coccyx length	75	68	65	-	47	64
46 sternum length	17	19	19	22	19	20
47 xiphoid angle (a, b, c)	(16 17 20)	(20 12 25)	(19 10 26)	(17 7 34)	(13 7 23)	(20 13 33)

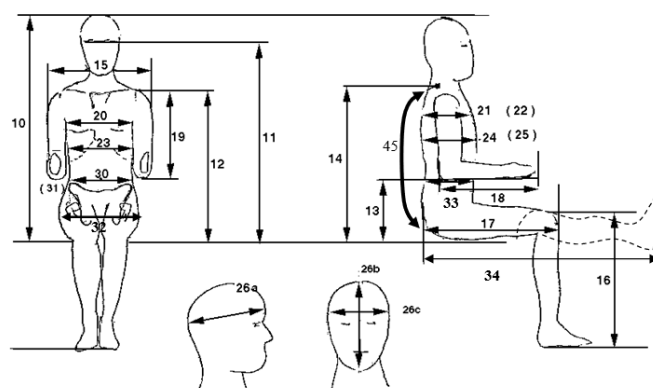





Table 6.3 Three different vehicles used in the impact experiments

Vehicle model	Pictures of vehicle	Partly parameters of vehicle
(a) Peugeot 307		Vehicle Height: 1510 mm Windshield Angle: 25.8° Bonnet Angle: 16.2° Bonnet length: 730 mm
(b) Citroen C4		Vehicle Height: 1491 mm Windshield Angle: 25.3° Bonnet Angle: 8.2° Bonnet length: 820 mm
(c) Renault Kangoo II		Vehicle Height: 1844 mm Windshield Angle: 38.4° Bonnet Angle: 8.2° Bonnet length: 540 mm

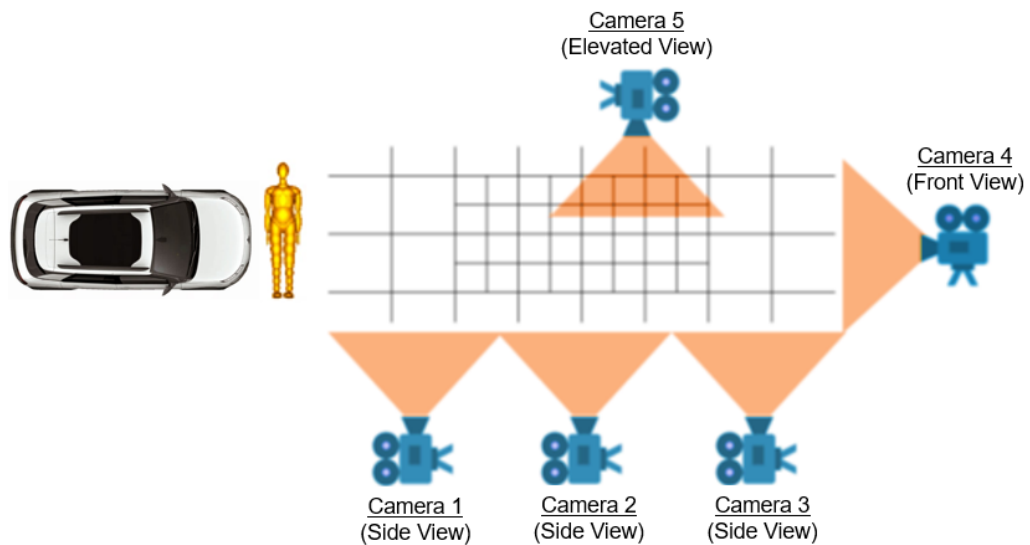


Figure 6.1 The general locations of the high-speed cameras

Table 6.4 Expected ground contact mechanisms [Crocetta *et al.* 2015]

Mechanism	Description
M1: wrap trajectory - pedestrian rotates 90°-180° before impacting ground head first	
M2: wrap trajectory - pedestrian rotates 0°-90° before impacting ground pelvis first, then head	
M3: wrap trajectory - pedestrian rotates 180°-270° before impacting ground head first	

The cadavers were held in position by a magnetic locking system which was automatically released just before the contact with the vehicle, see Figure 6.2 (a). Fiducial markers were used to record landmark positions on the head, extremities, pelvis, chest etc. The initial lower extremity joint angles are shown in Figure 6.3. Full braking ($\mu \approx 0.8$) was applied after the first pedestrian contact. For each test, six triaxial accelerometers (10 kHz sample rate with -3dB AA hardware filter) were inserted in the cadavers [see Figure 6.2 (b)]: one was inserted

in the chest, two were screwed on the left and right thigh bones, two were inserted in the ilium (left and right side) and one was inserted in the mouth to represent an approximate head CG. The mouth accelerometer was pressed against the palate and expanding foam was used to fill the mouth cavity. The accelerometer position was maintained during setting and curing. When dry, the surplus was removed and the head was equipped with a hood. Only the head accelerometer data is presented in this study.

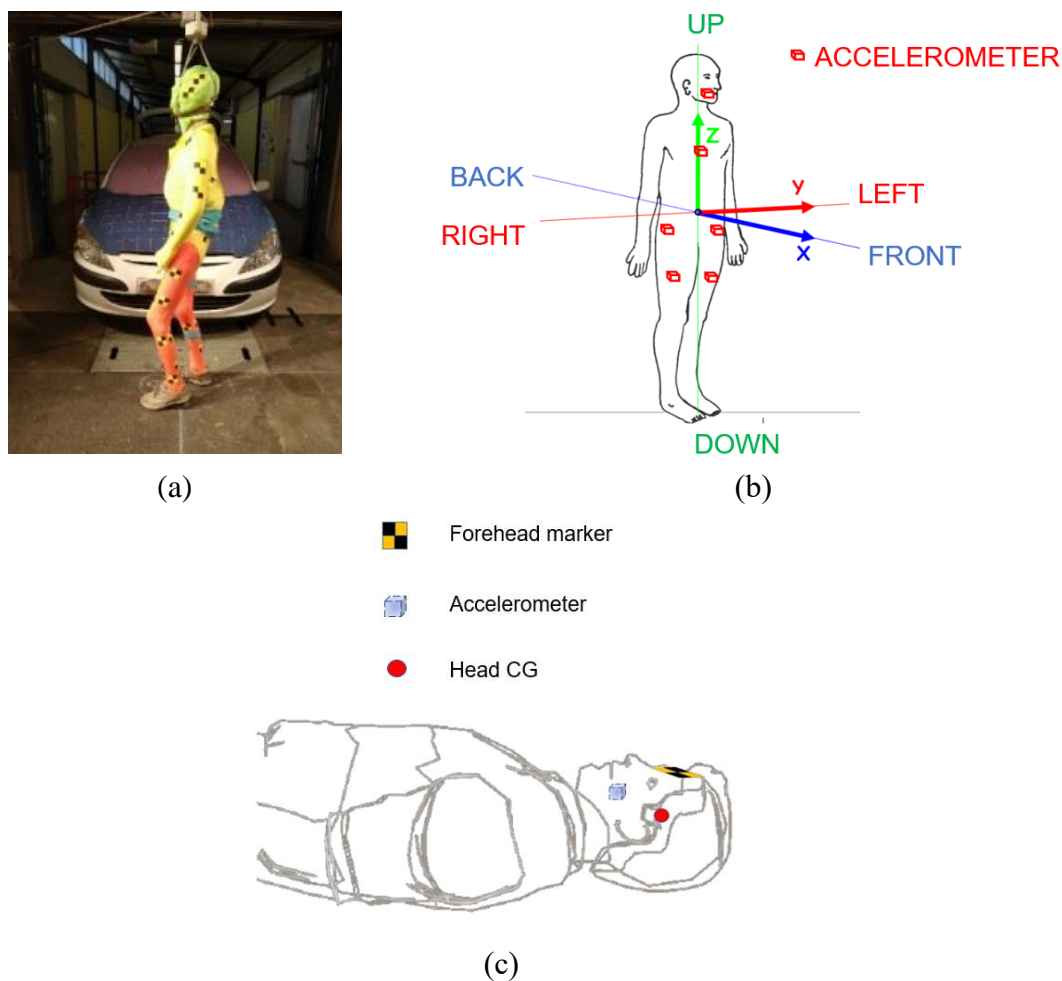


Figure 6.2 (a) Pre-impact scenario; (b) accelerometer positions and nominal orientations; (c) head accelerometer, CG and forehead marker positions



(a) Test 01



(b) Test 02



(c) Test 03



(d) Test 04



(e) Test 05



(f) Test 06

Figure 6.3 Knee joint angles of pedestrian pre-impact positions

6.2.2. Video Data Analysis

The global head trajectories in the X (vehicle forward direction) and Z (vertically upward) directions were estimated by manually tracking the location of the forehead marker [Figure 6.2 (c)] every 10ms using Matlab (ginput function). During contacts between the head and the vehicle and the head and the ground, marker trajectories were extracted every 1ms. Linear velocities were then obtained using a central difference scheme. Rotational kinematics for the head during both vehicle and ground contacts were estimated using Model Based Image Matching (MBIM), introduced by [Bahr and Krosshaug 2005, Krosshaug and Bahr 2005] and recently applied to head impacts [Tierney *et al.* 2015, Tierney *et al.* 2018]. MBIM uses multiple camera views to build an environment based on known background dimensions and then manually fits a skull model to the envelope of the head in all available videos at each time frame, see Figure 6.4. The rotation matrix for the head is then extracted at each time step, and a central difference scheme is used to compute body local angular velocity components. In this study, each case was reconstructed by two independent researchers. Tierney *et al* [Tierney *et al.* 2018] previously reported that MBIM is repeatable for both single and multiple researchers.

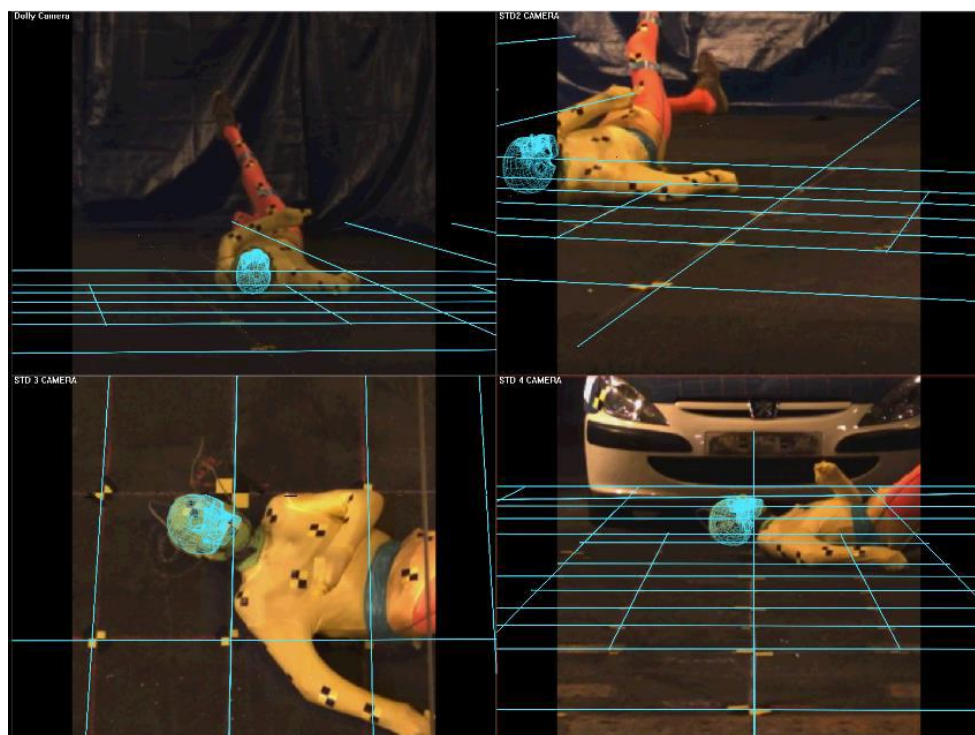


Figure 6.4 Sample head MBIM matching using multi-view camera images

6.2.3. Head injury assessments

The Head Injury Criterion (*HIC*) is commonly used to assess skull fracture risk [Versace 1971, Hutchinson *et al.* 1998], and is found from the resultant acceleration of the head mass centre as follows:

$$HIC = \left\{ \left[\frac{1}{t_2 - t_1} \int_{t_1}^{t_2} a_m(t) dt \right]^{2.5} (t_2 - t_1) \right\}_{max}, \quad \text{Equation 6.1}$$

where t_1 is the initial time and t_2 is the final time (in seconds) to maximize the *HIC*, and a_m is the resultant head CG acceleration (units of g), with time duration ($t_2 - t_1$) constrained to be less than 15 ms. However, since our accelerometers were fixed in the mouth instead of the head CG [Figure 6.2 (c)] for practical reasons, computation of the *HIC* was not possible with our available instrumentation. Instead, we define the “approximate Head Injury Criterion” (*aHIC*), calculated by applying the *HIC* computation to our head accelerometer data. To assess this approach, a virtual sensor was inserted in the same location in the 50th percentile male MADYMO pedestrian model to check the difference between *HIC* and *aHIC* in a simulation similar to those in [Shang *et al.* 2018b]. Results showed an approximate 10% difference, suggesting this approach is reasonable. The reported threshold for *HIC* (*aHIC* in *this study*) is 700 for an approximate 30% chance of skull fracture [Schmitt *et al.* 2010]. The 3ms acceleration criterion for the head was also calculated. This is used in regulations [ECE 2008, 2010] to assess energy dissipation of interior components in a vehicle, and it requires that accelerations of duration greater than 3ms do not exceed 80g [Got *et al.* 1978].

To assess the risk of rotationally induced brain injuries, the Brain Injury Criterion (*BrIC*) [Takhounts *et al.* 2013] during vehicle contact and ground contact was assessed on the basis of the MBIM results. The *BrIC* is associated with traumatic brain injuries (TBI), which has been used to assess the brain injuries of vulnerable road users [Kimpara and Iwamoto 2012, Mueller *et al.* 2015, Gabler *et al.* 2016, Gabler *et al.* 2018] and athletes [Aomura *et al.* 2016]. [Gabler *et al.* 2018] also proposed another criterion, *UBrIC*, to assess rotationally induced brain injury. However, evaluation of *UBrIC* requires a measure of angular acceleration which could not be reliably predicted with the available equipment. The *BrIC* score is found from the peak components of the body local head angular velocities:

$$BrIC = \sqrt{\left(\frac{\omega_x}{\omega_{xC}}\right)^2 + \left(\frac{\omega_y}{\omega_{yC}}\right)^2 + \left(\frac{\omega_z}{\omega_{zC}}\right)^2}, \quad \text{Equation 6.2}$$

where ω_x , ω_y and ω_z are the peak head angular velocity components and $\omega_{xC} = 66.3\text{rad/s}$, $\omega_{yC} = 56.5\text{rad/s}$, $\omega_{zC} = 42.9\text{rad/s}$ are the respective critical values proposed by Takhounts *et al.* [Takhounts *et al.* 2013]. The resulting *BrIC* score was used to estimate the risk of a rotationally induced AIS3+ brain injury using probability functions provided by Takhounts *et al.* [Takhounts *et al.* 2013].

6.3. Results

6.3.1. Pedestrian kinematics during the whole process of vehicle impact

Figure 6.5 and Table 6.5 summarize the overall kinematics, impact timings and intervals of the impact phases, with timings determined from the head accelerometer. Establishing the approximate contact time interval for both head-to-vehicle and head-to-ground contact in all tests was achieved by a combination of the filtered accelerometer and video data. For the onset of contact, a sharp change in the accelerometer time curve could be readily identified in each case and verified by comparison with the video data. Establishing the effective end time for each contact was more challenging and no general criterion could be applied. Instead, the end time was estimated by inspecting the acceleration time-history and comparing this to the video data. The time of the first contact between the vehicle and pedestrian is t_0 . The pedestrian rotates onto the bonnet during phase 1. The time of first head impact on the vehicle is t_1 . The pedestrian moves with the vehicle in phase 2. At t_2 , the pedestrian separates from the vehicle due to braking. The pedestrian has a flight period (phase 3) until t_3 , when first ground contact occurs (any body part). Then t_4 is the time of first head ground contact (in some cases $t_4 = t_3$). There follows a period of slide/roll and bounce (phase 4) until the pedestrian becomes stationary at t_5 . Appendix C shows the impact sequence of Test 01 at each key time on the speed time history curves. Figure 6.6 shows the pedestrian head trajectories in the X (horizontal) and Z (vertical) directions for all six tests. Head impact locations on the vehicle are shown in Figure 6.7.

Table 6.5 Key vehicle and ground contact events (s)

Key time	t ₀	Phase 1 duration	t ₁	Phase 2 duration	t ₂	Phase 3 duration	t ₃	t ₄	Phase 4 duration	t ₅
Description	1 st vehicle pedestrian contact		1 st head vehicle contact		pedestrian & vehicle separate		1 st ground contact (any)	1 st head ground contact		Pedestrian at rest
Test 01 (30.5 kph)	0	0.145	0.145	0.625	0.770	0.203	0.973	0.995	1.270	2.265
Test 02 (30.4 kph)	0	0.153	0.153	0.557	0.710	0.276	0.986	0.986	1.019	2.005
Test 03 (20.4 kph)	0	-	none	-	0.834	0.195	1.029	1.180	1.303	2.483
Test 04 (21 kph)	0	0.169	0.169	0.571	0.740	0.185	0.905	0.970	1.824	2.794
Test 05 (30.1 kph)	0	0.098	0.098	0.549	0.647	0.213	0.860	0.860	1.374	2.234
Test 06 (30.4 kph)	0	0.110	0.110	0.617	0.727	0.202	0.929	0.936	1.193	2.129

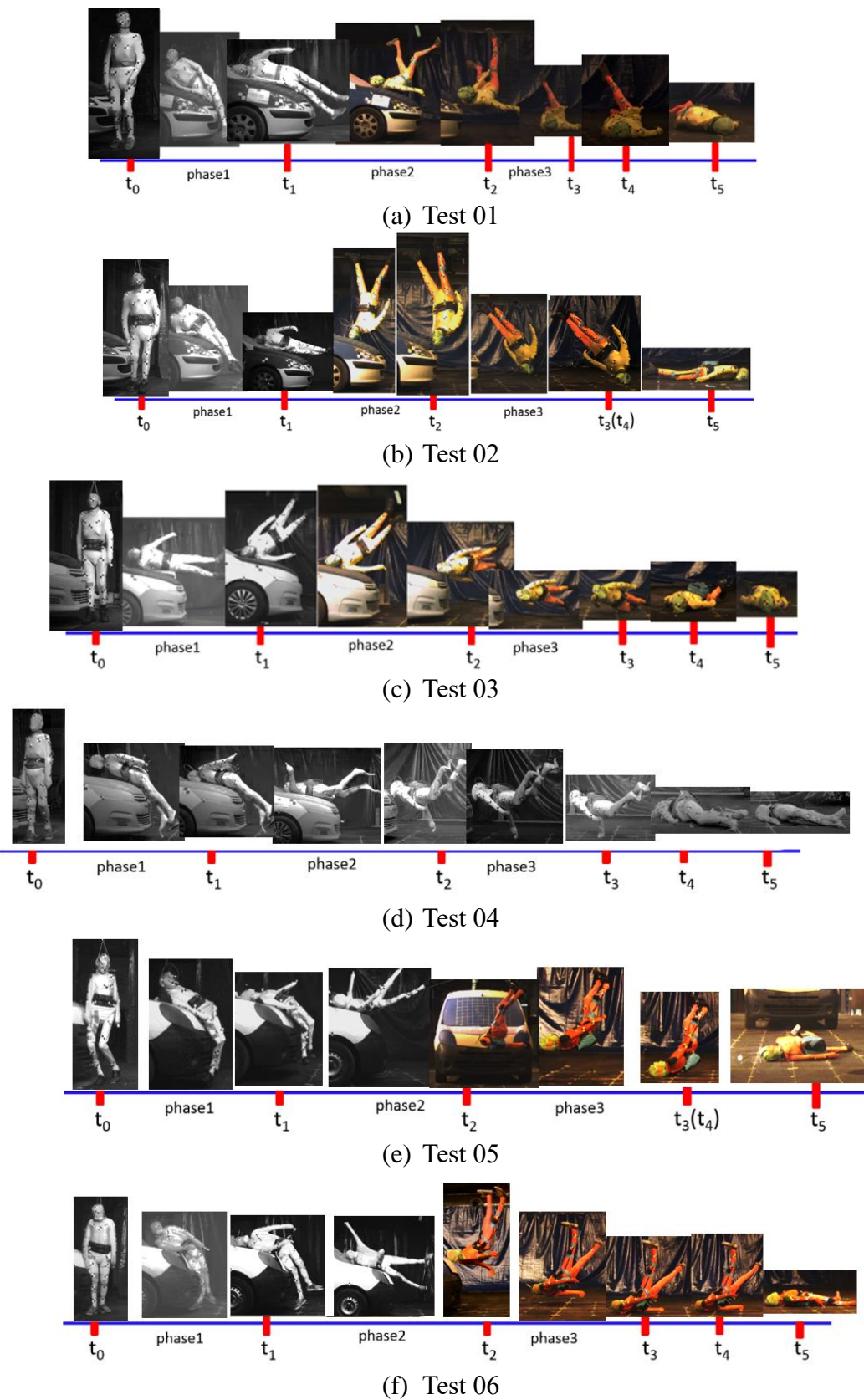
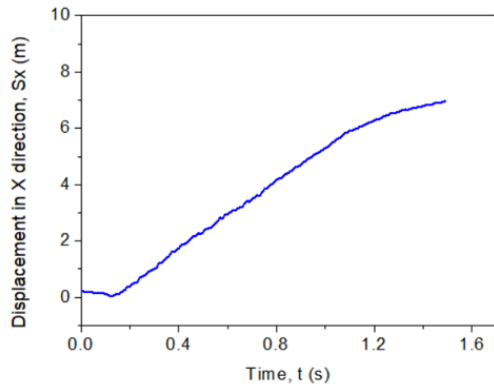
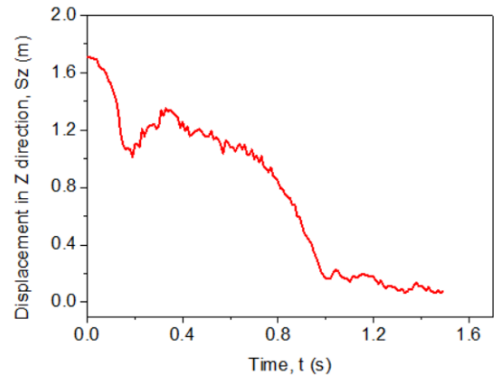


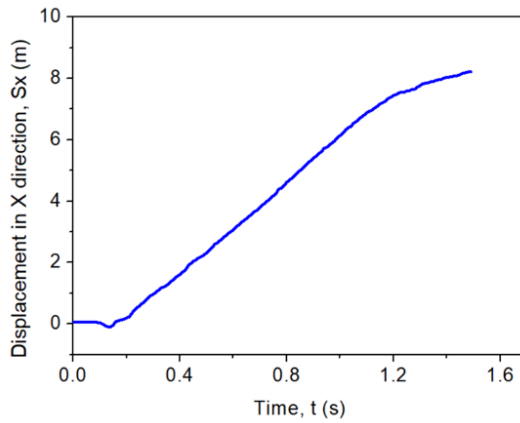
Figure 6.5 Sequences of vehicle-pedestrian impact for the six cadaver tests



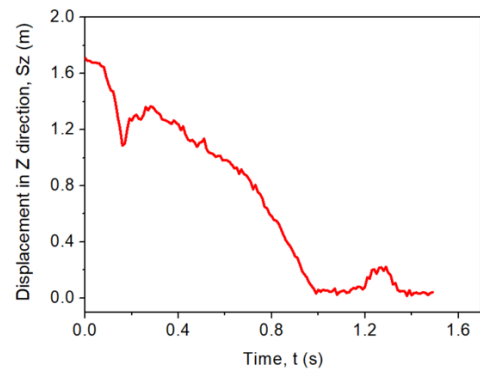
(a) Head position in X direction for Test 01



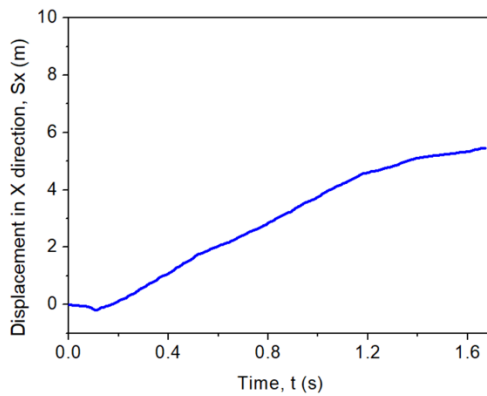
(b) Head position in Z direction for Test 01



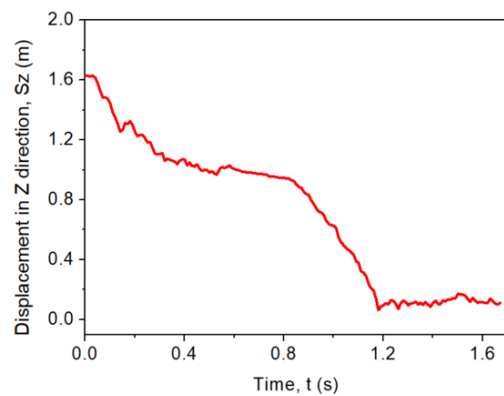
(c) Head position in X direction for Test 02



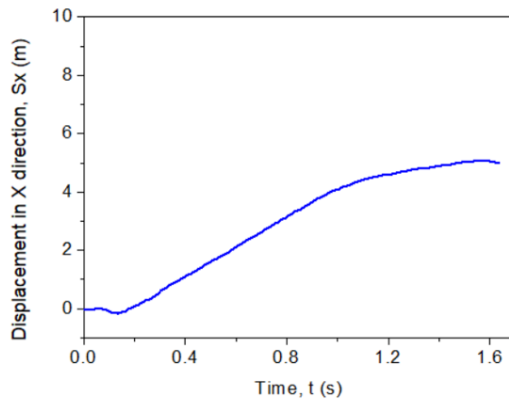
(d) Head position in Z direction for Test 02



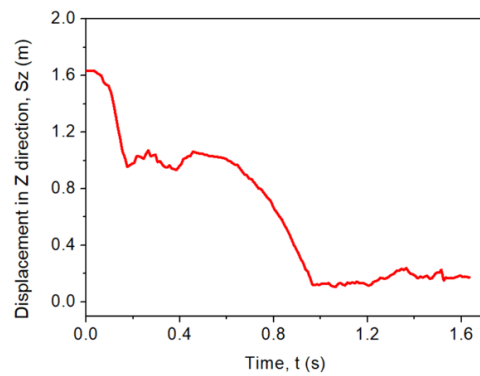
(e) Head position in X direction for Test 03



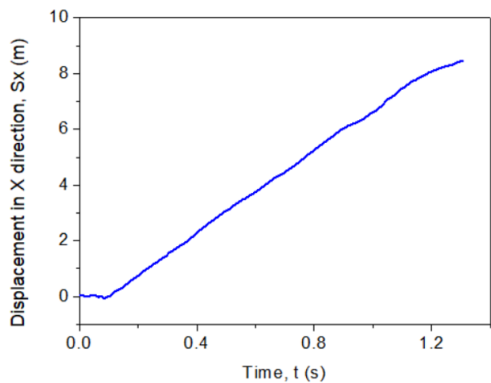
(f) Head position in Z direction for Test 03



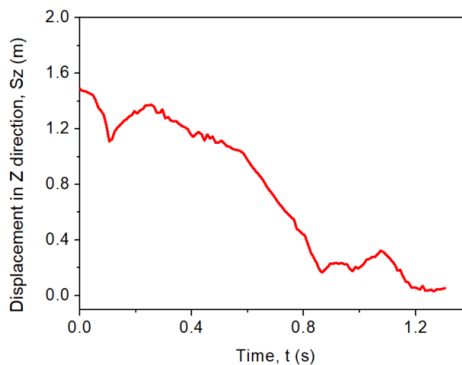
(g) Head position in X direction for Test 04



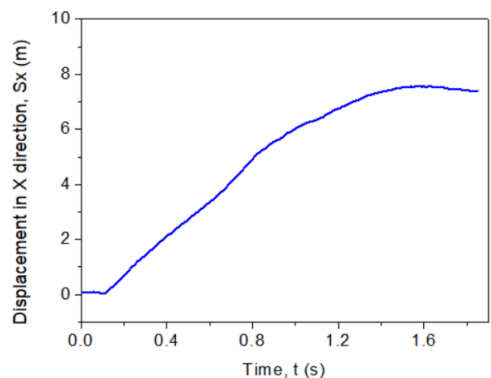
(h) Head position in Z direction for Test 04



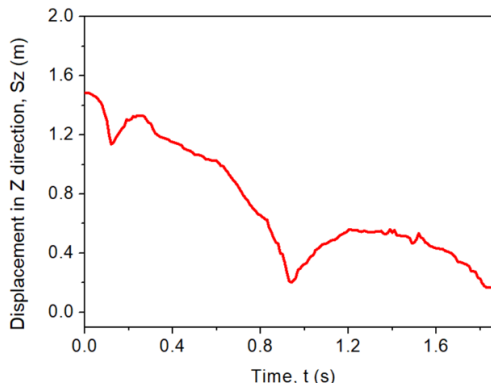
(i) Head position in X direction for Test 05



(j) Head position in Z direction for Test 05



(k) Head position in X direction for Test 06



(l) Head position in Z direction for Test 06

Figure 6.6 PMHS head displacement in X and Z directions for each test



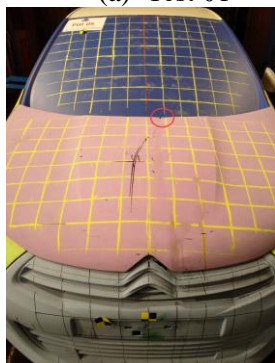
(a) Test 01



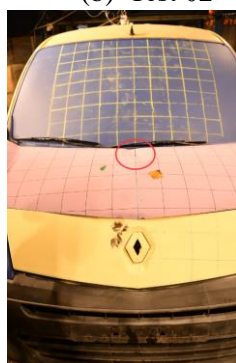
(b) Test 02

No head contact

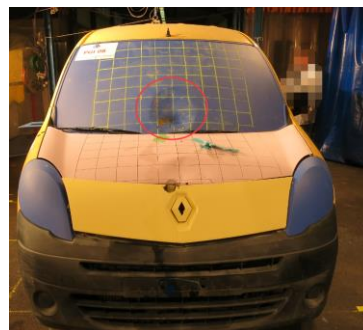
(c) Test 03



(d) Test 04



(e) Test 05



(f) Test 06

Figure 6.7 Pedestrian head impact location on vehicle

The vehicle contact phase is not described in detail here as it is well documented [Kerrigan *et al.* 2007, Subit *et al.* 2008]. Instead, our focus is on pedestrian kinematics after first vehicle contact, especially the subsequent ground contact. Following t_1 (first head contact on the vehicle, which occurs in all tests except Test 03 where shoulder contact/low impact speed prevent direct head contact), there is continued interaction of the pedestrian with the bonnet/windscreen area for about half a second until separation commences. Figure 6.8 shows the global velocity changes of the pedestrian's head during the entire impact process. To aid in understanding the impact processes and motivated by the principle of conservation of momentum, straight-line approximations for the head linear velocity between each impact phase have been added to Figure 6.8. These show that no significant impacts occur between head contact on the vehicle and separation from the vehicle. Following separation from the vehicle, the head acceleration is close to freefall acceleration under gravity. Contact with the ground is predominantly a vertical collision, with very small horizontal velocity changes of the head during ground contact. Figure 6.9 shows the head resultant acceleration during the vehicle and ground contact phases. Unfortunately, the accelerometer recording for Test 06 was corrupted during the ground contact (possibly become loose). Furthermore, to address potential accelerometer vibration (they were mounted in the cadaver's mouths using expanding foam), we employed a low-pass filter prior to injury risk assessments. Based on previous studies [SAE 1995, Kang and Xiao 2008] and motivated to achieve reasonable agreement between the predicted velocity changes during both vehicle and ground contact derived from differentiated video positions and integrated accelerometer curves (see Figure 6.10), we chose a CFC120 filter (3dB cut-off frequency = 200Hz), see Figure 6.9. With reference to Figure 6.10, a higher or lower cut-off threshold than 200Hz resulted in respectively over or under-prediction of the velocity change compared to the video-based estimates. The significance of this approach is further addressed in the Discussion.

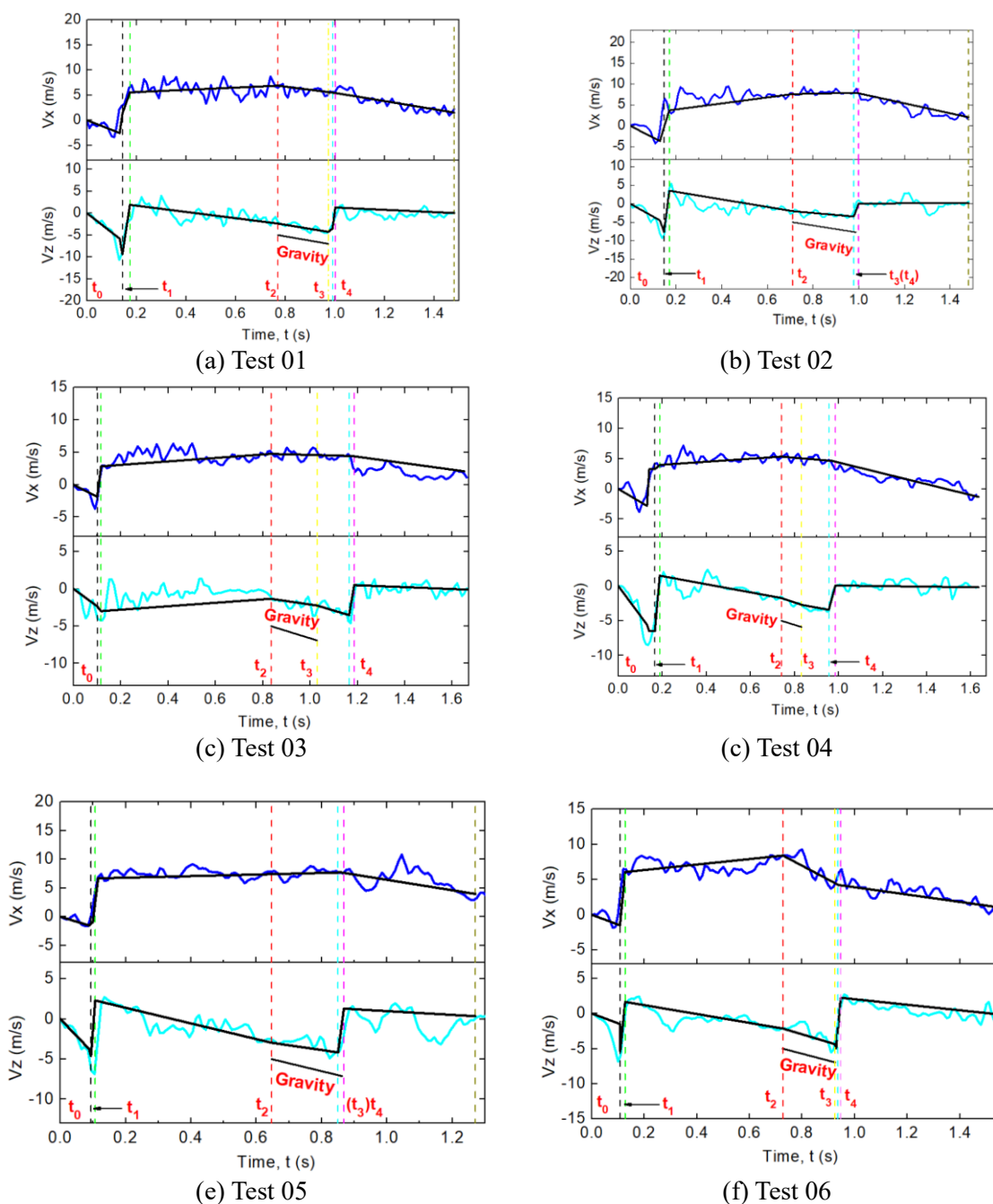


Figure 6.8 Head velocity time-histories from central difference (blue and cyan) with straight line approximations between major impact phases (black).

(Black dash: t_1 start; Green dash: t_1 end; Red dash: t_2 ; Yellow dash: t_3 ; Cyan dash: t_4 start; Purple dash: t_4 end)

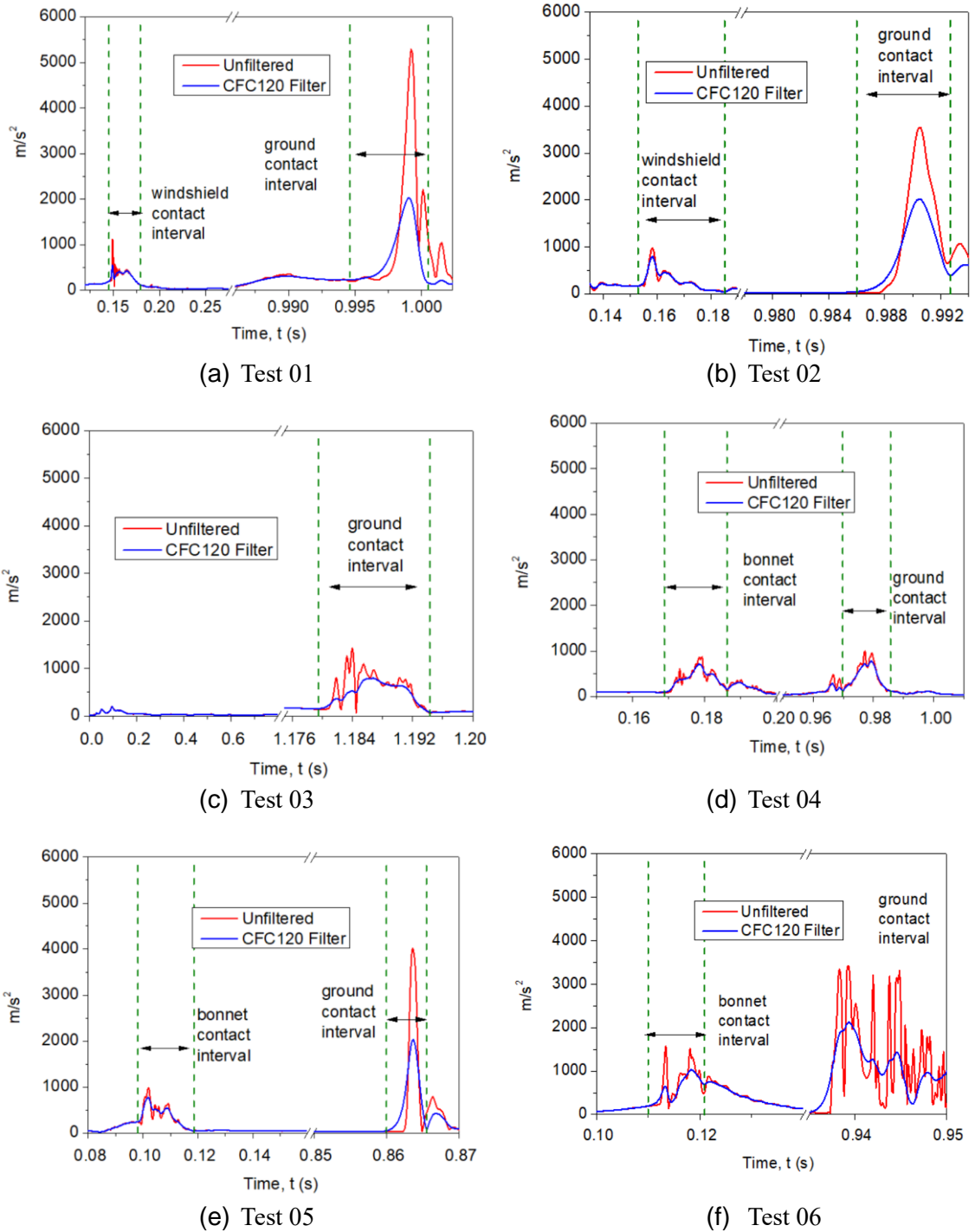


Figure 6.9 Filtered and unfiltered resultant head accelerometer time-histories during vehicle contact and ground contact

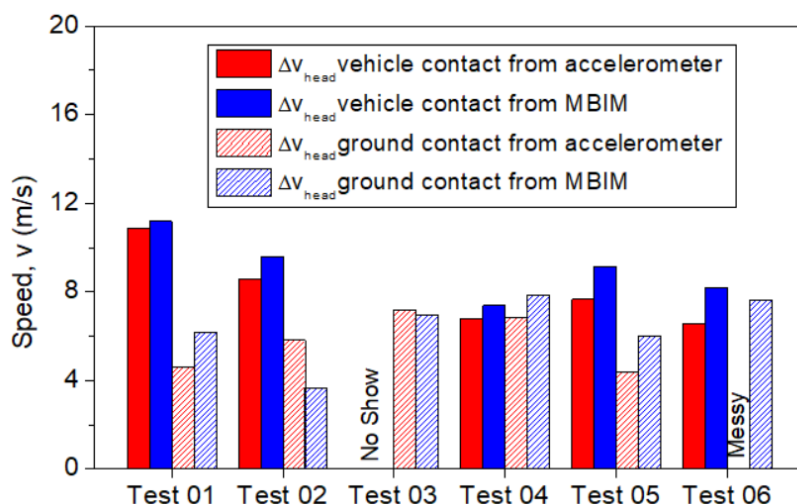


Figure 6.10 Comparison of head speed changes from MBIM and accelerometer

6.3.2. Head injury risk assessments

The *aHIC* scores for skull fracture risk based on the filtered acceleration curves for both vehicle and ground contacts are shown in Figure 6.11(a). The corresponding 3ms peak accelerations are shown in Figure 6.11(b), with head contact intervals in Figure 6.11(c). The *BrIC* score (including the range drive from the two independent MBIM estimates) and probabilities of AIS3+ brain injury risks are shown in Figure 6.11(d) & Figure 6.11(e) respectively. The comparisons of the variability in computed *BrIC* and linear velocity change scores between the two MBIM operators are given in Figure 6.12 and Figure 6.13. Table 6.7 & Table 6.8 summarize the vehicle and ground injury assessments. Figure 6.11(f) shows the average ground related rotational brain injury risk for 20km/h and 30km/h cases. Table 6.9 compares the expected and actual ground impact “mechanisms” using the categories of [Crocetta *et al.* 2015], while Table 6.10 compares the corresponding head impact speeds. The “agreement” in Table 6.9 is based on the proposed “mechanisms” obtained from a previous simulation study [Crocetta *et al.* 2015]. For pedestrian collisions from a compact car at 20 kph, almost all predicted cases were “M2”. For pedestrian collisions with a compact car or big car or SUV at 30 kph, the most frequently predicted mechanism was M1. If the mechanism observed from the cadaver test meets the most frequent mechanism from Crocetta *et al.*, the “agreement” in Table 6.9 was categorised as “Yes”. If the observed mechanism was one of the less frequently predicted ones, the agreement was “Partial”. If the observed mechanism was not predicted, then the agreement was “No”.

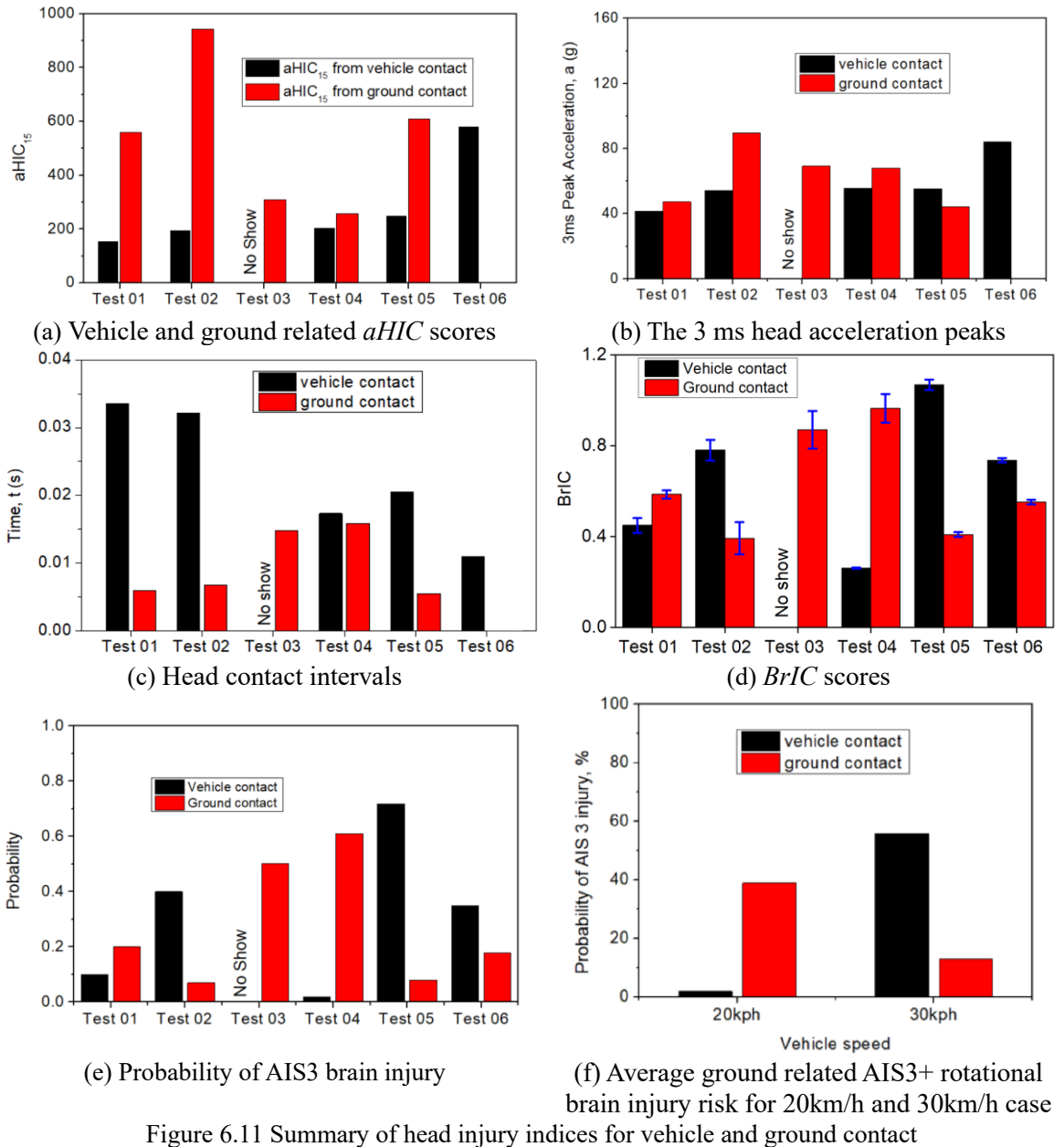


Figure 6.11 Summary of head injury indices for vehicle and ground contact

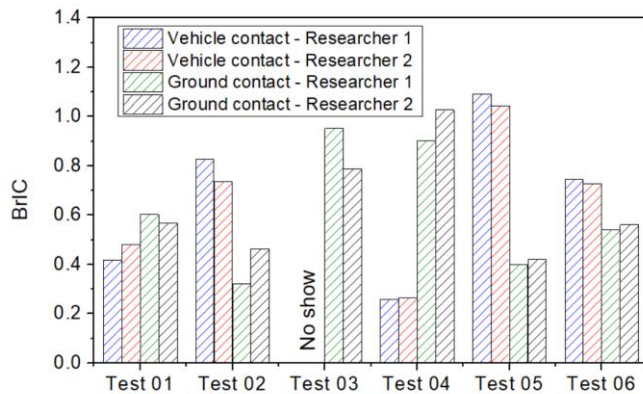


Figure 6.12 Comparison of $BrIC$ scores between researchers performing MBIM

Table 6.6-1 Intraclass correlation coefficients for two independent MBIM researchers for vehicle contact

	Test 01 Vehicle contact			Test 02 Vehicle contact			Test 03 Vehicle contact		
	Pos	Lin Vel	Ang Vel	Pos	Lin Vel	Ang Vel	Pos	Lin Vel	Ang Vel
x	0.928	0.335	0.844	0.995	0.325	0.945	NA	NA	NA
y	-0.048	0.95	NA	0.948	0.774	0.888	NA	NA	NA
z	0.992	0.98	NA	0.978	0.762	-0.015	NA	NA	NA

	Test 04 Vehicle contact			Test 05 Vehicle contact			Test 06 Vehicle contact		
	Pos	Lin Vel	Ang Vel	Pos	Lin Vel	Ang Vel	Pos	Lin Vel	Ang Vel
x	0.993	0.965	0.005	0.998	0.969	-1.402	0.998	0.567	0.984
y	-0.107	-0.371	0.981	0.749	0.901	0.967	0.749	0.64	NA
z	0.959	0.99	0.091	0.988	0.987	0.963	0.988	0.954	NA

Table 6.6-2 Intraclass correlation coefficients for two independent MBIM researchers for ground contact

	Test 01 Ground contact			Test 02 Ground contact			Test 03 Ground contact		
	Pos	Lin Vel	Ang Vel	Pos	Lin Vel	Ang Vel	Pos	Lin Vel	Ang Vel
x	0.992	0.335	-0.124	0.998	0.325	0.36	0.975	0.937	-3.142
y	0.977	0.95	0.05	0.969	0.774	0.691	0.877	0.582	0.906
z	0.995	0.98	0.919	0.938	0.762	0.933	0.996	0.649	0.841

	Test 04 Ground contact			Test 05 Ground contact			Test 06 Ground contact		
	Pos	Lin Vel	Ang Vel	Pos	Lin Vel	Ang Vel	Pos	Lin Vel	Ang Vel
x	0.994	0.965	0.982	0.998	0.985	0.949	0.997	0.567	0.002
y	0.582	-0.002	0.982	0.312	0.249	0.968	0.721	0.64	0.874
z	0.964	0.99	0.929	0.971	0.99	-0.023	0.958	0.954	-0.061

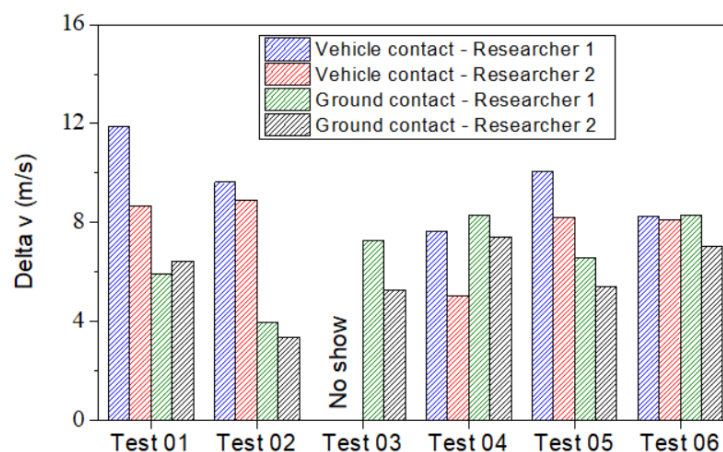


Figure 6.13 Comparison of linear velocity changes between researchers performing MBIM

Table 6.7 Summary of head/vehicle contact injury assessments

Test number	Impact speed (km/h)	NBLEH	HIC_{15}	3ms (g)	AIS 3+ (from <i>BrIC</i>)
Test 01	30	0.7	547	41.5	10%
Test 02	30	0.7	194	54.4	40%
Test 03	20	0.9	---	---	--
Test 04	21	0.9	203	55.5	2%
Test 05	30	1.2	248	55.3	72%
Test 06	30	1.1	579	84.1	35%

Table 6.8 Summary of head/ground contact injury assessments

Test number	Impact speed (km/h)	NBLEH	HIC_{15}	3ms (g)	AIS 3+ (from <i>BrIC</i>)
Test 01	30	0.7	559	47	20%
Test 02	30	0.7	943	90	7%
Test 03	20	0.9	309	69	50%
Test 04	21	0.9	258	68	61%
Test 05	30	1.2	608	44	8%
Test 06	30	1.1	--	---	18%

 Table 6.9 Expected and observed pedestrian ground contact mechanisms [Crocetta *et al.* 2015]

Test number	Expected	Actual	Agreement
Test 01	M1 (most frequent) or M3 (less frequent)	M1	Yes
Test 02	M1 (most frequent) or M3 (less frequent)	M3	Partial
Test 03	M2	M2	Yes
Test 04	M2	M2	Yes
Test 05	M2 (most frequent) or M1 (less frequent)	M1	Partial
Test 06	M2 (most frequent) or M1 (less frequent)	M1	Partial

Table 6.10 Expected and observed ground contact speeds [Crocetta *et al.* 2015]

Test number	Cadaver head velocity (m/s) at ground contact	Average \pm std dev. head velocity (m/s) at ground contact from multibody predictions
Test 01	5.1	4.7 \pm 0.8
Test 02	2.6	2.9 \pm 0.6
Test 03	5.1	3.2 \pm 1.4
Test 04	3.9	3.2 \pm 1.4
Test 05	4.4	4.7 \pm 0.8
Test 06	5.5	4.7 \pm 0.8

6.4. Discussion

6.4.1. Whole-body kinematics during the complete pedestrian impact process

This study presents the first detailed overview of the whole kinematic process of pedestrian collisions assessed using cadaver tests, starting with vehicle contact and ending with ground contact (see Figure 6.5 and Table 6.5). The very limited previous data on pedestrian ground contact from cadaver tests limit comparison to the published literature. Whole-body kinematics can be classified into several critical events and phases: phase 1 (duration \sim 100-170ms) starts with first pedestrian-vehicle contact and ends with first head-vehicle contact; in phase 2 (duration \sim 550-625ms) the pedestrian moves together with the vehicle; phase 3 (duration \sim 185-280ms) is separation and first pedestrian ground contact; phase 4 (duration \sim 1-1.8s) is slide, roll and bounce to rest. First head ground contact occurs after about 1s and the process is complete after about 2.0-2.8s. Pedestrian ground contact occurs at the end of a highly non-linear chain of events, such that small changes in initial configuration result in significant changes in head ground impacts (compare Test 01 to Test 02) and this has been well flagged in the literature [Simms and Wood 2009]. However, considering the ground contact mechanisms proposed by [Crocetta *et al.* 2015]– see Table 6.4, surprisingly good agreement was observed (Table 6.9) and head velocity prior to ground contact was similar to the range presented for each mechanism except for Test 03 (Table 6.10). These results show multibody modelling is generally successful at predicting whole-body motion of pedestrians during ground contact. Nonetheless, given the variations in head ground impact observed here in nominally similar cadaver tests (especially Test 01 vs Test 02), the capacity to predict injury risk in specific ground contact cases is low, and in line with earlier modelling observations [Li *et al.* 2017b].

6.4.2. *Head kinematics throughout the impact process*

The time-histories of head velocity changes (see Figure 6.8) clearly identify the head/vehicle and head/ground contact processes. It is instructive to conceive of the head velocity changes in terms of net forces acting vertically and horizontally: the horizontal head velocity changes in phase 1 are due to neck forces induced during whole-body rotation; then there is the vehicle contact, after which the horizontal velocity during phases 2 and 3 is largely constant (zero net force) during separation from the vehicle through to first pedestrian ground contact, after which sliding and rolling to rest during phase 4 reduce the horizontal velocity to zero. The vertical head velocity changes in phase 1 are again due to neck forces induced by whole-body rotation; then there is the vehicle contact, after which the vertical velocity changes approximately in accordance with gravity during separation from the vehicle through to first pedestrian ground contact, which again effectively reduces the vertical component of head velocity to zero.

6.4.3. *Head ground contacts*

The cadavers mostly struck the ground after around 1s (Test 05 has earlier contact but is unusual with subject mass only 38kg). The head impacts the ground more than once in each test, indicating significant restitution. However, attempts to estimate a consistent head ground contact stiffness for modelling purposes using a spring-mass model with restitution were largely unsuccessful Table 6.11 shows the tests in which the ground contact mechanisms were suitable for estimating head ground contact stiffness. Consequently, Table 6.12 shows the reasons for the remaining tests with linear stiffness estimates varying between ca. 180-1750 kN/m, see Table 6.13. This implies large stiffness variations (either between specimens or due to different contact locations on the skull) and/or a linear stiffness is a poor approximation. The head ground contact stiffness as listed at Table 6.13 was estimated basing on the following equation (which is adapted from [Nagurka and Huang 2004]) and assuming a head mass (M) of 4.5kg.

$$k = \frac{M}{(\Delta t)^2} \left[\pi^2 + (lne)^2 \right] \quad , \quad \text{Equation 6.3}$$

where e is the coefficient of restitution, which is defined as the rebound velocity divided by the velocity prior to contact [Nagurka and Huang 2004]. Values of pre/post impact velocity were taken from the MBIM results.

Figure 6.8 shows that ground contact is predominantly a vertical impact, with the horizontal velocity change during ground impact being undetectable from the video analysis in all six tests. In contrast, the vertical velocity change during ground contact is substantial and is chiefly responsible for the resultant acceleration peaks in Figure 6.9. The peak accelerations, *aHIC* and 3ms scores from ground contact are generally higher than those from vehicle contact, see Figure 6.11. The high stiffness of the ground contact evidenced by the shorter contact interval compared to the vehicle contact [Figure 6.11 (c)] is probably the main reason for this, since Figure 6.10 shows the speed change in the vehicle contacts is mostly higher than in the ground contacts. This highlights the need to find solutions to pedestrian ground contact injury for pedestrian protection at impact speeds of 20 - 30 km/h, where further improvements in vehicle front safety may be less beneficial than approaches to preventing pedestrian ground contact. These results are in line with our recent GIDAS analysis which found 72% of injury costs in pedestrian collisions below 30km/h are associated with ground related injuries [Shang *et al.* 2018d].

Table 6.11 Contact location for suitable cadaver tests

Suitable Tests	Impact Location
Test 01	Occipital/parietal bone
Test 04	Chin
Test 05	Occipital/parietal bone

Table 6.12 Reasons for unsuitable cadaver tests

Unsuitable Tests	Reason
Test 02	Force goes through the head and head, preventing head rebound
Test 03	Facial padding adds damping
Test 06	Acceleration is not available

Table 6.13 Head ground contact stiffness

Suitable Tests	Velocity before (m/s)	Velocity after (m/s)	e	Δt (ms)	<i>k</i> (kN/m)
Test 01	-5	0.75	0.15	5.9	1741
Test 04	-4	2.75	0.69	15.9	178
Test 05	-4.5	1.25	0.28	5.5	1709

6.4.4. Head accelerometer filtering

According to the X-ray after each test, there were no skull fractures. This provides further justification for the 200 Hz filter, as the peaks in the unfiltered accelerations in Figure 6.9 would almost certainly imply some skull fractures. Besides, a retrospective assessment of the GIDAS data analyzed for the work published in [Shang *et al.* 2018d] shows the proportion of crashes involving skull fracture from ground contact is less than 4% in the speed range 25-34 km/h and less than 1% in the speed range 15-34 km/h, which also complies with the absence of skull fractures in our cadaver tests.

6.4.5. Head Linear versus rotational loading ground contact

A comparison of the relationship between *aHIC*/3ms linear head injury risk with the rotationally assessed AIS 3+ risk computed from the *BrIC* score shows mixed results, see Figure 6.14. The *aHIC* score reduces with increased AIS3+ rotational head injury risk suggesting a compensatory pattern between head linear and angular injury risk which might depend on the geometry of head ground contact, but this pattern is not replicated for the 3ms score. It is thus unclear how to interpret these results and computational modelling may be needed to further elucidate this.

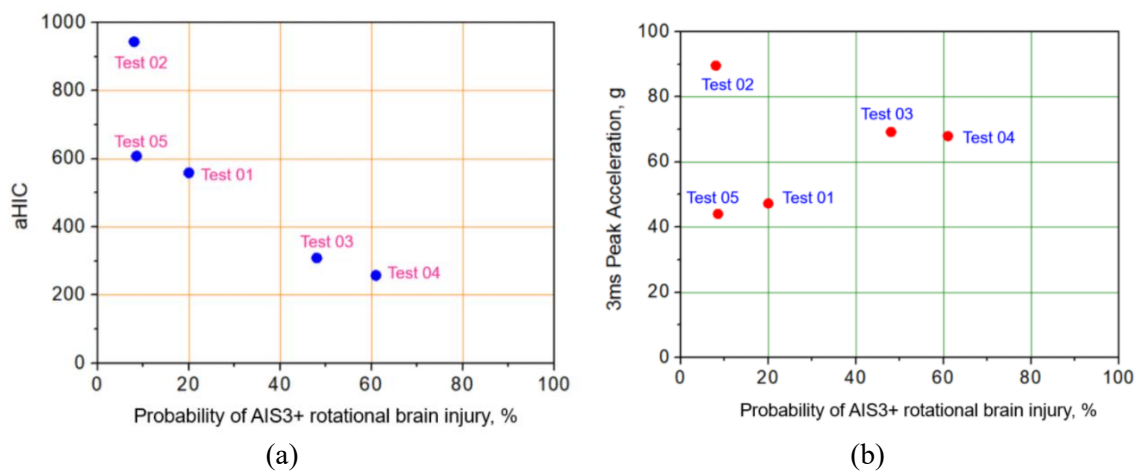


Figure 6.14: Comparison of the relationship between *aHIC*/3ms linear head injury risk with the rotationally assessed AIS 3+ risk for Test 01-05 (the accelerometer malfunctioned in the ground contact in Test 06)

6.4.6. Comparison with real-world crash video

By comparing these tests with real-world crash videos which analysed in Chapter 5, some differences can be observed. Around half of the pedestrians showed voluntary motions in the selected videos while this cannot occur in the cadaver tests. The voluntary motions may affect pedestrian post-impact kinematics and thus resulting in the variable ground contact mechanisms. The cadavers rotated less than 270 degrees before landing in all the 6 tests, while for the videos with estimated vehicle speed between 20-30 kph, pedestrian whole body rotation angles vary from 90 degrees to 450 degrees.

Table 6.14 and Table 6.15 illustrated the cases around 20 km/h and 30 km/h from Chapter 5, respectively. 5 cases were estimated as crashes around 20 km/h where 7 were estimated around 30 km/h. Both of the two cadavers in 20 km/h cases showed M2 mechanism in the experiments while only one of the five cases from real-world collisions showed similar mechanism, see Table 6.9. Similar to what happened in the tests, most pedestrians (4/5) were observed that their body stayed straight after the collisions. Moreover, the head impacts the ground first only occurred in one crash.

For 30 km/h cases observed from real-world collisions, mechanisms 1 and 3 occurred in 3 of 7. The largest whole body rotation was less than 270 degrees in the cadaver tests while in the real-world collisions, the rotation angles varied from 90 degrees to 495 degrees. In the cadaver tests, both headfirst impact ground and not were observed, so did the real-world collisions.

It should be noted that the pedestrian ground contact mechanisms observed from real-world collision videos do not exactly match the mechanisms defined by [Crocetta *et al.* 2015]. For instance, the impact mechanisms might be similar to that from cadaver tests, but the pedestrian rotated more angles before landing. The voluntary motions of the pedestrians, pedestrian initial speed and the impact location might be the reasons for the differences of kinematics observed in cadaver tests and real-world crash videos.

Table 6.14 Cases around 20 kph from Chapter 5 and Chapter 6

No.	Vehicle speed (km/h)	P whole-body rotation (degree)	Body stays straight or not	NBLEH	Head contact or not	first or not	Mechanism ([Crocetta <i>et al.</i> 2015])
2	21.6	225	Y	0.881	N		M3
4	18	90	Y	0.943	N		M2
6	21.6	225	Y	0.734	Y		M3
17	18	90	Y	0.825	N		M5b
25	21.6	90	N	0.825	N		M5b
Test 03	20.4	90	N	0.9	N		M2
Test 04	21.0	90	Y	0.9	N		M2

Table 6.15 Cases around 30 kph from Chapter 5 and Chapter 6

No.	Vehicle speed (km/h)	P whole-body rotation (degree)	Body stays straight or not	NBLEH	Head contact or not	first or not	Mechanism ([Crocetta <i>et al.</i> 2015])
5	28.8	180	Nearly	0.884	Y		M3
8	28.8	450	N	0.734	Y		M4
10	28.8	225	N	0.777	N		M3
13	32.4	495	Y	0.825	Y		M3
18	28.8	90	Y	0.825	Y		M1
22	28.8	450	Y	0.777	N		M4
29	28.8	90	Y	0.839	Y		M2
Test 01	30.5	180	N	0.7	N		M1
Test 02	30.4	270	Y	0.7	Y		M3
Test 05	30.1	180	N	1.2	Y		M1
Test 06	30.4	180	Y	1.1	N		M1

6.4.7. Unexpected Results

There were several unexpected findings that may lead to future insights.

Figure 6.11(f) and Table 6.8 show a substantially higher risk of rotationally induced brain injury for the two 20 km/h tests than the four 30 km/h cases. The reason for this is the combination of a larger ω_z component with the smaller threshold for this axis in the *BrIC* equation. By checking the head-ground contact mechanisms from the videos, the motion of the pedestrian heads in tests 03 and 04 was more complex (bending and twisting). In contrast, for the other tests, the heads showed mainly bending rotation during contact with the ground.

An underlying biomechanical explanation and whether this predicted increased risk at 20kph occurs in real-world collisions remains unclear, but future computational modelling may help elucidate this.

We had expected to identify a relationship between NBLEH and head injury risk as this was observed in our recent analysis of GIDAS data [Shang *et al.* 2018d], but Table 6.8 shows no clear relationship between either linear or rotational head injury risk assessments in ground contact and the NBLEH in our cadaver tests. The absence of a trend may be due to the small sample size.

A larger sample size would be needed to better understand the influence of vehicle design and pedestrian ground contact. However, the current experimental findings could be combined with computational modelling to better understand these effects. Additional high-speed cameras and markers on the head would have been beneficial for the MBIM process, as the region of interest to be covered during the whole process from the first contact to rest is large.

The accuracy of the angular velocity time histories derived from the MBIM process cannot be measured as there is no gold standard, and this is a limitation. However, compared to [Tierney *et al.* 2018], we expect a higher accuracy as the frame rate is higher and there are four cameras instead of three and the image resolution is better. The intraclass correlation coefficients for the results of the two independent researchers applying MBIM are given in Table 6.6.

A nine-accelerometer array suitable for computing head CG accelerations would have permitted more precise 3ms and *HIC* score computations. A method for enforcing known initial limb angles would be beneficial, but also difficult to achieve in these cadaver tests because the joints of the cadaver were very stiff to change the initial posture normally, what made the posture looks odd in Test 05. Furthermore, the cadavers' lack of muscle tone may result in different kinematics compared to live pedestrians, especially for the two 20 kph tests. In this chapter only head kinematics is presented, but the GIDAS data [Shang *et al.* 2018d] shows lower limb and spinal injuries also occur during pedestrian ground contact and these should be a focus of future work.

6.5. Conclusion

This chapter presents the first detailed analysis of pedestrian ground contact kinematics using staged cadaver tests addressing a range of vehicle shapes and pedestrian heights and impact speeds of 20 and 30 km/h. In addition to the well-established kinematics of pedestrians up to the time of head contact on the vehicle, we have observed around 500ms of continued interaction of the pedestrian on the vehicle until separation commences, followed by a flight period of around 200ms which terminates in ground contact. The linear accelerations in ground contact for vehicle impact speeds of 20 and 30 km/h are generally higher than the acceleration in the vehicle contact, though the contact intervals are shorter. No skull fractures were observed in any cases, but the 3ms scores are close to or above the threshold in several cases. The predicted risk of rotationally induced brain injury computed from model based image matching applied to ground contact is high for the 20 km/h tests, highlighting the risk of pedestrian injuries from ground contact even at very low speeds. We were unable to identify a clear relationship between vehicle shape/pedestrian height and ground contact head injury risk in these six tests. The data pertaining to these six pedestrian ground contact tests can be made available upon request for the purpose of human body model development.

7. Study 4: Assessment of multibody pedestrian model compared with real pedestrian during the crash

7.1. Introduction

The MADYMO 50 percentile male pedestrian model, as shown in Figure 2.6, developed by TNO Automotive, is one of the most commonly used multi-body pedestrian models for vulnerable road user crash reconstruction and numerical parametric study [van Hoof *et al.* 2003, van Rooij *et al.* 2003, Simms and Wood 2006, Untaroiu *et al.* 2009, Elliott *et al.* 2012, Xu *et al.* 2016b, Shang *et al.* 2018d]. The model was validated for both full model [Ishikawa *et al.* 1993a] and model segments such like tibia and femur static 3-point bending tests, PMHS side impactor tests for the pelvis, thorax and shoulder, PMHS leg impactor tests for bending moment and shear force of lower extremities [Kajzer *et al.* 1993]. Delange *et al.* [DeLange *et al.* 2006] verified the kinematics of multi-body pedestrian model with a large range (eighteen tests) of full vehicle-pedestrian impact tests. However, the model is only validated for vehicle contact [DeLange *et al.* 2006]. Coley *et al.* [Coley *et al.* 2001] verified two scaled human pedestrian models against cadaver tests and real-world crash reconstruction [Ishikawa *et al.* 1993a] by comparing the head, pelvis, knee and ankle trajectories and the resultant head velocities and accelerations.

Researchers also developed other multi-body or finite element pedestrian models for the vehicle-pedestrian collision. [Yang and Lovsund 1997] developed a 3D MB pedestrian model (see Figure 2.7) with emphasis on the head and lower extremities. As shown in Figure 2.7, the model consists of fifteen body segments and has fourteen joints. The leg segments of this model are breakable [Yang *et al.* 1993] and the knee joints are anatomical [Yang *et al.* 1995], which allows the model can predict the biofidelic response of the knees and leg fracture from vehicle-pedestrian impact simulation. The model was validated based on the pedestrian substitutes' kinematics, the body segments' accelerations, contact forces, and failure description from anatomical investigations of the pedestrian substitutes, compared with previously published cadaver impacts [Ishikawa *et al.* 1993a].

Finite element pedestrian models such as THUMS [Maeno and Hasegawa 2001, Iwamoto *et al.* 2003] and GHBM [Untaroiu *et al.* 2016] pedestrian models are developed to simulate

deformable vehicle-pedestrian impact scenarios. The models have muscles, brain, bones and soft tissues to assess the relevant injuries [Iwamoto *et al.* 2003]. Head impact and leg impact of THUMS' pedestrian model were validated by using subsystems and the trajectories of the head, T1 and T6 of the spine, and other body parts were compared [Yasuki and Yamamae 2010]. For the GHBMC pedestrian model, the knee model and overall model under lateral four-point bending impact loading was validated against previous PMHS test [Viano 1989, Kerrigan *et al.* 2007]. The kinematics during vehicle-pedestrian contact was also validated [Kerrigan *et al.* 2007]. Klug *et al.* [Klug *et al.* 2017] compared the trajectories of GHBMC and THUMS pedestrian models and head contact force by applying four generic vehicles at three impact velocities. The results approved the capabilities of simulating the kinematics during vehicle-pedestrian impact for both THUMS and GHBMC FE pedestrian model.

In summary, different kinds of pedestrian models including MB and FE models are developed and used in the field of vehicle vulnerable road user crashes, which has a significant meaning for pedestrian passive safety. The models were validated based on lower extremity bending and shear loadings, the head response like acceleration and force, head trajectories, whole-body kinematics etc. However, all models appear to be validated for the vehicle impact only, and model validations for ground contact are so far lacking. As the importance of pedestrian ground contact is growing [Shang *et al.* 2018d], it is also necessary to assess the performance of pedestrian models after vehicle impact. The staged PMHS impact test [Shang *et al.* 2020] provided a comprehensive reference including pedestrian kinematics and injury outcomes (skull fracture, *HIC* and *BrIC*) for multi-body model assessment.

Accordingly, the aims of this study are to:

- 1) reconstruct the PMHS impact tests of Chapter 6 to assess the capability of the MADYMO pedestrian model for use in ground contact scenarios.
- 2) assess the difference between the MADYMO multibody model and the cadaver in post-impact kinematics and head injury outcomes.
- 3) Perform sensitivity studies to assess the influence of the vehicle pedestrian contact characteristics, the influence of initial pedestrian position on subsequent pedestrian ground contact and the effect of internal damping on overall body kinematics.

If the pedestrian model can replicate kinematics and injury outcomes within a certain error tolerance, it may be suitable for application in a Virtual Test System (VTS). Moreover, it could be used for developing active countermeasures to prevent pedestrian ground contact related injuries, such as controlled braking or airbag technologies.

7.2. Materials and methods

MADYMO pedestrian multi-body model, as well as simplified vehicle models, were employed to assess the performance in ground contact. Before reconstructing the MB models against the PMHS impact tests presented in Chapter 6, it should be noted that uncertainties (loading and unloading functions in vehicle-pedestrian contact and pedestrian ground contact, damping inside the MB pedestrian model, pedestrian initial joint angles) exist. Figure 7.1 illustrates the flowchart of steps to assess the MB models.

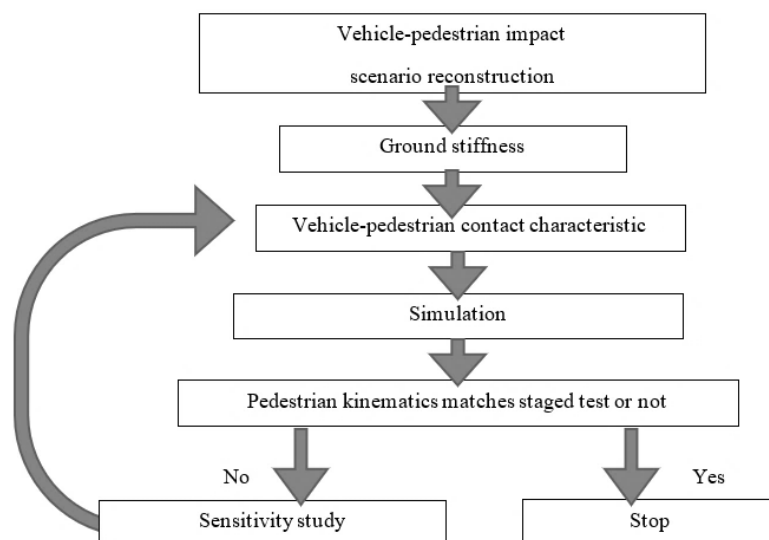
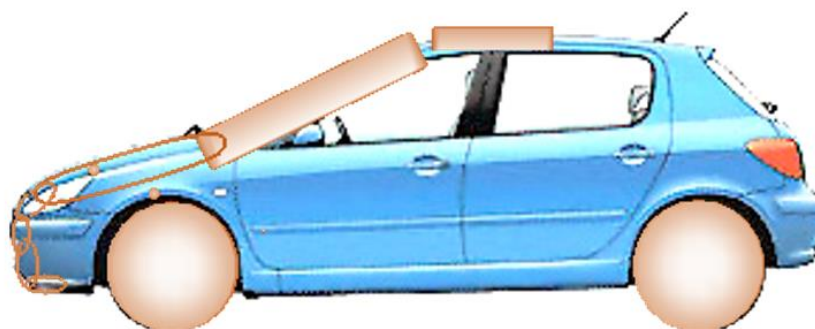


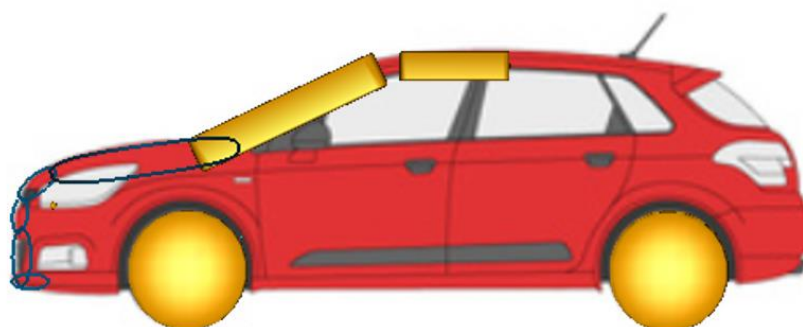
Figure 7.1 Flow chart of assessing the multi-body models

7.2.1. Multibody vehicle models

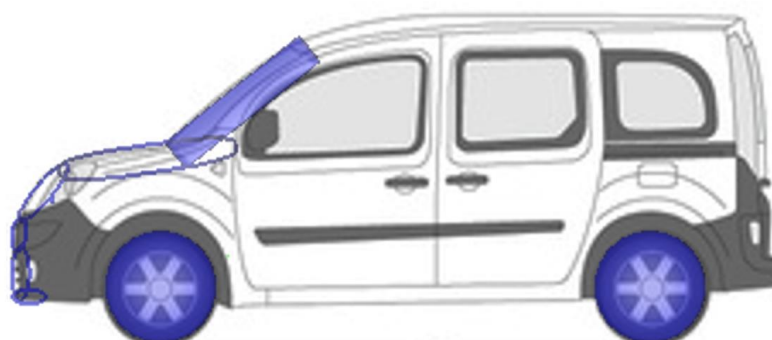
Simplified multi-body vehicle models are built in MADYMO, the geometry of each model is based on the profiles from the Blueprints [The-Blueprints] to represent the vehicles tested in Chapter 6. Each vehicle model consists of a lower bumper, bumper, bonnet leading edge, bonnet, windshield, wheels and roof. The overlapping side profiles of the vehicle models and simplified MADYMO models are shown in Figure 7.2.



(a) Peugeot 307



(b) Citroen C4



(c) Renault Kangoo II

Figure 7.2 The vehicle models with the simplified MADYMO models

7.2.2. Pedestrian models

Since the heights and weights of the PMHS pedestrians tested are different (as shown in Table 6.1) and the multi-body pedestrian model with same heights are not provided in the model database, it is necessary to scale the current MADYMO 50th percentile pedestrian model to represent the actual sizes of the PMHS pedestrians. A scaling tool based on a customized Matlab code was applied to obtain the scaled pedestrian models by inputting the pedestrian's height and weight. However, the scaling was solely based on the pedestrian's height and weight, so the body segment proportions might be different between the cadaver and the scaled model. The scaled MB models, as well as the corresponding PMHS pedestrians, are

demonstrated in Figure 7.3. The initial postures (joint angles) of the MB models were adjusted based on the photos of PMHS' pose from the side and the front views which captures pre-impact. Due to the joint limitation of the MB pedestrian model and the segment dimension differences, some differences between cadaver and MB model's posture exist, see the left forearm in Figure 7.3 (a). For Test 05 in Figure 7.3 (e), the posture looks odd because the joints of the cadaver were very stiff to change the initial posture normally.

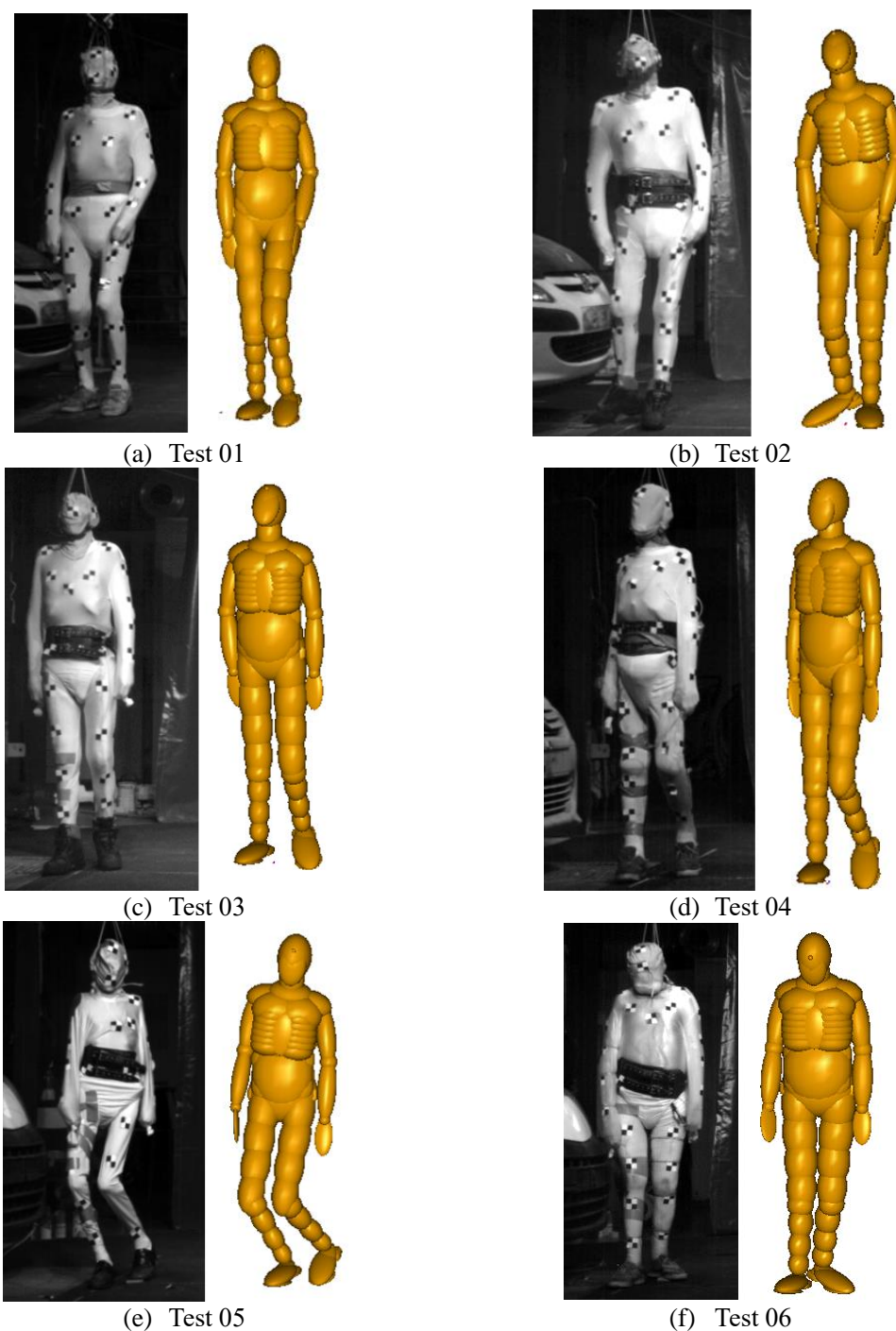
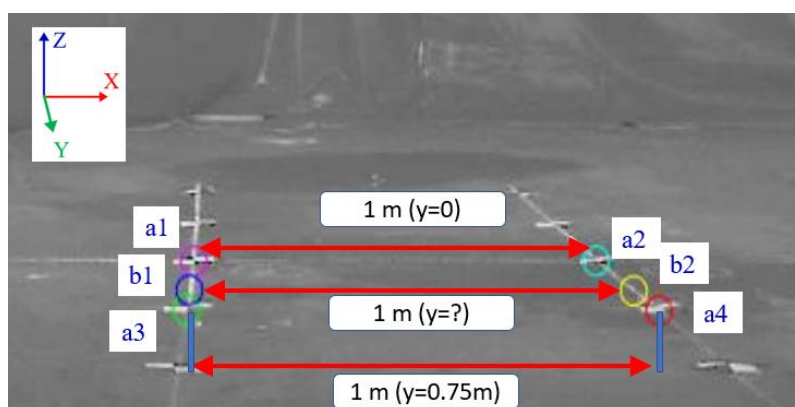


Figure 7.3 The initial postures of PMHS pedestrians and the corresponding multi-body models

7.2.3. Movement input of the MB vehicle models

The time-displacement curves in the X (horizontal) direction and the Z (vertical) direction, and the time-rotation curve of the vehicle, were extracted every 20ms using a customized Matlab script and were used to define the MB vehicle model's movement. The general steps for selecting the tracking point are as follows:

- (1) According to the width of the vehicle and the markers on the lab ground, using ginput function in Matlab to pick 2 pair of points (a1 and a2, a3 and a4) which defines 1 m in $y=0$ and $y=0.75$, then the expecting scale (b1 and b2) can be found based on the relation, see Figure 7.4 (a). The scale in Y direction depends on the coordinates of the points P1 and P2 in Figure 7.4 (b).
- (2) P1 is a reference point which can be used to find the tracking point P0 based on their relative positional relationship. Pick two points P1 and P2 in a line on the side of the vehicle, then the angular change of the vehicle can be calculated.



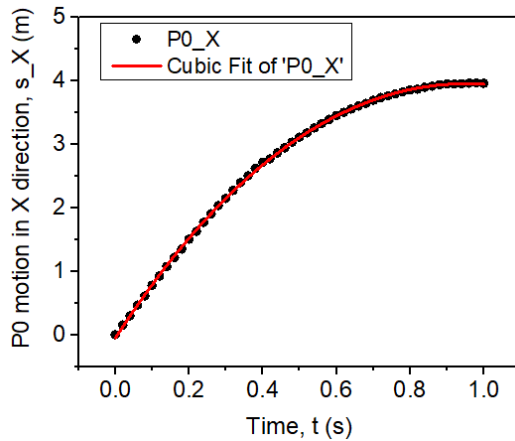
(a) Demonstration of choosing the scale



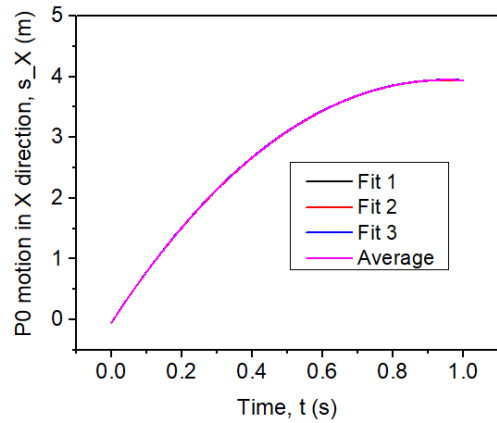
(b) Demonstration of choosing the tracking point P0

Figure 7.4 The steps of choosing the tracking point

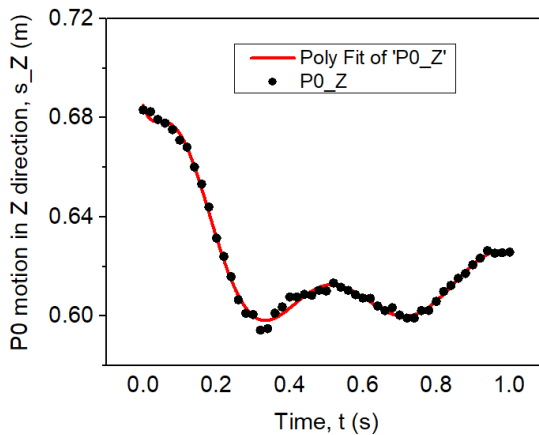
After the X and Z motion of the tracking point and the angle of the vehicle were calculated, the polynomial fittings (third-degree polynomial for X motion, ninth-degree polynomial for Z motion, fourth-degree polynomial for vehicle angle. Different orders were used for respective best matching fitting curve) were applied to fit the time history curves to ensure a smooth MB vehicle movement. Take Test 01 for instance, the motion of the tracking points corresponding the fitting curves are shown in Figure 7.5 (a), (c) and (e). It should be noted since the changes in the Z direction and theta (vehicle angle) are very small, a minor difference can result in relatively big errors when tracking the points P1 and P2. To reduce the error, the movements were tracked three times and averaged for each test, see Figure 7.5 (b), (d) and (f).



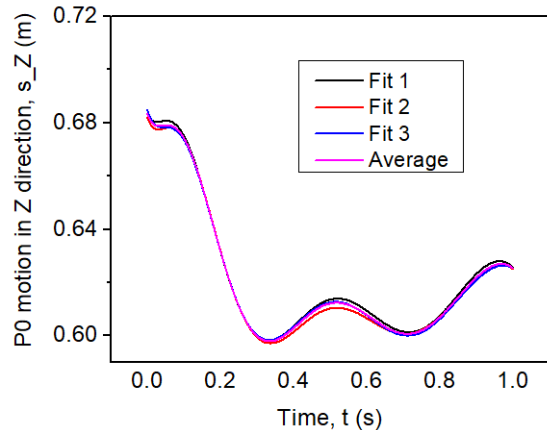
(a) Vehicle X motion



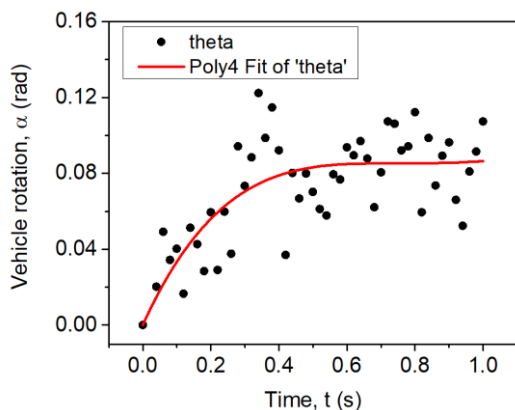
(b) 3 fitting curves of P0 X motion as well as the average curve



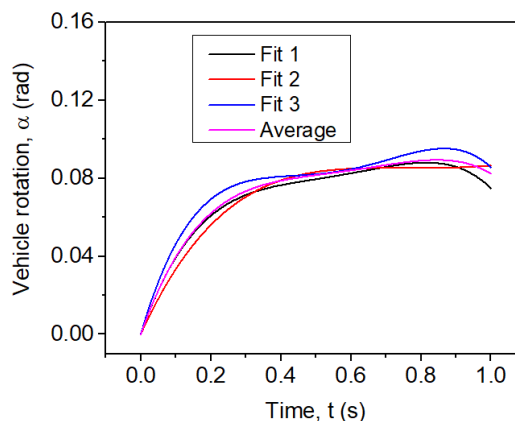
(c) Vehicle Z motion



(d) 3 fitting curves of P0 Z motion as well as the average curve



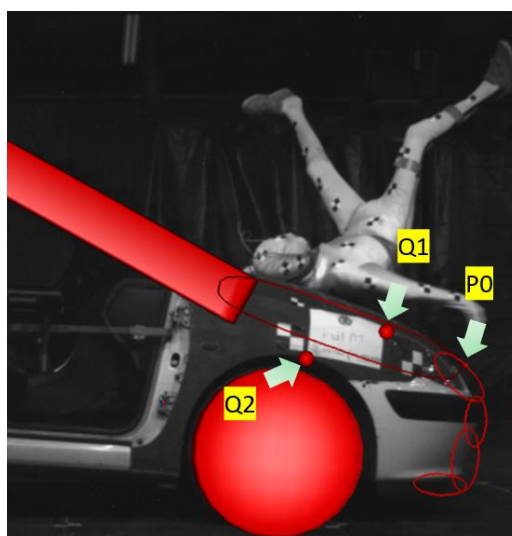
(e) Vehicle angle



(f) 3 fitting curves of vehicle angle as well as the average curve

Figure 7.5 The fitting curves of the motion of the tracking point

The input and output motions of the tracking point P0, as well as two other checking points Q1 and Q2 [as demonstrated in Figure 7.6 (a)], were compared to check whether the MB vehicle model moves as well as the input motions. Figure 7.6 (b) and (c) show that the movement of the tracking point P0 and the input is identical. For the two other reference points, the horizontal motion obtained from the video of the test and motion obtained from the MADYMO simulation output is closely related. The differences in vertical direction were small (up to 3 cm) and may be due to the vehicle’s rotation angle, which can be ignored. The checking point results indicate the feasibility of using the tracking system to capture the vehicle movement.



(a) The locations of two checking points

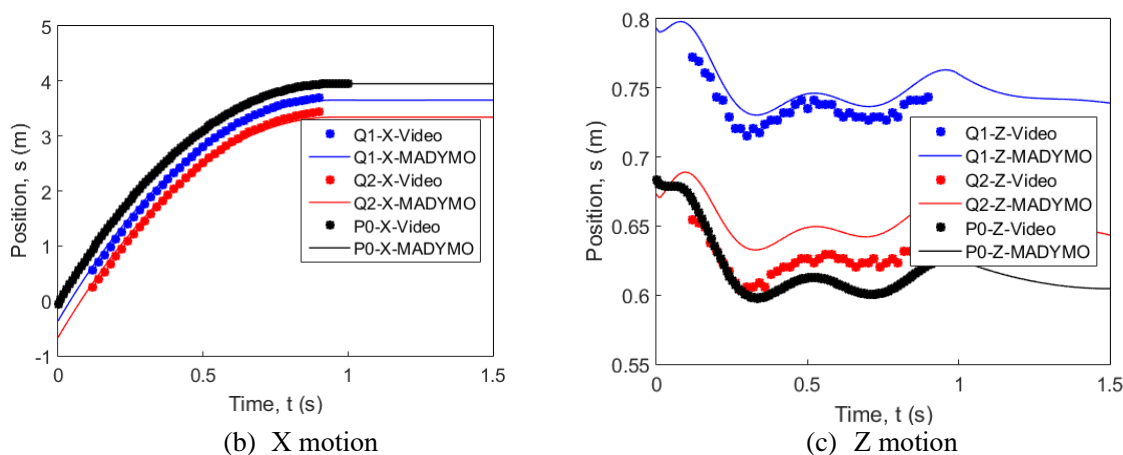


Figure 7.6 The comparison of input and output motions of checking points

7.2.4. Contact characteristic applied on the MB vehicle model

Three sources of vehicle contact characteristic were simulated. One is from [Martinez *et al.* 2007], one is from the test performed by the European New Car Assessment Programme (EURO-NCAP) [Euro-NCAP] and another one is from [Mizuno and Kajzer 2000] and [Liu *et al.* 2002]. The windshield stiffness and bonnet stiffness from [Mizuno and Kajzer 2000] were obtained by impactor tests and the stiffness of bonnet leading edge and bumper were assessed by [Liu *et al.* 2002]. This combination of vehicle contact characteristic has been used by [Li *et al.* 2016] for a previous virtual test system. Euro NCAP is a European car safety performance assessment programme backed by the European Union. Euro NCAP assesses the pedestrian safety performance of new cars with a rating (up to 5-star) based on sub-system impactor tests [Hobbs and McDonough 1998, Euro-NCAP 2010]. As demonstrated in Figure 2.25, the contact characteristic of vehicle bumper, bonnet leading edge, bonnet and windshield were obtained (step-by-step details which adapted from [Martinez *et al.* 2007] are attached in Appendix A) by lower legform, upper legform, child headform and adult headform tests with specified initial speed and impact angle, respectively. [Martinez *et al.* 2007] summarized 425 Euro NCAP tests then estimated a series of simplified average stiffness curves. The force-deformation curves of each tested vehicle from the Euro NCAP test as well as the force-deformation curves from [Martinez *et al.* 2007] and [Mizuno and Kajzer 2000] are shown in Figure 7.7. The detailed process of obtaining the vehicle front stiffness by using subsystem impactors can be found in [Martinez *et al.* 2007].

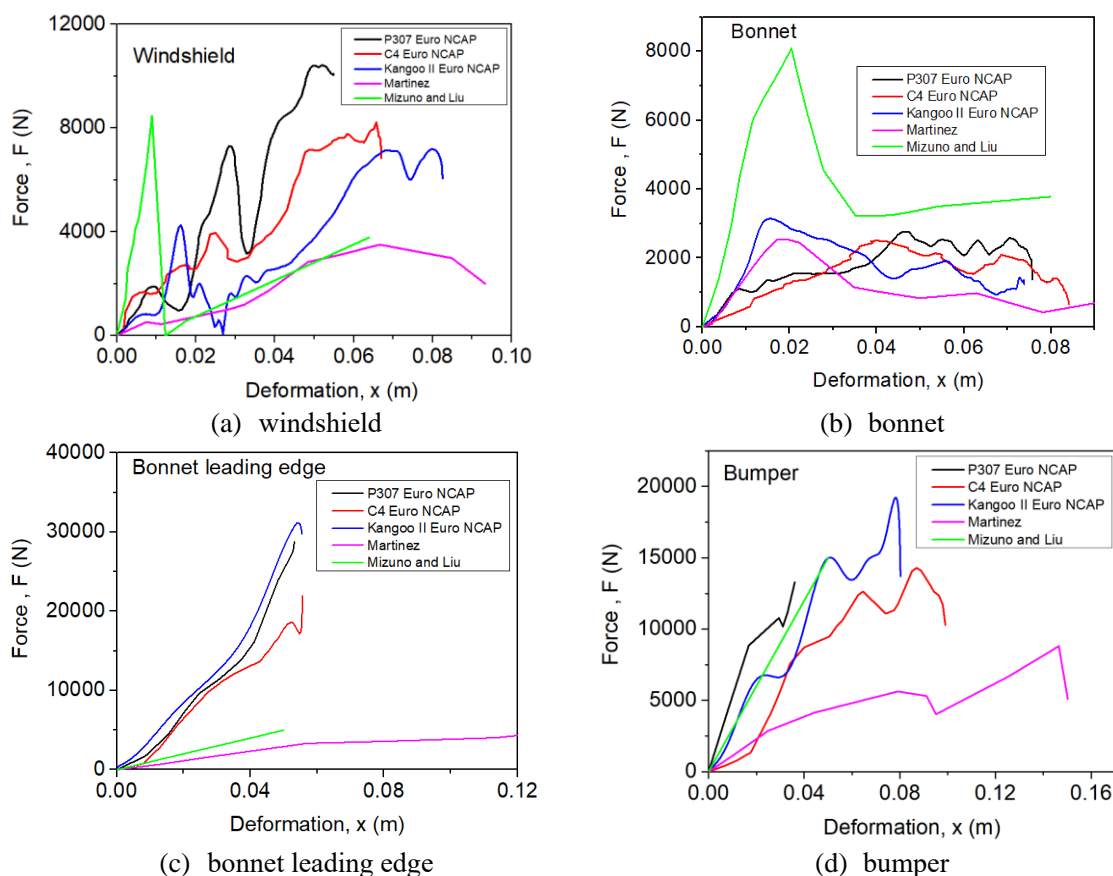


Figure 7.7 Force-deformation contact characteristics of vehicle front components from different sources

7.2.5. Ground contact stiffness

The ground contact stiffnesses are set different in MADYMO due to the individual differences of the tested PMHS and also the different locations on the head (some of the head contacts happened on the face while others occurred on the posterior side). To estimate the contact stiffness, an MB ball with initial linear and angular velocities was used to simulate the head impacts with the ground for the purpose of testing the head ground contact characteristic. The initial setup of the ball is listed in Table 7.1. Two methods were used to estimate the contact stiffness of the ground as shown in Equation 7.1 and Equation 7.2. The two methods of calculating the stiffness were based on the assumption that the head ground impact is simple harmonic motion [Triana and Fajardo 2013] and the acceleration is, therefore, a half-sine wave K_1 is calculated based on the peak acceleration and speed change while K_2 is calculated based on the impact time duration.

Table 7.1 The input parameter of the MB ball (simplified head model)

Parameter	Input
Head Mass	4.5kg
Inertia	(2.08e-02 2.37e-02 1.53e-02 0 0 0) kg·m ² (directly from MADYMO 50 percentile pedestrian model)
Linear speed	From MBIM results (Chapter 6)
Angular speed	From MBIM results (Chapter 6)
Initial position	0.02m high from the ground in vertical direction

$$\sqrt{\frac{m}{K_1}} = \omega = \frac{1}{\Delta T} = \frac{1}{\left(\frac{\Delta V}{Acc_{peak}}\right)} = \frac{Acc_{peak}}{\Delta V}$$

$$K_1 = m \times \left(\frac{\Delta V}{Acc_{peak}}\right)^2 \quad \text{Equation 7.1}$$

$$2\Delta T = 2\pi \times \sqrt{\frac{m}{K_2}}$$

$$K_2 = m \times \left(\frac{\pi}{\Delta T}\right)^2 \quad \text{Equation 7.2}$$

The stiffnesses calculated by two ways for each test are shown in Figure 7.8. The head ground contact characteristics for Test 06 was not listed as the acceleration measurement was noisy during ground contact, see Figure 6.9 (f). As the input of Test 06 was similar to Test 05 and the pedestrian ground contact mechanisms of the two tests were same, the stiffness of the ground for reconstructing Test 06 was set as same as that of Test 05. And the comparison of the accelerations obtained from the simplified head model test by using K_1 and K_2 as well as the curve from staged tests for each test are illustrated in Figure 7.9. The decision was to choose the average value of K_1 (K_1 gave better comparison than K_2 because it was difficult to define the period for the peak of acceleration) calculated from Test 01, Test 02 and Test 05, namely K_p (p: posterior), as shown in Figure 7.10, for the 30 kph tests, which have a relatively high ground stiffness due to the posterior head impact. In contrast, in Test 03 and Test 04, the front softer part of the head, such as the nose and face impacted the ground first, namely the anterior head impact, making the contact characteristic in head ground contact lower. The stiffness of the ground in these two tests was set as K_a (a: anterior), as shown in Figure 7.10, the average value of K_1 from the corresponding tests. The comparison of the head peak accelerations from cadaver tests and MADYMO simplified head ground impacts using K_p and K_a is shown in Figure 7.11. K_p and K_a will be chosen as head ground contact characteristic depending on which area of the head impacts the ground

first. Therefore, for the first round of simulation performed in section 7.3, it is necessary to check the head ground impact and then choose the appropriate contact characteristic.

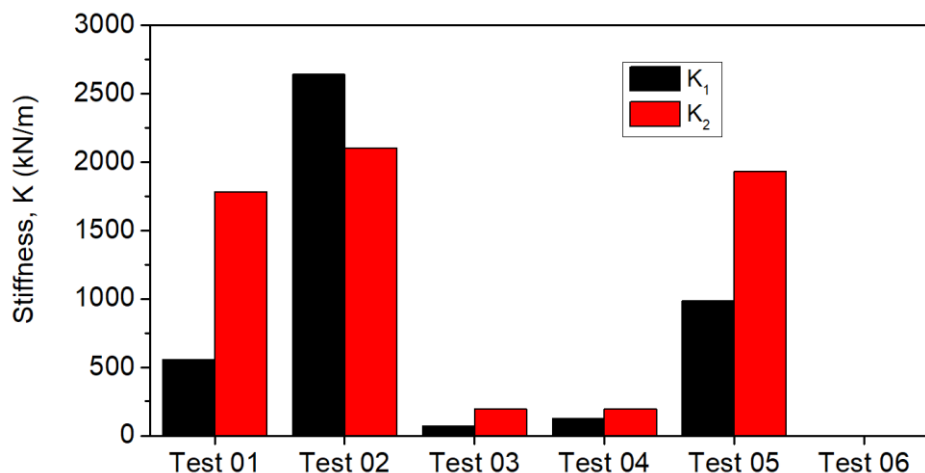
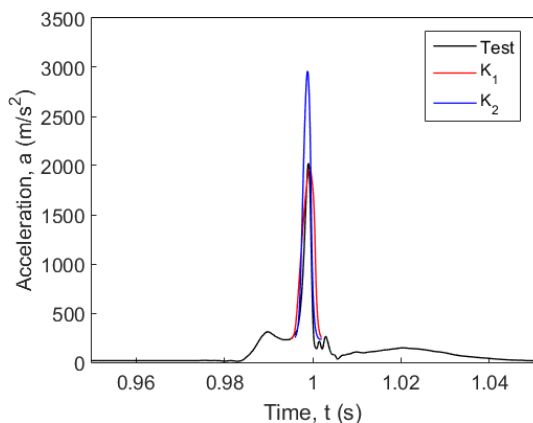
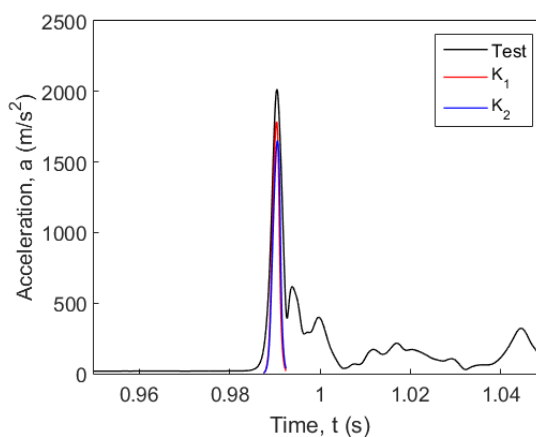


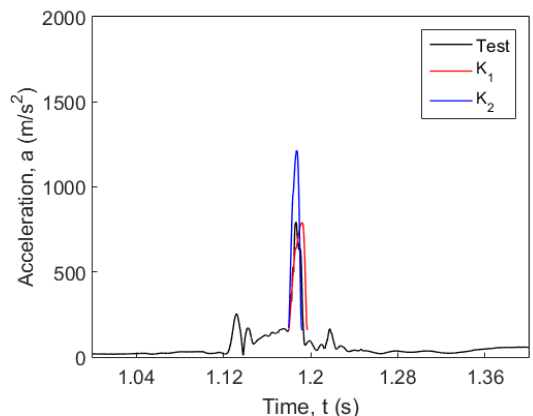
Figure 7.8 Ground stiffness for each test calculated by two methods



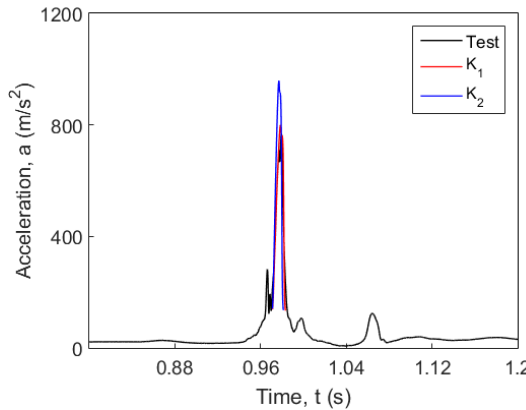
(a) Test 01



(b) Test 02



(c) Test 03



(d) Test 04

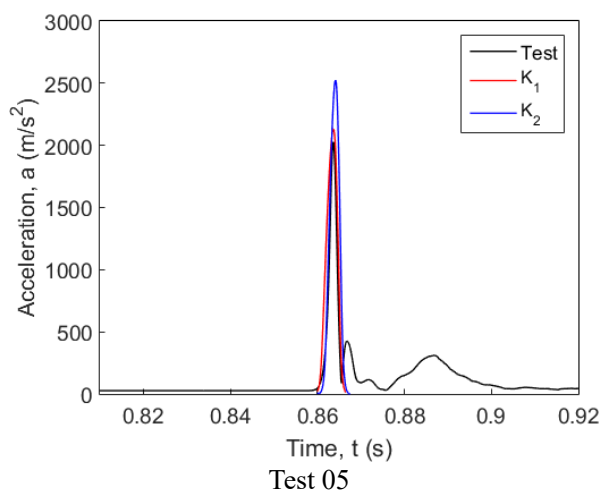


Figure 7.9 Comparison of the accelerations obtained from simplified head model test by using K_1 and K_2 (the comparison of Test 06 was not given because the head acceleration was corrupted signal during ground contact)

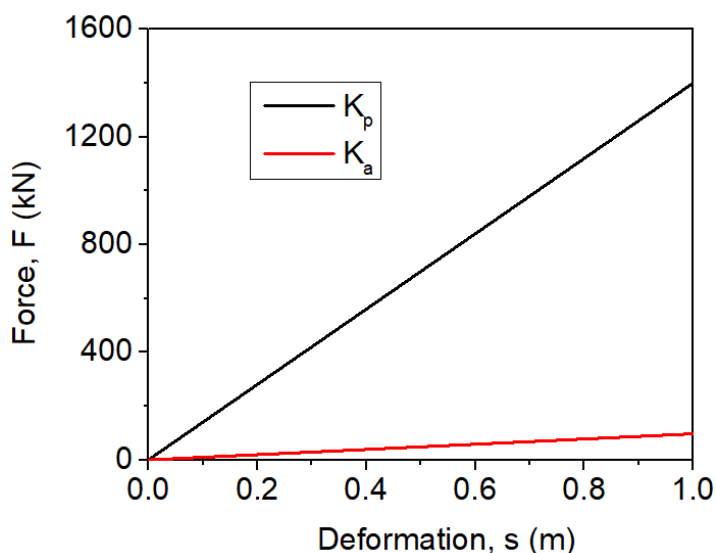


Figure 7.10 Two Stiffnesses of ground (k_p for Test 01, Test 02, Test 05 and Test 06; k_a for Test 03 and Test 04) applied in MADYMO simulation

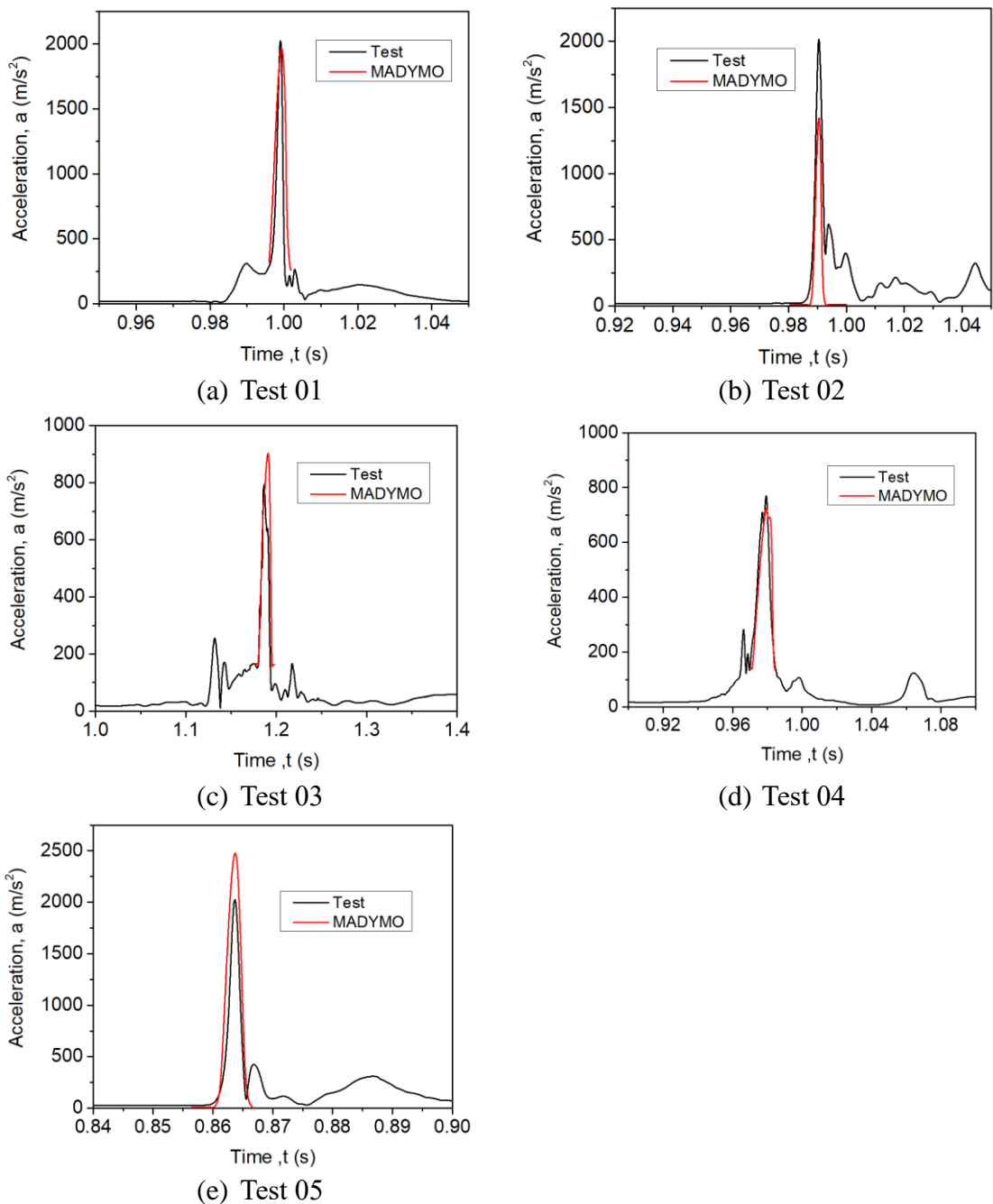
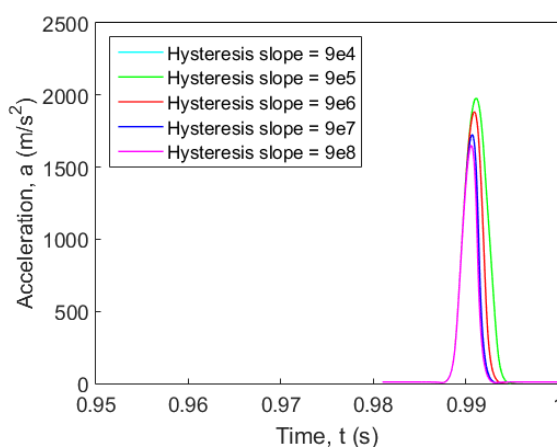


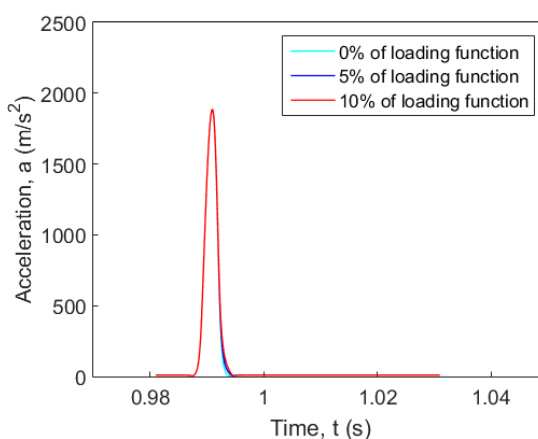
Figure 7.11 Comparison of acceleration peaks from cadaver tests and simplified MADYMO simulation in ground contact (the comparison of Test 06 was not given because the head acceleration was corrupted signal during ground contact)

There are two other variables in setting the contact characteristic in MADYMO: hysteresis slope and unloading curve. The effects were tested based on the simplified head model impact simulations. The hysteresis slope in 5 magnitudes ($9e4$, $9e5$, $9e6$, $9e7$ and $9e8$) and the unloading curves in 3 different ratios (0%, 5% and 10%) of loading curve were tested. The results are shown in Figure 7.12. Results showed that lower hysteresis slopes produced

relatively higher acceleration peaks and wider waves which can greatly impact *HIC* scores. The unloading curve seems to have almost no effect on the peak and impact time duration.



(a) Hysteresis slope



(b) Unloading curve

Figure 7.12 Testing of hysteresis slope and unloading curve effect on the contact

7.3. First round of simulation and results

The six staged tests were reconstructed and simulated using the MADYMO platform. Each test was simulated three times using vehicle contact characteristic from different sources. Pedestrian kinematics and head injury outcomes both from vehicle contact and ground contact were compared between staged experiments and their corresponding MB crash reconstruction, as shown in Figure 7.13 and Figure 7.14.

7.3.1. Pedestrian kinematics

The key event timings of the vehicle-pedestrian impact from staged tests and the reconstructed simulations as well as the ground contact mechanisms are compared, see Table 7.2 (Simulation 1: Mizuno and Liu; Simulation 2: Martinez; Simulation 3: EU NCAP). In Test 01 and Test 02, pedestrian vehicle separation times are generally earlier from MB reconstruction than those observed from the PMHS tests. While the head ground contacts occurred more than 100ms earlier for MB simulation in Test 01 but late in Test 02.

Table 7.2-1 Comparison of key events (s) of Test 01

Contact characteristic source	$t_{\text{head-vehicle contact}}$ (s)	t_{rebound} from the car (s)	$t_{\text{separation}}$ (s)	$t_{\text{head-ground contact}}$ (s)	Ground contact mechanism, from [Crocetta <i>et al.</i> 2015]
Staged test	0.145	0.269	0.770	0.995	M1
Mizuno and Liu ¹	0.140	0.200	0.595	0.845	M3
Martinez	0.140	0.200	0.615	0.875	M3
EU NCAP	0.145	0.205	0.610	0.865	M3

Table 7.2 -2 Comparison of key events (s) of Test 02

Contact characteristic source	$t_{\text{head-vehicle contact}}$ (s)	t_{rebound} from the car (s)	$t_{\text{separation}}$ (s)	$t_{\text{head-ground contact}}$ (s)	Ground contact mechanism, from [Crocetta <i>et al.</i> 2015]
Staged test	0.153	0.239	0.710	0.986	M3
Mizuno and Liu	0.150	0.235	0.625	1.045	M3
Martinez	0.150	0.230	0.615	1.020	M3
EU NCAP	0.150	0.225	0.655	1.070	M3

Table 7.2 -3 Comparison of key events (s) of Test 03

Contact characteristic source	$t_{\text{head-vehicle contact}}$ (s)	t_{rebound} from the car (s)	$t_{\text{separation}}$ (s)	$t_{\text{head-ground contact}}$ (s)	Ground contact mechanism, from [Crocetta <i>et al.</i> 2015]
Staged test	No show	-	0.834	1.180	M2
Mizuno and Liu	0.170	-	0.845	1.1170	M2
Martinez	0.170	-	0.805	1.1095	M2
EU NCAP	0.160	-	0.800	1.1130	M2

Table 7.2 -4 Comparison of key events (s) of Test 04

Contact characteristic source	$t_{\text{head-vehicle contact}}$ (s)	t_{rebound} from the car (s)	$t_{\text{separation}}$ (s)	$t_{\text{head-ground contact}}$ (s)	Ground contact mechanism, from [Crocetta <i>et al.</i> 2015]
Staged test	0.169	-	0.740	0.970	M2
Mizuno and Liu	0.185	-	0.745	1.030	M2
Martinez	0.185	-	0.745	1.255	M2
EU NCAP	0.185	-	0.705	1.190	M2

¹ The contact characteristics used in the simulations are from these authors correspondingly.

Table 7.2 -5 Comparison of key events (s) of Test 05

Contact characteristic source	$t_{\text{head-vehicle contact}}$ (s)	t_{rebound} from the car (s)	$t_{\text{separation}}$ (s)	$t_{\text{head-ground contact}}$ (s)	Ground contact mechanism, from [Crocetta <i>et al.</i> 2015]
Staged test	0.098	-	0.647	0.860	M1
Mizuno and Liu	0.120	-	0.735	1.790	M1/ M2
Martinez	0.120	-	0.735	0.990	M1/ M2
EU NCAP	0.115	-	0.735	1.040	M1/ M2

Table 7.2 -6 Comparison of key events (s) of Test 06

Contact characteristic source	$t_{\text{head-vehicle contact}}$ (s)	t_{rebound} from the car (s)	$t_{\text{separation}}$ (s)	$t_{\text{head-ground contact}}$ (s)	Ground contact mechanism, from [Crocetta <i>et al.</i> 2015]
Staged test	0.110	-	0.727	0.936	M1
Mizuno and Liu	0.135	-	0.725	0.945	M1/ M2
Martinez	0.135	-	0.690	0.895	M1/ M2
EU NCAP	0.130	-	0.680	0.925	M1/ M2

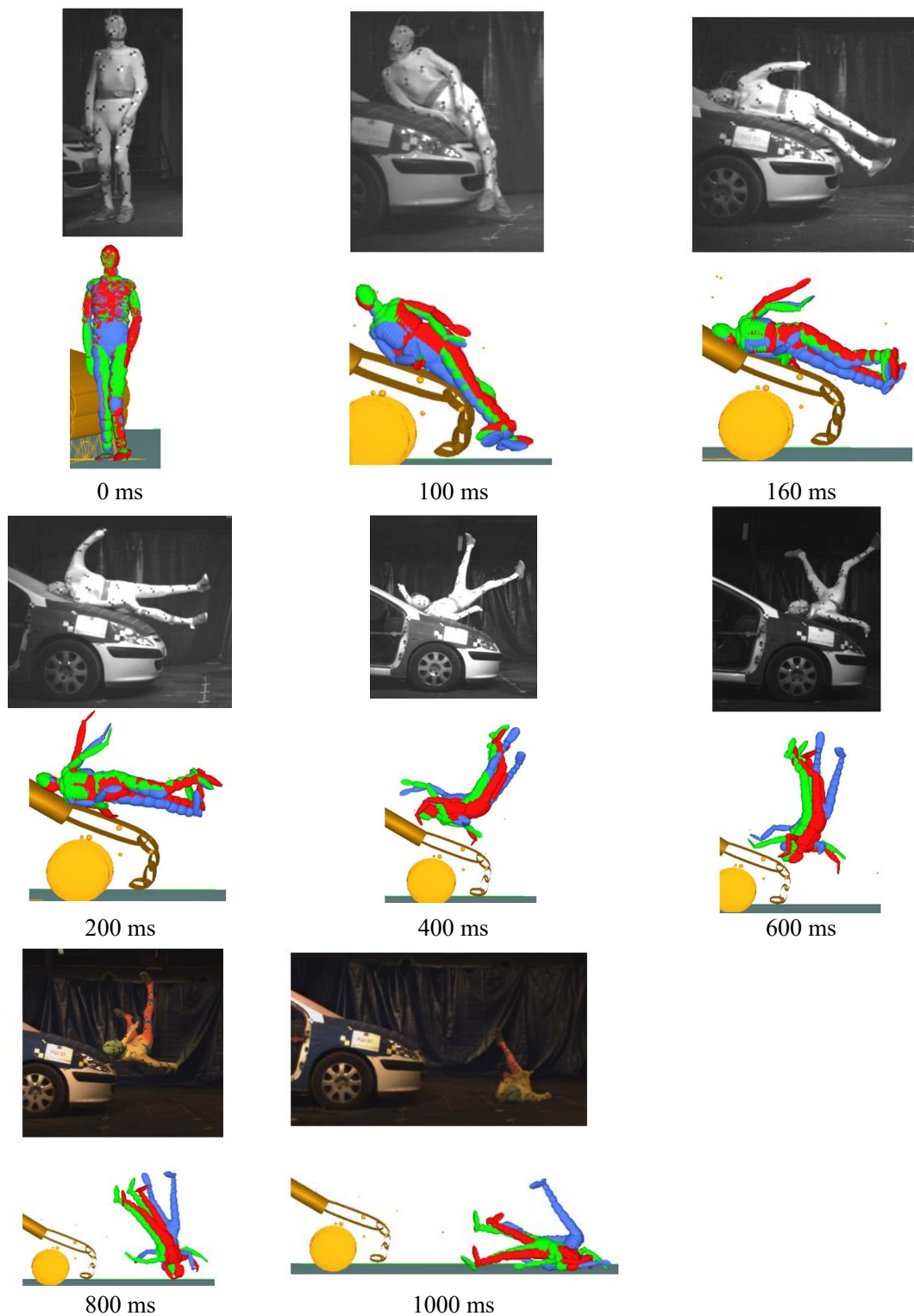


Figure 7.13-1 Test 01: Sequences of vehicle-pedestrian impact experiment compared with MB simulations. Contact characteristic of vehicle front applied from (Green model: EU NCAP; Blue model: Martinez; Red model: Mizuno)

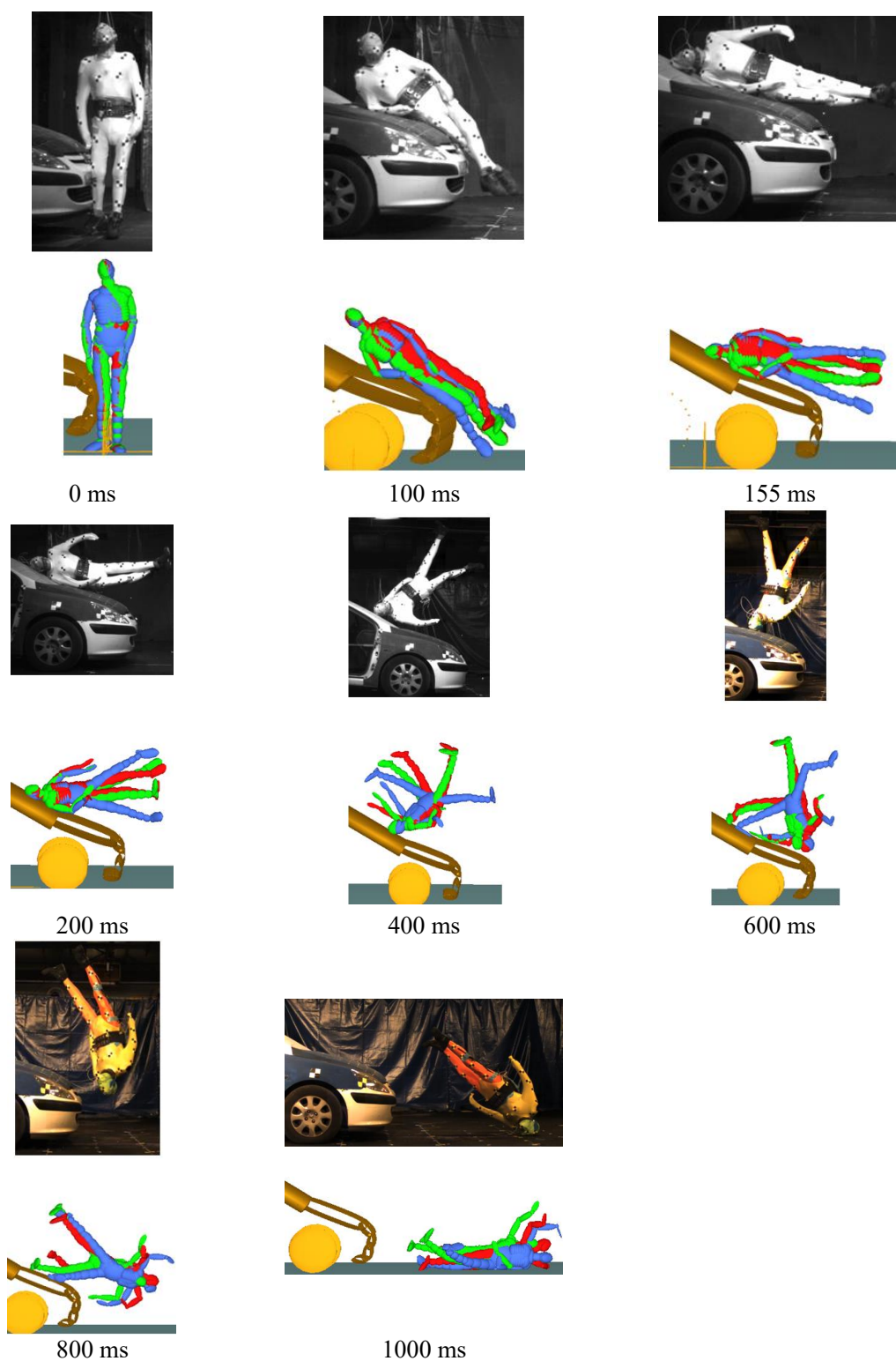


Figure 7.13-2 Test 02: Sequences of vehicle-pedestrian impact experiment compared with MB simulations. Contact characteristic of vehicle front applied from (Green model: EU NCAP; Blue model: Martinez; Red model: Mizuno)

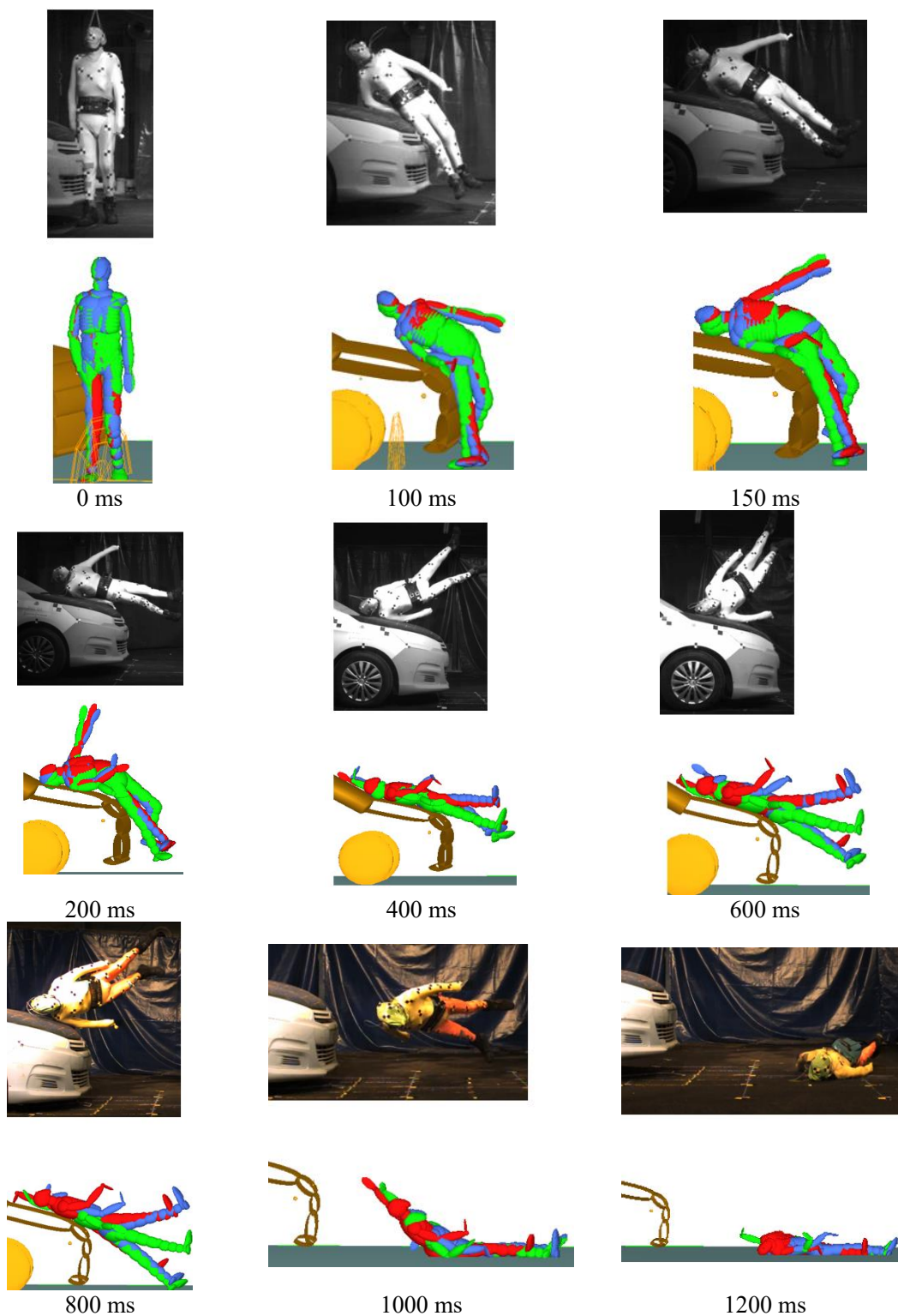


Figure 7.13-3 Test 03: Sequences of vehicle-pedestrian impact experiment compared with MB simulations. Contact characteristic of vehicle front applied from (Green model: EU NCAP; Blue model: Martinez; Red model: Mizuno)

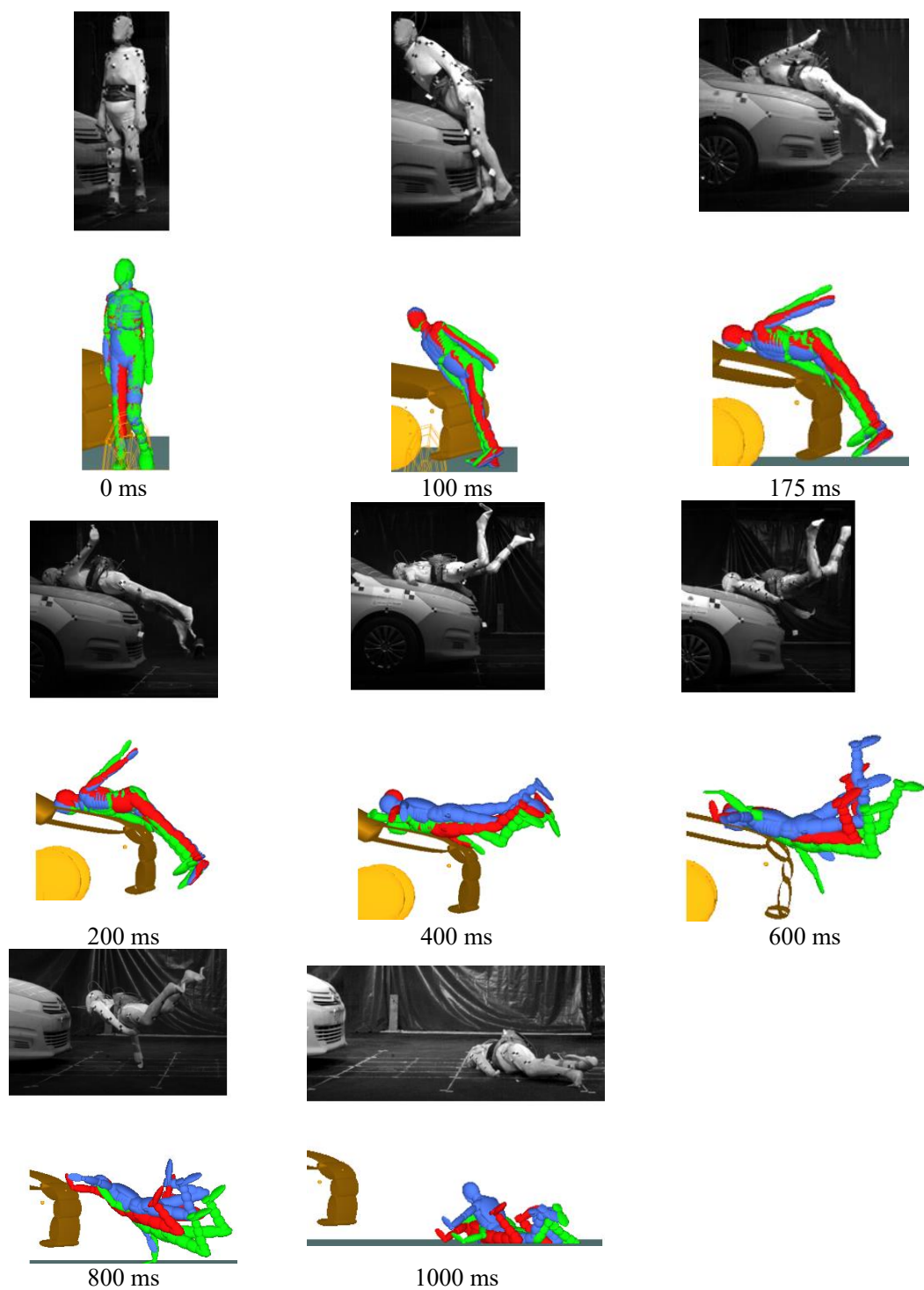


Figure 7.13-4 Test 04: Sequences of vehicle-pedestrian impact experiment compared with MB simulations. Contact characteristic of vehicle front applied from (Green model: EU NCAP; Blue model: Martinez; Red model: Mizuno)

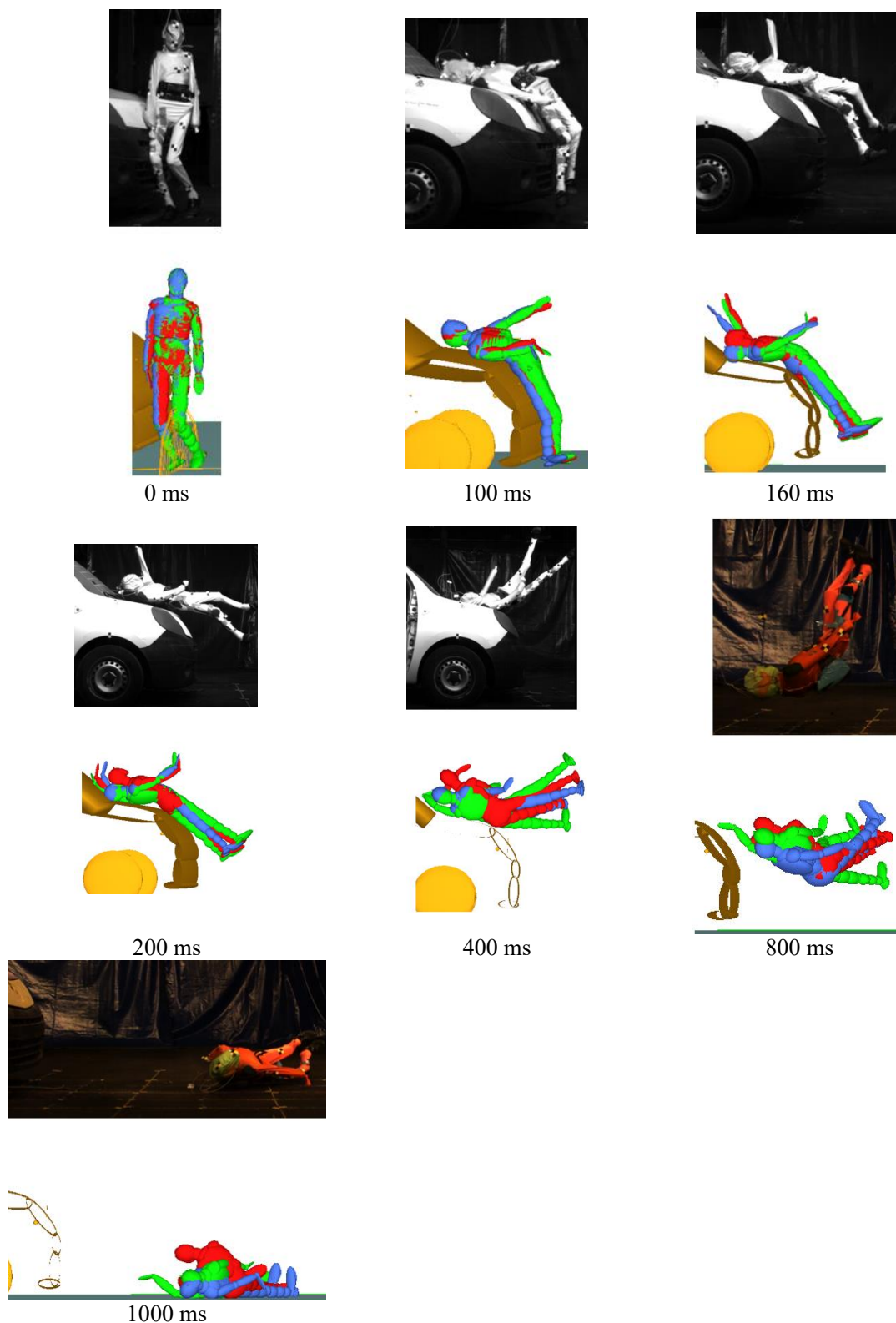


Figure 7.13-5 Test 05: Sequences of vehicle-pedestrian impact experiment compared with MB simulations. Contact characteristic of vehicle front applied from (Green model: EU NCAP; Blue model: Martinez; Red model: Mizuno)

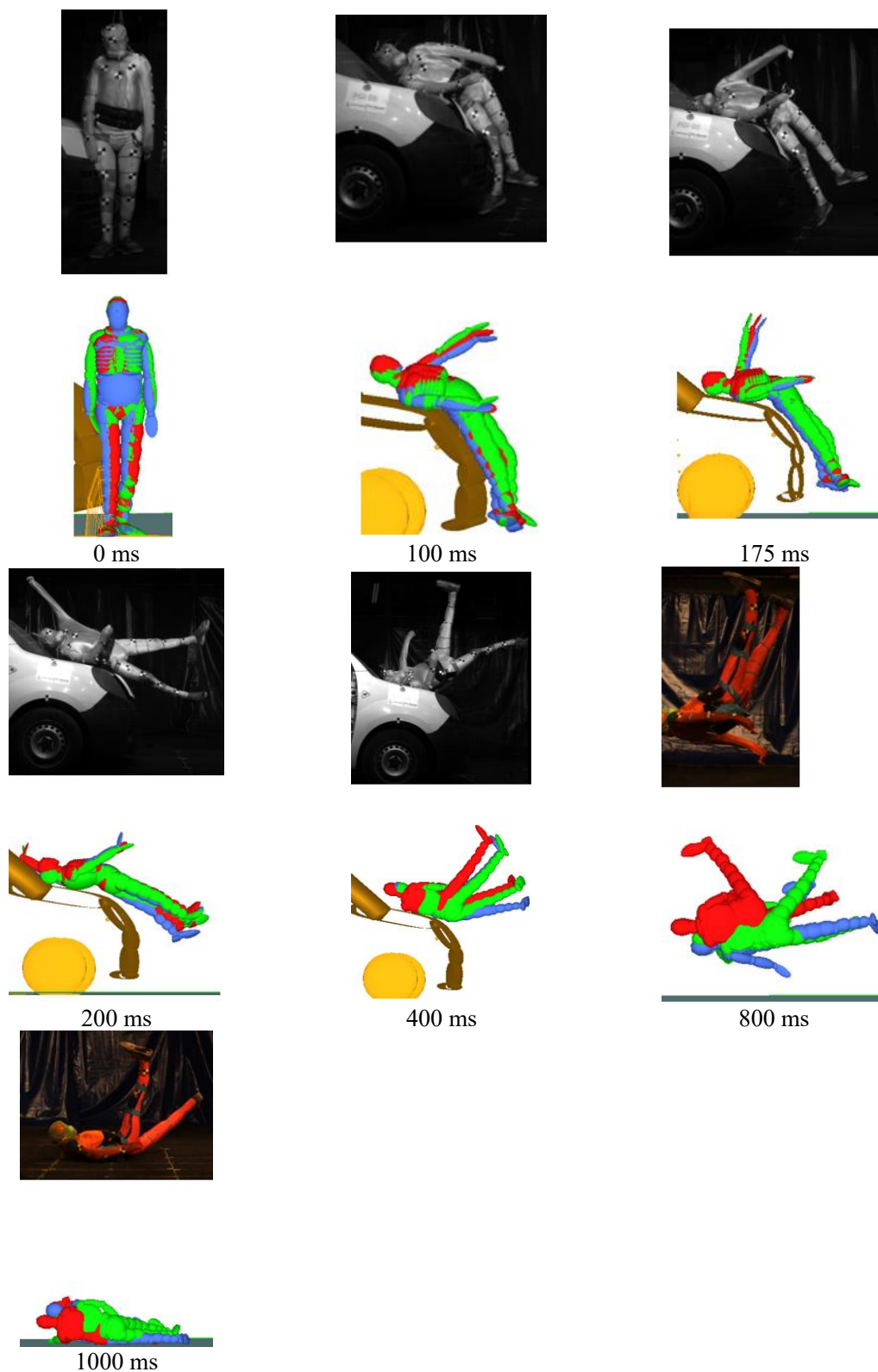
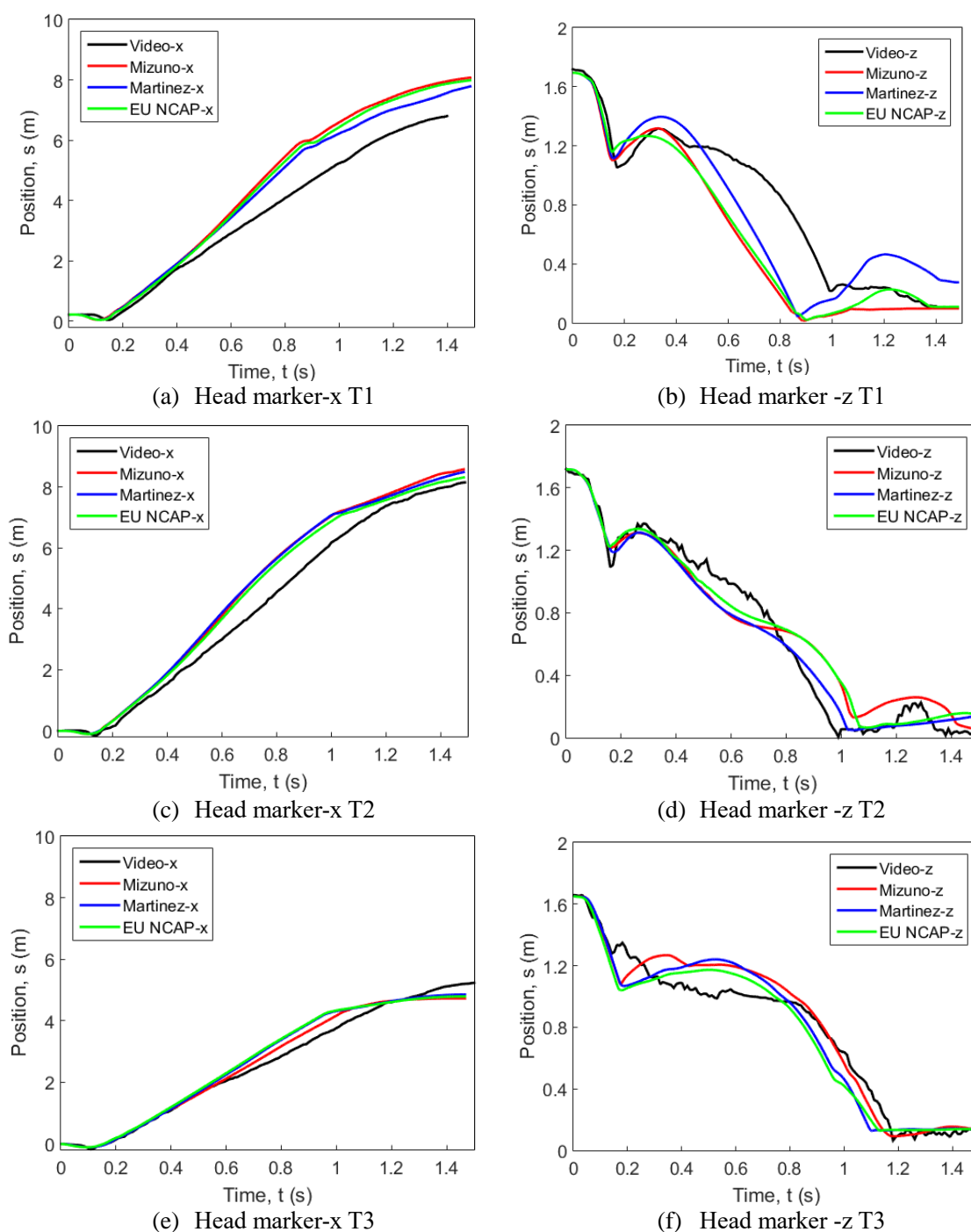


Figure 7.13-6 Test 06: Sequences of vehicle-pedestrian impact experiment compared with MB simulations. Contact characteristic of vehicle front applied from (Green model: EU NCAP; Blue model: Martinez; Red model: Mizuno)

7.3.2. Pedestrian head trajectories

Pedestrian head trajectories in both the X (horizontal) and Z (vertical) directions from staged tests and MB reconstructions are compared, see Figure 7.14. The MB Pedestrian's head projected further in the horizontal direction in simulations than the cadavers for Test 01 and Test 02.



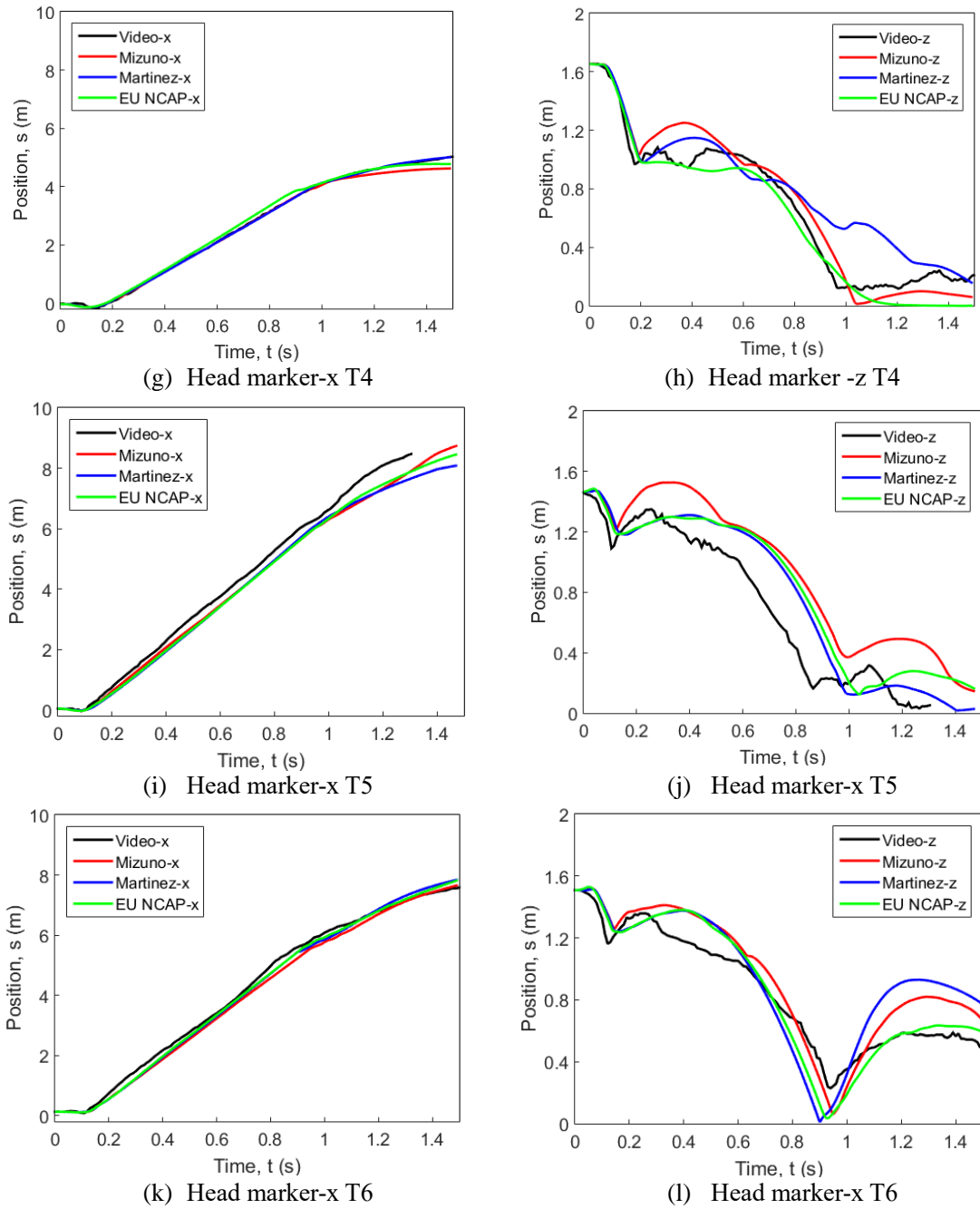
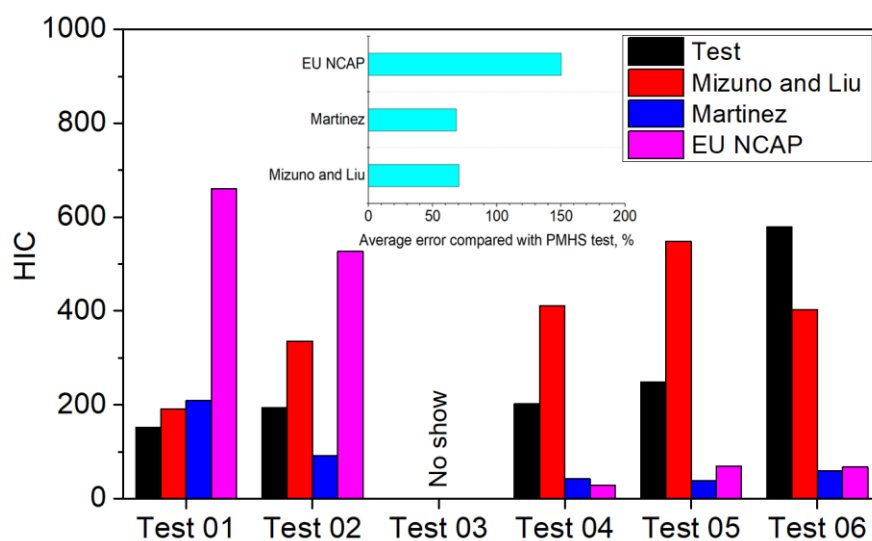


Figure 7.14 Comparison of pedestrian forehead trajectories between PNHS experiments and mathematic simulations

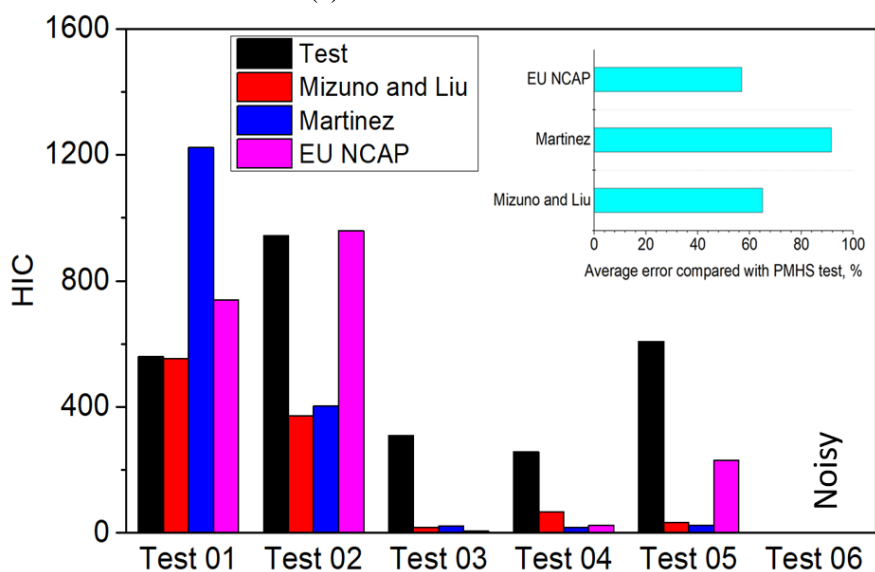
7.3.3. Pedestrian head injury criteria assessments

Pedestrian head injuries caused by translational accelerations were approximated using the *HIC* criterion, whereas injuries caused by rotational angular velocities were approximated using the *BrIC* criterion. These *HIC* and *BrIC* scores were calculated for both vehicle and ground contact for all six cases and were compared with the staged PMHS test results, as shown in Figure 7.15.

The overall average errors of the injuries obtained from simulation Mizuno and Liu, Martinez, EU NCAP compared with PMHS test are 51.3%, 62.0%, 73.3%, respectively.



(a) *HIC* from vehicle contact



(b) *HIC* from ground contact

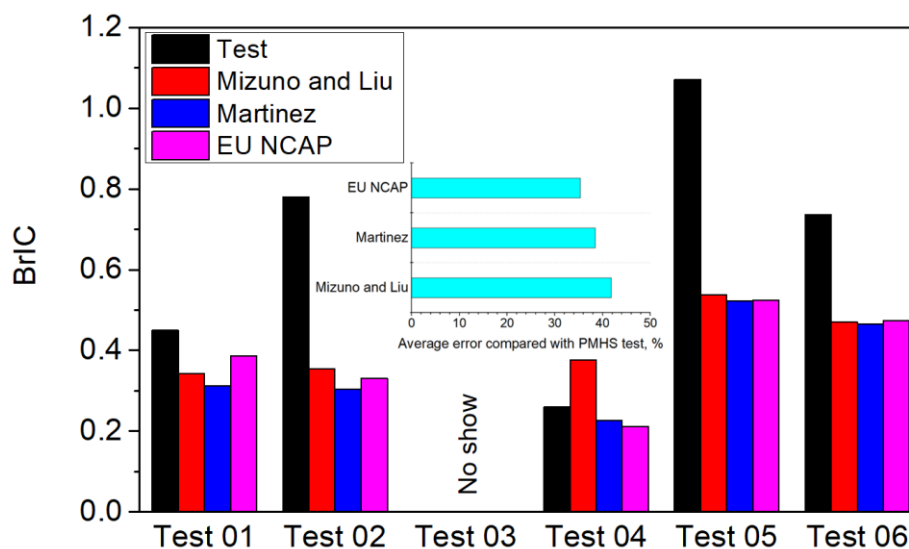
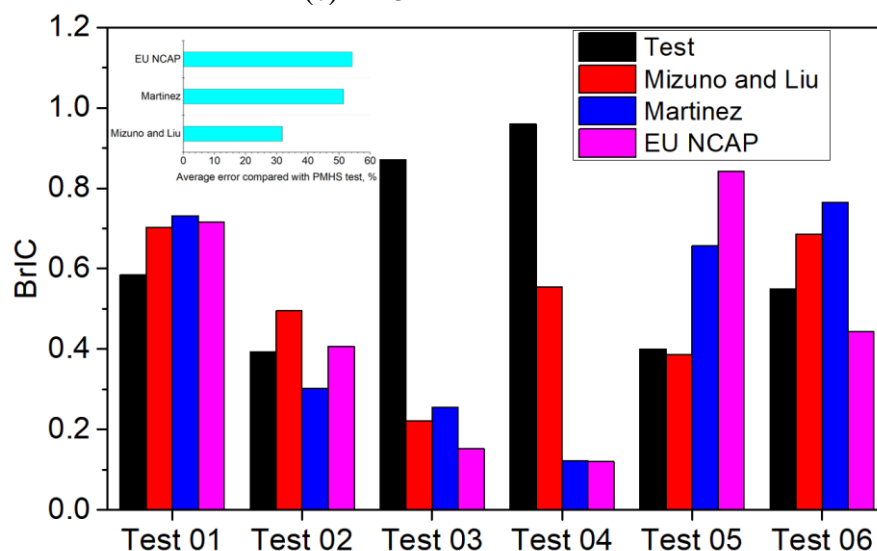

 (c) *BrIC* from vehicle contact

 (d) *BrIC* from ground contact

Figure 7.15 Comparison of head injury indices from vehicle and ground contact

7.4. Sensitivity study

Section 7.3.3 shows that the contact characteristic of the vehicle front has a great influence on the pedestrian head brain injury predictions caused by secondary ground contact. The influence of other uncertainties such as pedestrian initial joint angles and bending inside of the MADYMO pedestrian model will be assessed in the current study. Since vehicle contact characteristics resulted in relatively fewer errors of *HIC* and *BrIC* compared with the PMHS test results than the two other sources of contact characteristics. Mizuno and Liu's stiffness is then used as a baseline for further improvement by changing the contact characteristics of the windshield, bonnet, bonnet leading edge and bumper.

7.4.1. Sensitivity study of pedestrian initial joint angle

The initial posture effect was studied to check the degree of influence that the joint angle had over the resulting kinematics. Take Test 01 for instance, the initial hip angle, knee angle and ankle angle of the struck leg were changed ± 5 degrees in YZ plane (see Table 7.3) to check the influence on the ground related head injury indices. Only one parameter was changed each time and the other two were kept constant (baseline) for this sensitivity study. The results are shown in Figure 7.16. The injury indices obtained from the baseline model and the pedestrian with initial joint angle 2 (as illustrated in Table 7.3) are close while for the pedestrian with initial hip joint angle 2 and knee joint angle 2, the injuries showed noticeable differences when compared with the baseline results, as did the ground contact mechanisms, see Figure 7.17

Table 7.3 Initial angles of joint sensitivity study

Joint	Angle 1 (-5°)	Baseline angle (°)	Angle 2 (+5°)
Ankle	2	7	12
	21	26	31
	-5	0	5
Knee			
Hip			

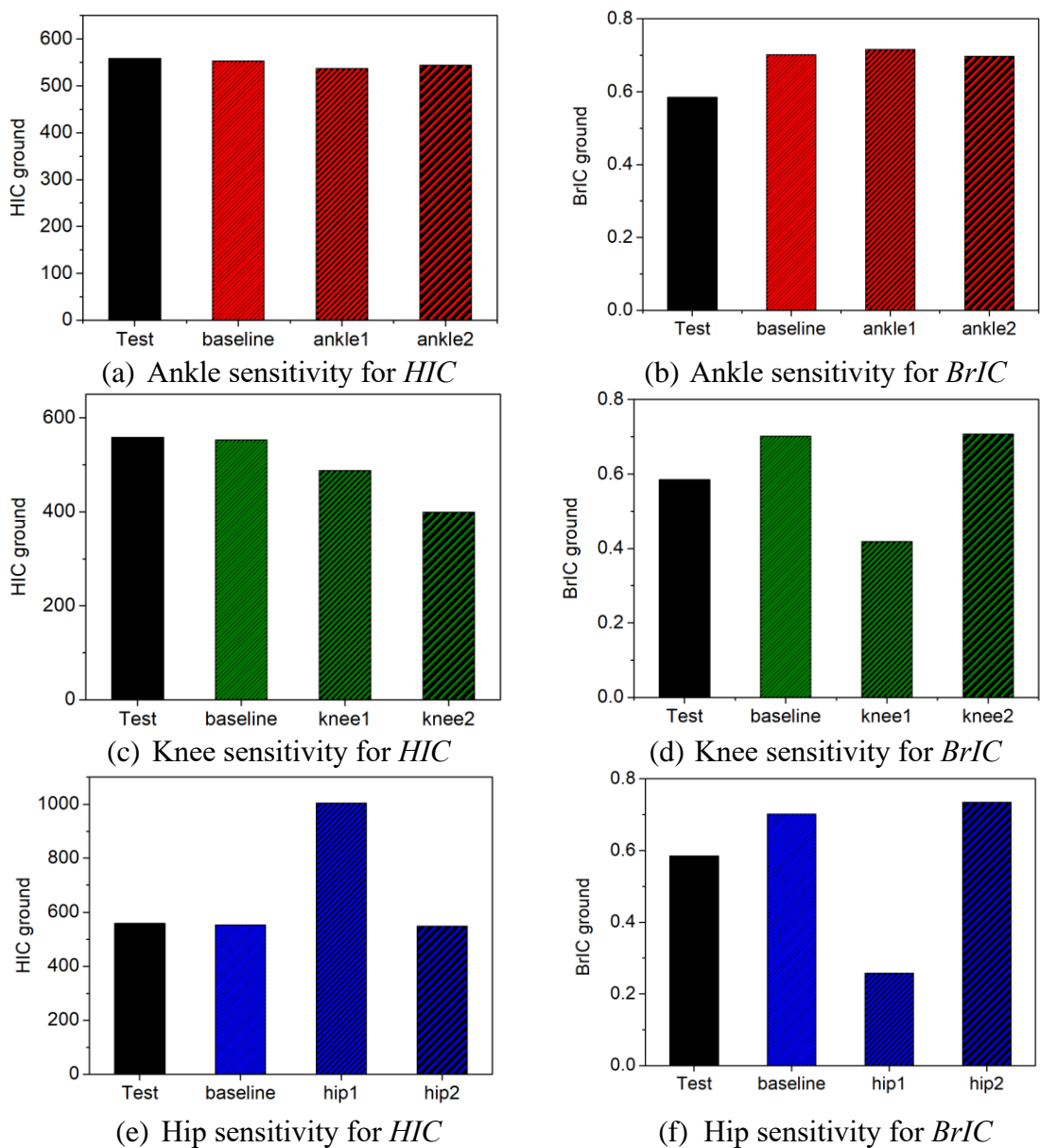


Figure 7.16 Initial joint angle effect on *HIC* and *BrIC* from ground contact

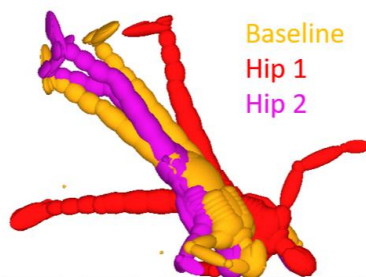


Figure 7.17 Pedestrian ground contact mechanisms from different initial hip angle from Table 7.3

7.4.2. Sensitivity study of bending of pedestrian model

As seen in the sequences of vehicle cadaver impact tests and MB reconstructions compared in Figure 7.13, the pedestrian model completely bounced off the vehicle after head windshield impact which was not present in the PMHS impact test. The potential reasons for the excessive bouncing could be the contact characteristic of the pedestrian model, the damping coefficient of the joints and the friction coefficient. A damping coefficient is the property of a material indicating whether the material will bounce back or return energy to a system. If the pedestrian bounce was caused by an unwanted vibration or shock, a high damping coefficient of the pedestrian joints will diminish the response. It will reduce the undesired reaction by absorbing the energy. A sensitivity study of human model bending was therefore performed, aiming to find the reason for the unexpected bouncing. A pedestrian model modified with a damping coefficient of 100 was used to reconstruct Test 01 and was compared with the baseline simulation. Both kinematics and injury outcomes (*HIC* and *BrIC* from ground contact) are compared, the results are shown in Figure 7.18 and Table 7.4. The bending added to the model did not significantly reduce the rebound but did affect the post-impact kinematics and the mechanisms of ground contact.

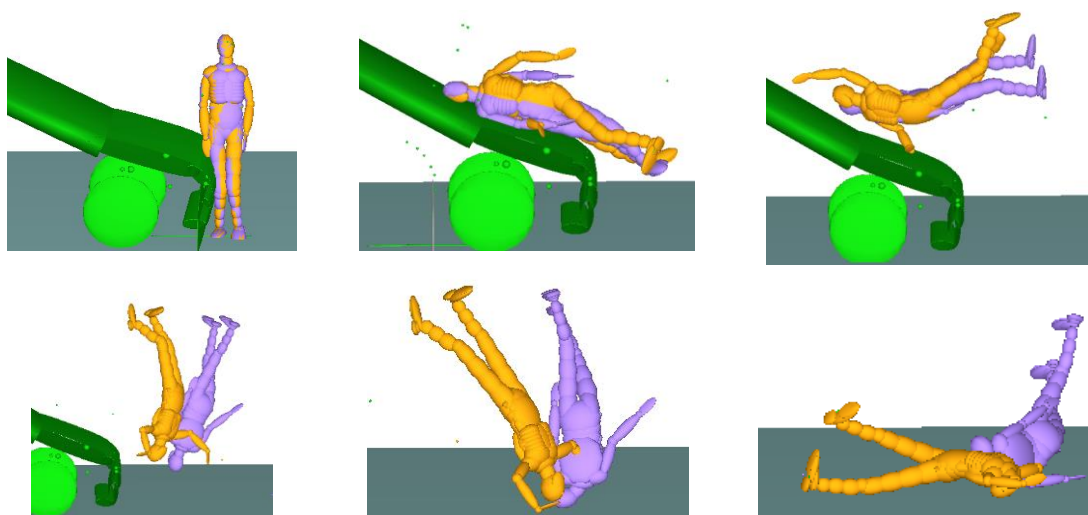


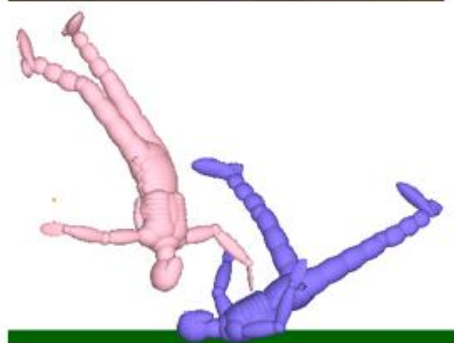
Figure 7.18 Sequence of baseline MB pedestrian model (orange) and the model with added bending kinematics in vehicle crash

Table 7.4 Comparison of *HIC* and *BrIC* in ground contact from baseline pedestrian model and the damping model

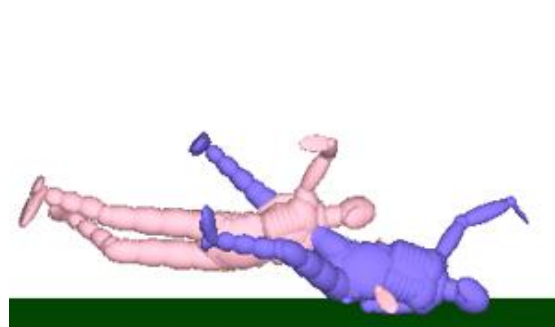
Injury indices	Baseline model	Damping model
<i>HIC</i>	553	1211
<i>BrIC</i>	0.7022	0.7758

7.5. Second round of reconstruction

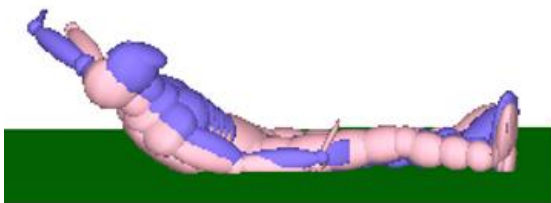
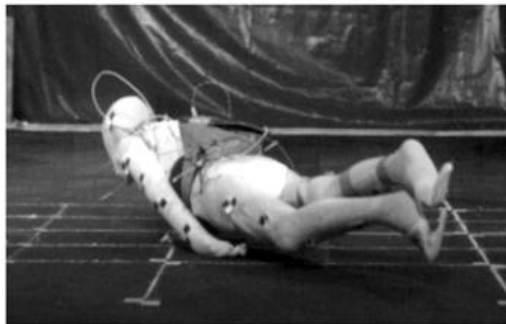
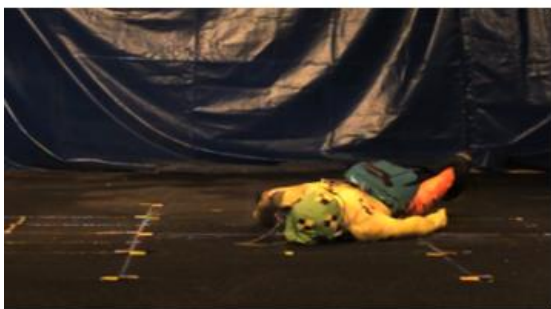
The study aims to represent the staged PMHS tests by using MB models. The results of the first round of simulations showed that the pedestrian kinematics could not be represented well for some of the tests. It is proved that the contact characteristics (the initial angle of pedestrian hip and knee joints, bending of MB pedestrian model) all effect the head injury indices during ground contact. The second round of reconstructed simulations were performed by changing the windshield/bonnet/bonnet leading/bumper contact characteristics which aimed to obtain a better kinematics matching of pedestrian models to the cadavers. The ground impact mechanisms are shown in Figure 7.19. Both of the ground impact mechanisms of the MB pedestrian models from the first and second rounds were compared with the cadaver tests. Pedestrian rotation in Test 01 and 02 were reduced. Test 05 is ignored because the cadaver could not represent the practical pedestrian posture due to the hard stiffness of the joints, see Figure 7.3 (e).



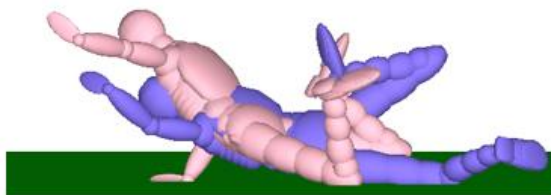
(a) Test 01



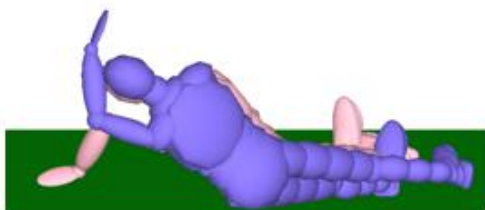
(b) Test 02



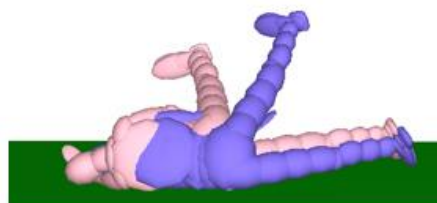
(c) Test 03



(d) Test 04



(e) Test 05



(f) Test 06

Figure 7.19 Comparison of pedestrian landing mechanisms between PMHS tests and MB reconstructions (Pink model: First round; Blue model: Second round)

The injury indices of the second round of simulations are compared with the results from the first round of simulations and the cadaver tests, as shown in Figure 7.20. For Test 01, *HIC* scores from both the vehicle contact and ground contact are significantly higher in the 2nd round simulations than *HIC* obtained from 1st round simulations and the cadaver tests. For Test 02, *HIC* obtained from ground contact in the 2nd round is more than twice as that in the 1st round, but it close to the cadaver test result. The differences of *BrIC* calculated from vehicle contact between two rounds of simulations are less than 0.2.

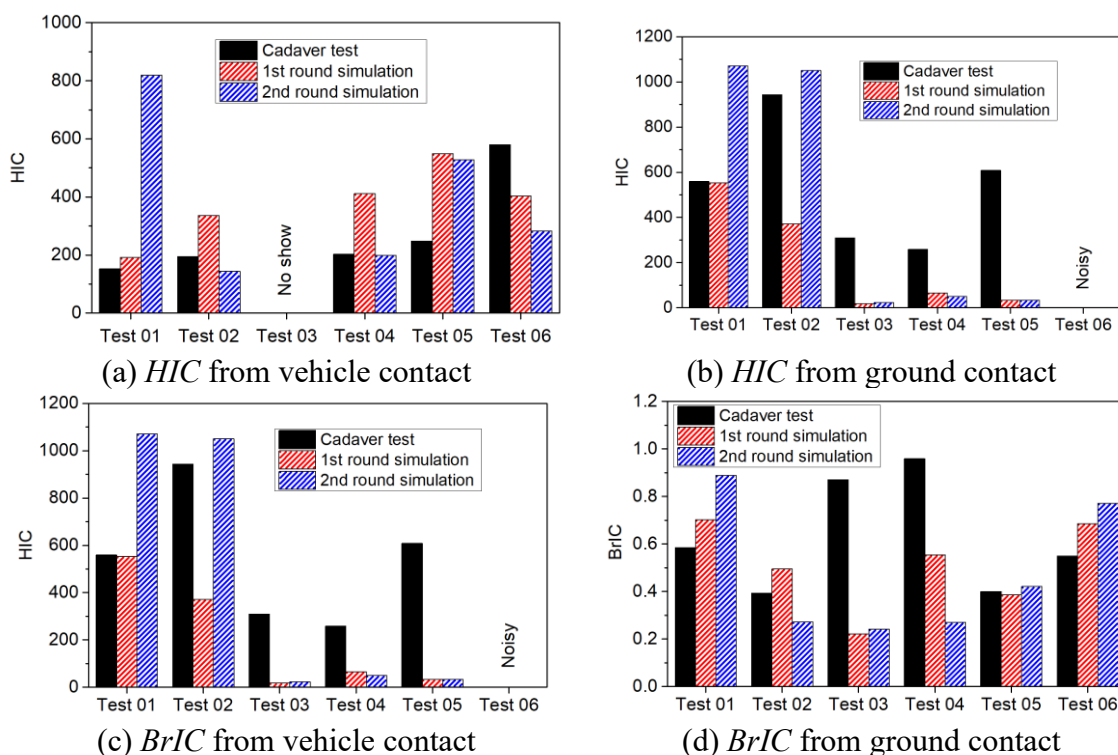


Figure 7.20 Comparison of head injury indices from PMHS tests, 1st round and 2nd round simulations

7.6. Discussion

This chapter presents the first kinematics assessment of an MB pedestrian model for the phases after vehicle impact by comparison with staged test data. The impact scenarios were built based on the PMHS tests (Chapter 6) and simulated with three different vehicle stiffnesses. Similar to the validation methods used in [Coley *et al.* 2001, DeLange *et al.* 2006], pedestrian kinematics and trajectories were assessed but unlike the validation of the head acceleration in the previous study [Coley *et al.* 2001], *HIC* scores which were calculated based on the accelerations were compared, the rotational brain injury indices (*BrIC*) were also compared (Figure 7.15). In Test 01 and Test 02 reconstructions, the

pedestrian models bounced off the vehicle after head windshield impact and this did not occur in the experiments. However, the bounces were observed in real-world collisions (Chapter 5). The damping coefficient inside the model was assessed to check if this could be held responsible for the rebound, but adding the bending could not eliminate the phenomena (Figure 7.18). In Test 01, the pedestrian left the vehicle earlier in the model and contacted the ground earlier than that observed from the experiments (Table 7.2). In addition, the ground contact mechanisms were not all representative of the landing mechanisms from the staged tests. The effect of pedestrian initial joint angles such as hip angle, knee angle and ankle angle of the struck leg was tested. Hip/knee joint angle 1 (-5°) greatly changed the injury indices because the postures were not matching the initial posture very accurately, angle 2 ($+5^{\circ}$) did not change the kinematics or injuries significantly.

The vehicle stiffnesses were changed to try to align the pedestrian kinematics with those seen in the experiments. For Test 01 and Test 02, pedestrian rotations can be increased or reduced by hardening or softening the contact characteristics of bumper and bonnet leading edge, see Figure 7.19. The ground impact mechanisms from the second round of simulations showed that the MB pedestrian better represented the experiments. While for low-speed test (20 km/h), Test 03, changing the contact characteristics of the vehicle's front components did not make any significant difference to the pedestrian ground impact mechanism, even though making the bumper/bonnet leading edge 100 times stiffer or softer than that in first round simulations. This discrepancy could be due to the low speed associated with relatively larger NBLEH in the model, which resulted in it being more difficult to change the pedestrian's post-impact kinematics significantly by changing the stiffness vehicle front-end components. For Test 05, the PMHS pedestrian was unusually stiff and the joints of the body were difficult to adjust, as shown in Figure 7.3(c), which could not represent the pedestrian's actual pose in the real-world. However, the mechanisms satisfied the classification of the previous MB parametric study [Crocetta *et al.* 2015] on ground impact. Even though the pedestrian kinematics improved in the 2nd round simulations, the injury indices were not generally close to that from cadaver tests compared with 1st round simulations (see Figure 7.20). Moreover, the mechanisms of pedestrian impacting with bumper/bonnet leading edge in 2nd round simulations were unreal (unexpected deep penetration) when softening the bumper/bonnet leading edge to match the ground impact mechanisms close to the cadaver tests.

Even though the impact mechanisms are similar, the HIC scores from computational models and the cadaver tests are obviously different, as shown in Figure 7.20, highlighting the uncertainty of MADYMO pedestrian model.

There are also several limitations to this study. Firstly, the MB pedestrian models were scaled basing on the MADYMO 50th percentile pedestrian male model, but the segments of each body parts were not scaled as the actual sizes of the PMHS. Secondly, the contact characteristics of PMHS should be individually different, but we did not change the stiffness of the pedestrian model because lacking related information.

7.7. Conclusion

This chapter of study first proposed a method to assess the multi-body models to represent the post-impact kinematics. The pedestrian models behaved similarly to the cadaver until head vehicle contact happened. Following the initial contact, they were found to bounce off the vehicle bonnet in Test 01 and Test 02, which did not occur in the staged cadaver tests. The injury indices obtained from MB models showed random differences with those of the cadaver tests. The sensitivity study found that the bending of the MB pedestrian model and the contact characteristics between pedestrian and vehicle had a discernable effect on the bounces which may change the kinematics in the air and the ground impact mechanisms. By changing the contact characteristics of vehicle front components, a second round of simulations were conducted to refine a model that would more accurately represent the kinematics of the cadaver. Despite Test 05, in which the initial pedestrian pose could not represent the actual pose, the pedestrian model rotations in most reconstructions, such as Test 01, Test 02, Test 04 and Test 06 can be amended similarly to the cadaver tests by hardening or softening the bumper and bonnet leading edge. In addition, the dominating factor that was the primary contributor to the bounces was found to be the stiffness of the vehicle front end. The bounce can be reduced by reducing the contact stiffness of bumper and bonnet leading edge. It indicated the potential possibility of human model development for pedestrian post-impact kinematics. The model is partially suitable for use in the virtual test system (VTS) under low-speed impact configurations.

8. Study 5: Assessment of vehicle front-end shape on pedestrian ground related injury considering a weighted impact configuration

8.1. Introduction

From previous studies [Simms *et al.* 2011, Hamacher *et al.* 2012, Han *et al.* 2012, Crocetta *et al.* 2015, Gupta *et al.* 2015, Li *et al.* 2017a, Yin *et al.* 2017], it is widely accepted that a vehicle's front end design influences the risk or severity of pedestrian ground contact injury. Several solutions were proposed to optimize the car to make it more pedestrian-friendly [Hobbs 2001, Carter *et al.* 2005, Park *et al.* 2010, Li *et al.* 2016]. As the results showed in Chapter 5, there was a correlation between the normalized bonnet leading-edge height and the risk of an adult experiencing AIS2+ head injuries caused by ground contact. However, the high variability of the real-world data hampered further insight into the role of the NBLEH. The cadaver tests also indicated that NBLEH has an influence on pedestrian ground impact mechanisms (Chapter 6). Nonetheless, it remains unclear how NBLEH influences pedestrian injury outcome in the broad range of real-world collision scenarios. Therefore, it is necessary to examine if a change in the vehicle front-end can reduce injuries from ground contact, considering a large range of impact configurations.

Li *et al.* [Li *et al.* 2016] used a Virtual Test System (VTS) to optimize vehicles' front end shape (by modifying the outer lines of bumper height, bonnet angle, bonnet leading-edge height *et al.*) and obtain the front end parameters of 'best shape' vehicle, which suffered lowest weighted injury costs in the collisions (in considering the distribution of vehicle impact speed from Chapter 5 and the performance of MB pedestrian model from Chapter 7, the vehicle speed is limited in 25kph). Inspired and based on this optimum solution, the current study attempts to conduct an MB numerical follow-up research on assessing vehicle front shape effect on ground contact using MATLAB and MADYMO. It is known from analysis of real-world pedestrian collisions that over 61% of the injury cost arises from ground contact for collisions speeds below 25 km/h. However, the potential for the reduction of ground related injury for low-speed collisions through the alteration of the vehicle front end shape over the range of real-world collision scenarios is not well understood. Earlier multibody modelling showed some effect of the normalised bonnet leading-edge height on

head injury outcome [Shang *et al.* 2018d], but here we look at the weighted ground contact injury cost for all body regions for vehicle shapes previously reported as either ‘good’ or ‘poor’ [Li 2016], for the three categories of passenger car (sedan), SUV and van.

The aims of this study are to assess whether the pedestrian injury costs subjected to ground contact are reduced in the optimized pedestrian-friendly (good) vehicle involved collisions compared directly with collisions involving poor vehicle designs.

8.2. Materials and methods

8.2.1. Pedestrian accident distribution

It has been stated [Simms and Wood 2006, Crocetta *et al.* 2015, Yin *et al.* 2017, Shi *et al.* 2018] that many factors such as vehicle impact speed, pedestrian size, pedestrian gait have effect on pedestrian ground contact mechanisms, also, the mechanisms are highly variable in actual collisions [Crocetta *et al.* 2015, Li *et al.* 2018]. In this study, the distribution of pedestrian size, gait, motion and vehicle speed are taken into consideration for the weighting.

8.2.1.1. Pedestrian size

In Li *et al.* [Li *et al.* 2016]’ study, there is no detailed pedestrian height distribution reported in the PCDS crash database [Mizuno and Ishikawa 2005]. They estimated the heights based on connecting their ages and anthropometric data [Pheasant and Haslegrave 2016] and then obtained the distribution [as shown in Figure 8.1(a)]. While in the current study, the distribution of height was extracted from the GIDAS database which has been studied by [Shang *et al.* 2018d], see Figure 8.1(b).

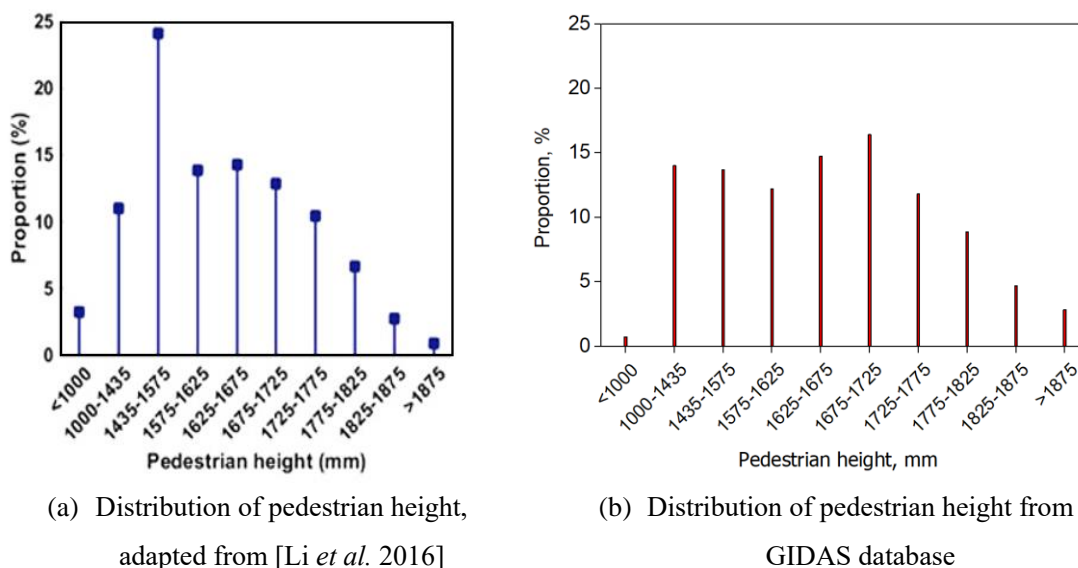


Figure 8.1 Distribution of pedestrian height in vehicle crashes from PCDS and GIDAS database

8.2.1.2. Pedestrian gait

Similar to [Crocetta *et al.* 2015, Li *et al.* 2016], a sample of pedestrian gaits were chosen from the whole gait cycle, defined by [Untaroiu *et al.* 2009], as shown in Figure 8.2. Considering that there is no available data on the distribution of pre-impact gaits, the proportions of gaits are selected equally as the study of [Li *et al.* 2016].

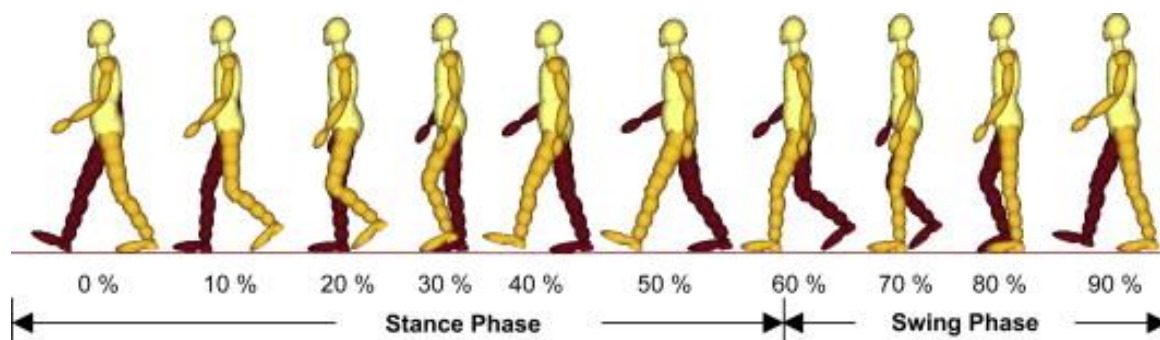


Figure 8.2 Pedestrian stances for different gait parameters (%) of the gait cycle, adapted from [Untaroiu *et al.* 2009]

8.2.1.3. Vehicle speed

Figure 8.3 (a) shows the distribution of vehicle impact speeds from a PCDS database [Mizuno and Ishikawa 2005], which was extracted by [Li *et al.* 2016] and applied in his VTS study. The distribution of the vehicle impact speeds from the GIDAS database was extracted and calculated from the study of [Shang *et al.* 2018d], as shown in Figure 8.3 (b) and the

proportions of the impact speed were normalized to maintain a sum of 100%. The vehicle speed is limited to less than 25 km/h, which is based on the observations of the real-world video study and the performance of the MB pedestrian model presented in Study 4 (Chapter 7),.

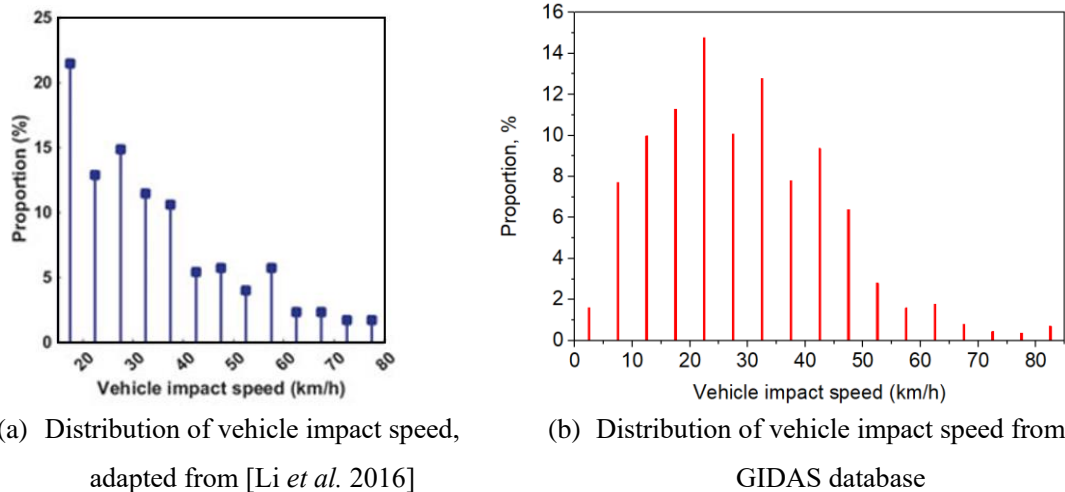


Figure 8.3 Distribution of vehicle impact speed in vehicle crashes from PCDS and GIDAS database

8.2.2. Pedestrian model

MADYMO pedestrian models are widely used to analyze kinetics and assess injuries in the field of vehicle-pedestrian safety [Simms and Wood 2006, Simms *et al.* 2011, Crocetta *et al.* 2015, Li *et al.* 2016, Yin *et al.* 2017]. In the current study, 5% percentile, 50% percentile, 95% percentile model, as well as scaled models (illustrated in Figure 8.4), are employed to represent a broad range of human sizes in real-world collisions. The model can be scaled to the needed height and weight based on the distribution in section 8.2.1.



Figure 8.4 MADYMO pedestrian models, 3 years old, 6 years old, 5% percentile, 160cm (scaled), 170cm (scaled), 50% percentile, 180cm (scaled), 95% percentile and 190cm (scaled), from left to right.

8.2.3. Vehicle model

Vehicles are modelled with ellipsoids using the MADYMO platform. Figure 8.5 (a) demonstrates the parameters of vehicle front-end shape and Figure 8.5 (b) presents the MB model impact scenario applied in this study. Each of the three different categories of vehicle, i.e., Sedan, van and SUV, were constructed using ellipsoids, as shown in Figure 8.5 (b). Six shapes, a good shape (results in lowest injury cost) and a poor shape (results in highest injury cost) for each vehicle categories obtained in the previous study [Li 2016], are chosen to check if it is feasible to apply the virtual test system to reduce ground related injuries.

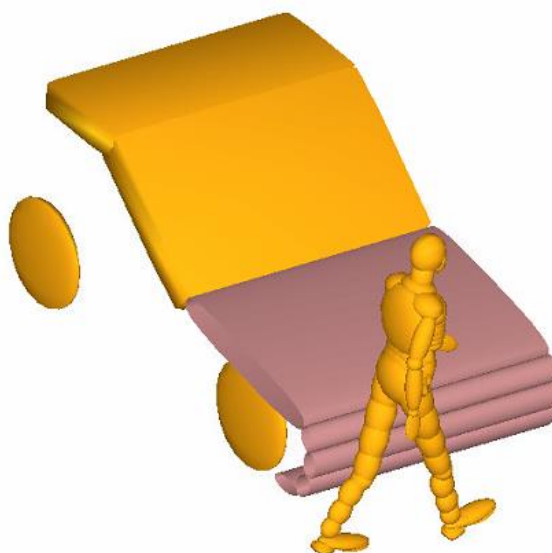
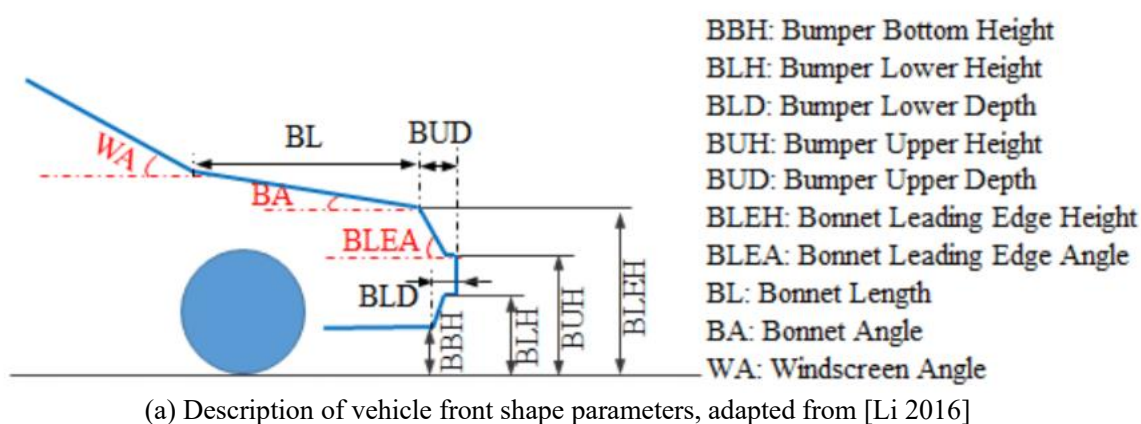


Figure 8.5 Description of vehicle front shape parameters and MB vehicle-pedestrian impact scenario

8.2.4. Numerical simulation

The basic vehicle-pedestrian impact scenario applied in this study was from [Li 2016], as shown in Figure 8.5 (b), the contact characteristics of vehicle contact are taken directly from the source of Mizuno and Liu in Chapter 7. Force–deformation curves of the bumper bonnet refer to those found in [Liu *et al.* 2002]. The stiffness of the windshield is obtained from the tests of [Mizuno and Kajzer 1999, Mizuno and Kajzer 2000], which has been applied in the optimization study of Li *et al.* [Li 2016]. The friction coefficients between vehicle and pedestrian are set as 0.3, which is used in previous studies [Lyons and Simms 2012]. For the pedestrian ground contact, since there is no validated pedestrian ground contact model, the ground is modelled as a rigid surface, the stiffness k_p in Figure 7.10 is applied as ground stiffness. The friction coefficient is set as 0.58, which represents a dry asphalt road [Crocetta *et al.* 2015]. And the constant deceleration of 0.75 g [Lyons and Simms 2012, Crocetta *et al.* 2015] is applied to the vehicles to simulate the braking.

8.2.5. Weighted Injury cost

Injury criterion values including head injury (*HIC*), neck injury (*Nij*), thorax injury (*TTI*), pelvis injury (lateral impact force), lower extremity injury (lateral bending moment), and knee injury (bending angle), which are extracted from the MADYMO simulations are categorized into AIS levels based on AIS 2005 [Gennarelli and Wodzin 2006] and the injury threshold obtained from previous studies [Tannous *et al.* 1999, Mo *et al.* 2014, TNO 2017]. The costs for each injury are listed in Table 4.1 and Table 4.2. Cost are then based on the distributions of pedestrian height (shown in Figure 8.1), vehicle speed (Figure 8.3) and an equal distribution of pedestrian gait. The product of the proportion of pedestrian height (p_{hi}), impact speed (p_{vi}), and pedestrian gait (p_{gi}) gives a weighting of a specific impact configuration (p_i) in the simulation test system, which is illustrated in Figure 8.1. The sum of the proportions for each distribution of influencing factors equals unity; as illustrated in Figure 8.2. Finally, the weighted injury cost (*WIC*) of each vehicle shape is the sum of the products of injury costs (*IC*) and weighting coefficient (p_i), see Figure 8.3.

$$p_i = p_{vi} * p_{hi} * p_{gi} \quad \text{Equation 8.1}$$

$$\sum_{i=1}^N p_i = \sum_{i=1}^N p_{vi} = \sum_{i=1}^N p_{hi} = \sum_{i=1}^N p_{gi} = 1 \quad \text{Equation 8.2}$$

$$WIC = \sum_{i=1}^N (IC * P_{vi}) \quad \text{Equation 8.3}$$


Where N is the simulation number.

8.2.6. Simulation test sample

Table 8.1 illustrated a simulation test sample (STS) of 60 (considering 3 vehicle impact speeds, 5 pedestrian heights and 4 pedestrian gait stances). In this study, the STS of 30 (3 vehicle impact speeds, 5 pedestrian heights and 2 pedestrian gait stances), 60 (6 vehicle impact speeds, 5 pedestrian heights and 2 pedestrian gait stances), 120 (12 vehicle impact speeds, 5 pedestrian heights and 2 pedestrian gait stances), 240 (12 vehicle impact speeds, 5 pedestrian heights and 4 pedestrian gait stances) were simulated. Different STS sizes were used for convergence when increasing the sample size. A detailed description of the STS is listed in Appendix D.

Table 8.1 A simulation test sample (STS) considering 6 vehicle impact speeds, 5 pedestrian heights and 4 pedestrian gait stances

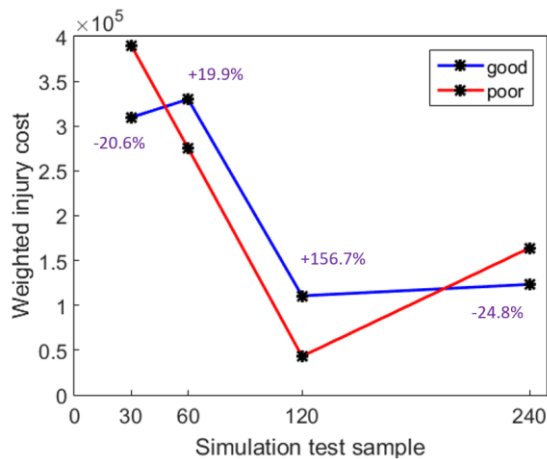
Group		1	2	3
Impact speed (km/h)	Range	1-8	9-16	17-24
	Mean	4.5	12.5	20.5
Pedestrian height (cm)	Range	<140	140-157	158-170
	Mean	120	151	164
Gait stance (%)	Range	20-30	40-60	70-80
	Mean	30	50	80



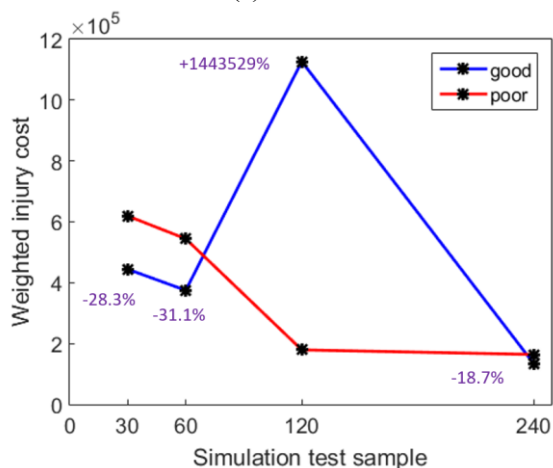
8.3. Results

The virtual tests are conducted in 30, 60, 120, 240 simulation numbers to represent a broad range of real-world crash configurations. Figure 8.6 (a), (b) and (c) show the WIC comparisons between previously proposed ‘poor shapes’ and ‘good shapes’ [Li *et al.* 2016] for the sedan, van and SUV, respectively as a function of the number of simulations included in the VTS. The percentages listed in the graphs mean pedestrians obtain higher (+) or lower

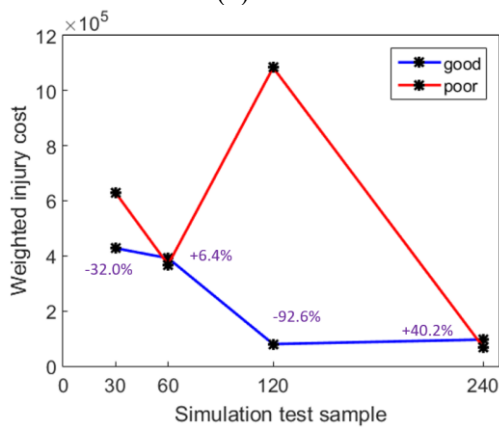
(-) WIC for good shape vehicle compared to the poor shape ones. It can be observed that in most cases, the weighted ground related injury costs that pedestrians obtained from good shaped SUVs are less than those from poor shaped SUVs, while for the sedan and van, the WIC changed more sporadically. Significant differences can be observed for the SUV and van groups when the STS was 120.



(a) sedan



(b) van



(c) SUV

Figure 8.6 WIC comparison between poor shape vehicles and good shape vehicles

8.4. Discussion

Based on vehicle front shape optimization, the feasibility of the virtual test focused on pedestrian ground contact was examined. The weighted ground related injury costs reduced with an increase in the simulation test sample (STS) for poor shape van, while for the sedan, SUV and the good shape van, the WIC showed randomness with the STS. When comparing the WIC obtained from the good shape and poor shape vehicles, no trends can be observed from all the 3 categories. Even though the differences of WIC between the poor sedan and good sedan are generally small, the differences are relatively large for SUV and van when $STS = 120$, as shown in Figure 8.6. The statistic was odd but no particular large value of weighted injury cost was found in each simulation, emphasizing there is a difficulty to obtain a convergency (while STS adapted from Table D.5 indicating the possibility of obtaining a convergency, as the results shown in Figure D1). Moreover, the optimized good shape vehicles did not improve the safety for pedestrian ground contact based on the WIC against poor shape vehicles. However, the results at the largest sample size ($STS = 240$) indicated for all three categories that there is not much difference for the weighted injury cost between the good shape and the bad shape. On the basis of this, we should continue to push the good shape because at the very least it's better for the primary contact (which was optimized based on the vehicle contact), and there is no discernable indication that it is more severe for the secondary contact.

There are some limitations in this VTS study: the vehicle speed distribution applied in this study is different when compared with the previous optimization work [Li 2016], and the speed was limited to less than 25 km/h. The optimization was based on the injury costs from vehicle and ground contacts while the current study only focused on the ground contact. In addition, the MB pedestrian models do not perform very well according to the assessment in Chapter 7, making the feasibility of running VTS remains uncertain.

8.5. Conclusion

Virtual tests are conducted in this study to assess whether the pedestrian ground related injury costs could be reduced in good shape vehicle collisions when compared to with poor shape vehicle collisions. Simulation tests samples (STS) of 30, 60, 120, 240 were applied in the VTS to represent the broad range of real-world vehicle-pedestrian crash configurations

from German in-depth Accident Database (GIDAS). However, convergence did not occur with an increase in the simulation sample size. The weighted injury costs from ground contact did not significantly reduce for good shape vehicle collisions when compared with the poor shape vehicle involved collisions. The differences of WIC obtained from good shape vehicles and poor shape vehicles are relatively small in all 3 categories except for van and SUV when the simulation tests sample was 120.

9. Discussion

Pedestrians can sustain injury in both vehicle and ground contact, but the research to date has primarily focused on the vehicle contact. Vehicle manufacturers are in the process of developing methods of reducing vehicle-based injuries, however, there has been insufficient research into the development of methods to mitigate ground-based injuries. In recent years there has been an increase in researchers [Otte and Pohlemann 2001, Simms and Wood 2006, Badea-Romero and Lenard 2013, Crocetta *et al.* 2015, Yin *et al.* 2017, Han *et al.* 2018a, Han *et al.* 2018b, Li *et al.* 2018, Shi *et al.* 2018] that have focused on the ground contact. For those who have focused on ground contact, most of the approaches have been through computational modelling [Isenberg and Chidester 1998, Crocetta *et al.* 2015, Yin *et al.* 2017, Shi *et al.* 2018, Zou *et al.* 2019], but the models were not validated. Accordingly, there are significant aspects of pedestrian ground contact which are not well understood, including:

- (a) no recent study of accident data for main factors (speed, age, height, vehicle shape effects)
- (b) no study of real-world collision kinematics
- (c) no cadaver studies
- (d) no validation of simulation models
- (e) no clarity on vehicle shape effects

Prior to the development of countermeasures, it is essential to complete a biomechanical analysis of pedestrian ground contact kinematics and injuries.

9.1. Pedestrian ground contact injuries from real-world accident database

An analysis of the German in-depth accident database (GIDAS) data related to the distribution of pedestrian injuries from ground contact was firstly reviewed in detail since 2001 [Otte and Pohlemann 2001]. Head injuries subjected to ground contact are found over all AIS levels except AIS 6, which is consistent with the general trend observed by [Ashton and Mackay 1983] in the 1980s. The proportion of ground contact injuries reduces quickly with an increase in AIS level. For both cases of MAIS 4 and MAIS 5, ground contact is responsible for only 4/28 cases, as shown in Figure 4.2.

Similarly to the results of previous studies [Kendall *et al.* 2006, Simms and Wood 2006] on

vehicle speed effect on pedestrian ground contact injuries, ANOVA tests (Figure 4.3 and Table 4.5) showed that increased vehicle speeds resulted in significantly higher ground related injuries. However, two cases with very serious (AIS 4+) ground related injuries occurred at low vehicle impact speeds (13km/h and 14km/h). Surprisingly, there were also four high speed cases larger than 100 km/h without AIS 2+ ground related injuries, and three of these were fatal due to the windscreen contact. These detailed cases highlight the variability of ground contact injuries, and also the relevance of ground contact injuries for low speed collision cases.

Age has a significant effect on the levels of pedestrian ground related injuries, as shown in Figure 4.5 and Figure 4.6. This is firstly reported even though other researchers [Niebuhr *et al.* 2016] observed a similar trend for injuries from vehicle contact. Moreover, the relation of age and injured body parts indicated that the average age of pedestrians with AIS 2+ ground related thorax injuries is substantially higher than for head, spine and extremities injuries, see Figure 4.6. Thus, the effects of age and speed can obfuscate the understanding of vehicle-related factors.

Figure 4.7 showed that the median NBLEH (Normalised bonnet leading-edge height) increases for the increasing AIS level of ground contact head injuries even though the Kruskal-Wallis analysis showed this effect is not significant. However, the logistic regression analysis shows for the first time a statistically significant influence of NBLEH on adult pedestrian ground contact head injury outcome, see Table 4.8. The results provided support for studies of [Tamura and Duma 2011a, Tamura *et al.* 2014, Crocetta *et al.* 2015, Yin *et al.* 2017] which have indicated vehicle shape could have influences on pedestrian ground contact injuries. The previous predictions [Tamura and Duma 2011a, Tamura *et al.* 2014, Crocetta *et al.* 2015, Yin *et al.* 2017] were conducted by mathematic modelling while the current result of NBLEH effect is the first data analysis from real-world collisions.

It also pointed out that more than half of the potential injury costs could be eliminated if ground contact injuries were prevented for the low speed collisions, as Table 4.9 illustrated.

9.2. Pedestrian kinematics observed from real-world collision videos

The videos of real-world vehicle-pedestrian collisions visually provided the display of vehicle-pedestrian impact. The results showed a high degree of variability and uncertainty of pedestrian ground contact mechanisms during the collisions, which has been stated in previous studies [Kendall *et al.* 2006, Kerrigan *et al.* 2007, Han *et al.* 2018a, Han *et al.* 2018b, Li *et al.* 2018, Shi *et al.* 2019]. It is observed that after being struck by a vehicle, the pedestrian sustained a larger projection with the increase of vehicle speed (as shown in Figure 5.2), which is consistent with [Wood *et al.* 2005, Yang *et al.* 2005].

Lower values of NBLEH produced larger whole-body rotations (see The relation of estimated NBLEH and whole-body rotations), which is first time this phenomenon has been clearly observed using real-world accident data. Therefore, it can be conclusively stated that NBLEH has a discernable effect on pedestrian post vehicle impact kinematics and the subsequent ground contact. A sharp drop-off in pedestrian post vehicle impact rotation was observed as the BLEH reached pelvic height. This strengthens the case for emphasizing the role of NBLEH in pedestrian collisions. Since these real-world videos are not clear enough to observe detailed pedestrian ground contact, it sets up the need for staged PMHS tests with high-quality videos. Most of the vehicle speeds in this study were estimated between 20 to 40 km/h, allowing us to focus on the pedestrian ground contact for these speeds.

9.3. Kinematics and dynamics of pedestrian head ground contact from cadaver tests

The six staged cadaver impact tests present the first detailed overview of the whole kinematic process of vehicle-pedestrian collisions, starting with first pedestrian vehicle contact and ending with rest on the ground following pedestrian ground contact (as shown in Figure 6.5 and Table 6.5). Pedestrian kinematics can be classified into several key phases and events: phase 1 (duration ~100-170ms) considers the first pedestrian-vehicle impact, terminating once the head impacts the windshield/bonnet, this phase is the most studied in previous research [Kerrigan *et al.* 2005, Subit *et al.* 2008]. Phase 2 is the process that the pedestrian moves with the car until they separate, this duration lasts around 550 to 625ms. Phase 3 is the dropping phase, and starts at the point of separation, ending with pedestrian ground contact, the duration is 185-280ms. Pedestrian ground contact mechanisms (see Table 6.9) are consistent with those proposed in [Crocetta *et al.* 2015]. Phase 4 is slide, roll and bounce

to rest, this phase can last 1-1.8s.

Head impact with the vehicle in Phase 1 and head ground impact in Phase 3 was extensively studied to investigate head injury predictions using translational and rotational indices (*HIC* and *BrIC*). First head ground contacts occur around 1s after the first vehicle-pedestrian impact, which is at the end of a highly non-linear chain of events, such that small changes in initial configuration result in significant changes in head ground impacts (e.g. Test 01 and Test 02, see Figure 6.3) and has been stated in the previous literature [Simms and Wood 2009].

Head-vehicle and head-ground contact processes were clearly identified by the time histories of the head velocity changes (see Figure 6.8). Obvious changes of head velocities in both horizontal and vertical directions were observed during head vehicle contact while for head ground contact, velocity changes were only observed in the vertical direction. No skull fractures were detected by X-ray examinations in all six tests. This complies with the finding from the GIDAS data analysis [Shang *et al.* 2018d] that less than 4% skull fractures occurred in collisions with a speed range of 25-34 km/h and less than 1% in the speed range of 15-34 km/h, suggesting that the modelled ground stiffness was too high [Simms and Wood 2006].

In addition to *aHIC* scores, the *BrIC* was used to assess the ground contact injuries for the first time, see Figure 6.11. *HIC* scores obtained from ground contact were generally higher than that from vehicle contact, this is consistent with the results of [Ashton 1975], which indicated that the injury risk is higher in ground contact than vehicle contact at low vehicle speeds. Figure 6.14 showed the *aHIC* score reduced with the increase of AIS3+ rotational head injury risk, suggesting a compensatory pattern between linear and angular head injury risk.

No clear patterns were observed for the NBLEH's effect on ground contact head injuries, which may be due to the small number of tests performed. However, this could be investigated by multi-body modellings. There are also further limitations of the cadaver tests, such as the PMHS being fixed until the second before vehicle impact, while half of the pedestrians were observed to voluntarily avoid the collision in the selected real-world crash videos. Furthermore, the PMHS's lack of muscle tone may result in different kinematics.

The influence of the braking applied in the impact tests was not analysed, while the recent study of MB modelling indicated that the severity of head ground contact can frequently be reduced by controlling vehicle braking [Zou *et al.* 2019].

9.4. Multi-body pedestrian model assessment for ground contact

This study presents the first kinematic comparison of an MB pedestrian model for the phases following a vehicle impact with cadaver tests data (the data is from Chapter 6). The MADYMO MB pedestrian model is only validated for the vehicle contact [Ishikawa *et al.* 1993a, Ishikawa *et al.* 1993b, Kajzer *et al.* 1993] even though it has been used in studying the ground contact [Crocetta *et al.* 2015, Yin *et al.* 2017]. In this study, the model was assessed by comparing the head trajectories and pedestrian kinematics with the data from cadaver tests. Similar methods were used in [Coley *et al.* 2001, DeLange *et al.* 2006] for model validation. *HIC* and *BrIC* were also compared to assess the injury risks caused by translative accelerations and rotational velocities.

The key events comparison between the staged tests and the MB reconstructions listed in Table 7.2 showed that the kinematics of cadavers and the corresponding MB pedestrian models were asynchronous in some events. For example, in Test 01 the separation happened 155-175ms earlier in the simulation than the cadaver test, and the ground contact mechanisms were not in the same category proposed by Crocetta *et al.* [Crocetta *et al.* 2015]. In Test 02, the pedestrian model separated from the vehicle earlier, and impacted the ground later than the cadaver due to it undergoing a greater number of rotation angles before landing. Figure 7.13 examined the vehicle-pedestrian impact sequences of the cadaver tests and MB simulations. In Test 01 and Test 02, the MB pedestrians bounced off the vehicle, which did not occur in the staged tests. However, bounce did occur in the real-world collisions which can be observed in the videos analysed in Chapter 5 (see Figure 5.1), and the cadavers could not represent voluntary action that a live pedestrian could. Future work will focus on a better understanding of this issue.

The effect of the pedestrian's initial joint positions and the damping coefficient of the joints were assessed but found no significant help to improve the post-impact kinematics and the *HIC/BrIC* (see Figure 7.16 and Figure 7.17). However, the initial posture did show an influence on pedestrian kinematics, which has been stated in previous research [Simms and

Wood 2006, Untaroiu *et al.* 2010]. The second round of simulations were conducted to try to obtain closer pedestrian ground contact mechanisms by changing the contact characteristics of the vehicle bumper and bonnet leading edge. Figure 7.19 showed the limited capability of the MB pedestrian model representing the kinematics in real-world collisions, and the resulting injury indices were not matching well (see Figure 7.20). The model could, however, be deemed reasonable for low speed (under 30 km/h) collisions.

9.5. Vehicle shape effect on ground related injury costs based on a virtual test system

[Li 2016] optimized the vehicle front end shape, aiming to obtain the least injury costs in vehicle crash when considering the distribution of vehicle speeds and pedestrian heights and gaits by using Virtual Test System (VTS). In the current study, only ground contact injury costs were assessed. Figure 8.6 showed that the WIC reduced with an increase of simulation test sample (STS) for poor shape van. While for the sedan, SUV and the good shape van, the WIC showed no convergence with the STS. The differences of WIC between poor shape vehicles and good shape vehicles are generally small in all three categories at the largest STS (240). However, when STS = 240, the sedan resulted in slightly higher WIC than van and SUV, which does not comply with the previous findings [Roudsari *et al.* 2005, Simms *et al.* 2011]. The patterns of vehicle front-end shape on pedestrian ground contact injury risks is unclear yet. This may be due to the different vehicle speed distributions used by [Li 2016]. In addition, the speed was limited to 24 km/h based on the estimated speed in real-world collisions (chapter 5). The optimization was based on the injury costs from vehicle and ground contacts while the current study only focused on the ground contact.

9.6. Potential practical work to reduce the risk and severity of ground related head injuries

Previous studies proposed several potential engineering solutions to make the vehicle much safer for pedestrians, in accordance with EEVC and Euro-NCAP regulations [Euro-NCAP, EEVC 2002]. In 2003, an active bonnet was proposed as an engineering solution to pedestrian safety [Krenn *et al.* 2003]. In 2004, designed bonnet and bumper for the safety of pedestrians were proposed by Lee *et al.* [Lee *et al.* 2004] which is based on experimental tests and computational simulations. A 2004 google patent [Mattsson and Ericsson 2004] presented the idea of a hood which can rise and fall to reduce the risk of a pedestrian head

injury. Beyond that, the pedestrian airbag is another important research direction, which was proposed in previous research and patents [Mori *et al.* 2008, Takimoto *et al.* 2010, Jakobsson *et al.* 2013, Lim *et al.* 2015]. Recently, researchers have focused on an adhesive outer airbag to keep the pedestrian stay on the bonnet to prevent the ground contact, or to reduce the bounce speed to lower the risk of suffering severe ground related injuries [Khaykin and Lerner 2016, Gupta *et al.* 2017, Shi *et al.* 2019].

Inspired by these ideas, potential solutions are proposed in this study to prevent or reduce the incidence and the severity of pedestrian injuries caused by ground contact. Based on the current and future results of chapter 5 and chapter 6, the virtual test system could be employed by vehicle industries to optimize their car front-end shapes, which is the safest design to pedestrian (both injuries from vehicle contact and ground contact are considered). In addition, pedestrian inflatable safety vest could be designed. The idea is when the pedestrian being hit by a car, the vest is triggered and then inflates and encase the head (see Figure 9.1), which protects the head when hitting the vehicle (similar to airbag used in bike helmet [Hovding 2019]) or the ground.

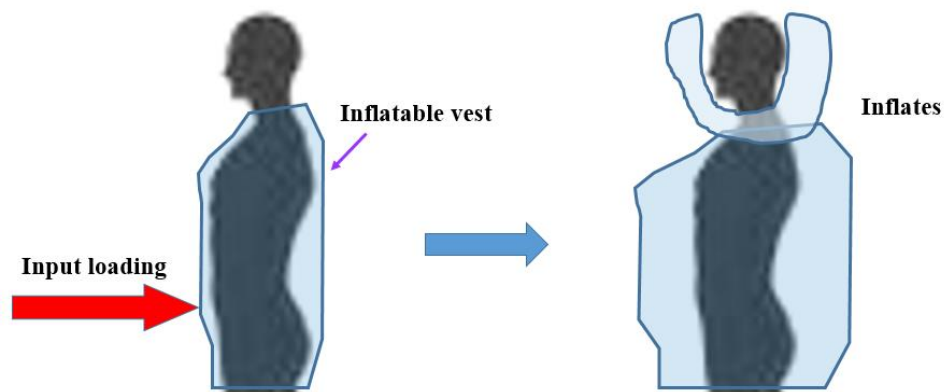


Figure 9.1 The idea of the inflatable safety vest

9.7. Summary

A recent real-world accident database was analyzed in detail to study ground contact injuries. Vehicle speed's effect on the severity of ground contact injury was consistent with previous research [Anderson *et al.* 1997, Otte and Pohlemann 2001, Wood *et al.* 2005, Hussain *et al.* 2019]. Vehicle front-end design is accepted to be one of the influencing factors on pedestrian ground related injuries [Roudsari *et al.* 2005, Simms *et al.* 2011, Hamacher *et al.* 2012,

Crocetta *et al.* 2015, Yin *et al.* 2017]. A statistically significant effect of NBLEH on the adult pedestrian ground related head injury is observed for the first time, see Table 4.8. A number of real-world vehicle-pedestrian videos were collected and analyzed to investigate NBLEH's effect on ground contact. The phenomenon of smaller values of NBLEH resulting in larger pedestrian rotations before landing on the ground was first observed, see The relation of estimated NBLEH and whole-body rotations . The rotation angle has a discernable influence on head ground contact mechanisms [Crocetta *et al.* 2015], thereby affecting the head injuries [Simms and Wood 2006, Yin *et al.* 2017]. However, the footage of the videos were not clear enough, only the general ground impact mechanisms can be observed, such as the landing kinematics in [Han *et al.* 2018b, Li *et al.* 2018], therefore, a series of cadaver tests were conducted and recorded in high-quality videos to have a better understanding of what happened in a complete process of vehicle-pedestrian collision as well as the head ground contact, which is also the first detailed analysis of pedestrian ground contact kinematics by PMHS tests. Figure 6.11(a) showed that the risk of head injuries due to translative contact with the ground is generally higher than those caused by vehicle contact. Previous studies [Ashton 1975, Simms and Wood 2006] have indicated that pedestrians may sustain more serious injuries caused by ground contact than from vehicle contact at low impact speeds. As Figure 6.11(f) and Table 6.8 showed, the risk of rotationally induced brain injury (*BRIC*) was substantially higher for the two 20 km/h tests (Test 03 and Test 04) when compared to the four cases with a vehicle speed of 30 km/h. The relation of either linear or rotational head injury risk and the NBLEH is unclear and this may be due to the small sample size (only six tests performed). A parametric study of the effect of NBLEH on ground contact injuries could be aided through the use of multi-body models combined with the cadaver tests. While the current MB pedestrian models were only validated for the vehicle contact [Coley *et al.* 2001, DeLange *et al.* 2006], model validation for ground contact is still limited. As the importance of pedestrian ground contact is growing [Han *et al.* 2018b, Li *et al.* 2018, Shang *et al.* 2018d, Shi *et al.* 2019, Zou *et al.* 2019], it is also necessary to assess the kinematic performance of the MB pedestrian model following the vehicle impact. Vehicle-pedestrian impact scenarios (from the cadaver tests analyzed in Chapter 6) were reconstructed and simulated using three different groups of vehicle contact characteristics: [Euro-NCAP], [Mizuno and Kajzer 2000] and [Liu *et al.* 2002], [Martinez *et al.* 2007]. In the reconstructions of Test 01 and Test 02 after head windshield impact, the pedestrian models bounced off the vehicle (see Figure 7.13), which did not occur in the PMHS experiments.

However, this bounce can be observed in some real-world collisions analyzed in Chapter 5. By changing the contact characteristics of bumper and bonnet leading edge, the performance of the MB pedestrian models improved in ground contact mechanisms, showing a limited capability representing the ground contact, this also should be a focal point in future work. Prior to the model validation, inspired by Li [Li 2016], a virtual test system (VTS) was performed to assess if changing the vehicle front-end shape can reduce injury costs subjected to ground contact considering a large range of vehicle speeds, pedestrian heights and gaits. The results illustrated in Figure 8.6 show no clear trends of sustaining the potential injury costs from pedestrian-friendly or unfriendly vehicle shapes, but the good shape vehicles are no worse than the poor shape vehicles in terms of pedestrian safety for ground contact.

10. General Conclusion and Future Work

10.1. General Conclusion

Significant new insights into pedestrian ground contact kinematics and injuries were developed in the course of this thesis.

(1) Analysis of the German collision database GIDAS showed:

The severity of ground related injuries is greatly affected by vehicle speed and pedestrian age. The average vehicle impact speed for AIS 2+ ground related upper extremity injuries is significantly lower than for head, thorax and spine injuries. Older pedestrians are more at risk of suffering thorax injuries. In terms of the effect of vehicle front shape, the proportion of ground related head injuries in AIS 2+ cases is higher for more recent vehicle models, but the difference is not statistically significant. Logistical analysis indicates that NBLEH is a predictor of the risk of AIS2 + ground related injuries. If all ground related injuries can be prevented for vehicle impact speeds below 40 km/h, there would be a substantial reduction in injury costs.

(2) Analysis of real-world videos showed:

Pedestrians showed voluntary motions such as standing still, stepping back, stooping backwards and pushing the bonnet with their arms in more than half of the selected collisions. Pedestrians impacted the ground head-first in approximately half of the collisions but the ground contact mechanisms were variable. Lower NBLEH values resulted in larger pedestrian rotation angles.

(3) Staged cadaver tests showed:

After the head-vehicle contact, there was approximately 500ms of continued interaction between the pedestrian and the vehicle until separation commences, which is followed by a flight period of around 200ms and terminates in ground contact. The linear accelerations in vehicle contact are generally lower than in the ground contact, while the contact intervals are longer. No skull fractures were observed in the tests, even though the 3ms scores are close to or above the threshold in several cases. The predicted risk of rotationally induced brain injury caused by ground contact is high for the 20 km/h tests.

A clear correlation between vehicle shape/pedestrian height and ground contact head injury risk was not observed in these six tests.

(4) Computational modelling showed:

Contact characteristics of vehicle front-end greatly influence pedestrian post-impact kinematics and the induced injury predictions. The model is partially suitable for use in a virtual test system (VTS) under low speed impact configurations and the VTS showed little difference for the weighted injury cost between the good shape and the bad shape for all three categories of vehicles. The good shape vehicles are at least not worse in pedestrian-friendly than the poor shape vehicles.

However, despite these advances, there remain significant aspects of pedestrian ground contact to investigate in the future, prior to the implementation of the injury prevention strategy.

10.2. Future work

This report was a basic analysis of pedestrian ground contact injuries that showed some promising correlations. Future work should focus on (1) more cadaver tests with broad range of vehicle speed and NBLEH to study vehicle shape effect on pedestrian post-impact kinematics and ground contact mechanisms in detail; (2) pedestrian model validation: improve the post-impact kinematic performance of MADYMO pedestrian model by changing the contact characteristic and the joint stiffness; (3) a virtual test system to improve the pedestrian safety by optimizing the vehicle front shape: when the MADYMO pedestrian model is improved for the capability of representing pedestrian post-impact kinematics and the predicted injuries, parametric studies can be conducted to study vehicle front shape effect on pedestrian ground contact injuries and propose a reverse measurement (vehicle front shape optimization) for pedestrian-friendly vehicle design; using same STS but not same impact configurations to study the effect on weighted injury costs; (4) re-analysing real-world crash videos: comparing cadaver tests with high quality real-world crash videos to study the similarities and differences; Crash videos with detailed injury information from hospital could help to better understand the relationship between contact mechanisms and ground related injuries; (5) engineering solutions for pedestrian safety: suggest combing the controlled braking with the active safety system to reduce the injury severity if the collisions

could not be prevented.

Potential solutions such as outer airbags and pedestrian inflatable safety vest which are proposed in section 9.6, are also important work in the future. In addition, inflatable safety vest that aim to protect the head could reduce the severity of head injuries not only from the vehicle contact but also from the ground contact. These solutions would benefit from collaboration with vehicle manufacturers.

References

- Abvabi, A., Nasr, A., Noorpoor, A., Kiasat, M.S., 2010. Investigation on the effect of impact location height on pedestrian safety using a legform impactor dynamic model. *Safety Science* 48 (5), 660-671.
- Anderson, R.W., Mclean, A.J., Farmer, M., Lee, B.-H., Brooks, C.G., 1997. Vehicle travel speeds and the incidence of fatal pedestrian crashes. *Accident Analysis & Prevention* 29 (5), 667-674.
- Aomura, S., Zhang, Y., Nakadate, H., Koyama, T., Nishimura, A., 2016. Brain injury risk estimation of collegiate football player based on game video of concussion suspected accident. *Journal of Biomechanical Science Engineering* 11 (4), 16-00393-16-00393.
- Arregui-Dalmases, C., Lopez-Valdes, F.J., Segui-Gomez, M., 2010. Pedestrian injuries in eight european countries: An analysis of hospital discharge data. *Accident Analysis & Prevention* 42 (4), 1164-1171.
- Ashton, S., 1975. The cause and nature of head injuries sustained by pedestrians. In: *Proceedings of the Proceedings of the International Research Council on the Biomechanics of Injury conference*, pp. 101-113.
- Ashton, S., Mackay, G., 1983. Benefits from changes in vehicle exterior design—field accident and experimental work in europe. SAE Technical paper.
- Badea-Romero, A., Lenard, J., 2013. Source of head injury for pedestrians and pedal cyclists: Striking vehicle or road? *Accident Analysis & Prevention* 50, 1140-1150.
- Bahr, R., Krosshaug, T., 2005. Understanding injury mechanisms: A key component of preventing injuries in sport. *British Journal of Sports Medicine* 39 (6), 324-329.
- Barrow, A., Reeves, C., Carroll, J., Cuerden, R., Liers, H., Marschner, M., Broertjes, P., 2014. Analysis of pedestrian accident leg contacts and distribution of contact points across the vehicle front. In: *Proceedings of the 6th International Expert Symposium on Accident Research (ESAR)*.
- Barry, F., Simms, C., 2016. Assessment of head-ground impact patterns in real world pedestrian-vehicle collisions. In: *Proceedings of the IRCOBI Conference Proceedings*.
- Bouquet, R., Ramet, M., Bermond, F., Cesari, D., 1994. Thoracic and pelvis human response to impact. *Proceedings of the 14th ESV*, 100-109.
- Carter, E., Ebdon, S., Neal-Sturgess, C., 2005. Optimization of passenger car design for the mitigation of pedestrian head injury using a genetic algorithm. In: *Proceedings of the Proceedings of the 7th annual conference on Genetic and evolutionary computation*, pp. 2113-2120.
- Cavallero, C., Cesari, D., Ramet, M., Billault, P., Farisse, J., Seriat-Gautier, B., Bonnoit, J., 1983.

- Improvement of pedestrian safety: Influence of shape of passenger car-front structures upon pedestrian kinematics and injuries: Evaluation based on 50 cadaver tests. SAE Technical Paper.
- Chawla, A., Mohan, D., Sharma, V., Kajzer, J., 2000. Safer truck front design for pedestrian impacts. *Journal of Crush Prevention and Injury Control* 2 (1), 33-43.
- Chen, H., Poulard, D., Crandall, J.R., Panzer, M.B., 2015. Pedestrian response with different initial positions during impact with a mid-sized sedan. In: *Proceedings of the 24th International Technical Conference on the Enhanced Safety of Vehicles (ESV)*.
- Chen, Q., Chen, Y., Bostrom, O., Ma, Y., Liu, E., 2014a. A comparison study of car-to-pedestrian and car-to-e-bike accidents: Data source: The china in-depth accident study (cidas). SAE Technical Paper.
- Chen, Q., Lin, M., Yan, L., Mao, Y., 2014b. Analysis of truck safety standards based on chinese in-depth accident study. *Cictp 2014: Safe, smart, and sustainable multimodal transportation systems*. pp. 2323-2336.
- CIDAS, 2017. <http://www.cidas.cn/page/cidas/cidas.php>.
- Cohen, J., 1988. Statistical power analysis for the behavioral sciences. *Journal of the American Statistical Association* 84 (363), 19-74.
- Coley, G., De Lange, R., De Oliveira, P., Neal-Sturgess, C.E., Happee, R., 2001. Pedestrian human body validation using detailed real-world accidents. In: *Proceedings of the Proceedings of the IRCOBI Conference*.
- Crocetta, G., Piantini, S., Pierini, M., Simms, C., 2015. The influence of vehicle front-end design on pedestrian ground impact. *Accident Analysis and Prevention* 79, 56-69.
- Decker, W., Koya, B., Pak, W., Untaroiu, C.D., Gayzik, F.S., 2019. Evaluation of finite element human body models for use in a standardized protocol for pedestrian safety assessment. *Traffic injury prevention*, 1-5.
- Delange, R., Vanrooij, L., Happee, R., Liu, X., 2006. Validation of human pedestrian models using laboratory data as well as accident reconstruction.
- Ding, C., Fredriksson, R., Sui, B., 2016. In-depth study of severe pedestrian accidents in china. In: *Proceedings of the IRCOBI Conference Proceedings*.
- ECE, 2008. Regulation no 21 of the economic commission for europe of the united nations (un/ece) — uniform provisions concerning the approval of vehicles with regard to their interior fittings.
- ECE, 2010. Regulation no 25 of the economic commission for europe of the united nations (un/ece) — uniform provisions concerning the approval of head restraints (headrests), whether or not incorporated in vehicle seats.
- EEVC, 2002. Improved test methods to evaluate pedestrian protection afforded by passenger cars. *Eevc Working Group Report (December 1998 with September 2002 updates)*.

- Elemance, 2019. <https://www.elemance.com/models/>.
- Elliott, J., Simms, C., Wood, D.P.J.a.A., Prevention, 2012. Pedestrian head translation, rotation and impact velocity: The influence of vehicle speed, pedestrian speed and pedestrian gait. 45, 342-353.
- ENFSI, 2015. Best practice manual for road accident reconstruction. pp. 37-40.
- Euro-NCAP, 2019. <https://www.euroncap.com>.
- Euro-NCAP, 2010. Pedestrian testing protocol.
- Gabler, L.F., Crandall, J.R., Panzer, M.B., 2016. Assessment of kinematic brain injury metrics for predicting strain responses in diverse automotive impact conditions. *Annals of Biomedical Engineering* 44 (12), 3705-3718.
- Gabler, L.F., Crandall, J.R., Panzer, M.B., 2018. Development of a metric for predicting brain strain responses using head kinematics. *Annals of biomedical engineering* 46 (7), 972-985.
- Gabler, L.F., Crandall, J.R., Panzer, M.B., 2019. Development of a second-order system for rapid estimation of maximum brain strain. *Annals of biomedical engineering* 47 (9), 1971-1981.
- Gayzik, F.S., Moreno, D.P., Vavalle, N.A., Rhyne, A.C., Stitzel, J.D., 2011. Development of the global human body models consortium mid-sized male full body model. In: *Proceedings of the International Workshop on Human Subjects for Biomechanical Research*.
- Gennarelli, T.A., Wodzin, E., 2006. Ais 2005: A contemporary injury scale. *Injury* 37 (12), 1083-1091.
- GIDAS, 2017. <http://gidas.org/en/willkommen/>.
- Goodarzi, N., Akbari, G., Razeghi Tehrani, P., 2017. Zinc chloride, a new material for embalming and preservation of the anatomical specimens. *Anatomical Sciences Journal* 14 (1), 25-30.
- Got, C., Patel, A., Fayon, A., Tarriere, C., Walfisch, G., 1978. Results of experimental head impacts on cadavers: The various data obtained and their relations to some measured physical parameters. SAE Technical Paper.
- Guillaume, A., Hermitte, T., Hervé, V., Fricheteau, R., 2015. Car or ground: Which causes more pedestrian injuries. In: *Proceedings of the Proceedings of the 24th International Conference on the Enhanced Safety of Vehicles (ESV)*, Gothenburg, Sweden, pp. 15-0084.
- Gupta, A., Alvarez, F., Daniel, T., Larner, D., 2017. Investigating the use of adhesively-coated external airbag to reduce post - impact kinematics. In: *Proceedings of the IRCOBI Conference Proceedings*.
- Gupta, V., Kalra, A., Shen, M., Chou, C.C., Yang, K.H., 2015. Effect of vehicle front end profile on pedestrian kinematics and biomechanical responses using a validated numerical model. In: *Proceedings of the ASME 2015 International Mechanical Engineering Congress and Exposition*.
- Gupta, V., Yang, K.H., 2013. Effect of vehicle front end profiles leading to pedestrian secondary head

- impact to ground. SAE Technical Paper.
- Hamacher, M., Eckstein, L., Kuhn, M., Hummel, T., 2011. Assessment of active and passive technical measures for pedestrian protection at the vehicle front. In: Proceedings of the 22st International Technical Conference on the Enhanced Safety of Vehicles (ESV 2011).
- Hamacher, M., Eckstein, L., Paas, R., 2012. Vehicle related influence of post-car impact pedestrian kinematics on secondary impact. In: Proceedings of the Proceedings of the International Research Council on the Biomechanics of Injury conference, pp. 717-729.
- Han, Y., Li, Q., He, W., Wan, F., Wang, B., Mizuno, K., 2017. Analysis of vulnerable road user kinematics before/during/after vehicle collisions based on video records. In: Proceedings of the IRCOBI Conference Proceedings.
- Han, Y., Li, Q., Qian, Y., Zhou, D., Svensson, M., 2018a. Comparison of the landing kinematics of pedestrians and cyclists during ground impact determined from vehicle collision video records. *International Journal of Vehicle Safety* 10 (3-4), 212-234.
- Han, Y., Li, Q., Wang, F., Wang, B., Mizuno, K., Zhou, Q., 2018b. Analysis of pedestrian kinematics and ground impact in traffic accidents using video records. *International Journal of Crashworthiness*, 1-10.
- Han, Y., Yang, J., Mizuno, K., Matsui, Y., 2012. Effects of vehicle impact velocity, vehicle front-end shapes on pedestrian injury risk. *Traffic injury prevention* 13 (5), 507-518.
- Hertz, E., 1993. A note on the head injury criterion (hic) as a predictor of the risk of skull fracture. In: Proceedings of the Proceedings: Association for the Advancement of automotive medicine annual conference, pp. 303-312.
- Hill, J., Thomas, P., Smith, M., 2001. The methodology of on the spot accident investigations in the uk. National Highway Traffic Safety Administration (DOT HS 809 220).
- Hobbs, A., 2001. Safer car fronts for pedestrians and cyclists. Brussels, European Transport Safety Council, Vehicle safety working party.
- Hobbs, C.A., McDonough, P.J.J.R., 1998. Development of the european new car assessment programme (euro ncap). 44, 3.
- Hovding, 2019. <https://hovding.com/>.
- Hu, J., Klinich, K.D., 2012. Toward designing pedestrian-friendly vehicles.
- Hussain, Q., Feng, H., Grzebieta, R., Brijs, T., Olivier, J., 2019. The relationship between impact speed and the probability of pedestrian fatality during a vehicle-pedestrian crash: A systematic review and meta-analysis. *Accident Analysis & Prevention* 129, 241-249.
- Hutchinson, J., Kaiser, M.J., Lankarani, H.M., 1998. The head injury criterion (hic) functional. *Applied Mathematics Computation* 96 (1), 1-16.
- Hutchinson, T.P., Searson, D.J., Anderson, R., Dutschke, J.K., Ponte, G., Van Den Berg, A., 2011. Protection of the unhelmeted head against blunt impact: The pedestrian and the car bonnet. In: Proceedings of the Proceedings of the Australasian road safety research, policing and

- education conference, pp. 1-10.
- IBM, 2015. Ibm spss statistics for windows. 24. Armonk, NY: IBM Corp.
- Isenberg, R.A., Chidester, A.B., 1998. Update on the pedestrian crash data study. In: Proceedings of the 16th International Technical Conference on the Enhanced Safety of Vehicles.
- Ishikawa, H., Kajzer, J., Schroeder, G., 1993a. Computer simulation of impact response of the human body in car-pedestrian accidents. SAE Technical Paper.
- Ishikawa, H., Yamazaki, K., Ono, K., Sasaki, A., 1993b. Current situation of pedestrian accidents and research into pedestrian protection in japan. In: Proceedings of the Proceedings: International Technical Conference on the Enhanced Safety of Vehicles, pp. 281-293.
- ISO, 2005. Iso 13232-5, motorcycles — test and analysis procedures for research evaluation of rider crash protective devices fitted to motorcycles Part 5: Injury indices and risk/benefit analysis.
- Iwamoto, M., Kisanuki, Y., Watanabe, I., Furusu, K., Miki, K., Hasegawa, J., 2002. Development of a finite element model of the total human model for safety (thums) and application to injury reconstruction. Proceedings of the 2002 International Research Council on Biomechanics of Injury, Munich, Germany, 31-42.
- Iwamoto, M., Omori, K., Kimpara, H., Nakahira, Y., Tamura, A., Watanabe, I., Miki, K., Hasegawa, J., Oshita, F., Nagakute, A., 2003. Recent advances in thums: Development of individual internal organs, brain, small female and pedestrian model. In: Proceedings of the Proceedings of 4th European LS Dyna Users conference, pp. 1-10.
- Jakobsson, L., Broberg, T., Karlsson, H., Fredriksson, A., Gråberg, N., Gullander, C., Lindman, M., 2013. Pedestrian airbag technology—a production system. In: Proceedings of the 23rd International Technical Conference on the Enhanced Safety of Vehicles (ESV).
- Jarrett, K., Saul, R., 1998. Pedestrian injury-analysis of the pcds field collision data. In: Proceedings of the 16th International Technical Conference on the Enhanced Safety of Vehicles.
- Jehu, V., Peavson, L., 1976. The trajectories of pedestrian dummies struck by cars of conventional and modified frontal designs.
- Kajzer, J., Cavallero, C., Bonnoit, J., Morjane, A., Ghanouchi, S., 1993. Response of the knee joint in lateral impact: Effect of bending moment. In: Proceedings of the Proceedings of the IRCOBI Conference, pp. 105-116.
- Kajzer, J., Cavallero, C., Ghanouchi, S., Bonnoit, J., Ghorbel, A., 1990. Response of the knee joint in lateral impact: Effect of shearing loads. In: Proceedings of the International IRCOBI Conference on the Biomechanics of Impacts, 1990, Bron, France.
- Kalra, A., Gupta, V., Shen, M., Jin, X., Chou, C.C., Yang, K.H., 2016. Pedestrian safety: An overview of physical test surrogates, numerical models and availability of cadaveric data for model validation. *International Journal of Vehicle Safety* 9 (1), 39-71.
- Kang, S., Xiao, P., 2008. Comparison of hybrid iii rigid body dummy models. In: Proceedings of the

- 10th International LSDYNA Users Conference.
- Kendall, R., Meissner, M., Crandall, J., 2006. The causes of head injury in vehicle-pedestrian impacts: Comparing the relative danger of vehicle and road surface. SAE Technical Paper.
- Kerrigan, J., Kam, C., Drinkwater, C., Murphy, D., Bose, D., Ivarsson, J., Crandall, J., 2005. Kinematic comparison of the polar-ii and pmhs in pedestrian impact tests with a sport-utility vehicle. Proceedings of the 2005 International Research Council on the Biomechanics of Impact (IRCOBI), Prague, Czech Republic.
- Kerrigan, J.R., Crandall, J.R., Deng, B., 2007. Pedestrian kinematic response to mid-sized vehicle impact. *International journal of vehicle safety* 2 (3), 221-240.
- Khaykin, A., Larner, D.L., 2016. Adhesive vehicle front end for mitigation of secondary pedestrian impact. Google Patents.
- Kimpara, H., Iwamoto, M., 2012. Mild traumatic brain injury predictors based on angular accelerations during impacts. *Annals of biomedical engineering* 40 (1), 114-126.
- Kimpara, H., Nakahira, Y., Iwamoto, M., Miki, K., 2006. Investigation of anteroposterior head-neck responses during severe frontal impacts using a brain-spinal cord complex fe model. *Stapp car crash journal* 50, 509.
- Klug, C., Feist, F., Raffler, M., Sinz, W., Petit, P., Ellway, J., Van Ratingen, M., 2017. Development of a procedure to compare kinematics of human body models for pedestrian simulations. In: Proceedings of the IRCOBI Conference: International Research Council on the Biomechanics of Injury.
- Koppel, S., Bohensky, M., Langford, J., Taranto, D., 2011. Older drivers, crashes and injuries. *Traffic injury prevention* 12 (5), 459-467.
- Krenn, M., Mlekusch, B., Wilfling, C., Dobida, F., Deutscher, E., 2003. Development and evaluation of a kinematic hood for pedestrian protection. SAE Technical Paper.
- Krosshaug, T., Bahr, R., 2005. A model-based image-matching technique for three-dimensional reconstruction of human motion from uncalibrated video sequences. *Journal of biomechanics* 38 (4), 919-929.
- Lawrence, G., Hardy, B., 1998. Pedestrian safety testing using the eevc pedestrian impactors. In: Proceedings of the 16th ESV Conference.
- Lee, J.-W., Yoon, K.-H., Kang, Y.-S., Park, G.-J., 2004. Vehicle hood and bumper structure design to mitigate casualties of pedestrian accidents. SAE paper (05-0105).
- Li, G., 2016. Optimization of vehicle front shape for pedestrian protection.
- Li, G., Lyons, M., Wang, B., Yang, J., Otte, D., Simms, C., 2017a. The influence of passenger car front shape on pedestrian injury risk observed from german in-depth accident data. *Accident Analysis & Prevention* 101, 11-21.
- Li, G., Yang, J., Simms, C., 2016. A virtual test system representing the distribution of pedestrian impact configurations for future vehicle front-end optimization. *Traffic Injury Prevention* 17

- (5), 515-523.
- Li, G., Yang, J., Simms, C., 2017b. Safer passenger car front shapes for pedestrians: A computational approach to reduce overall pedestrian injury risk in realistic impact scenarios. *Accident Analysis & Prevention* 100, 97.
- Li, Q., Han, Y., Mizuno, K., 2018. Ground landing mechanisms in vehicle-to-pedestrian impacts based on accident video records. *SAE Technical Paper*.
- Li, W., Li, G., Liu, F., 2015. Frontal structure safety analysis of minibuses based on chinese in-depth accident studies. *Icte 2015*. pp. 2973-2978.
- Lim, J.-H., Park, J.-S., Yun, Y.-W., Jeong, S.-B., Park, G.-J., 2015. Design of an airbag system of a mid-sized automobile for pedestrian protection. *Proceedings of the Institution of Mechanical Engineers, Part D: Journal of Automobile Engineering* 229 (5), 656-669.
- Lissner, H., Lebow, M., Evans, F., 1960. Experimental studies on the relation between acceleration and intracranial pressure changes in man. *Surgery, gynecology & obstetrics* 111, 329.
- Liu, X., Yang, J., 2003. Effects of vehicle impact velocity and front-end structure on dynamic responses of child pedestrians. *Traffic Injury Prevention* 4 (4), 337-344.
- Liu, X.J., Yang, J.K., Lövsund, P., 2002. A study of influences of vehicle speed and front structure on pedestrian impact responses using mathematical models. *Traffic Injury Prevention* 3 (1), 31-42.
- Lyons, M., Simms, C.K., 2012. Predicting the influence of windscreen design on pedestrian head injuries.
- Maeno, T., Hasegawa, J., 2001. Development of a finite element model of the total human model for safety (thums) and application to car-pedestrian impacts. *SAE Technical Paper*.
- Maki, T., Kajzer, J., Mizuno, K., Sekine, Y.J.a.A., Prevention, 2003. Comparative analysis of vehicle–bicyclist and vehicle–pedestrian accidents in japan. 35 (6), 927-940.
- Margulies, S.S., Thibault, L.E., 1992. A proposed tolerance criterion for diffuse axonal injury in man. *Journal of biomechanics* 25 (8), 917-923.
- Marjoux, D., Baumgartner, D., Deck, C., Willinger, R., 2008. Head injury prediction capability of the hic, hip, simon and ulp criteria. *Accident Analysis & Prevention* 40 (3), 1135-1148.
- Martinez, L., Guerra, L.J., Ferichola, G., Garcia, A., Yang, J., 2007. Stiffness corridors of the european fleet for pedestrian simulations. In: *Proceedings of the 20th International Technical Conference on the Enhanced Safety of Vehicles (ESV)* National Highway Traffic Safety Administration.
- Masoumi, A., Shojaeefard, M.H., Najibi, A., 2011. Comparison of steel, aluminum and composite bonnet in terms of pedestrian head impact. *Safety science* 49 (10), 1371-1380.
- Masson, C., Serre, T., Cesari, D., 2007. Pedestrian-vehicle accident: Analysis of 4 full scale tests with pmhs. In: *Proceedings of the 20th International Technical Conference on the Enhanced Safety of Vehicles (ESV)*

- Mattsson, M., Ericsson, M., 2004. Pedestrian safety device. Google Patents.
- Meng, Y., Pak, W., Guleyupoglu, B., Koya, B., Gayzik, F.S., Untaroiu, C.D., 2017. A finite element model of a six-year-old child for simulating pedestrian accidents. *Accident Analysis & Prevention* 98, 206-213.
- Midi, H., Sarkar, S.K., Rana, S., 2010. Collinearity diagnostics of binary logistic regression model. *Journal of Interdisciplinary Mathematics* 13 (3), 253-267.
- Mizuno, K., Kajzer, J., 1999. Compatibility problems in frontal, side, single car collisions and car-to-pedestrian accidents in japan. *Accid Anal Prev* 31 (4), 381-391.
- Mizuno, K., Kajzer, J., 2000. Head injuries in vehicle-pedestrian impact. SAE Technical paper.
- Mizuno, Y., Ishikawa, H., 2005. Summary of ihra pedestrian safety working group activities proposed test methods to evaluate pedestrian protection afforded by passenger cars.
- Mo, F., Arnoux, P.J., Cesari, D., Masson, C., 2014. Investigation of the injury threshold of knee ligaments by the parametric study of car-pedestrian impact conditions. *Safety Science* 62 (2), 58-67.
- Mori, K., Nagata, A., Sato, Y., Mizuno, Y., 2008. Pedestrian airbag system. Google Patents.
- Mueller, B., Macalister, A., Nolan, J., Zuby, D., 2015. Comparison of hic and bric head injury risk in iihs frontal crash tests to real-world head injuries. In: *Proceedings of the Proceedings of the 24th International Technical Conference on the Enhanced Safety of Vehicles*.
- Nagatomi, K., Hanayama, K., Ishizaki, T., Sasaki, S., Matsuda, K., 2005. Development and full-scale dummy tests of a pop-up hood system for pedestrian protection. In: *Proceedings of the Proceedings of the 19th International Technical Conference "Enhanced Safety of Vehicles" ESV, Washington*, pp. 05-0113.
- Nagurka, M., Huang, S., 2004. A mass-spring-damper model of a bouncing ball. In: *Proceedings of the Proceedings of the 2004 American control conference*, pp. 499-504.
- Neal-Sturgess, C., Carter, E., Hardy, R., Cuerden, R., Guerra, L., Yang, J., 2007. Aprosys european in-depth pedestrian database. *Age* 91, 95.
- Niebuhr, T., Junge, M., Rosén, E., 2016. Pedestrian injury risk and the effect of age. *Accident Analysis & Prevention* 86, 121-128.
- Oh, C., Kang, Y.-S., Kim, W., 2008. Assessing the safety benefits of an advanced vehicular technology for protecting pedestrians. *Accident Analysis & Prevention* 40 (3), 935-942.
- Otte, D., 2005. 3-d laser systems for scaled accident sketches and documentation of traces after traffic accidents as basis of biomechanical analysis. In: *Proceedings of the Proceedings of the International Research Council on the Biomechanics of Injury conference*, pp. 435-438.
- Otte, D., 2010. Head impact conditions and injury pattern in car crashes against pedestrians versus bicyclists in german in-depth-accident study gidas. In: *Proceedings of the International Crashworthiness Conference (ICRASH)*.
- Otte, D., Jänsch, M., Haasper, C., 2012. Injury protection and accident causation parameters for

- vulnerable road users based on german in-depth accident study gidas. *Accident Analysis & Prevention* 44 (1), 149-153.
- Otte, D., Krettek, C., Brunner, H., Zwipp, H., 2003. Scientific approach and methodology of a new in-depth investigation study in germany called gidas. In: *Proceedings of the Proceedings: International Technical Conference on the Enhanced Safety of Vehicles*.
- Otte, D., Pohlemann, T., 2001. Analysis and load assessment of secondary impact to adult pedestrians after car collisions on roads. In: *Proceedings of the Proceedings of the International Research Council on the Biomechanics of Injury conference*, pp. 143-157.
- Paas, R., Masson, C., Davidsson, J., 2015. Head boundary conditions in pedestrian crashes with passenger cars: Six-degrees-of-freedom post-mortem human subject responses. *International Journal of Crashworthiness* 20 (6), 547-559.
- Park, D., Jang, C., Lee, S., Heo, S., Yim, H., Kim, M., 2010. Optimizing the shape of a bumper beam section considering pedestrian protection. *International Journal of Automotive Technology* 11 (4), 489-494.
- Payne, A.R., Patel, S., 2001. Occupant protection & egress in rail systems (operas) project 427519. MIRA.
- Pheasant, S., Haslegrave, C.M., 2016. *Bodyspace: Anthropometry, ergonomics and the design of work* CRC Press.
- Ponte, G., Van Den Berg, A., Streeter, L.D., Anderson, R., 2004. Pedestrian protection in vehicle impacts: Further results from the australian new car assessment program. In: *Proceedings of the Proceedings of the 2004 Road Safety Research, Policing and Education Conference*, Perth, Australia, pp. 14-16.
- Rosén, E., Stigson, H., Sander, U., 2011. Literature review of pedestrian fatality risk as a function of car impact speed. *Accident; analysis and prevention* 43 (1), 25-33.
- Roudsari, B.S., Mock, C.N., Kaufman, R., 2005. An evaluation of the association between vehicle type and the source and severity of pedestrian injuries. *Traffic Injury Prevention* 6 (2), 185-192.
- SAE, 1995. Instrumentation for impact test—part 1—electronic instrumentation. SAE 211.
- Sawilowsky, S.S., 2009. New effect size rules of thumb. *Journal of Modern Applied Statistical Methods* 8 (2), 597-599.
- Schmitt, K.-U., Niederer, P., Muser, M., Walz, F., 2010. *Trauma biomechanics* Springer.
- Serre, T., Masson, C., Perrin, C., Chalandon, S., Llari, M., Py, M., Cavallero, C., Cesari, D., 2007. Real accidents involving vulnerable road users: In-depth investigation, numerical simulation and experimental reconstitution with pmhs. *International journal of crashworthiness* 12 (3), 227-234.
- Shang, S., Arnoux, P., Masson, C., Py, M., Simms, C., 2018a. A preliminary vehicle dummy impact test for validation of multi body pedestrian ground contact simulation. In: *Proceedings of the*

- Proceedings of the Bioengineering in Ireland Conference.
- Shang, S., Li, G., Otte, D., Simms, C., 2018b. An inverse method to reduce pedestrian-ground contact injuries In: Proceedings of the IRCOBI Asia 2018.
- Shang, S., Masson, C., Arnoux, P., Py, M., Simms, C.K., 2018c. Preliminary assessment of the madymo pedestrian model for predicting pedestrian ground contact kinematics. In: Proceedings of the Proceedings of the IRCOBI Conference.
- Shang, S., Masson, C., Teeling, D., Py, M., Ferrand, Q., Arnoux, P.-J., Simms, C., 2020. Kinematics and dynamics of pedestrian head ground contact: A cadaver study. *Safety Science* 127, 104684.
- Shang, S., Otte, D., Li, G., Simms, C., 2018d. Detailed assessment of pedestrian ground contact injuries observed from in-depth accident data. *Accident Analysis & Prevention* 110, 9-17.
- Shang, S., Otte, D., Simms, C.K., 2017. Pedestrian-ground contact injuries observed from german in-depth accident data. In: Proceedings of the Proceedings of the IRCOBI Conference, pp. 1.004-1.047.
- Shi, L., Han, Y., Huang, H., He, W., Wang, F., Wang, B., 2019. Effects of vehicle front-end safety countermeasures on pedestrian head injury risk during ground impact. *Proceedings of the Institution of Mechanical Engineers, Part D: Journal of Automobile Engineering*, 0954407019828845.
- Shi, L., Han, Y., Huang, H., Li, Q., Wang, B., Mizuno, K., 2018. Analysis of pedestrian-to-ground impact injury risk in vehicle-to-pedestrian collisions based on rotation angles. *Journal of Safety Research* 64, 37-47.
- Shigeta, K., Kitagawa, Y., Yasuki, T., 2009. Development of next generation human fe model capable of organ injury prediction. *Proceedings of the 21st Annual Enhanced Safety of Vehicles*.
- Simms, C., 2005. Sports utility vehicles and older pedestrians. *Bmj* 331 (7520), 787.
- Simms, C., Ormond, T., Wood, D., 2011. The influence of vehicle shape on pedestrian ground contact mechanisms. In: Proceedings of the Proceedings of IRCOBI Conference, Poland.
- Simms, C., Wood, D., 2009. *Pedestrian and cyclist impact* Springer Netherlands.
- Simms, C.K., Wood, D.P., 2006. Effects of pre-impact pedestrian position and motion on kinematics and injuries from vehicle and ground contact. *International Journal of Crashworthiness* 11 (4), 345-355.
- Stammen, J.A., Ko, S.W., Guenther, D.A., Heydinger, G.J., 2002. A demographic analysis and reconstruction of selected cases from the pedestrian crash data study. In: Proceedings of the SAE 2002 World Congress & Exhibition.
- Strandroth, J., Rizzi, M., Sternlund, S., Lie, A., Tingvall, C., 2011. The correlation between pedestrian injury severity in real-life crashes and euro ncap pedestrian test results. *Traffic injury prevention* 12 (6), 604-613.

- Subit, D., Kerrigan, J., Crandall, J., Fukuyama, K., Yamazaki, K., Kamiji, K., Yasuki, T., 2008. Pedestrian-vehicle interaction: Kinematics and injury analysis of four full scale tests. In: Proceedings of the Proceedings of IRCOBI Conference, pp. 275-294.
- Takhounts, E.G., Craig, M.J., Moorhouse, K., Mcfadden, J., Hasija, V., 2013. Development of brain injury criteria (bric). SAE Technical Paper.
- Takimoto, T., Kobayashi, Y., Nakamura, A., 2010. Pedestrian airbag apparatus. Google Patents.
- Tamura, A., Duma, S., 2011a. A study on the potential risk of traumatic brain injury due to ground impact in a vehicle-pedestrian collision using full-scale finite element models. *International Journal of Vehicle Safety* 5 (2), 117-136.
- Tamura, A., Duma, S., 2011b. A study on the potential risk of traumatic brain injury due to ground impact in a vehicle-pedestrian collision using full-scale finite element models. *International Journal of Vehicle Safety* 5 (2), 117-136.
- Tamura, A., Koide, T., Yang, K.H., 2014. Effects of ground impact on traumatic brain injury in a fender vault pedestrian crash. *International journal of vehicle safety* 8 (1), 85-100.
- Taneda, K., Kondo, M., Higuchi, K., 1973. Experiment on passenger car and pedestrian dummy collision. In: Proceedings of the Proceedings of the International Research Council on the Biomechanics of Injury conference, pp. 231-239.
- Tannous, R., Eppinger, R., Sun, E., Bandak, F., Haffner, M., Khaewpong, N., Maltese, M., Kuppa, S., Nguyen, T., Takhounts, E., 1999. Development of improved injury criteria for the assessment of advanced automotive restraint systems - ii. *Dummies* 54 (8), 151-152.
- The-Blueprints, <http://www.the-blueprints.com/>.
- Tierney, G., Krosshaug, T., Wilson, F., Simms, C., 2015. An assessment of a novel approach for determining the player kinematics in elite rugby union players. In: Proceedings of the Proceedings of the International Research Council on Biomechanics of Injury, pp. 180-81.
- Tierney, G.J., Joodaki, H., Krosshaug, T., Forman, J.L., Crandall, J.R., Simms, C.K., 2016. The kinematics of head impacts in contact sport: An initial assessment of the potential of model based image matching. In: Proceedings of the ISBS-Conference Proceedings Archive.
- Tierney, G.J., Joodaki, H., Krosshaug, T., Forman, J.L., Crandall, J.R., Simms, C.K., 2018. Assessment of model-based image-matching for future reconstruction of unhelmeted sport head impact kinematics. *Sports biomechanics* 17 (1), 33-47.
- Tillmann, B., 2006. Atlas der anatomie des menschen: Mit muskeltrainer Springer-Verlag.
- TNO, 2017. Madymo human body models manual release 7.7 june 2017. TNO MADYMO BV., Delft, 1-88.
- Toyota, http://www.toyota.com.cn/innovation/safety_technology/safety_measurements/thums.html.
- Triana, C., Fajardo, F., 2013. Experimental study of simple harmonic motion of a spring-mass system as a function of spring diameter. *Revista Brasileira de Ensino de Física* 35 (4), 1-8.
- Union, E., 2005. Directive 2005/66/ec of the european parliament and of the council of 26 october

- 2005 relating to the use of frontal protection systems on motor vehicles and amending council directive 70/156/eec. Europe Official Journal of The European Union, 37-40.
- Untaroiu, C.D., Crandall, J.R., Takahashi, Y., Okamoto, M., Ito, O., Fredriksson, R., 2010. Analysis of running child pedestrians impacted by a vehicle using rigid-body models and optimization techniques. *Safety science* 48 (2), 259-267.
- Untaroiu, C.D., Meissner, M.U., Crandall, J.R., Takahashi, Y., Okamoto, M., Ito, O., 2009. Crash reconstruction of pedestrian accidents using optimization techniques. *International Journal of Impact Engineering* 36 (2), 210-219.
- Untaroiu, C.D., Pak, W., Meng, Y., Schap, J., Koya, B., Gayzik, S., 2018. A finite element model of a midsize male for simulating pedestrian accidents. *Journal of biomechanical engineering* 140 (1), 011003.
- Untaroiu, C.D., Putnam, J.B., Schap, J., Davis, M.L., Gayzik, F.S., 2016. Development and preliminary validation of a 50th percentile pedestrian finite element model. In: *Proceedings of the ASME 2015 International Design Engineering Technical Conferences and Computers and Information in Engineering Conference*.
- Untaroiu, C.D., Shin, J., Crandall, J.R., 2007. A design optimization approach of vehicle hood for pedestrian protection. *International Journal of Crashworthiness* 12 (6), 581-589.
- Van Hoof, J., De Lange, R., Wismans, J.S., 2003. Improving pedestrian safety using numerical human models. SAE Technical Paper.
- Van Rooij, L., Bhalla, K., Meissner, M., Ivarsson, J., Crandall, J., Longhitano, D., Takahashi, Y., Dokko, Y., Kikuchi, Y., 2003. Pedestrian crash reconstruction using multi-body modeling with geometrically detailed, validated vehicle models and advanced pedestrian injury criteria. In: *Proceedings of the 18th ESV Conference*.
- Versace, J., 1971. A review of the severity index. SAE Technical Paper.
- Viano, D.C., 1989. Biomechanical responses and injuries in blunt lateral impact. SAE Technical Paper.
- Watanabe, R., Miyazaki, H., Kitagawa, Y., Yasuki, T., 2011. Research of collision speed dependency of pedestrian head and chest injuries using human fe model (thums version 4). In: *Proceedings of the 22nd International Technical Conference on the Enhanced Safety of Vehicles (ESV)*, WA, pp. 11-0043.
- WHO, 2013. Global status report on road safety 2013: Supporting a decade of action. World Health Organization.
- WHO, 2015. Global status report on road safety 2015 World Health Organization.
- Winckler, G., 1974. *Manuel d'anatomie topographique et fonctionnelle* Masson.
- Wood, D.P., Simms, C., Walsh, D., 2005. Vehicle-pedestrian collisions: Validated models for pedestrian impact and projection. *Proceedings of the Institution of Mechanical Engineers, Part D: Journal of Automobile Engineering* 219 (2), 183-195.

- Xu, J., Shang, S., Qi, H., Yu, G., Wang, Y., Chen, P., 2016a. Simulative investigation on head injuries of electric self-balancing scooter riders subject to ground impact. *Accident Analysis & Prevention* 89, 128-141.
- Xu, J., Shang, S., Yu, G., Qi, H., Wang, Y., Xu, S., 2016b. Are electric self-balancing scooters safe in vehicle crash accidents? *Accident Analysis & Prevention* 87, 102-116.
- Yang, J., 2005. Review of injury biomechanics in car-pedestrian collisions. *International journal of vehicle safety* 1 (1-3), 100-117.
- Yang, J., Kajzer, J., Cavallero, C., Bonnoit, J., 1995. Computer simulation of shearing and bending response of the knee joint to a lateral impact. SAE Technical Paper.
- Yang, J., Lovsund, P., 1997. Development and validation of a human-body mathematical model for simulation of car-pedestrian collisions. In: *Proceedings of the Proc. of the Int. IRCOBI Conf., Hanover (Germany)*, pp. 133-49.
- Yang, J., Lövsund, P., Cavallero, C., Bonnoit, J., 2000. A human-body 3d mathematical model for simulation of car-pedestrian impacts. *Traffic Injury Prevention* 2 (2), 131-149.
- Yang, J., Rzymkowski, C., Kajzer, J., 1993. Development and validation of a mathematical breakable leg model. In: *Proceedings of the Proceedings of the International Research Council on the Biomechanics of Injury conference*, pp. 175-186.
- Yang, J., Yao, J., Otte, D., 2005. Correlation of different impact conditions to the injury severity of pedestrians in real world accidents. In: *Proceedings of the Proceedings of the 19th International Technical Conference Enhanced Safety of Vehicle, Washington, DC*.
- Yao, J., Yang, J., Otte, D., 2008. Investigation of head injuries by reconstructions of real-world vehicle-versus-adult-pedestrian accidents. *Safety science* 46 (7), 1103-1114.
- Yasuki, T., 2006. Using thums for pedestrian safety simulations. *Autotechnology* 6 (4), 44-47.
- Yasuki, T., Yamamae, Y., 2010. Validation of kinematics and lower extremity injuries estimated by total human model for safety in suv to pedestrian impact test. *Journal of Biomechanical Science and Engineering* 5 (4), 340-356.
- Yin, S., Li, J., Xu, J., 2017. Exploring the mechanisms of vehicle front-end shape on pedestrian head injuries caused by ground impact. *Accident Analysis & Prevention* 106, 285-296.
- Zeng, B., Liu, X., Zhang, Y., 2016. The structure optimization analysis of electric vehicle in small offset rear end collision. *Procedia engineering* 137, 103-108.
- Zhang, G., Cao, L., Hu, J., Yang, K.H., 2008. A field data analysis of risk factors affecting the injury risks in vehicle-to-pedestrian crashes. In: *Proceedings of the Annals of Advances in Automotive Medicine/Annual Scientific Conference*, pp. 199.
- Zou, T., Shang, S., Simms, C., 2019. Potential benefits of controlled vehicle braking to reduce pedestrian ground contact injuries. *Accident Analysis & Prevention* 129, 94-107.

Appendices

Appendix A. Subsystem impactor tests stiffness calculation, adapted from [Martinez *et al.* 2007]

Stiffness calculation from headform tests

- (1) The time t_0 is determined when the headform fore-aft acceleration (A_{FH}) exceeds $2g$.
- (2) In the interval of $(t_0, t_0 + 1 \text{ ms})$, the normal angle at the impact point with respect the fore-aft direction (α_N) is obtained as illustrated in Figure A1.
- (3) The resultant normal acceleration (A_{RN}) is obtained from the vertical and the fore-aft acceleration which projected with respect the normal of impact.
- (4) Multiply the A_{RN} with the headform mass M_H , to obtain the normal force F_N .
- (5) The initial normal velocity (V_{0N}) at t_0 is obtained by projecting the impact velocity (V_0) to the normal of impact.
- (6) Double integrate the A_{RN} to get deflection D_N using the V_{0N} as the initial velocity, making the displacement zero at t_0 .

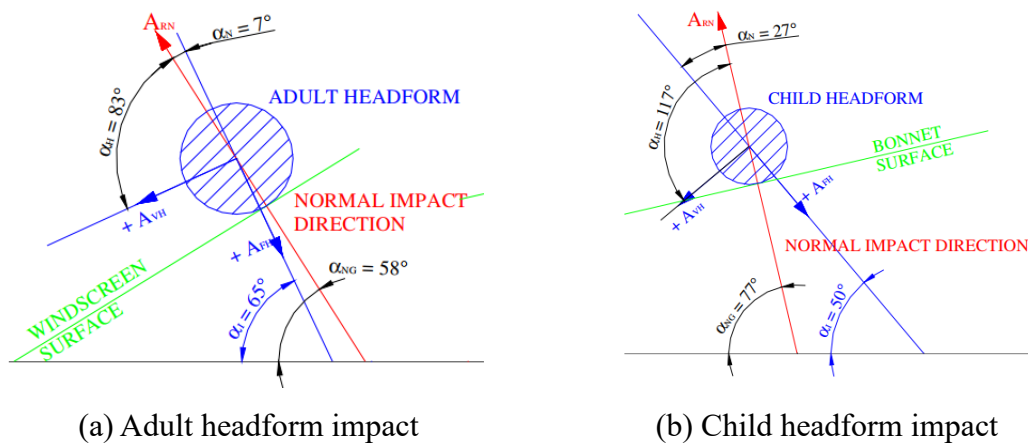


Figure A1. Angles of the headform impact tests, adapted from [Martinez *et al.* 2007]

Stiffness calculation from legform test

- (1) Define time t_0 of the legform impact test.
- (2) The force in the impact F_L is obtained by multiplying the tibia acceleration A_T (channel output) with the impactor mass M (given).
- (3) The displacement (D_L) is obtained by double integrating the A_T , using V_0 as the initial velocity and making the displacement zero at t_0 . It should be noted that the displacement includes the displacement of car structure together with the crush of the impactor (approximately 20 mm).

Stiffness calculation from Upper legform test

- (1) Define time t_0 of the upper legform impact test.
- (2) Divide the sum of forces (F_S) with the upper legform mass behind the load transducer (M_{LC}) to obtain the whole device acceleration (A_{UL}).
- (3) The total Force (F_T) is obtained by multiplying the calculated acceleration A_{UL} with the total mass of upper legform (M_{UL}).
- (4) Double integrate the A_{UL} to get the displacement using the V_0 as the initial velocity and making the displacement zero in the very first moment of impact D_{UL} . Again, the displacement includes the car structure displacement together with the crush in the impactor (approximately 40 mm).

Appendix B. Real-world crash video sequences used in Chapter 5

The online sources of the real-world crash videos are listed as below,

<https://www.youtube.com/watch?v=ZU8hXY8KiAg> (0:35, 2:27, 2:37, 3:14)

<https://www.youtube.com/watch?v=Pm9sln6coyM> (11:07, 11:12, 11:20, 11:25, 11:31, 13:00 14:02,)

https://www.youtube.com/watch?v=Khuie6_axRg (0:08)

https://www.youtube.com/watch?v=vXMdtZz_EOk (1:21, 1:43, 3:03, 4:08, 5:49, 8:30, 9:10)

https://www.youtube.com/watch?v=4VzE3vqGsTs&oref=https%3A%2F%2Fwww.youtube.com%2Fwatch%3Fv%3D4VzE3vqGsTs&has_verified=1 (0:09, 0:22, 0:34, 8:03, 8:15)

<https://www.youtube.com/watch?v=tZ5BoHnIFNE> (0:30, 3:22, 4:46, 6:53)

<https://www.youtube.com/watch?v=2Azs-JI0jTY> (5:29)



(01)

(02)

(03)



(04)

(05)

(06)



(07)

(08)

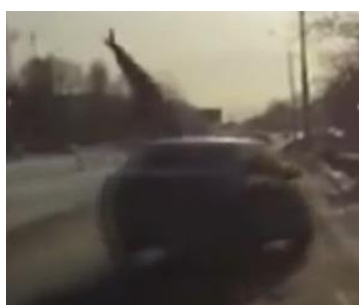
(09)



(10)

(11)

(12)



(13)

(14)

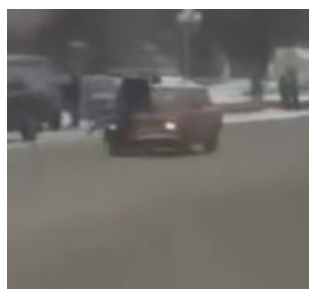
(15)



(16)

(17)

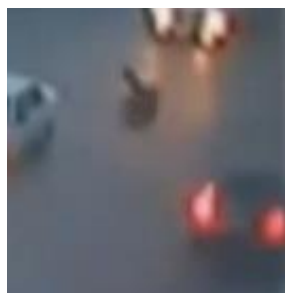
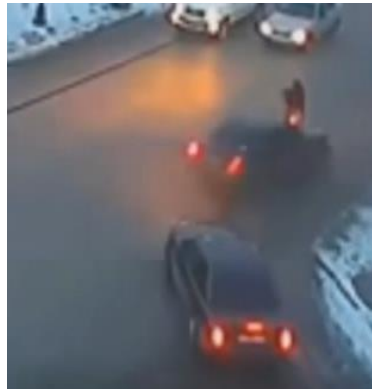
(18)



(19)

(20)

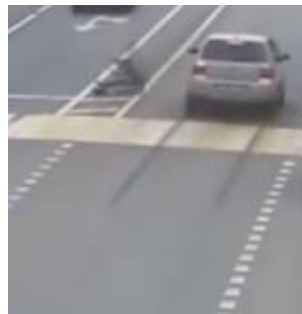
(21)



(22)

(23)

(24)



(25)

(26)

(27)



(28)

(29)

Figure B1 29 sequences of vehicle-pedestrian collision captured by video

Appendix C. Sequence of vehicle-pedestrian impact for cadaver test 01 with video data

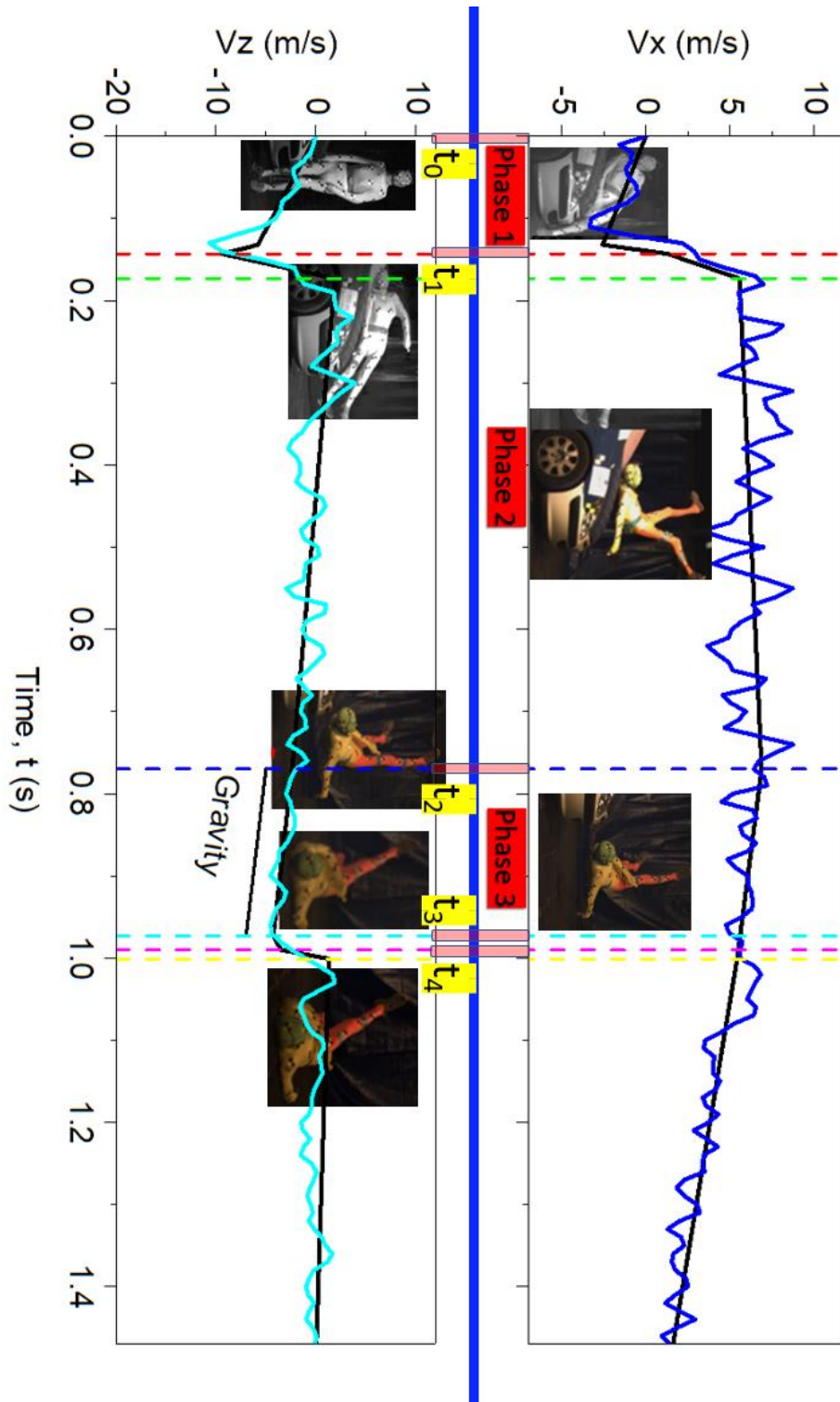


Figure C1 Sequence of vehicle-pedestrian impact for cadaver test 01 with head linear velocities from video data

Appendix D. Simulation test sample (STS) used in Chapter 8

Table D.1 STS = 30 (3 vehicle impact speeds, 5 pedestrian heights and 2 pedestrian gait stances)

Group		1	2		3	
Impact speed (km/h)	Range	1-8	9-16		17-24	
	Mean	4.5	12.5		20.5	
Pedestrian height (cm)	Range	<140	140-157	158-170	171-177	>177
	Mean	120	151	164	174	185
Gait stance (%)	Range	30-70		80-20		
	Mean	50		100		

Table D.2 STS = 60 (6 vehicle impact speeds, 5 pedestrian heights and 2 pedestrian gait stances)

Group		1	2	3	4	5	6
Impact speed (km/h)	Range	1-4	5-8	9-12	13-16	17-20	21-24
	Mean	2.5	6.5	10.5	14.5	18.5	22.5z
Pedestrian height (cm)	Range	<140	140-157	158-170	171-177	>177	
	Mean	120	151	164	174	185	
Gait stance (%)	Range	30-70		80-20			
	Mean	50		100			

Table D.3 STS = 120 (12 vehicle impact speeds, 5 pedestrian heights and 2 pedestrian gait stances)


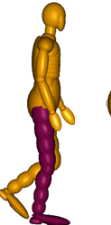






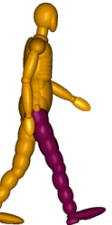

Group		1	2	3	4	5	6	7	8	9	10	11	12
Impact speed (km/h)	Range	1-2	3-4	5-6	7-8	9-10	11-12	13-14	15-16	17-18	19-20	21-22	23-24
	Mean	1.5	3.5	5.5	7.5	9.5	11.5	13.5	15.5	17.5	19.5	21.5	23.5
Pedestrian height (cm)	Range	<140			140-157			158-170		171-177		>177	
	Mean	120			151			164		174		185	
Gait stance (%)	Range	30-70				80-20							
	Mean	50				100							
													
		10%	20%	30%	40%	50%	60%	70%	80%	90%	100%		

Table D.4 STS = 240 (12 vehicle impact speeds, 5 pedestrian heights and 4 pedestrian gait stances)


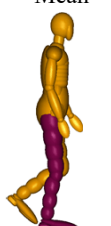




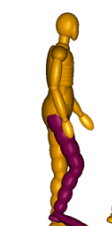
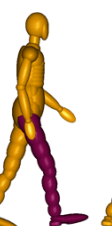
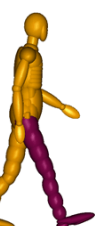

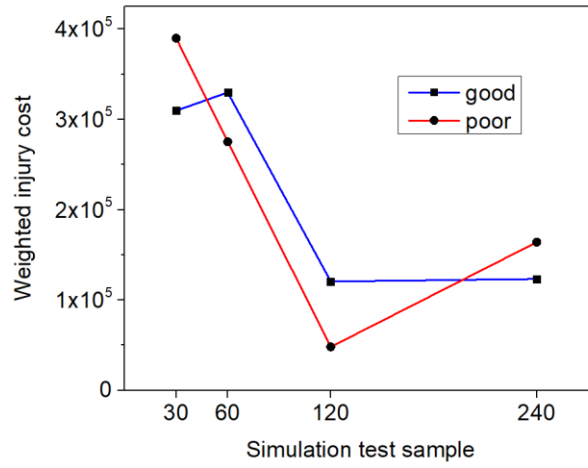
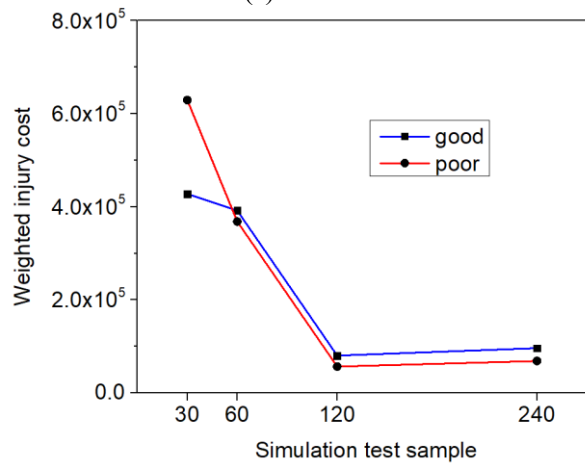
Group		1	2	3	4	5	6	7	8	9	10	11	12
Impact speed (km/h)	Range	1-2	3-4	5-6	7-8	9-10	11-12	13-14	15-16	17-18	19-20	21-22	23-24
	Mean	1.5	3.5	5.5	7.5	9.5	11.5	13.5	15.5	17.5	19.5	21.5	23.5
Pedestrian height (cm)	Range	<140			140-157			158-170		171-177		>177	
	Mean	120			151			164		174		185	
Gait stance (%)	Range	20-30		40-60		70-80		90-10					
	Mean	30		50		80		100					
													
		10%	20%	30%	40%	50%	60%	70%	80%	90%	100%		

Table D.5 STS = 120 (6 vehicle impact speeds, 5 pedestrian heights and 4 pedestrian gait stances)

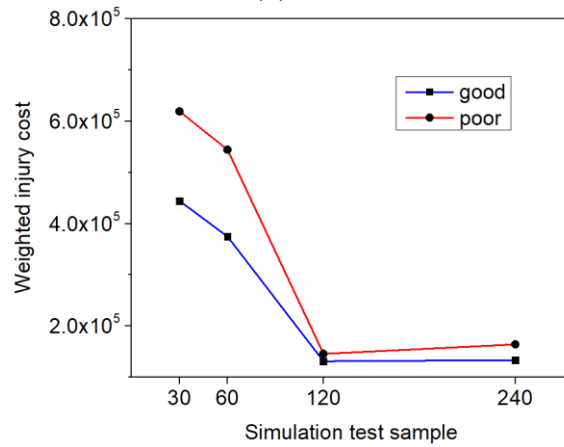
Group		1	2	3	4	5	6
Impact speed (km/h)	Range	1-4	5-8	9-12	13-16	17-20	21-24
	Mean	2.5	6.5	10.5	14.5	18.5	22.5z
Pedestrian height (cm)	Range	<140	140-157	158-170	171-177	>177	
	Mean	120	151	164	174	185	
Gait stance (%)	Range	20-30	40-60	70-80	90-10		
	Mean	30	50	80	100		



(a) sedan



(b) van



(c) SUV

Figure D1 WIC comparison between poor shape vehicles and good shape vehicles (STS adapted from Table D.5)